Poly Ether Ether Ketone (PEEK) polymers for High Temperature Laser Sintering (HT-LS)

Doctoral thesis submitted to the University of Exeter in fulfilment of the requirements of the degree of Doctor of Philosophy in Engineering

Berretta, Silvia

May 2015

Poly Ether Ether Ketone (PEEK) polymers for High Temperature Laser Sintering (HT-LS)

Submitted by Silvia Berretta to the University of Exeter

in fulfilment of the requirements of the degree of

Doctor in Philosophy in Engineering in May 2015

I certify that all of the material in this thesis which is not my own work has been identifies and that no material has previously been submitted and approved for the award of a degree by this or any other university.

Signature ……………………………

Abstract

Laser sintering (LS) is an additive manufacturing technique that allows production of prototypes and fully functional components characterised by the highest level of freedom of design currently achievable. High customisation, multi-functional integration, design optimisation and the potential for reducing cost and production time of a single item are the most outstanding characteristics of the LS process. However, the small number of polymers at present available constitutes a significant drawback for many engineering applications, especially in the automotive and aerospace industrial sectors where seemingly only one commercial high temperature grade, Poly Ether Ketone (PEK) HP3, can meet the high material performance required.

With the aim to expand the choice of materials for LS and especially High Temperature Laser Sintering (HT-LS) manufacturing, this research project has focused on the investigation and implementation into LS of a new high temperature polymer, Poly Ether Ether Ketone (PEEK). This study has examined some of the key requirements needed for the successful development of new materials in LS processes at experimental and theoretical levels.

Two generic PEEK grades 150PF and 450PF have been quantitatively investigated in parallel with well-established LS polymers in terms of particle size, particle morphology and flow behaviour. A calculation of the inter-particle interactions has been evaluated for all the materials proposed. These analyses, coupled with two strategies for the improvement of powder flowability, have formed a systematic and fundamental approach for studying powders in LS. The PEEK 450PF grade has been selected for optimisation into the HT-LS system, EOSINT P 800. The HT-LS processing parameters and their effect on the mechanical characteristics of the laser sintered units have been investigated and optimised, and new insights into the HT-LS mechanisms and functionalities of the EOSINT P 800 system are presented. A basic technique for the prediction of one of the HT-LS processing temperatures is proposed. A formula for linking material properties to processing parameters has also been assessed. Lastly, the medical equivalent grade of PEEK 450PF, PEEK-

OPTIMA® LT1, has been utilised for the manufacture and test of two medical components.

"Quello che impari non te lo toglie nessuno"

A mamma, papà e Gaia

Acknowledgements

I will never find the appropriate words of gratitude for the opportunity to undertake this research project. The completion of this thesis is an accomplishment that can only be properly acknowledged by thanking all whose help has been invaluable at several levels. With this intent the following represent my occasion to finally, fully and, hopefully, properly thank those who made this achievement possible and always worthwhile along the way.

Firstly, I would like to thank my supervisors Prof Oana Ghita and Prof Ken Evans, whose advice and support guided me throughout the duration of this course. Oana especially has been not only an inspiring academic but also a valuable mentor. I am grateful for the knowledge and skills I have learned by discussing problems and ideas with her. But most of all, I thank her because she was never afraid to challenge and guide me. As a student, I believe this is the most important characteristic that you wish for in a supervisor.

Much credit is given to Invibio biomaterials solutions and Victrex for the resources support necessary for carrying out this research. I would like to thank Andy Anderson for his technical assistance and also Dr Adam Chaplin, Dr Alan Wood, Chris Newman and Dr Mark Brady.

Special thanks are owed to the X-AT advanced technologies group (X-AT, CALM and CALMARE) and its staff. I have felt welcomed since the first day and although this was the result of the contribution of everyone, I owed some special recognition to some. There are two people that need to be thanked before everyone else. Firstly, many and many thanks go to my "P 800 instructor", the engineer specialist Richard Davies. It has been an immense pleasure working with him and learning from him. He has become a valuable friend and I am glad I turned him into a black no sugar coffee lover like me. This is the appropriate time to cony the expression "vitamin R". Secondly, but not really, I would like to express my sincere thanks to Tommy (Dr Yat-Tarng Shying) for the great job done in the labs in terms of maintenance and management, for providing training and for being always open to discuss anything it was in my mind with such a friendly attitude. I mostly thank him for teaching me what a PhD really means: Passion, Humility and Dedication. I will never forget the times

Nate, Alex, Melek, Pam and David. I wish I had spent more time with the last two of you.

Last but not certainly least, the most important thanks are for Edward James. I do not know how he put up with my ranting in the last months…it really must be love! Or maybe I am so awesome and beautiful, and smart, and funny and nice anyway! I forgot humble! Okaaay…jkg.

<div align="right">Silvia</div>

Dissemination

Journal Papers

1. Ghita O., James E., Davies R., **Berretta S.**, Singh B., Flint S. and Evans K.E., *High Temperature Laser Sintering (HT-LS): An investigation into mechanical properties and shrinkage characteristics of Poly (Ether Ketone) (PEK) structures*, Materials & Design, Volume 61, September 2014, Pages 124-132, ISSN 0261-3069, http://dx.doi.org/10.1016/j.matdes.2014.04.035.

2. **Berretta S.**, Evans K.E. and Ghita O., *Morphology of polymeric powders in Laser Sintering (LS): From PA to new PEEK powders*, European Polymer Journal, Volume 59, October 2014, Pages 218-229, ISSN 0014-3057, http://dx.doi.org/10.1016/j.eurpolymj.2014.08.004.

3. **Berretta S.**, Evans K.E. and Ghita O., *Processability of PEEK, a new polymer for bespoke High Temperature Laser Sintering (HT-LS)*, European Polymer Journal, Volume 68, May 2015, Pages 243-266. doi:10.1016/j.eurpolymj.2015.04.003

Conference Papers

4. **Berretta S.**, Evans K.E., Ghita O., Newman C. and Anderson A., *Size, shape and flow of powders for use in Selective Laser Sintering (SLS)*, High Value Manufacturing: Advanced Research in Virtual and Rapid Prototyping - Proceedings of the 6th International Conference on Advanced Research and Rapid Prototyping, VRAP 2013, Leira, Portugal (2014)

5. **Berretta S.**, Davies R., Anderson A. and Ghita O, *PEEK OPTIMA® LT1 for High Temperature Laser Sintering (HT-LS)*, 2nd International PEEK meeting, Washington DC, USA (2015)

Contents

List of Figures

27

List of Equations

List of Tables

List of Abbreviations

AOR	Angle Of Repose
AR	Aspect Ratio
CAD	Computer Assisted Design
CB	Carbon Black
CT	Computer Tomography
DMA	Dynamic Mechanical Analysis
DSC	Differential Scanning Calorimetry
ED	Energy Density
EMR	Energy Melt Ratio
HA	Hydroxyapatite
HT	High Temperature
HT-LS	High Temperature Laser Sintering
LS	Laser Sintering
MFI	Melt Flow Index
PA	Polyamide
PAEK	Poly Aryl Ether Ketone
PEEK	Poly Ether Ether Ketone
PEK	Poly Ether Ketone
PS	Post Sintering
PSD	Particle Size Distribution
SEM	Scanning Electron Microscopy
STL	Standard Tessellation Language (file format)

TGA   Thermo-Gravimetrical Analysis

List of Symbols

A   Hamaker constant

β   Heating rate in TGA analysis

C_p Specific heat capacity

$CaCO_3$ Calcium carbonate

E′   Storage modulus

E″   Loss modulus

$\tan \delta$ Loss factor tan

E_A Activation energy

E_D Energy leading to material degradation

E_{melt} Energy required to melt a given material

ED   Energy density

ED_{vol} Energy density per volume unit

EMR   Energy melt ratio

EMR_D Energy melt ratio leading to material degradation

h_f Enthalpy of melt

M_w Molecular weight

P   Laser power

P_D Laser power leading to material degradation

Q   Material density or bulk density

Φ   Packing fraction

S_a Surface roughness

SC   Scan count

SS	Scan spacing
T_D	Onset degradation temperature (1% weight loss)
T_b	Part bed temperature
T_m	Melt temperature
T_{max}	Maximum temperature in the 1st derivative of the TGA scans used in the Kissinger method
ν	Scan speed
z	Layer thickness

1 Introduction

1.1 Research context and research objectives

Laser Sintering (LS) is an additive manufacturing process that has drastically shortened the gap between industrial design and manufacturing by allowing production of parts of any geometry directly from a Computer Assisted Design (CAD) file. This fact alone explains why LS has been developed for metals, plastics, ceramics, glass and composites of any sort, including organic materials such as wood.

The LS process also exhibits the highest freedom of design currently available and many industrial sectors have started to make use of it. While advantages of this high fabrication freedom can be easily identified for manufacturing industries such as jewellery, fashion and consumer goods, the exceptional cases are the applications for high-tech engineering areas. For instance, freedom of design allows patient specific customised implants in the medical sector, whereas the aerospace, defence and automotive industries have been utilising LS for production of design optimised light weight components.

Polymer LS refers to the LS process that uses polymeric powders and their composites. Contrary to other LS areas such as metal LS, where the technology has advanced more, only an extremely limited number of polymers are available for this technology. Most polymeric LS grades exhibit mechanical and material properties that are not suited to applications requiring high material performance such as for example tensile strength, wear resistance, thermal stability and chemical neutrality.

In 2010 EOS [1] announced the launch of the first commercial High Temperature Laser Sintering (HT-LS) system able to process materials above 200 ˚C, EOSINT P 800. In parallel, EOS [1] released the first HT-LS optimised grade "EOS PEEK HP3", a Poly Ether Ketone (PEK) High Temperature (HT) engineering polymer.

This research project is based on the investigation of the HT engineering plastics known as Poly Ether Ether Ketone (PEEK) grades for their implementation into the HT-LS process. Belonging to the same chemical family of PEK, PEEK and PEK share similar properties and performance. As PEK, PEEK offers a high operating temperature which allows its use in applications requiring elevated thermal and

chemical stabilities. Additionally, PEEK exhibits a lower melting temperature than PEK, hence leading to an easier (lower) processing window. While these benefits are strictly related to the intrinsic properties of the PEEK material over the PEK counterpart, the market cost of PEEK powder per kg is lower than the HT-LS optimised PEK powder and therefore PEEK could be more attractive for industry.

This study aims to investigate and propose a new HT polymeric material option for HT-LS manufacturing.

The objectives of this project are the following:

a) In depth understanding of the HT-LS process and its unique characteristics (variable size building chamber and post sintering phase);
b) Optimisation of the processing parameters of HT-LS of PEEK with special attention to their effects on the microstructure and mechanical properties of HT laser sintered PEEK components;
c) Proposing a method for temperature prediction for new polymeric powders in HT-LS;
d) Providing two case studies based on the findings developed from point a) to point c): manufacture and test of two medical components (cranial implant and inter-body fusion spinal cages).

This three year research project with title "Poly Ether Ether Ketone (PEEK) polymers for High Temperature Laser Sintering (HT-LS)" has been conducted with the support of Victrex [2] and Invibio biomaterial solutions [3] and it is the first to report on the use of PEEK in the commercial HT-LS system, EOSINT P 800.

1.2 Thesis outline

The thesis is structured into four main areas: (a) introduction and state of the art; (b) description of materials and experimental techniques used; (c) materials investigation, HT-LS manufacturing and optimisation, prediction techniques of LS processing parameters, and lastly, manufacture and test of two long term medical implants: cranial implants and spinal inter body-fusion cages; (d) conclusions.

An exhaustive review of the literature available on PEEK material, polymer LS, particle morphology, powder flow characteristics and LS processing parameter optimisation is presented in chapter 2.

Materials, analytical methods and characterisation techniques used in this work are described in chapter 3.

Experimental characterisation of PEEK powders in terms of particle morphology, flow behaviour, spreading performance and melt rheology are described in parallel with well-established LS materials, used as benchmark, in chapter 4. Strategies for the improvement of the particle flow behaviour are also included in this section.

Analysis of the unique characteristics of the HT-LS process and optimisation of the processing parameters for HT-LS of PEEK structures are discussed in chapter 5. The results of the systematic mechanical tests applied to the HT laser sintered PEEK components are also presented in this chapter.

A method for prescribing one of the processing temperatures in HT-LS for HT polymers is provided in chapter 6. A LS formula known as "Energy melt ratio" that couples material properties and LS processing parameters is also examined in relation to feasible HT-LS conditions, mechanical performance and material degradation for PEEK 450PF.

Manufacture and test of two real medical case studies are reported in chapter 7.

Lastly, conclusions and suggestion for further investigations are provided in chapter 8.

The full structure of the thesis is illustrated in the following page.

	Thesis outline
Chapter 1	Introduction
Chapter 2	Literature review: • PAEK polymers • Laser sintering (LS) • High Temperature Laser Sintering (HT-LS)
Chapter 3	Materials and experimental methods
Chapter 4	Powder characterisation • Melt viscosity • Particle size • Particle morphology • Inter particle interactions (Hamaker constant) • Flowability and spreading tests • Strategies to improve the powder flow behaviour
Chapter 5	HT-LS manufacturing of PEEK • Variable build chamber size • Optimization of the processing parameters versus mechanical performance • Post sintering
Chapter 6	Prediction of processing parameters in HT-LS
Chapter 7	Medical case studies: • Cranial implants • Inter body fusion spinal cages
Chapter 8	Conclusions and suggestions for further development

2 Literature review

This chapter provides a review of the different topics that either have had an impact or have been analysed in this research project. A description of the Poly Aryl Ether Ketone (PAEK) materials is followed by the explanation of the Laser Sintering (LS) process with special attention to the material properties and processing parameters affecting this fabrication method. Lastly, the High Temperature Laser Sintering (HT-LS) process is introduced and thoroughly discussed. The structure of this literature review is illustrated in Figure 1.
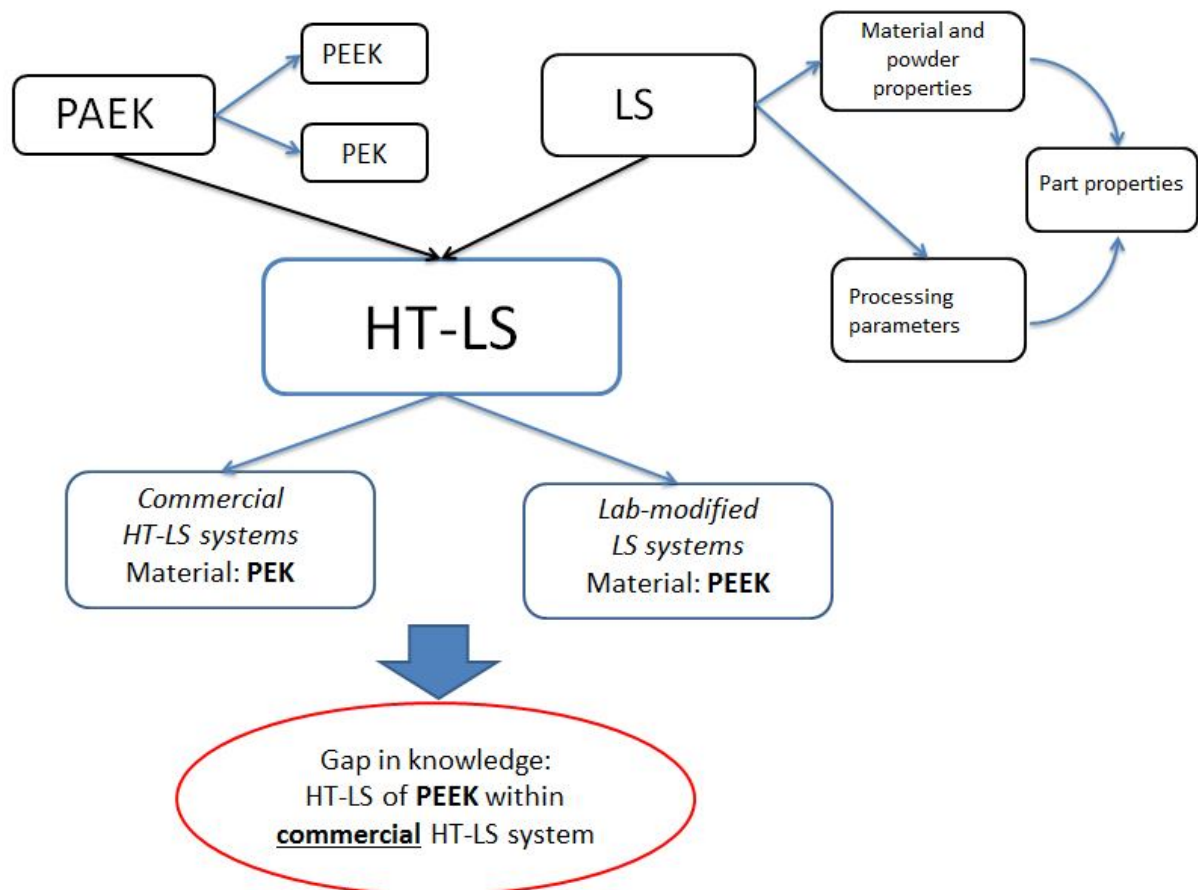
Figure 1. Structure of chapter 1: literature review

2.1 Poly aryl ether ketones

2.1.1 Structure

Poly Aryl Ether Ketones (PAEKs) represent a family of HT thermoplastics and semi-crystalline polymers characterised by a common chemical structure: an aromatic backbone chain interconnected by ketone and ether functional groups in different configurations and proportions [4] (Figure 2).
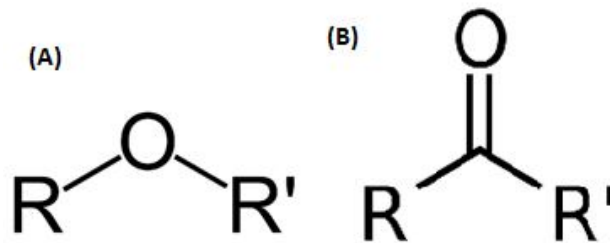
Figure 2. Ether group (A) and ketone group (B)

Some of the most known materials are Poly Ether Ketone (PEK), Poly Ether Ether Ketone (PEEK) and Poly Ether Ketone Ketone (PEKK), whose chemical and crystal structures are reported in Table 1.
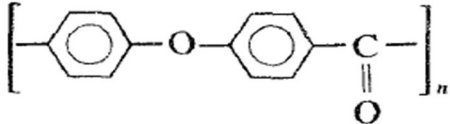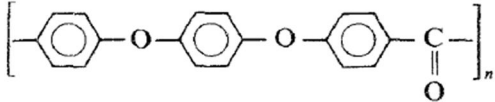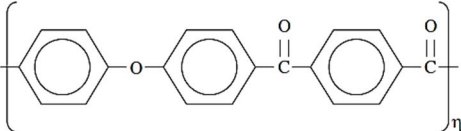
Material	Ketone content [5]	Chemical structure	Crystal Structure	Lattice parameters $(10^{-10}$ m)
PEK	50%		Orthorhombic cell	a = 7.63 - 7.65 b= 5.96 - 5.97 c= 10.00 - 10.09 [6, 7]
PEEK	33%		Orthorhombic cell	a= 7.75 - 7.83 b= 5.86 – 5.94 c= 9.86 – 10.06 [6, 7]
PEKK	67%		Orthorhombic cell	a= 4.17 b= 11.34 c= 10.08 [8]

Table 1. Chemical composition and crystal structure of PAEK materials

PAEKs share a similar crystal structure [6-12]. Dawson and Blundell [7] explained that the high similarity found in the crystal units of these materials is due to the ability of the ketone and ether links to be interchanged with a minimum of distortion of the chain packing and only slight variation of the lattice parameters. As the ketone content increases, the axis a and the axis b of the crystal cell decreases and increases, respectively [8]. This phenomenon is clearly evident in PEKK, the material with the highest amount of ketone groups. A representation of the PEEK chain configuration and the orthorhombic crystal cell is shown in Figure 3.
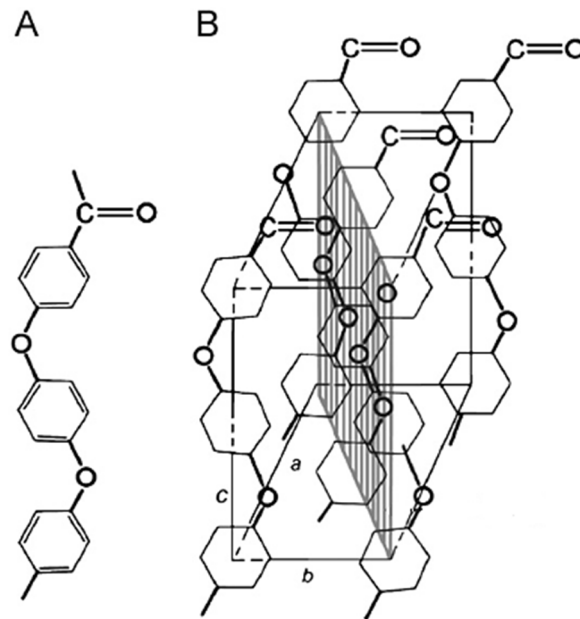
Figure 3. PEEK material: (A) chain configuration and (B) orthorhombic crystal cell [4]

The interest in the crystal cell and relative lattice parameters arises from the need to understand the crystallisation mechanism and thermal behaviour of PAEKs, which affect the final properties of a manufactured PAEK part.

This polymeric family is characterised by high mechanical performance, high thermal resistance and excellent chemical neutrality. While the aromatic structure is responsible for chemical resistance and high stability at high temperatures for prolonged times, the semi-crystalline nature confers good mechanical properties such as elevated Young's modulus and high impact strength [12], provided that thermal history and processing conditions have not been detrimental for the material. PAEKs also exhibit indefinite shelf life [13], biocompatibility of certain grades of the family and the possibility to add fillers to enhance mechanical properties or to match biological performance values [14]. Thanks to these properties, PAEKs find applications in many industrial sectors, ranging from aerospace and automotive to medical device technology.

2.1.2 Thermal behaviour and crystallinity

In terms of thermal behaviour, PAEKs undergo glass transition, (possible) cold crystallisation, melting and crystallisation (also named melt crystallisation). Variants in the chemical structure cause differences in the temperature at which the above phenomena occur. As the ketone content rises above the ether content, melting and glass transition temperatures shift to higher values. While a large number of experimental data can be found in the literature [8, 11, 12, 15, 16], Harsha et al. [15] provided a diagram showing the relationship between ketone/ether ratio and the melting and glass transition temperatures (Figure 4).
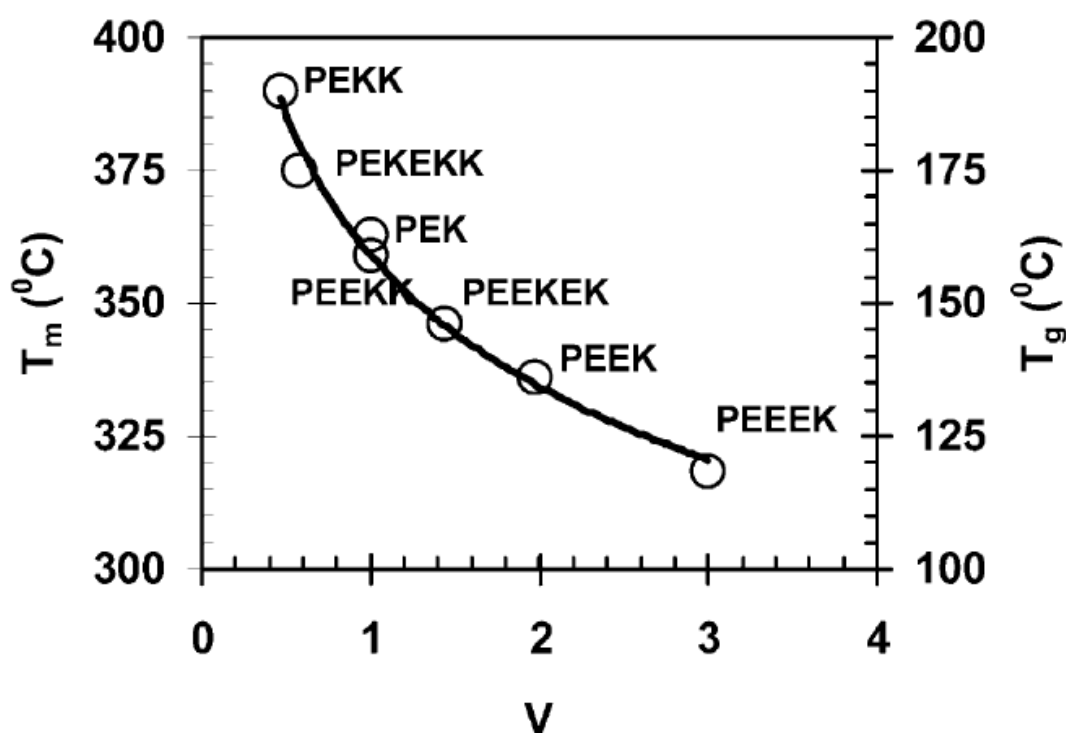
Figure 4. Relationship between the thermal properties and the chemical composition of the PAEK polymers. T_m = Melting temperature, T_g = glass transition temperature and V = ketone/ether content ratio [15]

While PEEEK exhibits the lowest melting temperature, at just above 315 °C, and glass transition lower than 125 °C, PEKK, the material with the highest amount of ketone groups, shows a melting temperature of nearly 390 °C and glass transition above 190 °C (Figure 4).

Although glass transition and melting points are key parameters for defining the processing conditions of a PAEK component, much more attention has been given to the understanding of the crystallisation dynamics of the PAEK materials. It is well known for example that a high degree of crystallinity results in high tensile strength. It is as result of this interest in tensile strength that the crystallisation behaviour of PAEKs has been deeply analysed. Zimmerman et al. [12] studied the crystal structure and crystallisation mechanism of PEEK, PEK, PEEKK and PEKEKK with the same molecular weight of approximately 30,000 g/mol. By using several analytical techniques, such as Differential Scanning Calorimetry (DSC) and Wide Angle X-ray Scattering (WAXS), the ketone content was found to be responsible for affecting the glass transition and melting temperatures, but not the crystallinity content, which was instead shown to be only a function of the thermal history. The WAXS results also showed a common orthorhombic crystallisation cell for all the materials. The authors outlined that increasing annealing temperatures made all materials rearrange with better packing, causing the cell volume to decrease and the crystallinity density to increase. As it occurred in all the materials analysed, this characteristic was considered independent from the ketone content. Day et al. [17] analysed only PEEK samples instead. The specimens were thermally treated between 380 °C and 420 °C up to 120 minutes in air and nitrogen atmospheres. The longer the annealing time, the higher the temperature of the molten material became and the lesser was the amount of material able to re-crystallise, especially for the samples treated in air. Those samples of PEEK treated in air above the melt temperature crystallised at slower rate than the corresponding samples treated in nitrogen. These results pointed out how thermal effects should be carefully taken into consideration for the processing setting of PEEK manufacturing and for all those cases, like repair, where additional thermal events will be added to the samples.

Vasconcelos et al. [18] studied the crystallisation mechanisms in PEKK and PEEK by DSC. PEKK showed heterogeneous nucleation with growth of elements having disc geometry and crystallisation velocity too fast to be studied isothermally. PEEK showed instead that crystallisation took between 5 and 15 minutes for heating rates ranging from 5 to 20 °C/min, indicating that the material does not need to be held at higher temperature for too long in order to get a good crystalline content. The authors also noticed that while lower heating rate favoured the growth of disc type

elements, higher heating rates led to bat type. No clear definitions or illustrations of disc and bat shapes were though supplied.

Thermal degradation of PAEKs has also been thoroughly analysed. Hay and Kemmish [19] studied the thermal degradation of disc samples cut from moulded sheets of PEK and PEEK (supplied by Victrex, UK [2]). The samples, pre-dried at 100 °C and moulded at 400 °C for 90 seconds, showed no changes in molecular weight up to 300 °C in nitrogen and 200 °C in air. Discolouring and an increase of the insoluble fractions were noticed after long exposure when kept at 400 °C for 16 hours. PEEK and PEK were found to decompose in a similar manner and at a similar rate with a random homolytic scission of either the ether or the carbonyl bonds in the polymer chains; crosslinking occurred at an early stage in the decomposition. Unlike Hay and Kemmish, Day et al. [20] instead studied decomposition of ground PEEK powder 450P. The results showed that PEEK remained stable up to 400 °C up to 6 hours in a non-oxidative environment (nitrogen). Chain branching and crosslinking occurred when the samples were conditioned in air atmosphere.

In terms of manufacturing processes, most PAEK grades, especially PEEK and PEK, are utilised in traditional methods, such as compression and injection moulding [21].

Part of the reason for the attraction of PEK in traditional manufacturing is that PEK shows excellent properties such as chemical resistance, radiation protection, thermal stability, high melting point and high continuous service temperature. These mechanical properties lend it to aerospace, aeronautics and automotive applications. PEK crystallises in an orthorhombic lattice and exhibits a crystallisation mechanism similar to that of PEEK (spherulites, narrow lamellae and packed bundles [22]). Density is around 1300 Kg/m³ and the viscosity can vary according to different grades from the same companies [1, 2]. The thermal behaviour is characterised by: a glass transition at 152 °C (154 °C [16], 150 °C [23]), followed by a sharp exotherm (cold crystallisation) and then a melting endotherm at about 370 °C (367 °C [16]). By crystallising amorphous samples of PEK at different temperatures, the glass transition is no longer so distinct; however, it does exhibit a double peak melting behaviour. The smaller peak occurs approximately 20 °C above the crystallisation temperature, while the bigger peak occurs at 373 °C and it is independent to the crystallisation temperature.

50

PEEK is one of the most studied polymers in the PAEKs family. It is tough, ductile, abrasive-resistant and exhibits excellent fatigue characteristics and load bearing properties even at high temperature. It is in glassy state at room temperature, presents low flammability, high continuous service temperature, chemical resistance to a wide range of organics and inorganics solvents in terms of dissolution and solvent stress cracking. It is only damaged by 98% sulphuric acid. It is also particularly resistant to high temperature water/steam and the resistance to damage occurs in term of radiation (sterilisation) as well. It is processed in various manufacturing equipment at temperatures between 390-420 ˚C [4]. Similarly to PEK, the density is reported to be around 1300 Kg/m³ (ISO 1183) [2] . The viscosity can vary significantly, for example ranging between 130-450 Pa·s, at 400 ˚C (ISO 11443) amongst different grades of the same material from the same manufacturer [2]. As it can be used in several manufacturing technologies, its thermal properties and crystallisation behaviour has been studied through the use of various techniques, including: DSC, thermo-gravimetric analysis (TGA), small angle and wide angle X-ray diffraction (SAXD and WAXD respectively), scanning and transmission electron microscopy (SEM and TEM respectively) and Fourier Infrared Transform Spectroscopy (FTIR) [18, 24-44]. PEEK has a melting point between 335-343 ˚C, glass transition between 143-150 ˚C, cold crystallisation at several temperatures (177 ˚C, 180 ˚C, 220 ˚C) and crystallisation from the melt around 290-305 ˚C. Moreover PEEK, like PEK, presents double melting peaks. The lower peak appears 10-15 ˚C above the crystallisation temperature [25], while the higher peak appears at around 340 ˚C [10] and it is independent from the crystallisation temperature.

These double melting peaks have prompted a number of conflicting interpretations and interestingly occur when PEEK and PEK have undergone a slow crystallisation process or an annealing treatment. According to Bassett et al. [25] the temperature of the lower peak depends on the temperature of the crystallisation or annealing treatment applied to the sample under test. This lower peak always appears at 5-10 ˚C higher than the annealing or crystallisation temperature, or in other words, if a sample was slow crystallised at 200 ˚C, the lower melting peak would happen at 210 ˚C. The higher melting peak occurs at 340 ˚C and 370 ˚c for PEEK and PEK respectively. The temperature of this higher melting peak is not affected in case the specimens underwent previous annealing or slow crystallisation treatments. Several

attempts have been made to explain this phenomenon [25, 38, 40, 45, 46] and essentially three models have been proposed, all of them inaccurate to some extent. According to the first model, the low endotherm (melting peak) is enthalpy recovery of the physically aged amorphous portion. However, the results were found inaccurate when attempts were made to achieve the same conclusion with a technique different from standard DSC. In the second model, the high melting peak represents the melt of thicker lamellae (primary crystals), while the low melting peak represents the melting of secondary crystals characterised by thinner lamellae grown between the main lamellae. Again this model was not found to be fully correct. Lastly, the third model hypothesises the presence of crystals with lower melting temperature and their ability to re-crystallise into thicker and more perfect lamellae during the annealing or heating. Only recently Jin et al. [22] have been able to explore the crystallisation behaviour of PEEK by means of Flash DSC, a DSC system that allows a heat rate of 10,000 °C/min. The authors suggest that the double melting peak is due to the slow heating and cooling capability of standard DSC. In other terms, it is believed to be an artefact.

In summary, PEEK is considered to crystallise in both lamellae and spherulites forms and crystallisation occurs from heterogeneous nucleation [26]. When PEEK mostly develops lamellae, they can further differentiate into primary and secondary lamellae. The differences between those two structures are thickness, location and time of formation during the thermal history of a sample. Instead, when PEEK crystallizes isothermally, crystallinity and lamellar thickness increase with crystallisation temperature [10]. Moreover, when PEEK is subjected to an annealing treatment, the crystallinity increases as the annealing time increases [47].

Crystallisation is environmentally dependent: if the process takes place in an oxidative environment, crosslinks will be more likely to happen [17]. The longer the time and the higher the temperature at which PEEK is held in molten status, the lower is the fraction of original material able to re-crystallise and the longer will be the annealing time required for crystallisation [17]. The mechanical behaviour of PEEK has been evaluated by varying strain rates and testing temperature. At room temperature and for low strain rate PEEK shows a linear relationship between stress and strain in tensile and compression tests [4]. As a thermoplastic polymer, the mechanical properties are subjected to a drop above the glass transition

temperature. Fatigue behaviour and wear resistance of PEEK has been largely proven [48-51]. One of the most interesting works was carried out by Zhang et al. [52].The authors analysed the behaviour of PEEK in term of tribological properties after plasma surface treatments and identified a micro cutting dynamics followed by delamination as wear debris mechanism of PEEK [51].

A comparative study between the mechanical properties of PEEK and PEK was carried out by Tregub et al. [23]. The samples of both polymers were crystallised at different temperatures between 160-300 °C in order to produce samples with different crystallinity contents. The results of tensile and thermo-elastic tests performed at room temperature were not significantly different between PEEK and PEK, allowing the authors to conclude that the different ketone content in the two materials did not have an effect on tensile strength and mechanical moduli. Following tests performed with samples crystallised at different temperatures were carried out at the same testing temperature of 200 °C. The samples that crystallised at higher crystallisation temperatures exhibited higher tensile stress values because of the higher crystal perfection. Moduli of PEEK and PEK produced similar results, proving that differences in mechanical performance are unaffected by the ketone content.

The use of PEEK as biomaterial is well-established thanks to the high biocompatibility, good mechanical properties and the possibility to incorporate or add fillers to improve a number of properties. Mano et al. [52] report the use of PEEK in hip prosthesis, spinal cord elements, screw, plates and pins. Kulkarmi et al. [53] describe the results obtained with cervical PEEK cages for cervical spondylitis radiculopathy or myelopathy with an average follow up of 18 months. The work showed high fusion rate, no migration or extrusion of the cage, low subsidence, stability and facilitation of radiological assessment. Kurtz and Devine [4] review all the current uses of PEEK as biomaterial ranging from trauma implants to scaffold structure for tissue reconstruction. Nieminen et al. [54] report the mechanical properties of injection moulding PEEK plates after three years of in-vitro and in-vivo animal implantation. They managed to produce two types of plates with different percentage of crystallinity in order to evaluate every possible response. Han et al. [55] report the result of electron-deposition of titanium coating on PEEK structure and the relative enhanced biological properties in terms of osseointegration and cell

proliferation during in vitro and vivo tests. Lethaus et al. [56] developed an algorithm to manufacture cranial implants in PEEK and tested them, especially in compression performance. For the purposes of this research project (chapter 7) unfortunately the authors did not provide data on the geometrical accuracy of the implants. It is clear that although interesting research had been produced on PEEK components fabricated on traditional manufacturing methods, studies on parts fabricated by HT-LS within an ad-hoc HT-LS system are still missing.

2.2   General laser sintering, material properties and parameters

Laser Sintering (LS) is a manufacturing method able to build prototypes and physical components in layer wise manner directly from a 3D Computer Aided Design (CAD) file, previously sliced in 2D cross sections. The setup of this technology consists in a powder bed where a laser consolidates particles of raw materials layer upon layer according to the cross-sections of the object to manufacture. The process offers the highest freedom of design currently available in manufacturing, and several types of materials can be used in the process: metals, ceramics, glass, polymers and their composites [57].

LS of polymers is one of the most promising processes in the powder bed fusion group. It offers the possibility to use and develop new engineering plastics and composites with a potentially broad range of performance and at reduced specific density when compared to metals.

To date, most commercial LS systems have been developed for polyamide (PA) based polymers with low glass transition and melting temperatures and only a few elastomers [58]. In this context, most research works focused on the investigation of properties and applications of materials such as PA 6, PA 11, PA 12 and their composites [58-71]. However, materials such as polypropylene, polystyrene, polycarbonate, polyoxymethylene and styrene-acrylonitrile copolymers have also started to be considered [72-77]. While Goodridge et al. [58] exhaustively reviewed properties of most low melting temperature polymers and composites, Athereya et al. [59] provided evidence of the better performance of LS components of PA 12-carbon black over specimens in the same materials manufactured with traditional techniques (compression and injection moulding). The laser sintered samples showed higher

mechanical performance which was explained by more uniform carbon black dispersion in the LS samples by the authors. Chung et al. [60] instead laser sintered and tested PA 11 structures made with different contents of glass bead fillers. The results showed that tensile and compressive moduli increased with higher glass bead concentration, while the elongation at break decreased. Davidson [78] investigated the implantation and optimisation of TPU elastomers for the development of user customised running footwear applications, while Vasquez [79] researched low temperature LS polymers for the production of snowboard bindings. In the medical area, LS has been employed in several areas, ranging from tissue engineering to orthopaedics and maxillofacial implants. Although PA is not a biomaterial, LS of PA components has been used for production of physical models of anatomical structures, directly obtained from medical data [80]. The study had several purposes: teaching, training, surgery planning and fabrication of moulds to produce endoprosthesis through other manufacturing technologies [81]. Williams et al. [82], for example, report on the case of a 29-year old male with orbital blowout fracture that, after noticing the poor quality of a stereo lithography mould designed for the production of his long term titanium implant, prompted his surgeon to produce the same mould by LS with glass-filled PA grade. The model appeared better in terms of geometry accuracy and surface finishing and it was then used for production of the highly accurate long term titanium implant.

It is clear, then, that as LS allows the highest freedom of design currently available, this property has led to a level of end-user customisation never before achieved, as well as the optimisation of physical components, i.e. complex lighter parts whose original functional requirements are not compromised. The design freedom and the benefits of light weight offered by LS manufacturing increasingly interested the aerospace and automotive industries [57]. Most of the low temperature polymers are successful in the consumer goods industry, where, for example LS of PA has helped to develop new models of business economy, such as Shapeways [83]. However, the use of these polymers in the aerospace or automotive application is limited fields because of the low mechanical material properties.

Hence, research into new potential LS powders, including carbon fibre reinforcements, metallic coating and PEEK fillers, has started to appear, with the aim of enhancing the final part properties [61, 65, 66, 69, 70, 84].

In 2010, the first ad hoc designed HT-LS system able to process materials above 200 ˚C was released on the world market. EOS (Germany, [1]) launched the HT-LS EOSINT P 800 system in parallel with the first HT-LS optimised grade PEK, a HT thermoplastic belonging to the PAEK family, traded under the name "EOS PEEK HP3". While marketing reasons were used to justify this commercial name, the author will refer to it as "PEK HP3".

The introduction of the HT polymer PEK HP3 and of the HT-LS system EOSINT P 800 opened the way to the manufacture of extended performance laser sintered components applicable in high demanding engineering areas.

Although small differences may arise between systems operating different classes of materials, a LS machine (Figure 5) usually presents two side sections, collecting and supplying powder, and a central one called "building chamber" where the laser sintering takes place.
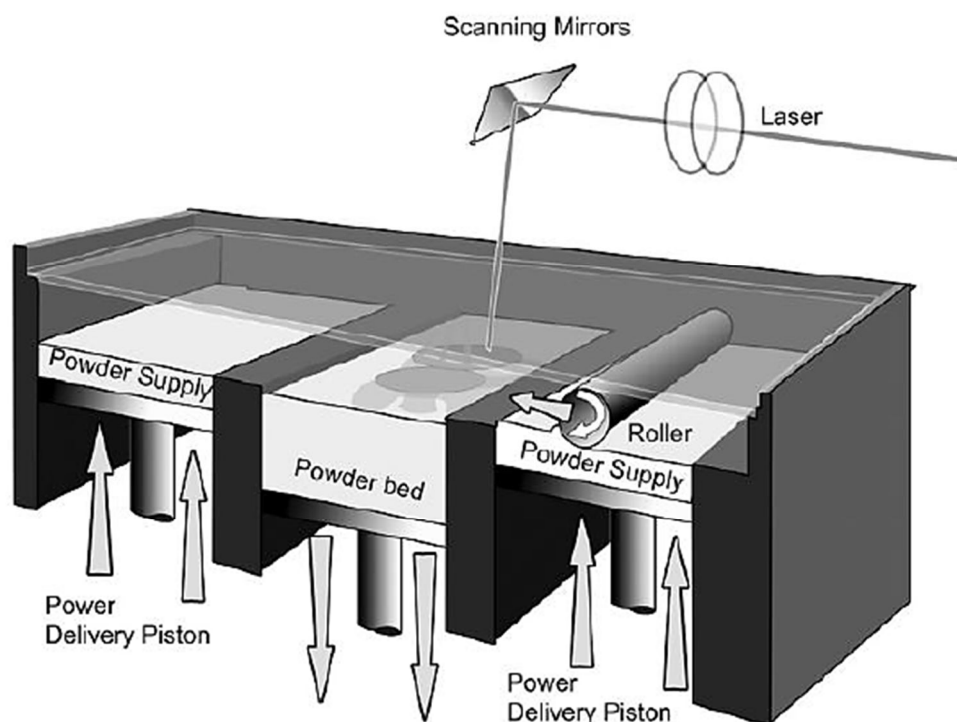
Figure 5. A typical LS system [85]

A building operation has three phases: warm up, building period and cooling. In the first stage, the material powder is slowly heated up to a temperature below its

melting point. When the building environment becomes thermally stable and uniform, the building stage can start. A certain amount of powder is therefore dispensed and spread from the side sections over the build chamber into a uniform layer, generally 100 μm thick; the laser then induces the solidification of some specific regions in the powder bed corresponding to the cross-sections of the parts to fabricate; once finished, the building chamber is lowered of the height of a layer, fresh powder is dispensed and spread and the laser-scanning starts again, causing sintering either across the current layer and between the two successive layers. The sequence spreading-sintering-lowering goes on until all the components are fully completed. Then, a long controlled cooling procedure of the system begins.

The process takes places in an inert atmosphere (95% nitrogen) throughout the three phases. The temperature at which the powder is kept before the laser exposure is below the melting temperature of the material, a condition that allows the laser just to supply the surplus energy necessary for the consolidation of some selected areas while avoiding sintering of unwanted regions. The un-sintered particles that surround parts and components act therefore as supporting structures during a manufacturing operation.

In LS, as in other manufacturing processes, processing parameters and material properties are strictly connected and mutually affect the properties of the produced parts. Yet, parts of a LS building operation also affect each other. This characteristic is due to the fact that parameters- like parts positioning within the building chamber of a LS system and in respect to the other parts, number of parts for layers, manufacturing energy settings, time necessary for the LS completion of one layer (layer time), whole duration of the building job - are all interconnected and might affect the final properties of each part. For example, a component built in a job operation with high density of parts might present some differences from the same component built in a building process with a very small part density. The orientation of the part in respect with the build direction also changes the mechanical performance and geometrical accuracy of a laser sintered component.

The parameters involved in LS processing are described in the following paragraph; however, a graphical illustration of the parameter classification is provided in Figure 6.
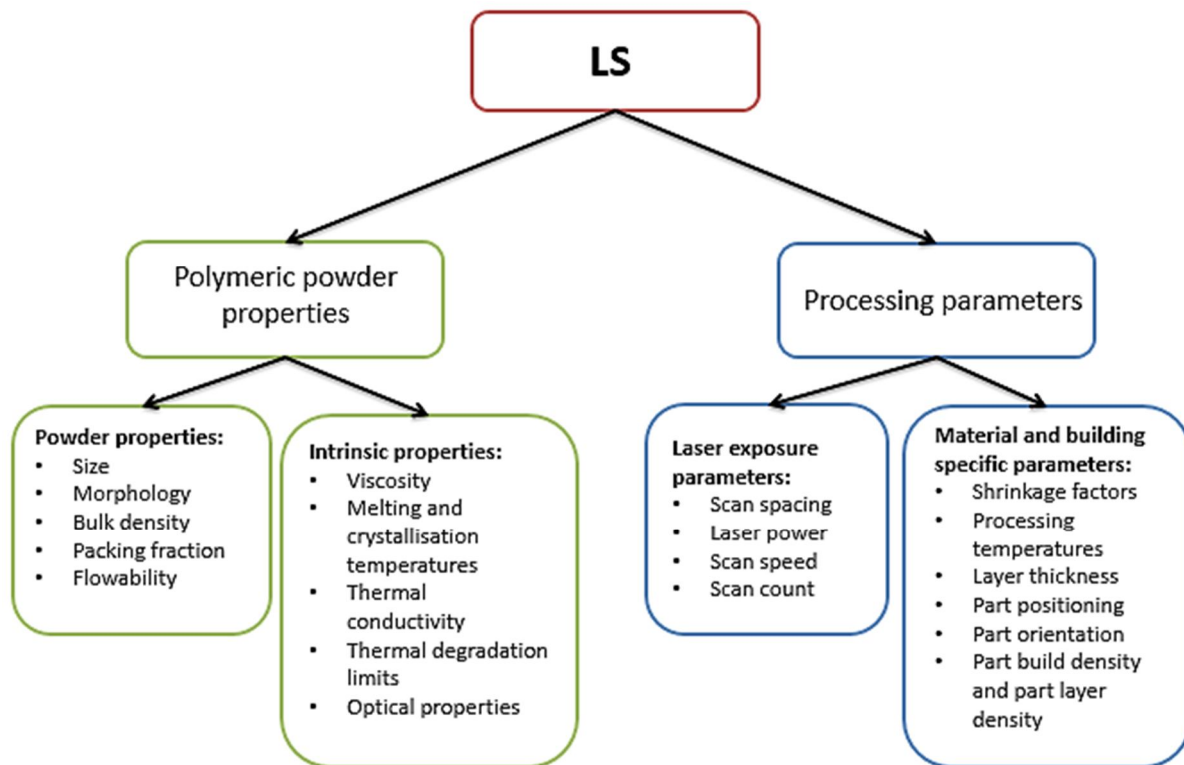
Figure 6. Parameters involved in LS

2.2.1 Polymeric powder properties

The material parameters involved in LS manufacturing both include material properties that constitute the particles and properties that are due to the powder form of the materials, i.e. particle size, morphology and flow conditions.

2.2.1.1 Size, morphology and flow behaviour of polymeric powders in LS

Size, shape, structure, density and surface features of the particles of a given material significantly affect its physical, thermal, optical, mechanical and electrical properties.

Particle size refers to measurement of a physical length or "diameter" in a population of particles. Different particle size techniques evaluate different equivalent diameters [86]. Powder materials are usually the collection of particles with different dimensions; therefore particle size results are generally expressed in terms of particle size distributions.

Particle morphology aims instead to evaluate the shape characteristics of the particles. As seen for particle size, several parameters have been defined and implemented in the characterization of particulate solids. While Heywood [86] defined the shape of a particle as the contribution of two factors, form (cuboid, spheroid, etc.) and relative proportion ("which distinguish the shape of one from another of the same form" [86]), particle processing sectors tend to rely on the determination of geometrical factors like circularity (overall shape of a particle) and roundness (edges profile of a particle).

Powder density is often considered a synonym for bulk density. The latter is defined as the mass of particle of a certain assembly divided by the total volume (sum of particle volume, inter-particle voids volume and internal pore volume) that the particles occupy. However, if a powdered material undergoes a compaction process, the volume occupied by the particles will change and so will the final density. As a consequence of powder handling, many definitions and methods are available for the evaluation of powder density.

Flowability depends on several factors: the powder itself (particle size distribution, particle shape, particle surface features); the environmental conditions (temperature, moisture); and, according to some authors, to the flow test adopted (angle of repose, Carr indices, compressibility, etc.) [87, 88]. Schulze [88] reports the basic concepts about bulk solid materials and flowability, and he describes the main physical factors affecting flowability, such as adhesive strength and wall friction. Prescott and Barnum [87] suggest distinguishing between "powder flow properties" and "powder flowability". Powder flow properties are defined by the interactions between the individual particles and affect the flow performance: powder density, compressibility, cohesive strengths within the particles and wall friction. Powder flowability instead refers to how a given material will flow in specific equipment, implying that the same material will behave differently in different flow equipment conditions. In this case, it is largely recommended the use of a test able to simulate as closely as possible the flow in the real scenario, utilising the equipment that will ultimately be used for manufacturing. Clearly, the two methods of defining powder flow properties (stand-alone tests or real scenario test) are not particularly satisfactory, because they outline the lack of a general method able to precisely predict the flowability of a material under any conditions when its flow properties are known.

While powder technology is a wide and well-established area of research, specific studies and knowledge that can be transferred to the additive manufacturing area are missing. LS powders have to provide high resolution in the final parts therefore finer materials are generally preferred. However, very fine particles can negatively affect the required good flow behaviour by agglomerating. Fine particles can also be source of undesired sintering [58, 74], fog the optic elements within a LS system during the laser exposure in a building process and hinder the removal of un-sintered powder from the manufactured products [89]. Particles of size equal or less than 10 μm have to be avoided because they are considered difficult to spread and separate, especially at HT due to their high inter-particle friction [60]. The required thickness of a layer during a LS process in order not to affect the final parts resolution has to be at least two times the size of the particles used. It then appears clear that for a layer thickness of 100-200 μm, particles in the range 10-150 μm are preferred [60]. Drummer et al. [90] recommend an average size of 60 μm with absolute absence of particles with diameter of equal or less than 10 μm. However, more than one researcher has reported the use of nanoparticles [60, 90-93].

Yet, it is not only preferred a certain particle size distribution; requirements on the particle morphology have been also proposed for powder flow behaviour, structural and mechanical performance of the laser sintered parts. Goodridge et al. [58] point out that a good flow behaviour is achieved with spherical or nearly spherical particles. Evans et al. [94] in their method for the development of new LS materials suggest that powder flowability and high density parts are strictly connected and a good flow condition can be achieved if the powder flows more "like sand than baking flour" with a tap density of 50%, but regardless, the final verdict will be the final mechanism in the LS machine. Dupin et al. [62] studied two types of PA 12 with small differences in particle morphology and particle size and they characterised their effect on the extent and morphology of porosity in the laser sintered parts. While rounder and bigger particles were believed to lead to better results with higher density, in reality broader size distributions with significant content of particle of size 8 μm led to less part porosity even at lower manufacturing energy densities. Gibson and Shi [63] mention the particle size as one of the factors affecting the laser depth penetration during LS. Goodridge et al. [58] recommend a particle size range of 45-90 μm with the suggestion to avoid particles smaller than 45 μm. Works using bigger

irregular particles are mentioned and powders made through different process (polymerisation or cryogenic grinding) are found to have different morphology, which is responsible for the improvement or drop of the mechanical properties. McAlea et al. [95] recommend an average particle size greater than 75 µm. Hao et al. [96] have demonstrated that larger particles lead to higher surface roughness and larger and more surface pores in the laser sintered samples than smaller particles. Furthermore, the percentage of internal pores was found to increase in the samples manufactured with higher particle size powders. Liu et al. [97] have studied the effect of particle size distribution on selective laser melting and proved that it has an effect on final part properties. Broader particle size distributions cause higher bed density, greater density in the manufactured specimen and smoother surface, while narrower particle size distribution was responsible for better flowability and parts characterised by higher ultimate tensile strength and hardness. Kumar [98] reports that regular, equiaxed, non-porous particles lead to the improvement of metal powders. Kolan et al. [99] investigated the effect of the particle size of a binder in bioactive glass.

Clearly, particle characteristics might have an impact on part properties. However, also powder deposition mechanisms might affect the conditions of the powder bed during LS processing (powder bed compaction, homogenous density all across the bed) and ultimately the part properties. Based on this assumption, Van Der Schueren et al. [100] analysed three deposition methods in selective metal sintering. According to the authors, the flow is mainly influenced by the inter-particle friction. Therefore the powders, whose particle morphology leads to the minimum inter-particle friction, will also flow better and consequentially achieved better powder bed conditions. Not surprisingly, a spherical shape was found to ensure the minimum contact between powder particles and caused a reduction in friction, allowing better flow, deposition and LS powder bed characteristics, which lastly will facilitate the creation of more performing parts.

Amado et al. [101] also focused on the characterisation of powders for LS. Powdered materials were characterised by using an image-based powder analyser system formed by a rotational drum and image acquisition system. By recording the powder free surface and the cross sectional area of the powder inside the drum, the material was analysed in terms of flow and fluidised behaviour. The indexes used were: avalanche angle, surface fractal, volume expansion ratio, fluidized volume slope,

fluidized height slope and final settling time. The authors examined nine types of materials of different chemical nature and different compound method and formulation. The materials having nearly spherical particles and those composed by convex shape particles (a particle is defined to exhibit a convex shape when any line segment between two points on the profile of the particle never goes through the core of the particle) showed higher performance in flow behaviour, packing density and capacity to achieve a fluidised state. The materials composed by less regular shaped particles, and especially flake like powders, presented: poorer flow and packing density, small fluidization tendency with additional complexity such as dilatancy. According to the authors, the advantage of this instrumentation was that the rotational drum could be set at the same speed performed in commercial LS machines. In a more recent work [102], the same authors analysed some of the above properties for PA and polypropylene grades at a testing temperature higher than their glass transition temperature. Findings showed that the temperature strongly affects the flow performance.

2.2.1.2 Intrinsic properties

One of the main characteristics required for LS powdered materials is the ability to show a processing window, i.e. a temperature interval between the onset temperatures of melting and crystallisation. This window (Figure 7) called "Super-cooling window" [73] is defined on the basis of the thermal properties of melting and crystallisation of the material under test in relation to the temperature at which the material is held during a LS building operation. If the LS processing temperature is lower than the material onset crystallisation temperature and therefore located outside the window, major and localised shrinkage will occur during and just after the laser exposure that, in turn, will lead to deleterious effects on the mechanical properties of the laser sintered parts. If the LS processing temperature is higher than the material onset melting temperature, therefore again outside this proposed window, uncontrolled melting will occur all across the powder bed without even the laser exposure [73, 77, 103]. Any LS processing temperature inside the window instead will lead to controlled and effective sintering without any undesired and detrimental thermal event in the powder. It is largely believed that it will be easier to

optimise processing temperatures for LS a material having this wide temperature window.

Powders are also required to exhibit sharp melting and crystallisation peaks. Such conditions should allow more uniform melting and crystallisation mechanisms, while avoiding overlapping of these two thermal events.
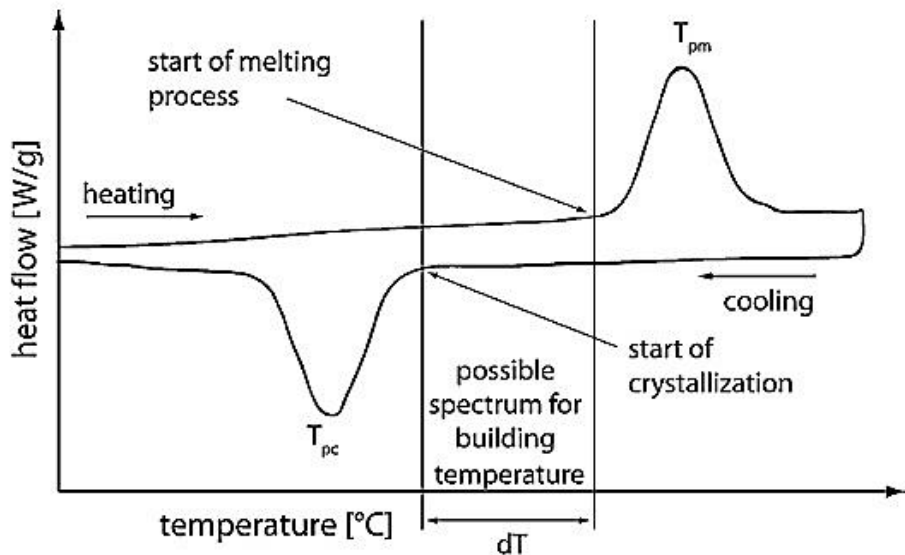
Figure 7. Super-cooling window, LS processing window [73]. The curve shows the DSC thermoscan of PA 12. T_{pc} = crystallisation temperature, T_{pm}= melting temperature

Figure 7 illustrates the thermal profile obtained through DSC of the polymeric grade PA 12. T_{pm} and T_{pc} represent the melting and crystallisation peak temperatures of the polymer, while the "possible spectrum for building temperature" is the super-cooling window. Interestingly, this window represents a method for selecting new material for the LS technology based on the knowledge of their thermal properties. It would also provide a predicting estimate of processing temperatures for a given material within a LS system before a trial-and-error approach. This method seems to apply well to PA based grades and it largely used in literature [77]. However, it cannot be applied to elastomeric polymers, a class of polymers that do not undergo melting and crystallisation, yet are used in the LS technology.

To overcome the limitations of the super-cooling window, Vasquez et al. [104] introduced the concept of a "stable sintering region" (Figure 8). In this method, the

temperature at which the material is completely molten and the temperature at which a first sign of material degradation occurs delimit the range of potential processing temperatures for LS. More precisely, the lower temperature is identified by the combination of DSC analysis with hot stage testing, while the upper limit temperature is the value at which 1% weight degradation loss takes place under a heating rate of 10 °C/min in a TGA test. An example of stable sintering region for the PA 12 is shown in Figure 8.
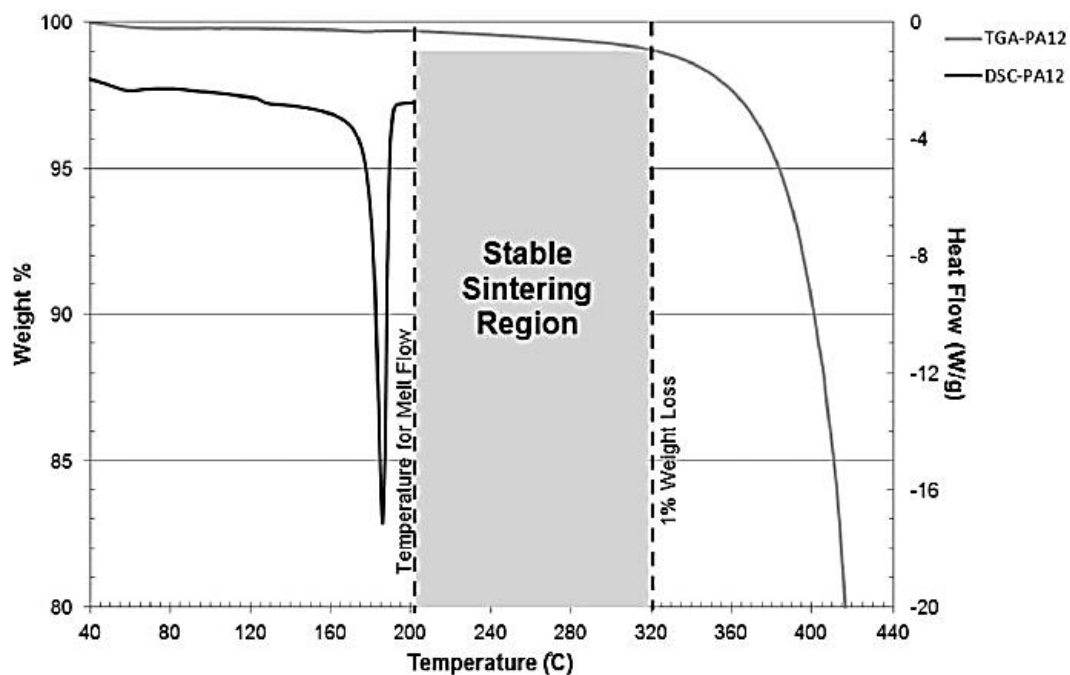
Figure 8. Stable sintering region of a PA 12 grade for LS, according to Vasquez et al. [104]

This alternative window represents, to date, the most widely applicable and complete approach to predict ideal processing temperatures, especially those related to the laser exposure strategy, for new and established materials in LS. This technique does not mainly aim to predict the processing temperature of new materials inside a LS system. It offers a prediction of a spectrum of temperatures that the material can undergo without degrading during the laser exposure during a LS building operation, providing *a priori* a limit for LS processing parameters on the basis of material properties. Interestingly, this window could be applied to elastomeric polymers by

choosing as lower limit the softening temperature of these materials, providing therefore a more general method than the super-cooling window.

For HT polymers such as PEEK, only Rechtenwald et al. [105] have attempted to define a LS processing window. According to the authors, the lower boundary of this window was represented by the manufacturing settings leading to very weak laser sintered samples, impossible to be further examined. The higher limit instead was constituted of those parameters causing dark discolouration in the samples, interpreted as a sign of polymer degradation. Contrary to the super-cooling window and stable sintering region, this approach did not include raw material properties, but only LS processing parameters found by trial-and-error.

LS polymeric powders are expected to go through the three stages of standard building operations (warm up, building and cooling) without experiencing any thermal degradation effect, especially during the cooling period, in which the particles remain at a temperature above their glass transition temperature for a fairly long amount of time. Again, the method introduced by Vasquez et al. [104] is the only one including this requirement in the prediction of processing windows for potential new LS materials.

Low thermal conductivity is also demanded in LS in order to avoid undesired fusion of particles surrounding a component and to guarantee a good separation between molten and solid phases [58, 90].

Concerning the material viscosity, a low value is usually preferable, because it is believed to be responsible for good interfusion of the polymer chains, high particle necking and satisfying layer to layer adhesion [58]. It is also suggested that a fairly low viscosity allows a fast and more efficient sintering dynamics that will lead to more fully dense parts. Contradictorily, it is reported that the possible highest molecular weight which is often synonym of high viscosity will allow the manufacture of components with the highest mechanical properties [77]. However, when the viscosity is too low, a higher shrinkage and poor part accuracy in the sintered parts are expected to occur [77, 106, 107]. According to Kruth et al. [77] the ratio between surface tension and melt viscosity gives a velocity parameter that can define the limit for a successful LS of polymers. Materials like PA 12 that have a melt viscosity of

65

100 Pa·s can be fully sintered under surface tension of 30 mN/m thanks to the obtained velocity equal of $3 \cdot 10^{-4}$ m/s. Polymers like polycarbonate, with melt viscosity of 5000 Pa·s and dissimilar surface tension, cannot. However, this examination was carried out on only two polymers and it was not clarified by the authors how surface tension value was determined. Interestingly, viscosity and the correlated quantity Melt Flow Index (MFI) are good indicators in the LS area for evaluating the recyclability of PA powders. Shi et al. [108] studied the effect of several material properties including viscosity for two grades of polystyrene with different molecular weights. The authors suggest that the molecular weight by affecting directly the melt viscosity of a molten material, have a strong impact on the quality of laser sintered components. More precisely, the components of polystyrene built with the grade with lower melting viscosity exhibited higher densities than the specimens built with the higher viscous grade.

Material properties such as viscosity, particle size and building temperature are also involved in the particle coalescence event. Particle sintering or particle coalescence is the process where two or more adjacent particles form necks and bond together because of a reduction of the free surface energies of the particle involved. A high pressure or an elevated temperature can make the surface free energy to drop and trigger the sintering process. When this mechanism takes place in other manufacturing process such as rotational moulding or ceramic sintering, the temperature is equal or lower than the melting temperature of the material involved; in LS, however, the laser supplies a quantity of energy for a short amount of time that is considered to raise the powder temperature much higher than the melting temperature, inducing the partial melting of the particles [109, 110]. Particle sintering is generally modelled by the Frenkel method [111]. While the final neck diameter between two particles affects the final micro-structure of the laser sintered components, the sintering rate indicates whether or not the material particles can effectively bond in the time scale of the LS process. Vasquez et al. [112] evaluated the sintering neck and timescale of several low temperature polymers already established and yet to optimise for the LS process. The materials included semi-crystalline and elastomeric polymers. According to the authors, when the quantity defined as the ratio between average diameters of two initial particles of a given material and the final particles neck diameters is near to one, on a time scale up to

66

50 seconds, the material could be successfully implemented in the LS technology. However, longer time scales do not *a priori* exclude new material candidates.

Lastly, optical properties such as absorptance also play a key role in LS. Absorptance depends on the combination of powder material properties and the wavelength of the laser used in a LS system. According to Tolochko et al. [113, 114], the absorptance of polymeric powders increases with higher wavelengths of the laser sources involved. Interestingly, pores in the powder bed due to the powder form of the materials act as blackbodies, leading to higher material absorptance overall if compared with the value of the same but fully dense material. According to this finding, porous bed arrangement will absorb more effectively the laser energy than highly compacted powder energy densities. This is a surprising fact as porous powder beds are believed to be responsible for poor LS. It is then not clear how higher laser absorptance of the powder bed particles and final part properties affect each other. Tolochko et al. [113, 114] also outline that the powder absorptance changes with time during the LS, and the greater the absorptance of a powder, the less the energy input necessary for sintering. However, the laser energy density required for sintering powdered materials is determined by the melting temperatures and the absorptance coefficients of such materials. When the laser input required for sintering a low melting point material is fairly high, it means that such material has a very low absorptance value.

2.2.2 Processing parameters

Several processing parameters are involved in LS and can be used to optimise the performance of a component or a material. They can be divided in two groups: parameters that depend on the laser exposure (laser power, laser speed, scan count and scan spacing) and parameters that depend on the specific material and building process (processing temperatures, layer thickness, part orientation, part positioning, part build densities and shrinkage factors).

2.2.2.1 Processing parameters that depend on the laser exposure

The laser exposure is the way the laser induces the consolidation of the powder particles in the powder bed and depends on scan speed, scan spacing, scan count and laser powder.

Scan speed (v), or laser speed or beam speed, is the velocity at which the laser scans the regions to be consolidated in the powder bed. Although it can be changed, it is usually on the range of 2000-2500 mm/s.

Laser power (P) is the energy delivered by the laser to the powder particles located in those regions of the powder bed that correspond to the cross-sections of the components to be fabricated. This parameter is material-dependent and it can be modified to improve the manufacturing results. However, if a laser power that is too high is utilised, shear stresses between layers can occur, which result in increased liquid flow and in a more probable incidence of curling and distortion of the parts. Generally, lasers utilised in LS equipment are carbon dioxide with wavelength of 10.6 μm.

The Scan Spacing (SS) is the distance between two parallel laser scans and it will be further explained in chapter 5.2.5. The scan spacing is recommended to be 3-6 times smaller than the laser beam diameter in order to allow multiple laser exposures to the particles [58].

The Scan Count (SC) indicates the number of times that the same segment is exposed by the laser. It is generally set equal to 1.

The parameter called "Energy Density" (ED) is commonly used in the LS community for considering the combined effect of the laser exposure parameters on the part properties. ED is the function of the laser power (P), scan spacing (SS), scan count (SC) and scan speed (v) and is given by (Equation 1).

$$ED = \frac{P \times SC}{SS \times v}$$

Equation 1. Energy density equation [58] within the LS process. ED = Energy density, SC = scan count, SS = scan spacing and v = laser speed

P is measured in W, SC is dimensionless, SS in mm, v in mm/s and therefore ED is measured in $J \cdot mm^{-2}$.

Another definition of ED available in the literature [104] includes the layer thickness (z) set during a LS build process. This volumetric ED (ED_{vol}) is given by Equation 2:

$$ED_{vol} = \frac{ED}{z}$$

Equation 2. Volumetric ED. ED = Energy Density, z = layer thickness

ED is measured in $J \cdot mm^{-2}$, z is the layer thickness measured in mm and therefore ED_{vol} is measured in $J \cdot mm^{-3}$.

It is believed that that ED, part density and ultimately part mechanical performance are related and mutually affect each other. Generally, a higher ED leads to higher part density and better mechanical properties. However, an ED that is too high causes deterioration and degradation of the material during the process. Goodridge et al. [58] showed that the increase of the ED caused higher part density and higher tensile strength of the specimens. The ED is a material-dependent parameter which means that the best combination between laser power, scan spacing and scan speed should be evaluated for every material processed in LS.

2.2.2.2 *Processing parameters that are material and building specific*

During a LS operation, more than one temperature is set within a LS system. In general one temperature refers to the powder layer ready to be exposed by the laser and another one (or more) refers to the powder layers scanned previously. Both temperatures (or sets of temperatures) are critical as they affect the laser exposure and the thermal conditions at which the consolidated regions will start to cool down. In the case of the EOSINT P 800, three temperatures are defined in every building process (chapter 5.2.4): process chamber temperature or part bed temperature (temperature of the powder before the laser scan); building platform temperature and

frame temperature (temperatures related to the walls and bottom of the build chamber containing the produced parts and the un-sintered powder).

The part bed temperature is one of the most significant parameters during the LS process, and in order to achieve particles sintering, it is higher than the onset crystallisation temperature of the processed material but slightly below its melting temperature. The part bed temperature has to be set carefully as response of three simultaneous requirements. Firstly, it should allowing the laser to supply only the exact surplus of energy necessary for the triggering the melting of the desired areas of the powder bed. Secondly, once the laser exposure is completed, the part bed temperature should allow the just molten material to slowly cool down retaining a flat position instead of curling up because of thermal gradient in the process chamber of the LS system. Curling up of the just sintered regions can hinder completely further progression in the LS process. Thirdly, it should not be the cause for exposure of the powder under test and especially the un-sintered particles to unnecessary high temperatures.

The other processing temperatures are instead required to provide the optimal thermal conditions for the cooling of the laser sintered components.

All the processing temperatures are material- and machine-dependent. Material-dependent means that the processing temperatures are strongly connected to the thermal properties of a specific powder material in use, while machine-dependent means that LS systems from different manufacturing companies might require slightly different processing temperatures for the same material or that machines with powder bed of different size need different processing temperatures.

Another parameter is constituted of the shrinkage factors. These values are material- and machine-dependent. These factors, provided by the LS systems manufacturers, should compensate for differences between nominal design and actual geometry of the parts, hence the name "shrinkage compensation factors". The shrinkage factors are usually determined in the development phase of the LS equipment by sintering specimens in the different locations of the powder bed and measuring the discrepancies between model size and specimen size. The shrinkage is usually provided for three reference axes within the LS building system and appears to be location-dependant. An additional correction is also applied for deep builds. It must

be noted, though, that sometimes these values have to be recalibrated. Soe et al. [115] have reported on the shrinkage factors found within the largest LS system available for PA, EOSINT P 700. The authors evaluated an exhaustive map of thermal discrepancies in the powder and suggested rules for good part assembling. However, machine to machine variation is still present and variation within a build is still happening. The most common strategies are to apply compensation factor to the software of the LS system, which is building-chamber-size dependent and material-dependant, or to scale up the input model data directly. In both cases the corrections could be made specific to the LS system or to target a given part application.

The number of parts in a build - part build density - and the number of parts per layer - part layer density - have an effect on the duration of the laser exposure on each layer and on the cooling cycle of the LS system. Both durations can ultimately influence the laser sintered part properties to some extent. The higher the part layer density, the higher the time that the laser needs to expose all the interested regions in every layer. If the number of the scanned areas in the powder bed is large, layer time and the cooling time of the whole build might increase. Interestingly, the same condition could be achieved by a low part layer density due to few components with considerably big cross-sections. In this case, a large scanned area not only can increase layer time and cooling cycle but is also likely to cause distortion and geometrical inaccuracies.

Similar considerations are valid for the part build density, i.e. the higher the part build density, the longer the layer time and cooling cycle could be. If two hypothetical LS builds present the same part layer density but different build height, it is clear than the deeper build will have higher part build density than the shallow build. The build with higher part build density will be exposed for a longer time to HT than the build with lower part build density and ultimately this condition could affect to some level the properties of the laser sintered parts and impact on the recycle behaviour of the un-sintered particles.

Layer thickness is the width of the layer of fresh powder delivered before the laser exposure. Generally equal to 100-150 µm, it is recommended to be two or three times the suggested average particle size of the material utilised [90]. This condition should allow the particle coalescence to occur as a direct contact of the laser on the

71

particles rather than relying on particle-to-particle conduction. Moreover, if a layer is too thin, namely as thick as the average particle size, the realization of a uniform layer of powder would be not guaranteed. Layer thickness can also change the properties of the final parts and a well-established rule can be found in the industry-based LS community. Smaller layer thickness will lead to the manufacture of smoother parts; however it will increase the building and cycling time. Thicker layers will, on the other hand, reduce the building time but step-side effects will appear on the surface and profile of the component.

Part positioning is the location of products and components during manufacturing within the building chamber of a LS system. While part location has been found to be responsible for shrinkage effects on the components built in certain regions of the building chamber [115] and [116], Gibson and Shi [63] showed that part location had an effect also on the mechanical properties of the laser sintered components. The authors found that the components built at central location and height within the building chamber of the LS system in use exhibited higher mechanical performance, particularly tensile strength, than the specimens built elsewhere. The author explained this finding by assuming that particular manufacturing position helped to achieve better sintering because of better thermal condition of the powder bed.

Part build orientation, or simply part orientation, refers to the building direction in which a component has been laser sintered. Build orientation is considered to play an important role in part accuracy and significantly affects the mechanical performance of laser sintered components. It is well known in the LS industry and academic community that the layer bonding of the LS process causes mechanical anisotropy in the laser sintered structures. Components built along the Z direction of the referencing system of a LS system will show a considerable drop, up to 50%, of the tensile strength compared to the same components built along X and Y axes [63, 116]. The combination of part orientation and part positioning can also affect the geometrical accuracy of laser sintered components. With this intent, a few researchers have investigated iterations of job assemblies for studying geometry distortion [116, 117].

Manufacturers generally indicate good practice rules [118] concerning the orientation and positioning of the parts in a build in the processing guides of the LS machines.

Examples could be the rule to leave at least a 6 mm gap around all the profile and in any direction (X, Y and Z) of a part for components built in PEK HP3 or the recommendation to position a component in such a way that the scanning area will increase with the building direction (Z axis).

The optimisation of all the processing, parameters in LS varies with the requirement of the component to manufacture. For instance, tissue engineering applications require the fabrication of small components with high pore content, while high porosity is deleterious for those engineering components where internal voids are a source of structural failure. The most common approach for parameters optimisation in the LS sector is to carry out an identical build iteratively by changing one parameter at a time and to test each batch of components. This practice, although successful in terms of data reliability, is time-consuming and, according to material cost, very expensive. The lack of testing equipment able to reproduce the condition of the LS process has prevented the development of a better methodology. Yet, the successful impact of LS manufacturing in diverse sectors is now prompting the exploration of new materials, thus requiring a more theoretical understanding of the fundamental mechanism involved in LS.

Several attempts to optimise the LS process are available in the literature. Most of them focus on the influence of ED on the mechanical performance of laser sintered parts. Ho et al. [119] evaluated the effect of the ED parameters on polycarbonate structures, while a similar approach was adopted by Drummer et al. [90, 120] and Caulfield et al. [121] for the analysis of PA structures. The increase of the ED causes the mechanical properties, especially tensile strength, to improve to reach a plateau. Franco et al. [122, 123] focused on the efficiency of the LS against more traditional manufacturing methods in terms of energy consumption. While some structures were laser sintered only for feasibility purpose, rather than for mechanical characterisation, the authors offer a model of LS that includes processing parameters and fundamental material properties for the first time, something not possible in any of the previous models, which were based on the ED factor only.

Vasquez et al. [104] report on the investigation of a parameter called Energy Melt Ratio (EMR), where material characteristics obtained by DSC, gel permeation

73

chromatography and TGA analysis are used for predicting the processing settings leading to material degradation. The EMR parameter is given by Equation 3.

$$EMR = \frac{ED_{vol}}{Enery\ required\ to\ melt\ a\ given\ material} = \frac{ED}{E_{melt}\ \times z}$$

$$= \frac{\dfrac{P\ \times SC}{SS \times\ v}}{[C_p\ (T_m - T_b) + h_f] \times Q\ \times \Phi \times z}$$

Equation 3. Energy Melt Ratio (EMR)

P, SC, SS, v, C_p, T_m, T_b, h_f, Q, Φ and z are laser power (W), scan count (dimensionless), scan spacing (mm), scan speed (mm/s), specific heat capacity ($kJ \cdot kg^{-1} \cdot$ °C^{-1}), melting temperature (˚C), LS part bed temperature (˚C), enthalpy of melt (J/kg), material density ($kg\ \cdot m^{-3}$), packing fraction (dimensionless) and layer thickness (mm) respectively. EMR is therefore dimensionless.

The numerator represents the ED, i.e. the applied ED in the LS process during laser exposure, while the denominator is the theoretical energy required to melt a given material in the process. A high value of EMR could mean that the amount of energy applied through the processing setting is far higher than the energy required theoretically to melt that specific material. For validation, the authors built and tested samples at different Energy densities. The EMR factor predicted well the parameters for which the material degradation started to occur during the process, especially for the PA 12 grade. Additionally, the mechanical properties of the laser sintered specimens manufactured at increasing ED were plotted against the EMR values evaluated for the corresponding increasing ED settings. The graph obtained by plotting tensile strength performance of laser sintered PA 12 components is shown in Figure 9.
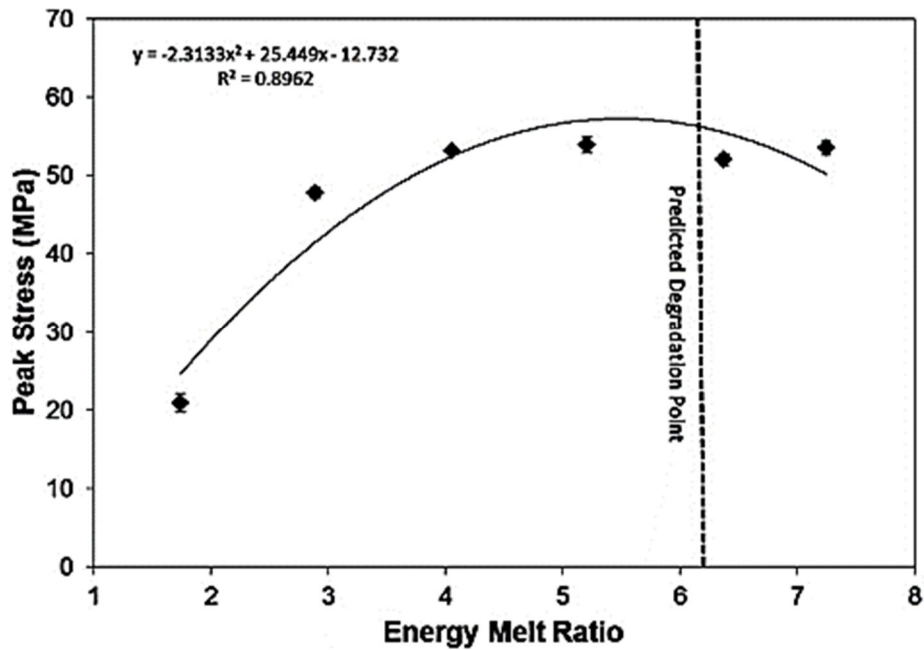
Figure 9. A plot showing the tensile strength (peak stress) of laser sintered PA 12 components manufactured at increasing ED plotted against the corresponding values of the Energy Melt Ratio (EMR) parameter [104].

Not surprisingly, the mechanical performance of the laser sintered samples under test improved with increasing values of ED, and therefore EMR (Figure 9), until it reached a peak value. Interestingly, the EMR value predicting material degradation was found to be relatively close to the limit value of the tensile strength, thus giving an acceptable estimate of material degradation affecting part performance.

Clearly, when the EMR parameter is desired to be used in relation to the mechanical performances of laser sintered structures a limited number of build trials will still have to be carried out.

2.3   High Temperature Laser Sintering (HT-LS)

High Temperature Laser Sintering (HT- LS) refers to the LS process having an operating temperature higher than 200 °C. The kinds of polymers that can be used in this process have higher melting temperatures and higher mechanical performance when compared to the polymers of traditional LS. This is a key point, because HT-LS polymers can replace metals for some applications that require operating

temperatures up to 250 °C and can also provide a lower material density than metals. It is not surprising that aerospace, defence, automotive industries have been looking into HT-LS for the manufacture of lightweight and designed optimised components. Correspondingly, a relatively high mechanical performance, low material density and the capacity not to degrade at exposure to high temperature are also key requirements for the medical industry.

The first HT-LS system was released in 2010 causing the development of two main groups of research in PAEK LS: LS of PAEK in lab-modified equipment and, later, LS of PEK in ad-hoc HT-LS equipment.

2.3.1 HT-LS in customised machines

The first reported attempt to laser sinter PEEK was carried out by Tan et al. (2003) [91] using PEEK 150XF (Victrex UK, [2]) in a LS PA designed machine, Sinterstation 2500 (3D Systems, USA [124]). The aim was to develop scaffold structures for tissue engineering. The authors processed PEEK in a low temperature chamber by significantly increasing the laser power and optimised the LS processing parameters with a trail-and-error approach. The authors also evaluated the incorporation of hydroxyapatite (HA), a substance responsible for activating the tissue regeneration mechanism, by sintering samples with different compositions in weight of PEEK and HA. Unfortunately, the analysis of the specimens was mainly qualitative (imaging by scanning electron microscope) and did not include mechanical data.

In later studies, the same group (2005) [93] sintered HA/PEEK scaffolds with specified porosity, micro-porosity, pore size and surface-to-volume ratio probably using the same LS machine. The sintered specimens were analysed in terms of: structural shape, porosity, biocompatibility and bioactivity of the HA content. Such tests analysed the apatite formation in similar body fluid test conditions and monitored the response of the primary human fibroblasts in in-vitro cell cultures (cell adhesion and cell proliferation evaluation). Although the PEEK matrix showed bio-inert behaviour, the HA indicated a promising apatite formation.

Another study from Tan et al. (2005) [92] reported a comparison between LS of PEEK/HA with other LS polymeric materials such as polycaprolactone, poly (L-lactic

acid), poly(vinyl alcohol). The work did not add any information about LS of PEEK above the findings of their previous works [93].

Rechtenwald et al. (2005) instead [105] laser sintered PEEK in a modified version of the LS system designed for PA 12, the EOSINT P 380 (EOS, Germany [1]). The machine was equipped with an in - lab made additional structure called a "heating dome", located within the building chamber, which allowed to reach a temperature of 350 °C. PEEK samples were sintered at different Energy densities by varying the processing parameters and four materials were utilised: a commercial LS PA grade (trademark PA 2200 [1]) used as reference material and three types of PEEK from Victrex [2]: PEEK 450PF, PEEK 150PF and PEEK 150XF. The difference between 450PF and 150PF is the molecular weight and therefore melt viscosity, while the difference between 150PF and 150XF is the average size of the particles. The authors evaluated the properties of single layer specimens by impact testing and defined for each type of PEEK a processing window having as a lower limit those parameters leading to mechanical stability, therefore allowing further examination of the samples and upper limit those parameters causing the onset of degradation effect, such as discolouration of the polymer. PEEK was successfully sintered, and the authors pointed out that a higher preheating temperature (part bed temperature, temperature within the building chamber before the laser exposure) than the one achievable with the heating dome should lead to better mechanical performance of the parts.

Pohle et al. (2007) [125] provided new findings in the use of PEEK for tissue engineering applications. The authors sintered discs made of different mixtures of Carbon Black (CB) (Evonik, Germany [126]) to improve the flowability and β-tricalciumphosphate (β-TCP) to enhance the bioactivity of the sintered parts. Because of its wide particle size distribution, PEEK was sieved below 63 µm as average size. The addition between the PEEK powder and the organic fillers was achieved by compounding and the following blends in weight were examined: pure PEEK; PEEK + 1% CB; and PEEK + 1% CB + 10% β-TCP. All the samples were laser sintered at a part bed temperature of 340 °C in the commercial machine EOSINT P 380 (EOS, Germany [1]) equipped with the heating dome structure. Cell vitality and cell proliferation were examined over a period of 14 days: the samples containing CB showed surprisingly higher cell proliferation than those of pure PEEK;

a reduced proliferation was noticed for the samples containing β-TCP, which differed from what was expected and no cytotoxic effect was found in any specimen.

Schmidt et al. (2007) [127] reported on the LS of samples in PEEK 150PF (Victrex, UK [2]) mixed with 1% in weight of soot used as lubricant. The samples were analysed in terms of preheating temperature (part bed temperature) range, porosity, density and bending stress. However, details of the LS system used are not provided.

Von Wilmowsky et al. (2008) [128] extended the work of Pohle et al. [125], adding bioglass in the PEEK blends. Discs of different dimensions (diameter of 14.5 mm, height of 1.7 mm and cylindrical centre-hole with a diameter of 2.5 mm) were laser sintered by using the following compositions in weight obtained through sieving and compounding: pure PEEK; PEEK + 1% CB; PEEK + 1% CB + 10% β-TCP and PEEK + 1% CB + 10 % bioglass. The samples were processed in the EOSINT P 380 system equipped with the "heating dome". Machine parameters such as layer thickness of 0.15 mm, part bed temperature of 334 °C, laser power of 10 W, scan speed of 4.5 m/s and scan distance of 0.2 mm were kept constant throughout all the sintering operations. Cell morphology, cell viability and cell proliferation were examined for a longer period, i.e. 28 days: all the samples exhibited cell proliferation, CB seemed not to affect the in vitro osteoblast behaviour; bioglass led to the highest osteoblast growth and β-TCP demonstrated a significantly lower proliferation at any time of the survey.

In a more recent piece of work, Von Wilmowsky et al. (2009) [129] laser sintered within the same modified machine and with same processing parameters [128] PEEK implants containing β –TCP. The implants were surgically incorporated in the frontal skull of ten pigs and later retrieved for biocompatibility examination. The medical grade PEEK OPTIMA® LT3 supplied by Invibio biomaterial solutions (UK, [3]) was used in this investigation. Two types of laser sintered PEEK implants were fabricated: pure laser sintered PEEK implants and laser sintered PEEK implants containing β-TCP. The laser sintered components were studied in parallel with a compression moulded PEEK implant used as control sample. More than one sample was produced for each material formulation in order to evaluate the in vivo response at different times. The implant containing β-TCP exhibited the best results in terms of

osseous-integration, biocompatibility, bioactivity and shear polymer bone interface strength. Interestingly, the behaviour of β-TCP between in vivo was much better than in the in-vitro conditions.

It is interesting to note that studies on the sintering of PEK, PEEK 450PF and PEEK 150PF mixed with carbon black in different percentages were also carried out by Wagner et al. [130] and Woicke et al. [131] in previous years, 2004-05. However, these attempts were performed at room temperature and consisted of smoothing the layers manually over a flat surface and sintering single layer specimens by using an Nd: YAG laser equipped with a scanner module.

Recently, Kroh et al. [132] also sintered samples of PEEK 150PF and 450PF (Victrex, UK [2]). The authors investigated Young's modulus and tensile strength of the samples and applied an additional heating phase after the laser exposure of every layer. The mechanical properties of the LS PEEK 450PF samples manufactured with this additional heating time were compared to the parts laser sintered without it. The specimens produced with the additional heating phase showed higher tensile strength and strain. When an additional heating time of 80 seconds per layer was applied in the LS process, the mechanical properties of the laser sintered samples were almost comparable with those of the specimens of the same material manufactured by injection moulding samples Unfortunately, this work lacks any description of the LS system utilised and it is not discussed how an additional heating phase of 80 seconds per layer could negatively affect the whole thermal histories of LS specimens or the geometrical accuracy of potential components.

All the attempts to laser sinter PEEK, then, were focused on production of medical devices that, although demanding strict requirements of chemical stability, thermal resistance and accuracy, limit the potentials of the PEEK material to other engineering areas. It is possible that the lack of an unmodified HT-LS system before 2010 inhibited the exploration of laser sintered PEEK structures for aerospace and automotive components.

2.3.2 HT-LS in the EOSINT P 800

The HT-LS process in the only commercial EOSINT P 800 systems takes places at temperatures higher than 200 °C and unlike the LS described in 2.2 it applies an additional heating phase at the end of the laser exposure of every layer, called "Post sintering". The P 800 system also offers the possibility to manufacture components in variable building chamber size. These two P 800-specific functionalities are discussed in chapter 5.

University of Exeter has recently provided a systematic characterisation of HT laser sintered PEK HP3 samples. Beard et al. [133] analysed 16 standard-shaped dog bones in terms of topology, microstructure, thermal stability and mechanical performance. The authors report high thermal and mechanical properties (tensile strength above 90 MPa) and density independent from the building position of the samples within the building chamber.

Ghita et al. [116] examined the mechanical, shrinkage and degradation characteristics of PEK HP3 samples manufactured along X, Y and Z axes of the EOSINT P 800 system. A higher shrinkage for samples built in the middle of the building chamber of the system and a drop of the tensile properties for samples built along the Z direction are presented.

In a later work, Ghita et al. [134] HT laser sintered and studied for the first time HP3 PEK samples blended with used HP3 PEK powder (material that has already been through the manufacturing process). Both raw powders and sintered specimens were analysed. Although used powder showed higher melting and crystallisation temperatures, a satisfactory sintering stage between used and virgin particles was shown. Tensile strength, thermal properties – melting, crystallisation and degradation temperatures-, surface roughness and microstructure of the sintered components were investigated. Interestingly, the specimens incorporating used HP3 PEK powder (30% used / 70% virgin PEK powder, weight percentage) showed a drop of the tensile strength values of only 17%.

The only work mentioning the use of PEEK processed in the EOSINT P 800 equipment has been carried out by El Halabi et al. (2011) [135]. A human cranial implant was HT laser sintered by EOS [1] within the EOSINT P 800 using

conditioned PEEK 450PF supplied by Victrex [2] .This work mainly focused on the 3D model simulation of the implant and it lacks any description about the manufacturing process or the component mechanical performance. This research performed under a European project named "Custom IMD project: SME Supply Chain Integration for Enhanced Fully Customisable Medical Implants, using New Biomaterials and Rapid Manufacturing Technologies, to Enhance the Quality of Life for EU Citizens."

2.4 Conclusions

PEEK is a HT polymer that is characterised by high mechanical performance, excellent chemical stability, superior thermal resistance and well-established biocompatibility. These properties have prompted the use of PEEK in additive manufacturing techniques such as polymeric LS.

Polymeric LS is a powder-based additive manufacturing process in which a variety of parameters contribute to the production of performing products and components. The characteristics of the raw powder materials affect both fundamental steps within the LS process and the properties exhibited by the laser sintered parts. Yet, a quantitative methodology for selecting and optimising new and existing powders for LS has still not been fully accomplished. Hence, an in-depth investigation into the powder properties of established and new materials can help to draw light into the development of new LS and HT-LS powders and represents one of the objectives of this research project.

Besides the limited choice of materials commercially optimised for LS, especially for HT-LS, dimensional accuracy, surface finish and component anisotropy are still areas where laser sintered parts remain inferior to parts produced by more traditional manufacturing methods [57]. However, LS affords the highest freedom of design in the manufacturing sector and requires no tooling and supporting structures. The LS process also offers high customisation, lightweight manufacturing, multi-part production, functional integration, design optimised fabrication and leads to an extreme time reduction between design and manufacturing. It is clear that LS manufacturing does not currently aim to replace the most traditional manufacturing methods using polymers, but rather offers an alternative for those applications which

are currently hindered by a limited freedom of design of the more traditional fabrication processes. Although an enhanced design freedom is accomplished by other additive manufacturing processes such as fused deposition modelling, LS is the only process that allows multi parts production without any kind of supporting structures.

The recent release of the EOSINT P 800 system has made the processing of HT polymers, such as PEK, feasible in non-modified LS systems. This condition ensures a more controlled thermal processing environment, which is a fundamental requirement for a successful building process, and literally started the manufacture of performing PEK HP3 components with high mechanical, thermal and chemical properties. In order to distinguish this process and its potential from LS occurring at lower processing temperatures, the name "High Temperature Laser Sintering" was introduced by our research group.

Several attempts to laser sinter PEEK have been carried out within lab-modified LS equipment and discussed here. The reliability of those systems remained uncertain, the laser sintered parts were only partially investigated in terms of mechanical properties and often only produced for small tissue engineering components (scaffolds).

HT-LS instead opens the way to process PEEK in a non-modified LS system.

At present, a study into the development and optimisation of the PEEK material within the tailored system EOSINT P 800 is still missing and therefore it constitutes the main investigation of this thesis work. HT-LS can provide PEEK components for high demanding engineering applications in a wide range of industrial areas, including aerospace, automotive and medical industries. HT-LS of PEEK could also rely on a lower processing temperature window than PEK because of the 30° C lower melting temperature of PEEK. This property could enhance the recyclability of the un-sintered PEEK powder because of the exposition to lower processing temperatures.

In conclusion, the HT-LS process remains extremely worthwhile and useful for research, development and manufacturing at academic and industrial levels.

3 Materials and experimental techniques

Powder materials, HT laser sintered samples and medical implants have been investigated by using several analytical techniques. This chapter provides: (a) a description of all materials analysed, (b) an explanation of the methods used for characterisation of the powders, (c) a description of the methods used for the analysis of the HT laser sintered samples and (d) a summarisation of the testing techniques used for the investigation of the two medical implant case studies.

3.1 Materials

The materials used in this research project are described according to the following classifications: powders already optimised for the low and HT-LS processes and already available commercially (LS grades); new potential PEEK grades for investigation into their use in HT-LS system and lastly additives and fillers utilised for analysing the effect of particle shape, size and physicochemical nature on the flow behaviour of a powder blends. The treatments applied to powders are also explained.

3.1.1 LS grades

LS grades are powder materials that have been already optimised for LS technology and therefore well-established. The performance of these materials, measured from the experimental techniques, have been compared with new potential PEEK grades, with the aim to identify the key parameters necessary for the selection of a new polymeric LS grade.

3.1.1.1 *PA 2200 and PA 1101*

PA 2200 is a PA 12 based powder and PA 1101 is a PA 11 based powder that are both supplied by EOS (Germany [1]). PA 2200 is white in colour, has a melting temperature 176 ˚C [136] and an onset crystallisation temperature of 150-152 °C (Table 26). Available in a discrete number of composite materials optimised for LS, PA 2200 is one of the most well established materials for LS. The powder exhibits

good chemical resistance, high strength and stiffness, biocompatibility and offers the potential for surface finishing [1]. Component mechanical properties depend on the building direction within the building chamber: according to material datasheet, XY samples exhibit tensile strength of 48 MPa, while YZ (and XZ) samples have tensile strength of 42 MPa. One of the main advantages of this material is its high recyclability to a content of 50% by weight for a new generic LS process [137]. The success of this powder then is not only because of its good properties in terms of flow and processability but also due to its cost that it is made competitive through its high recycling performance. According to Kruth et al. [77], PA powder can be recycled for a certain number of runs, until the flowability becomes detrimental for the spreading of the powder within a LS system and the melt viscosity increases up to a point that causes deleterious surface finishing effects in the parts, known as "orange peeling".

In order to provide a realistic analysis of this benchmark material, the pure virgin PA 2200 and the most common PA blend used in LS manufacturing, 50% used / 50% virgin by weight, referred by the author as PA 2200 50/50 used/virgin, have both been analysed in terms of their powder characteristics (chapter 4) and thermal properties (chapter 6) .

PA 1101 is also white in colour and exhibits a melting temperature of 201 $^\circ$C and and an onset crystallisation temperature of 163 °C (Table 26). PA 1101 has impact and elongation at break and presents better thermal resistance than PA 2200. According to the material datasheet [1], LS samples have tensile strength of 48 MPa for all the building orientations. In this research work, PA 1101 has been used as an additional benchmark material only in the analyses presented in chapter 6.

3.1.1.2 PEK HP3

PEK HP3 is the only HT polymeric grade available for HT-LS. The material is essentially Poly Ether Ketone (PEK), with a melting temperature of 373 $^\circ$C [138] and an onset crystallisation temperature of 338 °C (Table 26). PEK exhibits high mechanical performance, elevated thermal and chemical resistance and is allowable for applications requiring an operating temperature above 250 $^\circ$C and important mechanical performance [139]. It is inherently flame retardant and has excellent

wear resistance [1]. The main advantage of this powder grade is the possibility to replace metallic parts in those applications requiring lighter parts without the loss of the functional demands. Although some studies have been recently provided on the recyclability of PEK, the cost of the powder is still more expensive than PA based powder materials and this has somehow limited the potential of the material itself. In this research work PEK HP3 has been used as benchmark for the new potential HT PEEK grades in terms of powder characteristics and performance of the laser sintered structures.

3.1.2 New potential HT-LS grades

The new potential HT materials for HT-LS are two types of the PEEK polymer: PEEK 150PF and 450PF, both supplied by Victrex (UK [2]). Both materials present a melting temperature of 343 °C and an onset crystallisation temperature in the range 300-314 °C (Table 26). As they belong to the same chemical family of PEK HP3, both types of PEEK have high mechanical properties, low wear factor, high thermal and chemical stability, operating temperature above 250 °C and certain grades are approved for biocompatibility [140]. Contrary to PEK, PEEK presents a lower melting temperature and a lower glass transition temperature - therefore a better processability - with the same operating temperature of 250 °C of PEK. Available at a lower cost than PEK HP3, PEEK powders can offer competitive material performance. The principal difference between the two grades of PEEK used in this work is the molecular weight.

3.1.2.1 PEEK 150PF

PEEK 150PF represents a PEEK polymer having a molecular weight of 83,000 g/mol [4] and melt viscosity of 130 Pa·s (at 400 °C ISO 11443) [141]. It is suited for applications requiring a high flow condition of the molten material.

3.1.2.2 PEEK 450PF

PEEK 450PF represents a PEEK grade having a molecular weight of 115,00 g/mol [4] and therefore a higher viscosity than PEEK 150PF, i.e. of 350 Pa·s (at 400 ˚C ISO 11443) [142].

3.1.2.3 PEEK OPTIMA® LT1

PEEK OPTIMA® LT1 is the medical equivalent grade of PEEK 450PF and is supplied by Invibio biomaterial solutions (UK [3]). This grade is approved for biocompatibility and well-established for long term implant application and medical diagnostics components [3, 4].

3.1.3 Fillers

Several fillers with different particle shapes and sizes have been utilised into this analysis in order to evaluate their effect on the flow behaviour when dry mixed with the PEEK 450PF grade. The effect of the fillers has been evaluated in different percentages and a limit of 30% by weight has been imposed in order to preserve the mechanical performance of a potential composite. Previous studies [92] have indeed shown that the mechanical properties of a laser sintered PEEK based composite decrease when the filler concentration by weight is higher than 40%.

3.1.3.1 Spheriglass 2000

Spheriglass 2000 is a LS optimised grade consisting of spherical soda lime particles (Potters, UK [143]). The material presents a softening temperature of over 800 ˚C and a median diameter in the range 27-36 µm [143]. Spheriglass has been chosen in order to understand the effect of inclusion of particles with similar size but very round and smooth surfaces into the PEEK particles.

3.1.3.2 Calcium Carbonate

Calcium carbonate ($CaCO_3$) supplied by Ashgrove [144] presents a decomposition temperature of 900 ˚C and white appearance [145]. Although the median size of the

CaCO$_3$ was not provided in the material datasheet, after the scanning electron microscopy screening these particles resulted having size smaller than 10 µm. The CaCO$_3$ material was then chosen in order to evaluate the effect of small particles on the PEEK particles during a flow test.

3.1.3.3 Hydroxyapatite

HydroxyApatite (HA), nano powder (≤ 200 nm) supplied by Sigma Aldrich [146], present a melting temperature of 1100 °C and are insoluble in water [146]. This material was chosen because HA particles are round with quite complex nano-structures and are of similar size to PEEK particles (chapter 4.2). This property allowed the experimental techniques to focus on the effect of the different shapes on the flow performance.

3.1.4 Aerosil Pharma 200

Aerosil 200 Pharma, supplied by Evonik [126], is a nano silica powder (particle size ≤ 12 nm) designed for improving the flow in pharmaceutical products [33]. The mixtures PEEK 450PF / Aerosil (99:1) and 150PF / Aerosil (99:1) (by weight) were dry-mixed using a high speed mixer and sieved.

3.2   Conditioning of HT powders

3.2.1 Drying and sieving powders

The role of water absorption during shelf-storage on the spreading results within the LS systems (chapter 3.1.8) of the PAEK materials was investigated. PEEK powders and HP3 PEK were dried in an air ventilated air-oven at 150 °C for 2 hours before the test, according to PEEK material processing guide supplied by Victrex [147]. The sieving was carried out by using an automatic sieve with a mesh size of 100 µm.

In order to guarantee the elimination of any absorption effect within the HT-LS system EOSINT P 800, a testing temperature of 250 °C was set. Undried PEK HP3 was also tested under the same conditions and used as a reference.

3.2.2 Thermal conditioning of PEEK 150PF and 450PF

The thermal conditioning of the PEEK grades was carried out by following the patent "PAEK powder, in particular for the use in a method for a layer-wise manufacturing of a three-dimensional object, as well as method for producing it" [148], where the increase of the powder bulk density is considered beneficial for LS [1]. The procedure consists in gradually heating the powder to a temperature 50 °C above the glass transition and 20 °C below the melting temperature and holding the material at that temperature for at least 24 hours. PEEK 150PF and PEEK 450PF were gradually heated up to 250 °C in an air circulating oven for 24 hours, then left to cool down to room temperature. The materials were then sieved, left resting for at least a day in order to avoid electrostatic charging and used for characterisation analyses, spreading tests and HT-LS manufacturing. In order to understand the effect of the thermal conditioning on the particles, thermally conditioned PEEK 150PF and 450PF were analysed by SEM imaging, shape characteristics, angle of repose performance and spreading ability. These tests are described in the following paragraph.

In summary, the list of the powder materials utilised in this thesis are reported in Table 2.

LS grades	Grades to optimise for LS	Fillers	Additives	Dried and sieved grades	Thermally treated/tempered grades
PA 2200	PEEK 150PF	CaCO$_3$	Aerosil Pharma 200	PEK HP3	PEEK 150PF
PA 2200 50/50 virgin/used	PEEK 450PF	HA		PEEK 150PF	PEEK 450PF
PEK HP3	PEEK OPTIMA® LT1			PEEK 450PF	PEEK OPTIMA® LT1

Table 2. List of powder materials used in this research project: LS established powders, new potential HT PEEK grades, fillers and additive

3.1 Powder characterisation methods

3.1.1 Melt flow index

Melt Flow Index (MFI) is the mass of molten polymeric material passing through a die of standardised dimensions in ten minutes. The MFI parameter is related to the viscosity of the material under test and the lower, the higher the viscosity of the polymer. The MFI test was carried out using the Melt Flow Tester 6941 CEAST (UK, [149]) according to standard ISO 1133 and ASTM D 1238-04 with a material heating time of 5 minutes. The testing temperature is a material dependent parameter and was chosen as 23 °C above the melting temperature for each material. When the material was not so viscous to last for 10 minutes and was extruded in a much lower time, the time was recorded and used for scaling up the mass of the extrudate in a theoretical test of 10 minutes. A minimum of three measurements were carried out on each material. The MFI test was chosen over other techniques aimed to measure polymeric rheology because of its simplicity, velocity and large utilisation in industry. The aim of the test was to check the viscosity performance of the HT polymers, i.e. PEK HP3, PEEK 150PF and PEEK 450PF.

3.1.2 Particle size distribution

The Particle Size Distribution (PSD) test gives the size distribution of the single units, particles or grains, constituting a bulk material. The scope of this technique has been to evaluate the particle size distribution of established LS materials and new potential powders. Most of the tests were determined using a Saturn DigiSizer 5200 (Micromeritics, US [150]). In this instrument gives the particle size distribution of a sample is detected by light scattering. The specimen is suspended in a specific solution and hit by a laser source, hence creating a diffraction pattern specific to size of the particles involved. A solution of 0.4% sodium hexametaphosphate (more precisely, 6.7 g sodium hexametaphosphate and 1.3 g sodium hydrogen carbonate for 2 L deionized water) was used. The analysis of the PA based powders was instead carried out using the Mastersizer equipment (Malvern Instrument [151], UK) supported by Microplus software version 2.19 software. The tests were carried in the same testing conditions of the Saturn DigiSizer test.

Three measurements were performed on each material and the average results of the three repeats were reported. Although this test assumes that the particles are spherical or nearly spherical, it is widely used in the LS community and therefore utilised here.

3.1.3 Angle of repose

Angle of Repose (AOR) is a single-point test which quantifies the angle of the cone that a bulk material forms when poured over a flat surface, assuming that each material has its own specific angle of repose. The cone is formed by dropping the material through a funnel of standardised dimensions and the angle considered is the inner angle formed between the cone surface and the flat surface. The smaller the angle of repose, the higher the flowability. The test was designed by following the ASTM C 144 standard [152]. A glass funnel of angle of 60-61 °and nozzle diameter of 8 mm was used. The test was performed at room temperature with the funnel (tip of the nozzle) placed at a height of 38.1 mm (H) from the flat surface according to the standard. The powder was fed through the funnel until the cone of deposited material reached the tip of the nozzle. The AOR was evaluated by measuring the diameters of the cone in 4 positions (horizontal, vertical and the two main diagonals) by using a Mitutoyo digital Vernier calliper and following Equation 4 and Equation 5.

$$Da = \sum \frac{di}{4}$$

Equation 4. Average Diameter (Da) of the four diameters (di) of the base of the cone [152]

$$AOR = \tan^{-1} \frac{2 * H}{Da}$$

Equation 5. AOR formula [152]

Six measurements were performed on each material and the average value and the standard deviation were reported. A few modifications were made in order to carry

out the tests: the interior of the glass funnel was covered with paper in such a way to perfectly fit the angle of the funnel and to facilitate the flow of powder; the powders were added in small amounts; the powder was supplied through the funnel until the cone of deposited material reached the tip of the nozzle.

The experimental set up is shown in Figure 10.
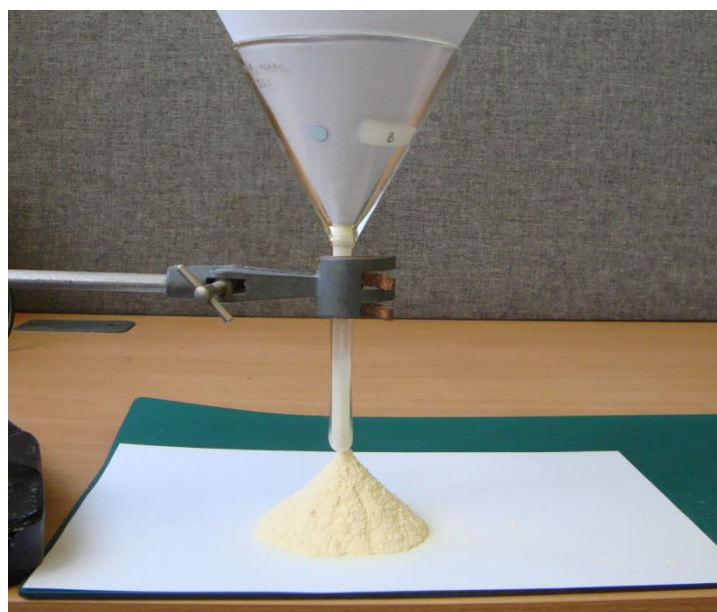
Figure 10. AOR experimental setup. Material: PEK HP3

3.1.4 Scanning electron microscopy of powder samples

The Scanning Electron Microscopy (SEM) examination of the powder materials was performed with a Hitachi S - 3200N scanning electron microscope. The powders were thinly spread on metallic stubs and then coated with 10 nm of gold coating in order to reduce the surface charging. The electron secondary imaging was set with an accelerating voltage of 25 kV.

3.1.5 Particle shape analysis

The particle shape analysis was carried out in order to quantitatively evaluate the shape of the particles constituting LS powders and potential new grades. SEM images of the particles were used in this analysis. The shape descriptors circularity,

roundness, Aspect Ratio (AR) and solidity were estimated through the measurements of perimeter and area of a large number of particles for each material. Circularity (Equation 6) evaluates the general shape of a particle. An overall circular polygon has circularity equal to 1, while an elongated shaped element has a value close to zero.

$$Circularity = 4\pi \times \frac{Area}{(Perimeter)^2}$$

Equation 6. Circularity parameter used in the particle shape analysis of LS powders and PEEK grades

Roundness (Equation 7) gives information about the edges profile of the particles. Particles with very round edges have values close to one, while particles with roundness values close to zero correspond to very sharp and angular particles.

$$Roundness = 4 \times \frac{Area}{\pi \times (Major\ Axis)^2}$$

Equation 7. Roundness parameter used in the particle shape analysis of LS powders and PEEK grades

Circularity and roundness are often simultaneously analysed in order to better visualize the type or bulk material units in consideration. The guideline relationship between circularity and roundness values for a particle has been plotted and presented in Figure 11.
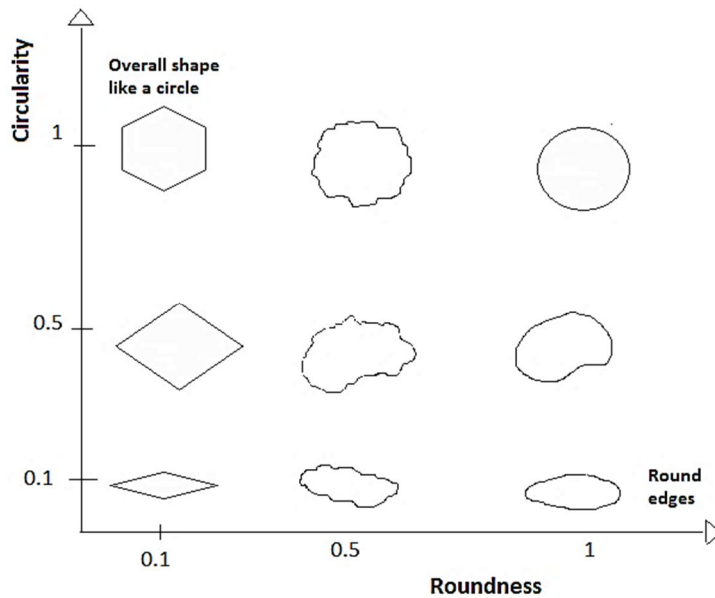
Figure 11. Relationship between roundness and circularity

Particles with low values of roundness and high values of circularity are located in the top left of the graph (Figure 11) where the particle presents an overall circular shape but with pointed edges. Particles with simultaneous high values of circularity and roundness are instead on the top right of this graph, indicating the case of nearly spherical units. Low values of circularity and roundness are represented in the bottom left of Figure 11 by highly elongated particles with sharp edges. Low values of circularity and high values of roundness can be visualized in the bottom right of the graph where the particle appears fairly long with smooth and round edges.

Aspect ratio (Equation 8) is the ratio between the major and the minor axes of a particle (Figure 12) [153]. Values close to 1 indicate the presence of equiaxed particles that can correspond to different shapes, i.e. circles, squares, overall circular polygons; while higher values identify highly elongated particles. An example of the major and minor axes of a particle is shown in Figure 12.

$$AR = \frac{Major\ Axis}{Minor\ Axis}$$

Equation 8. AR parameter used in the particles shape analysis of LS powders and PEEK grades
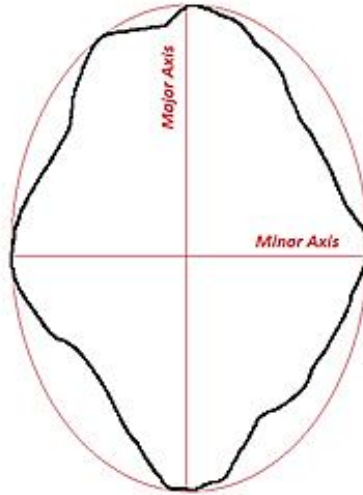
Figure 12. AR: major and minor axes of a particle

Solidity (Equation 9) is the ratio between the measured area of a particle and its corresponding convex area (Figure 13). High values (close to 1) represent very bulky particles, while lower values characterise particles which exhibit irregularities and protuberances on their surface such as flakes, lumps and outwards elongations.

$$Solidity \; = \; \frac{Area}{Convex\;Area}$$

Equation 9. Solidity parameter used in the particle shape analysis of LS powders and PEEK grades
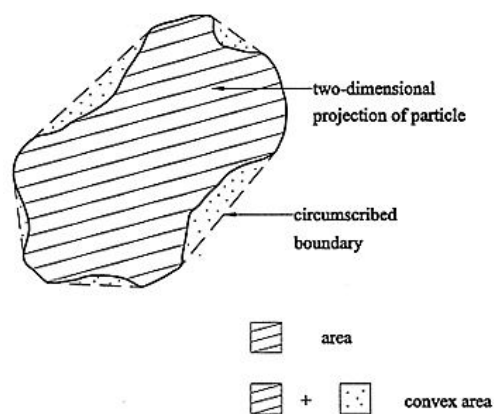
Figure 13. Convex area [154] of a particle. The convex area is used in the evaluation of the particle shape descriptor solidity

95

3.1.5.1 Method

The shape analysis was carried out by using the image processing program "Image J" [155]. The software is capable of evaluating the shape descriptors on specimen images. SEM images were used and processed according to the following procedure (Figure 14): setting of the scale, conversion to binary image, drawing the edges of particles using the automatic wand and the freehand tool, evaluation of the shape parameters through the ROI manager window. The particles analysed were not overlapping and not lying on the edges of the image. Circularity, roundness, AR and solidity were the shape descriptors evaluated for all the powder samples [155]. The shape analysis was carried out on HP3 PEK, virgin PA 2200, 50/50 virgin/used PA 2200, PEEK 450PF, PEEK 150PF and thermally conditioned PEEK 450PF. The numbers of particles evaluated for each grade were: 1174, 1538, 1539, 1154 and 1498, respectively. The number of particles analysed for the thermally conditioned PEEK 450PF grade was 1201.
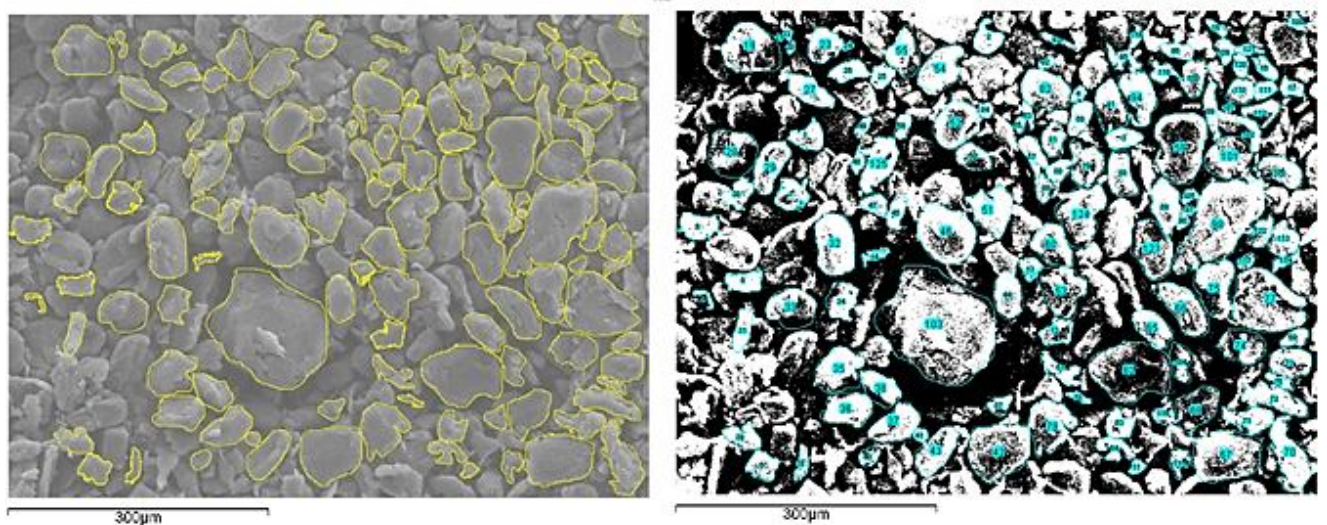
Figure 14. Image J processing using SEM images: conversion of the original SEM image into a binary file for detection of the particles

Average values and standard deviations of the main shape descriptors are reported along with their distribution.

3.1.6 Mahalanobis distance

To better represent the relationship between the shape descriptors roundness and circularity (chapter 3.1.5) of the powder materials analysed in the shape analysis, the Mahalanobis distance was used. The Mahalanobis distance is a statistic descriptor able to evaluate the centroid of a data set and the distances of all the data points from it. More precisely, this distance has been calculated by using the function "Mahal" in the computing software Matlab [156] with number of iterations equal to 300. An example of evaluation of the Mahalanobis distance for more than 20,000 data points of bivariate population is shown in Figure 15.
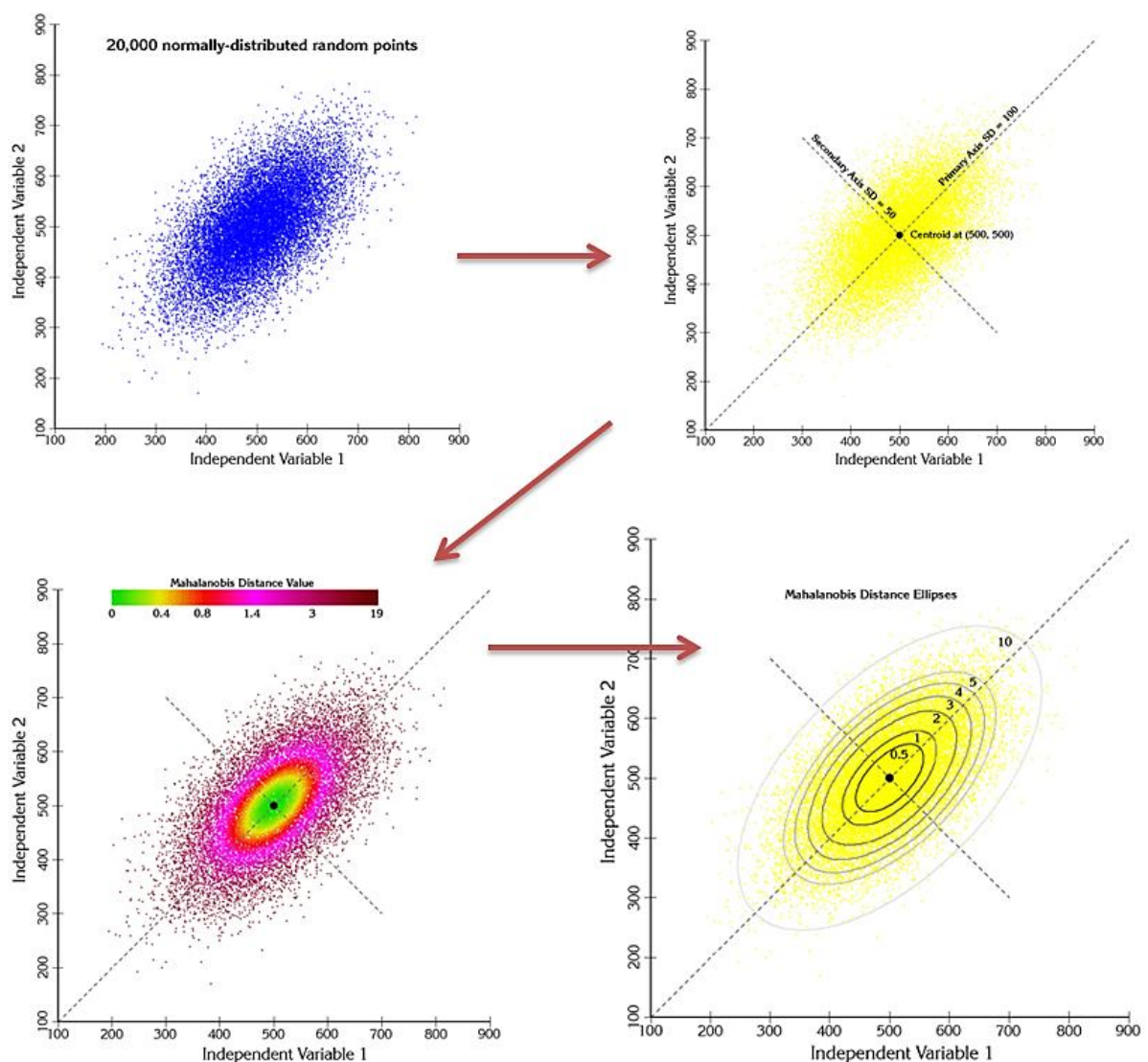
Figure 15. Example of the evaluation of the Mahalanobis distance for more than 20,000 data points [157]

97

Figure 15 shows how the Mahalanobis distance works when applied to large dataset depending on two independent variables. A centroid of all data points found is calculated and a colour scale is applied to the data points accordingly to their distance from the centroid, allowing a clearer visualisation of distance distribution.

3.1.7 Hamaker constant

Powder materials can be cohesive or free flowing due to different factors such as particle morphology, size, chemical nature and interacting medium [158]. Van der Waals forces are electromagnetic interactions that are often taken into account to evaluate the intermolecular interactions responsible of macroscopic properties between the particles of a given material [86]. The Hamaker constant is the Van Der Waals force constant able to predict or estimate the inter-particle interactions by considering the physicochemical nature of the materials involved [159-163]. In general, in the interaction of two spheres, the smaller the Hamaker constant, the smaller the Van der Waals forces are likely to be [164] and therefore the better the particles will flow. The Hamaker constant can be estimated by two methods: Hamaker and Lifshitz. The Lifshitz's theory [164] is more rigorous, overcomes limitations of the Hamaker's approach by treating bodies as continua and therefore can be applied to macroscopic bodies such as powder particles. The calculation of the Hamaker constant is derived from Maxwell's equations and is done by using the refractive indices and the dielectric constants of the powder materials involved and of the medium in which the particles interact [164]. The dielectric constant is a measure of the ability of a material to store electrical energy when subjected in an electrical field. The refractive index refers to finite velocity of propagation of electromagnetic fields in matter (retardation effect). As van der Waals forces are electromagnetic interactions between macroscopic bodies (Lifshitz's approach) both dielectric constant and refractive index that respectively indicates how strong the inter-particle attraction is and how fast it propagates through the materials involved, influence the final value of the Hamaker constant. The formula of the Hamaker constant evaluated according to the Lifshitz's method is shown in Equation 10.

$$A \approx \frac{3}{4} K_B T \left(\frac{\varepsilon_1 - \varepsilon_3}{\varepsilon_1 + \varepsilon_3}\right) \left(\frac{\varepsilon_2 - \varepsilon_3}{\varepsilon_2 + \varepsilon_3}\right) + \frac{3}{8} \frac{h\upsilon_e}{\sqrt{2}} \frac{(n_1^2 - n_3^2)(n_2^2 - n_3^2)}{\sqrt{(n_1^2 + n_3^2)} \sqrt{(n_2^2 + n_3^2)} \left\{\sqrt{(n_1^2 + n_3^2)} + (n_2^2 + n_3^2)\right\}}$$

Equation 10. Hamaker constant (A)

K_B is the Boltzmann constant equal to $1.38 \cdot 10^{-23} J \cdot K^{-1}$; T is the temperature and equal to 300 K; h represents the Plank constant equal to $6.63 \cdot 10^{-34} J \cdot s$; υ_e is the electron orbiting frequency equal to $3 \cdot 10^{15} Hz$; ε_1, ε_2, ε_3 are the dielectric constants of phase 1, 2 and interacting medium, respectively; n_1, n_2, n_3 are the refractive indices of phase 1, 2 and interacting medium, respectively. Phase 1 and phase 2 are the powder materials utilised, while medium is air.

The values of the dielectric constants and the refractive indices were found in the literature and are listed in Table 3.

Material	Refractive index	Dielectric constant
Air	1	1
PEEK	1.65 - 1.77 Mean = 1.71 [165]	3.38 [166-168]
PA 12	1.52 [169]	4.82 [169]
Spheriglass	1.51 [170]	6.9 [170]
HA	1.649 - 1.641 Mean = 1.645 [171, 172]	4.95 - 13.55 Mean = 9.25 [173]
CaCO$_3$	1.486 - 1.658 Mean = 1.572 [174]	6.1 - 9.1 Mean = 7.6 [175]
Aerosil Pharma 200	1.45 [126]	4.5 [175]

Table 3. Refractive indices and dielectric constants used for the evaluation of the Hamaker constant of the powder materials (LS grades, PEEK and blends)

The same value of refractive index and dielectric constant was used for PEEK 150PF and 450PF as it was not possible to obtain grade-specific parameters.

3.1.8 Spreading tests

The ability of a powdered material to be uniformly and evenly spread in layers was tested by spreading the materials in two types of LS machines. Several materials were tested:, PEEK 150PF, PEEK 450PF, dried PEK HP3, sieved PEK HP3, sieved PEEK 150PF, dried PEEK 150PF, dried PEEK 450PF, sieved PEEK 450PF, thermally conditioned PEEK 150PF and 450PF, PEEK 150PF and 450PF with the addition of 1% Aerosil (by weight).

Two LS system machines were used: the LS PA designed machine Sinterstation 2000 (3D systems, USA [124]) and the HT-LS system EOSINT P 800 (EOS, Germany [1]).While the Sinterstation 2000 system is equipped with an counter-rotating roller spreading device, the EOSINT P 800 is provided with a double blade recoater. The powder spreading devices are shown in Figure 16.
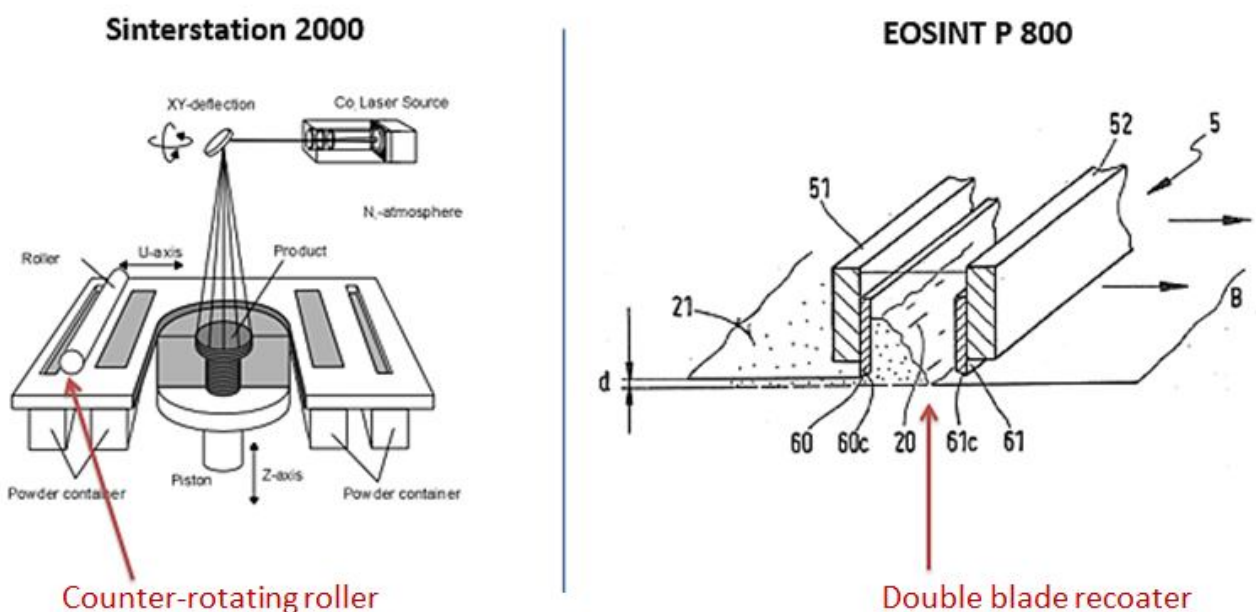
Figure 16. Powder spreading tools in the LS systems Sinterstation 2000 and EOSINT P800: counter-rotating roller [176] and double blade recoater [177], respectively.

A 15 mm thick powder base was spread in both systems according to EOS guidelines for a building operation [118]. The test, carried out a room temperature, consisted of spreading up to ten fresh layers of powders and evaluating the spreading conditions for each layer. Pictures of each layer and each material were taken for every layer.

The test was performed in the two machines in order to estimate the effect of the spreading device on the spreading results. However, as one of the interests of this research was to investigate and optimise the processing of PEEK within a HT-LS system, more tests in several conditions were carried out in the EOSINT P 800.

Up to ten layers of powder were spread and examined in the EOSINT P 800 for those powders that showed good spreading performance. If a powder exhibited such poor spreading conditions as did not allow the spreading of a successive layer, only a few layers of powder were spread and visually analysed.

The tests carried out in the EOSINT P 800 were performed at various temperatures: well-above the glass transition temperature of PEEK and PEK materials (250 ˚C) and at their processing temperatures (332˚, 339˚ and 365 ˚C).

In order to reduce the quantity of fresh powders discarded after this test within the EOSINT P 800, all the spreading tests were carried out over half of the building area, i.e. in half building mode chamber (chapter 5.2.2.1).

The list of materials, equipment and testing conditions is shown in Table 4.

LS system	Testing temperature	Materials
Sinterstation 2000	T_{Room}	- PEK HP3 - PEEK 150PF - PEEK 450PF
EOSINT P 800	T_{Room}	- PEK HP3 - PEEK 150PF - PEEK 450PF - Thermally conditioned PEEK 450PF - Thermally conditioned PEEK 150PF - PEEK 450PF + 1% Aerosil - PEEK 150PF + 1% Aerosil
EOSINT P 800	250 °C	- Dried PEK HP3 - PEK HP3 - Dried PEEK 150PF - Dried PEEK 450PF
EOSINT P 800	Processing temperatures	- PEK HP3 (at 365 °C) - PEEK 150PF (at 339 °C) - PEEK 450PF (at 332 °C)

Table 4. Spreading tests: LS equipment, testing conditions and materials

3.1.9 Differential scanning calorimetry

Differential Scanning Calorimetry (DSC) allows the study of a wide range of thermal properties of materials. Melting and crystallisation temperature, and crystallinity contents of powder samples were analysed using the DSC 821e/700 (Mettler Toledo [178], UK) with sample weight of approximately 10 mg. The powders were heated from room temperature up to well-above their melting temperature (200 °C for low temperature polymers such as PA and 400 °C for PAEK powders) with heating and cooling rates of 10 and -10 °C/min, respectively. Nitrogen was used as protective gas with flow of 50 ml/min. The evaluation of the thermal properties such as melting temperature, enthalpy of melt, crystallisation peak and enthalpy of crystallisation have been assessed by using the Stare package software (Mettler Toledo [178], UK).

The evaluation of the first derivative of the heating segment of an entire DSC thermoscan has been also evaluated for the powder materials. The operation is carried out automatically within the Stare software by setting the number of sampling points equal to 26. A minimum of three measurements were carried out for every material analysed.

The DSC scan used in the evaluation of the stable sintering region (chapter 6) was carried out on thermally conditioned PEEK 450PF powder sample of mass approximately equal to 10 mg. The sample was heated from room temperature to 400 ˚C at 10 ˚C/min with purge gas flow (nitrogen) of 50 ml/min.

3.1.10 Thermo-gravimetrical analysis

Thermo-Gravimetrical Analysis (TGA) is an analytical technique used for the study of thermal degradation phenomena on materials. The test shows the weight loss of a sample when exposed to a user defined thermal programme. The results can be interpreted versus time or temperature. The TGA tests on powder samples of mass of approximately 10 mg were carried out using the Mettler Toledo TGA/DSC 1-1100 ˚C (Mettler Toledo [178], UK).

The TGA data of thermally conditioned PEEK 450PF powder sample used in the evaluation of the stable sintering region (chapter 6) was obtained by heating the material from room temperature to 900 ˚C at a heating rate of 10 ˚C/min and using nitrogen as protective gas at 50 ml/min flow.

The TGA data used for the calculation of the EMR_D (3.1.12) was performed on thermally conditioned PEEK 450PF powder sample heated from room temperature to 900 ˚C at a heating rate of 10 ˚C/min and nitrogen as protective gas at 50 ml/min flow.

The TGA data used in the evaluation of the Kissinger method (3.1.12.1) were carried out on thermally conditioned PEEK 450PF powder samples heated from room temperate to 900 ˚C at different heating rates indicated in 3.1.12.1 and nitrogen as protective gas at 50 ml/min flow.

PEEK 450PF and thermally conditioned PEEK 450PF powder samples used in chapter 6 for investigating thermal degradation, were heated from room temperature to 900 ˚C at a heating rate of 10 ˚C/min and nitrogen as protective gas at 50 ml/min flow.

3.1.11 Packing fraction measurement

The bulk density is the density of loose and uncompressed powder per unit volume. The packing fraction is a numerical parameter that indicates how well a bulk material (powder or grain) can compact, i.e. occupying the smallest volume with the highest number of particles. When this value is close to zero indicates that a material has poor packing behaviour with many voids within the unit volume. When instead it is close to 1 the material has good packing performance with a large number of particles occupying the unit volume and very few or nil voids. This parameter represents a key property in powder bed fusion processes where a good degree of compaction in the powder bed is necessary for the creation of fully dense components. The value of the packing fraction of thermally conditioned PEEK 450PF has been measured by evaluation of the ratio between the bulk density of the powder and the true density of the material equal to $1320 \; kg/m^3$ [179, 180].

The measurement of the bulk density consisted of:

- Measuring the weight of a plastic 100 ml cylinder (m_0)
- Pouring a powder material through a plastic funnel until it reached the 100 ml mark while keeping the end of the funnel 2 cm above the cylinder.
- Measuring the new weight (m_1)
- Carrying out three measurements
- Evaluation of the bulk density (Q) according to Equation 11
- Evaluation of the packing fraction Φ according to Equation 12 with the true density of PEEK ($\rho = 1320 \; kg \cdot m^{-3}$).

$$\rho = \frac{m_1 - m_0}{100}$$

Equation 11. Bulk density

$$\Phi = \frac{Q}{\rho}$$

Equation 12. Packing fraction

3.1.12 Energy melt ratio

Energy Melt Ratio (EMR) is a numerical parameter introduced by Starr et al. [181] and later further investigated by Vasquez et al. [104] when studying the relationship between manufacturing parameters and mechanical properties of laser sintered PA specimens. As described in chapter 2.2, it represent the ratio between the energy applied in LS, ED_{vol}, and the theoretical energy required for melting a given material (E_{melt}). ED_{vol} is given by Equation 13.

$$ED_{vol} = \frac{ED}{z}$$

Equation 13. Volumetric ED. ED = Energy Density described in chapter 2, z = layer thickness

ED is measured in $J \cdot mm^{-2}$, z is the layer thickness measured in mm and therefore ED_{vol} is measured in $J \cdot mm^{-3}$.

EMR is given by Equation 14 and Equation 15.

$$EMR = \frac{ED_{vol}}{E_{melt}} = \frac{ED}{E_{melt} \times z}$$

Equation 14. EMR as ratio between ED, $\boldsymbol{E_{melt}}$ and layer thickness (z)

$$EMR = \frac{\dfrac{P \times SC}{SS \times v}}{[C_p (T_m - T_b) + h_f] \times Q \times \Phi \times z}$$

Equation 15. EMR parameter in LS

105

P, SC, SS, v, C_p, T_m, T_b, h_f, Q, Φ and z are laser power (W), scan count (dimensionless), scan spacing (mm), scan speed (mm/s), specific heat capacity ($kJ \cdot kg^{-1} \cdot °C^{-1}$), melting temperature (˚C), LS powder bed temperature (˚C), enthalpy of melt (J/kg), material density ($kg \cdot m^{-3}$), packing fraction (dimensionless) and layer thickness (mm) respectively. EMR is therefore dimensionless.

LS processing parameters were the experimental values described in chapter 5. Bed temperature was found experimentally as described in chapter 5.3. The melting temperature and enthalpy of melt were measured using DSC analysis (chapter 3.1.9). Material density and packing fraction were measured according to 3.1.11. The remaining parameters were found in the literature and reported in chapter 6.

At present, EMR is the only factor that couples processing parameters with properties of LS materials. In this form the EMR equation can be used for evaluating the relationship between properties of a LS powder material for different processing parameters, i.e. over a range of EMR values. However, EMR can also be formulated and solved for those processing parameters that lead to material degradation. The theoretical energy degradation of a material (E_D) can be determined using Equation 16.

$$E_D = [C_p(T_D - T_m) + \frac{E_A}{M_w}] \times Q$$

Equation 16. Energy leading to material degradation

C_p, T_D, T_m, E_A, M_w and Q are specific heat capacity ($kJ \cdot kg^{-1} \cdot °C^{-1}$), onset degradation temperature (˚C), melting temperature (˚C), activation energy for degradation (kJ), molecular weight (g/mol) and material density ($kg \cdot m^{-3}$), respectively. Onset degradation temperature and energy of activation were evaluated experimentally using TGA analysis as described in chapter 3.1.10. Melting temperature was evaluated experimentally using DSC analysis (chapter 3.1.9). Material density was measured according to 3.1.11. The remaining parameters were found in the literature and indicated in chapter 6.

The EMR value corresponding to material degradation (EMR_D) is shown in Equation 17.

$$EMR_D = \frac{E_D}{E_{melt}}$$

Equation 17. EMR leading to material degradation

The optimisation of the HT-LS processing parameters on PEEK has been carried out by varying the laser power and holding constant the other processing parameters (beam speed, scan distance and count). Solving Equation 17 for the value of ED responsible for the onset of the material degradation, it is possible to find the processing parameters leading to degradation during a LS building process (Equation 18). Therefore, the laser power (P_D) leading to material degradation was calculated by solving the equation of the energy density of degradation (ED_D) in Equation 18 and is reported in Equation 19.

$$ED_D = EMR_D \times E_{melt}$$

Equation 18. Energy density of material degradation

$$P_D = \frac{EMR_D \times E_{melt} \times SS \times v \times z}{SC}$$

Equation 19. Laser power causing material degradation during LS

In this project, the EMR equation has been used for both purposes.

3.1.12.1   Kissinger method and evaluation of the activation energy

The measurement of the activation energy (E_A) leading to thermal degradation of thermally conditioned PEEK 450PF was carried out according the Kissinger method. The obtained value was then used for the calculation of the EMR_D.

The Kissinger method consists of several TGA experiments carried out at different heating rates (β), - every experiment at a different heating rate - . The exothermic peak temperature (T_{max}) was recorded at varying heating rates and the data were used for the evaluation for a straight line fit in the plot having the factor $\ln \frac{\beta}{T_{max}^2}$ as Y axis and the parameter $\frac{1000}{T_{max}}$ as X axis. The slope of the straight line multiplied by the gas constant (R = $8.314\, J \cdot mol^{-1} \cdot K^{-1}$) is the activation energy value for thermal degradation of the material analysed.

The peak temperature T_{max} has been measured by evaluating the peak of the first derivative of the TGA results. The heating rates of 5, 10, 15 and 20 K/min were used for the evaluation of the activation energy E_A of PEEK materials.

The onset degradation temperature was evaluated with the STARe software [178] function "Step horizontal" with step equal to 1%. The right temperature value was then utilised in Equation 16 is at the temperature at which 1 % weight loss occurred on the TGA data carried out at heating rate of 5 K/min.

3.2 Sample testing methods

The testing of HT laser sintered samples has involved several techniques and methods that are described in the following paragraphs.

3.2.1 Tensile testing

Tensile samples were manufactured with ISO 527-2-1A [182] geometries along the X direction of the referencing system within the building chamber. Tensile testing experiments were performed by using a LLOYD instruments EZ 20 mechanical testing machine at room temperature (20 ˚C). The testing speed was equal to 2 mm/min and the gauge length was 85 mm. At least 20 samples were manufactured and tested for every build. The average ultimate tensile strength and the standard deviation were evaluated. The measurement of sample elongation was not carried out because of the lack of an extensometer module on the tensile test equipment.

3.2.2 Post treatment of HT laser sintered tensile bars

In the attempt to push the limits the tensile strength of LS sintered samples, an additional build according to the parameters of build 6 (chapter 5.5.2) was repeated and the HT laser sintered samples were subjected to a post treatment after the LS manufacturing. According to the material guidelines [147], the samples were dried at 150 °C for 3 hours and annealed at 250 °C for 5 hours within an air-ventilating oven. The samples were tested and compared with the tensile testing results (tensile testing procedure described in 3.2.1) of build 6.

3.2.3 One and ten layer samples

One and ten layer samples were HT laser sintered specimens specifically built for studying the effect of the post sintering phase (chapter 5.2.2.2) on the surface roughness, microstructure and layer bonding. The samples were XY cross sections (Figure 17) of the tensile samples manufactured with ISO 527-2-1A geometries along the x direction of the referencing system within the building chamber produced with the processing parameters corresponding to build 5 and different PS times.
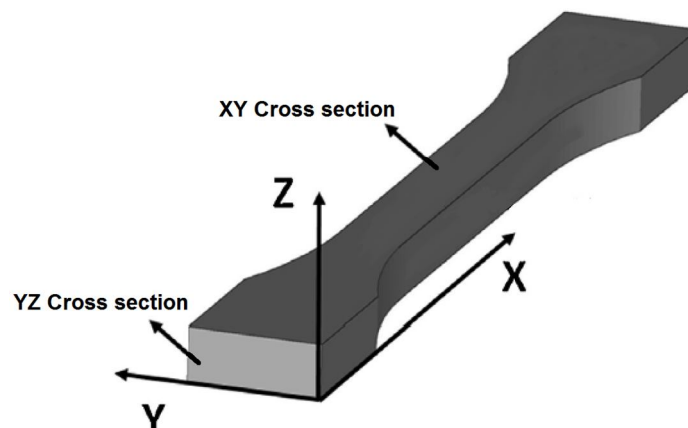
Figure 17. XY cross section of one and ten layer samples. YZ cross section used for imaging layer bonding properties

One layer specimens were tensile samples exposed only once to the laser followed by the post sintering phase. Once one exposure was completed, the process was manually interrupted and the samples left to cool down naturally.

Ten layer specimens were tensile bars exposed to the laser, followed by the PS and the recoating phases, ten times. The purpose of the production of these specimens was to understand the effect of the PS time: it was expected that looking at the molten and solidified surface of one layer and ten layer would give an indication of the importance of this heating phase.

One and ten layer samples in thermally conditioned PEEK 450PF were manufactured with PS times of 6 s, 9 s, 12 s and 15 s. Similarly one and ten layer samples in PEK HP3 produced according to manufacturing parameters of build 5 and with standard recommended PS of 12 s were built and used as benchmark for the PEEK samples.

3.2.4 Dynamic mechanical analysis

Dynamic Mechanical Analysis (DMA) allows the study of the viscoelastic behaviour of a given material by the measurement of the complex modulus. While the real part of the complex modulus represents the elastic behaviour (Storage modulus E') of a material, the imaginary part (Loss modulus, E") represents its viscous performance [183]. The tests were carried out using the Mettler Toledo DMA-1(Mettler Toledo, UK [178]). All the specimens were built with nominal dimension of 30 mm x 7 mm x 2 mm and tested in three-points-bending mode (Frequency 1 Hz and strain displacement 10 µm). During the test, each sample was heated from 30 ˚C to 300 ˚C at heating rate of 3 ˚C/min. At least, four repeats were carried out for each type of processing conditions.

3.2.5 Surface roughness measurements

The surface roughness of one and ten layer specimens were evaluated using a Taylor-Hobson Talyscan 150 surface profiler. An area of 3 mm x 3 mm was scanned on the XY surface of each sample at 1000 µm/s with spacing along the X axis of 3

µm and of 5 µm along the Y axis. The evaluation of the descriptor surface roughness (S_a) and the imaging of surface profiles were performed using the software Talymap.

3.2.6 Micro-computer tomography (micro-CT)

In order to investigate the internal structure, samples built at different manufacturing settings (cubic samples of about 5 mm x 5 mm x 5 mm) were analysed by microcomputer tomography. The tests were carried out using an X-Tek Bench top CT 160 Xi System with resolution of 3 µm. The samples were examined with voltage of 65 kV, current of 82-90 µA under rotation angle of 360 ˚. The data was then reconstructed using the software CT Pro 3D [184] and imaged with the software VG Studio Max 2.1 [185]. The samples were investigated qualitatively and quantitatively in terms of pore size and the material density within the VG Studio Max 2.1 software package. The pore size was evaluated by selecting the pore and applying the distance tool. The material density evaluation, which is shown in Figure 18, was carried out according the following steps:

- Selection of the largest region of interest on the sample data
- Application of a contrast mask that highlighted in yellow the material and left unselected (black appearance) the pores within the sample structure
- Measurement of the yellow percentage over the whole sample. This number equates the estimated material density.
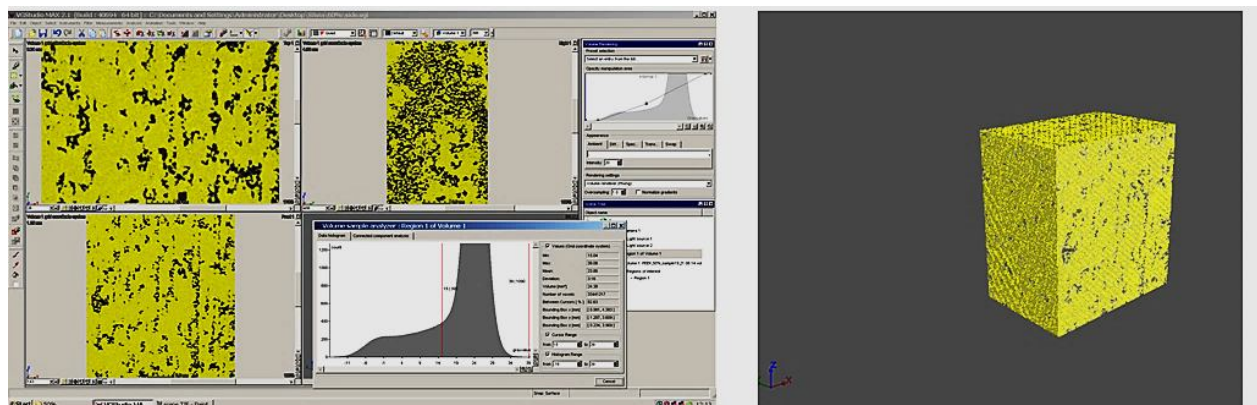
Figure 18. Material density evaluation using micro-CT scanning

One sample for each set of manufacturing settings was analysed using micro-CT scanning because of the duration of the scanning time.

3.2.7 ANOVA statistical analysis

The software package IBM SPSS Statistics version 21 [186] has been used for evaluating the statistical differences between data groups of samples built with different manufacturing parameters. Experimental results have been analysed using the post-hoc analysis of the ANOVA with Tamhane T2 at a confidence level of 95%. The statistical results are presented in terms of 'P-Values'. Any P-value found smaller than 0.05 means that there is a significant difference between the compared groups of data. Significant difference indicates that the variation of the means values between two or more datasets is not due to the natural variation of the results, but to the conditions with whom the data were generated.

3.2.8 SEM of HT laser sintered samples

SEM examination of HT laser sintered structures was carried out by using a Hitachi S - 3200N scanning electron microscope. The samples were coated with 10 nm of gold/palladium in order to reduce the surface charging. The electron secondary imaging was set with an accelerating voltage of 25 kV.

Also the one and ten layer specimens of thermally conditioned PEEK 450PF and PEK HP3 were analysed using SEM. In order to investigate the layer bonding properties as function of the post sintering time the ten layer samples were cooled down with liquid nitrogen and manually snapped. The fracture surface (YZ cross sections in Figure 17) was then analysed with SEM imaging according to the settings described above.

3.2.9 TGA analysis

The HT laser sintered PEEK 450PF sample manufactured with the processing parameters from build 3, used in chapter 6, was heated from room temperature to

900 ˚C at a heating rate of 10 ˚C/min and nitrogen as protective gas at 50 ml/min flow.

3.3 Medical case studies

Two types of medical implants were manufactured with the HT-LS process using the PEEK grade "PEEK OPTIMA® LT1", supplied by Invibio biomaterial solutions [3]. PEEK OPTIMA® LT1 is the medical equivalent of PEEK 450PF. As PEEK 450PF, PEEK OPTIMA® LT1 was thermally conditioned before use in the HT-LS system, according to the procedure described in 3.2.2.

3.3.1 Cranial implants

The CAD model (STL file) of a cranial implant originated from true patient data was supplied by the "Custom IMD project: SME Supply Chain Integration for Enhanced Fully Customisable Medical Implants, using New Biomaterials and Rapid Manufacturing Technologies, to Enhance the Quality of Life for EU Citizens" project [187]. The cranial implants were manufactured in the EOSINT P 800 system in reduced chamber mode with build 5 processing parameters described in chapter 5.5.2. The implants were manufactured at different orientation in respect with the building orientation within the P 800 system and tested in terms of dimensional accuracy. The build orientation of each part is showed in chapter 7 along with the results of the dimensional accuracy measurements.

3.3.1.1 Dimensional accuracy measurements

The dimensional accuracy of the interior and exterior surfaces of each cranial implant was analysed using a Renishaw Cyclone [188] scanning and measuring system with a 2 mm diameter stainless steel cylindrical probe and an accuracy of 5 µm. The scanning test consists of the probe scanning all over the surface of the cranial implant at a time, as shown in Figure 19.
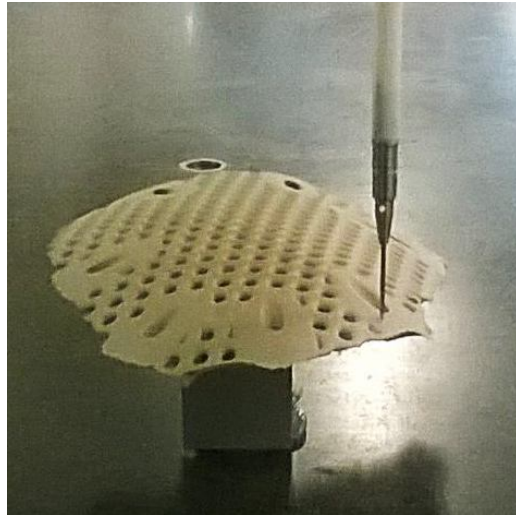
Figure 19. Renishaw Cyclone. A cylindrical probe scanning the exterior surface of one of the high temperature laser sintered cranial implants

The implants were mounted on customised laser sintered cylindrical fixtures manufactured in PA 12, one for the interior surface and one for the exterior surface. The top surface of each fixture was manufactured by Boolean subtraction of the cranial implant surface from the jig. The jig therefore exhibited the best match fit with the samples. The implant was mounted on the fixture by means of three points of fixation (metallic screws). This *modus operandi* provided a safe way to mount organic shape than glue fixation, helped to scan samples in the same position and orientation and lastly reduced the tiding stage and the errors introduced by the alignment of the scanned data with the results. The jigs are shown in Figure 20.
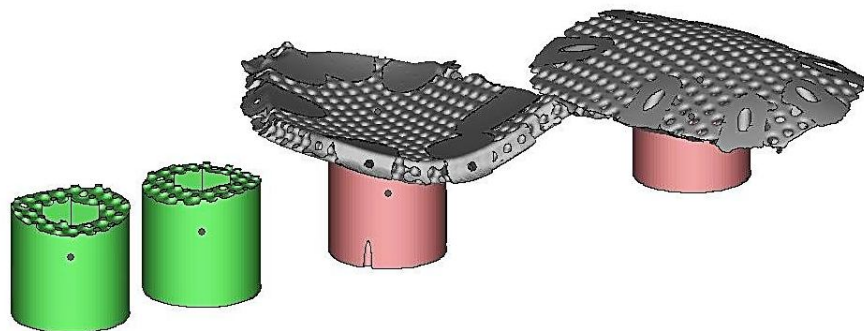
Figure 20. Laser sintered mounting fixtures for dimensional accuracy analysis of cranial implants

The scanned data has been compared to the original data of the implant CAD model (STL file) utilising the software package Geomagic Studio v10 [189]. More precisely, the scanning and the comparison with original model data has been carried out with the following steps:

- Scanning of a surface and generation of a dataset or point cloud
- Creation from the point cloud of a STL file (scan data STL file) with triangular mesh
- Cleaning of the scan data STL file from noise using the software package Materialise Magics RP v18 [190]
- Rough alignment of the scan data STL file to the original model (original STL file) in Magics RP v18
- Final alignment of the scan data STL file to the original model (original STL file) in Geomagic Studio v10 using the best fit alignment tool
- Deviation analysis in Geomagic Studio v10 using the 3D compare tool.

Both surfaces have been aligned to the CAD model by using the best fit alignment tool, and analysed with the 3D compare tool. In order to carry out a deviation analysis that resulted in a colour mapping operation of the aligned files, critical values and nominal tolerances had to be chosen. No data for dimensional accuracy of HT laser sintered cranial implants are currently available. Therefore, the nominal tolerances were set equal to the established LS industry based nominal tolerance of ± 100 μm, while the choice for the critical values (minimum and maximum critical values) was chosen taking into consideration the LS resolution by a factor 2, i.e. 1 mm. In summary, maximum and minimum critical values were set at ± 1 mm, while the maximum and minimum nominal tolerances were set at ± 0.1 mm.

The area within the nominal tolerances was mapped in green colour in Geomagic Studio v10. This green area was quantified (pixel area) using the software package Image J [191] by setting the plugin "Colour threshold" limited to the green range. The area within the nominal tolerances (green area) was also compared to the overall area of the surface of the cranial implant under test. This area was evaluated using the same software image plugin "colour threshold" excluding the background pixel and selecting the threshold option. The percentage ratio of the area within nominal tolerance over the whole area was calculated according to Equation 20.

$$Nominal\ tolerance\ ratio\ (\%) = \frac{Area\ wihtin\ nominal\ tolerances\ \cdot 100}{Overall\ area}$$

Equation 20. Nominal tolerance ratio

An example of (from the left) the deviation analysis results, the evaluation of the area within the nominal tolerances and the overall area are shown in Figure 21.
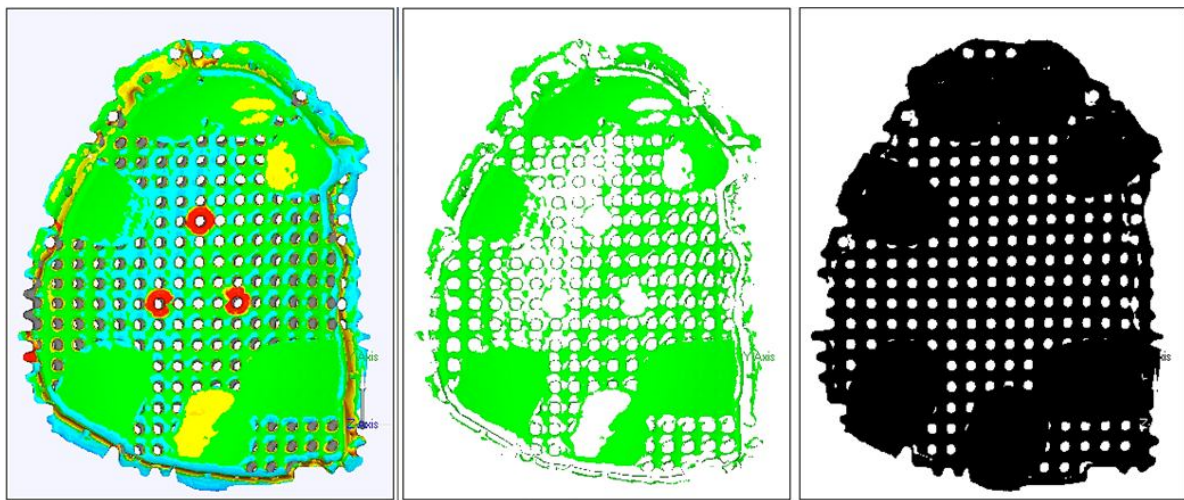
Figure 21. From the left, deviation analysis result on the inner surface of a HT laser sintered cranial implant; evaluation of the area within nominal tolerances (green area) and overall area. Software package: Image J [155]

3.3.2 Spinal inter-body fusion cages

The CAD files of different spinal inter-body fusion cages were supplied by Invibio biomaterial solutions [3]. The spinal inter-body fusion implants were manufactured within the EOSINT P 800 system in reduced chamber mode and with the processing parameters from build 5 described in chapter 5.5.2. While one type of spinal cages and corresponding test results are reported in chapter 7 (courtesy of Invibio biomaterial solutions), the other implants are undergoing testing at Invibio biomaterial solutions [3] and are protected by intellectual property restrictions.

3.3.2.1 *Static axial compression test*

The HT laser sintered spinal inter-body fusion lumbar cages were tested and compared with traditional machined cages of the same design and material in terms of static axial compression performance. This test was carried out by Invibio biomaterial solutions [3]. Stainless steel load block matching the outer geometry of the cages were used as static loading during the compression test. The geometrical centre and the centre of the spherical bearing were aligned and an intradiscal height of 100 mm was used, in accordance to standard testing procedure for lumbar cages (ASTM F 2077). The test was performed at room temperature in dry conditions with an axial loading rate of 2 mm/min. The implants were tested until failure or maximum load capacity of the testing machine.

3.4 Conclusion

A significant number of powder materials and HT laser sintered samples have been analysed using the characterisation methods and techniques described in this chapter and the results are reported in chapters 4, 5 and 6. Two case studies of medical components have also been manufactured and some of their properties investigated (chapter 7).

The quantitative particle shape analysis, spreading tests and calculations of the Hamaker constant represent innovative techniques for the characterisation of powder materials in LS. The techniques including tensile testing, DMA, micro-CT, SEM and surface roughness measurement offer the opportunity to provide a systematic analysis of mechanical and micro-structural properties of HT laser sintered components manufactured in varied conditions and parameters. The DSC and TGA methods help estimate potential HT-LS processing conditions on the basis of the powder material properties. Lastly, the mechanical compression testing of inter-body fusion spinal cages and probe contact scanning of HT laser sintered PEEK cranial implants offer the possibility to respectively present mechanical performance data of a real medical application and a dimensional stability study of complex organic shape specimens of cranial implants generated from true patient data.

For clarity, a summary of the materials and experimental techniques used in this research project is shown in Figure 22.
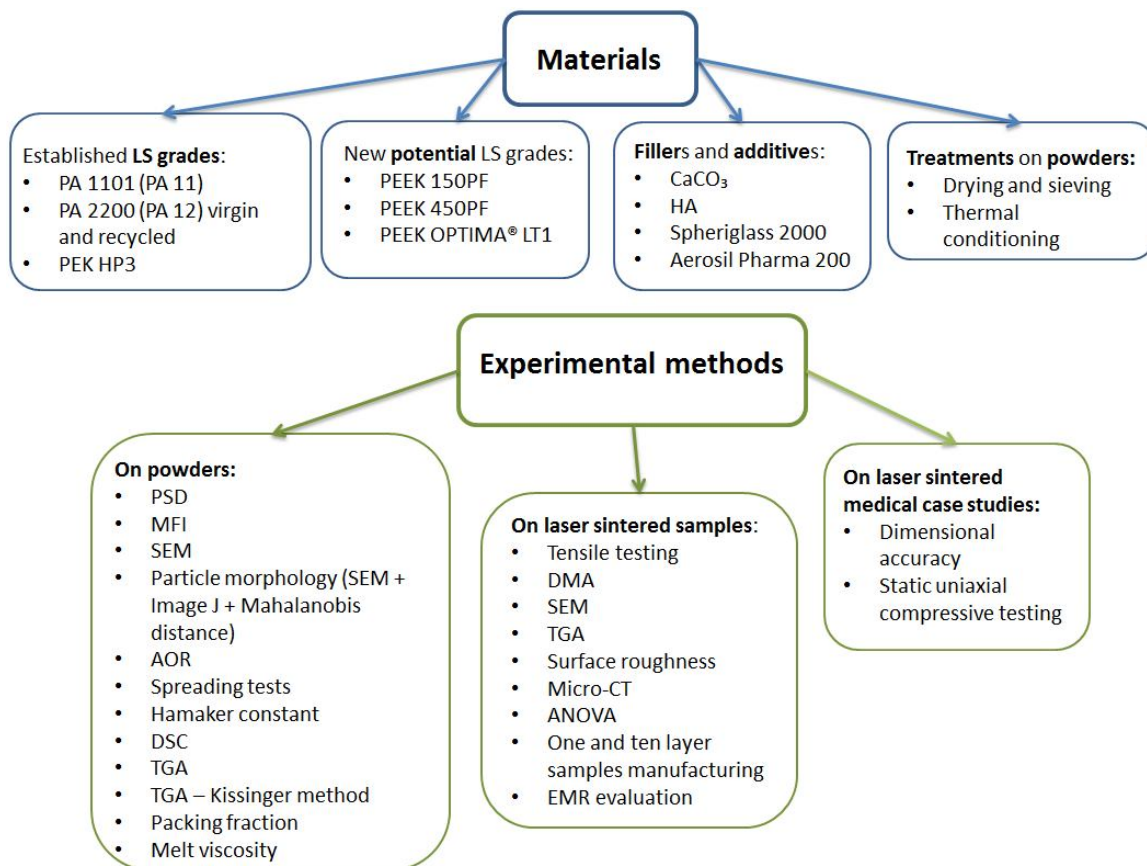
Figure 22. Summary of the materials and experimental techniques used in this research project (chapter 3)

4 Powder characterisation

The characterisation of the PEEK polymeric powders (material description provided in chapter 3.1) described in this chapter includes the analysis of the particle size distributions, the quantitative and qualitative study of the particle morphology characteristics and the flow performance (angle of repose and spreading performance). PEEK 150PF and 450PF powders have been tested and compared against well-established LS materials such as PA 2200 (low melting temperature LS grade) and PEK HP3 (high melting temperature LS grade). The strategies adopted for the optimisation of the flow properties of the powder particles are also supplied along with the experimental analyses and results obtained. A scheme of the structure of this chapter is shown in Figure 23.
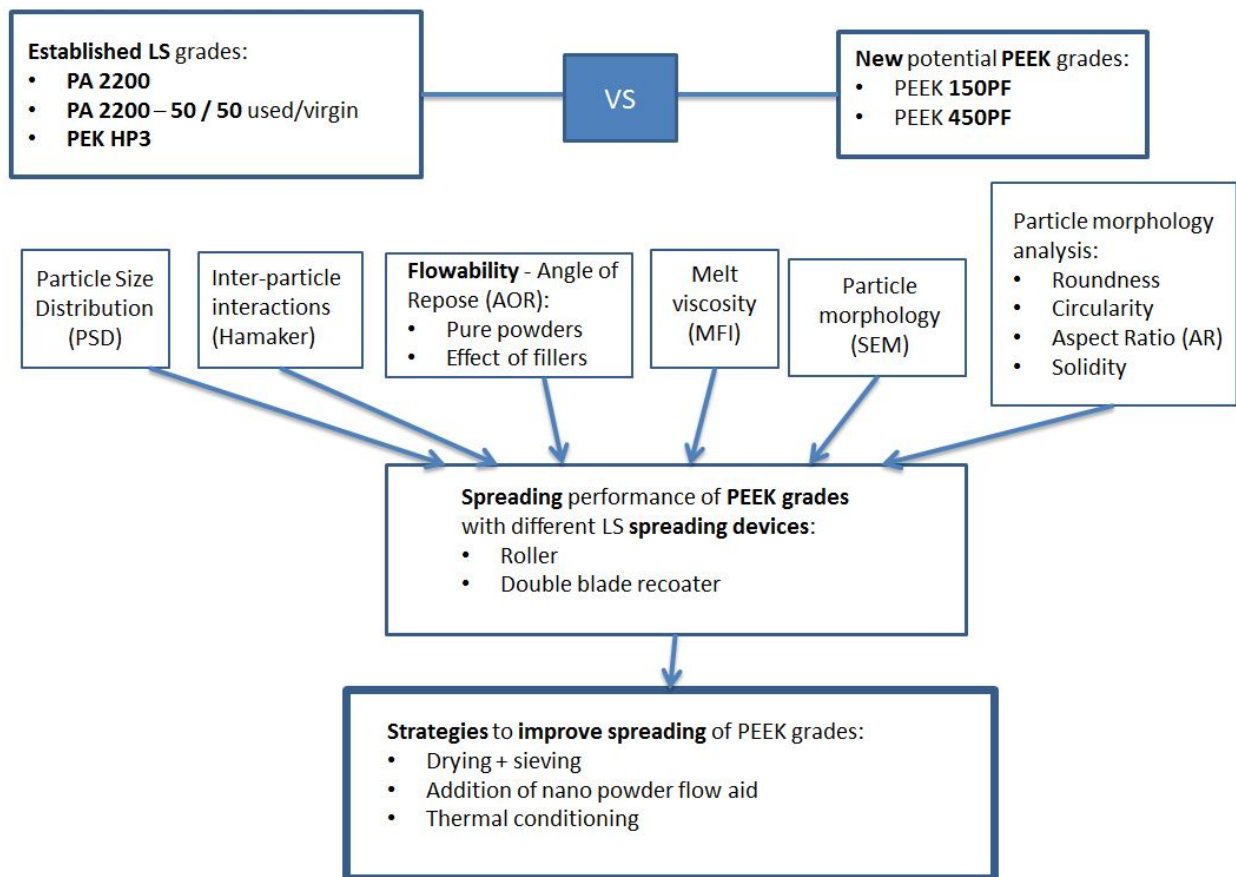
Figure 23. Structure of chapter 4: powder characterisation

4.1 Melt flow index

Melt Flow Index (MFI) indicates how viscous a polymeric molten material is. The smaller the MFI value is, the more viscous the polymer. The experimental results obtained for PEEK 150PF, PEEK 450PF and PEK HP3 are listed in Table 5.

Material	Testing temperature (°C)	MFI (g/10 min)
PEK HP3	395	10.73 ± 0.11
PEEK 450PF	365	1.83 ± 0.04
PEEK 150PF	365	27.92 ± 0.97

Table 5. MFI results of HT polymers, average values and standard deviations

PEEK 150PF shows the highest value of MFI, while PEEK 450PF the lowest. PEEK 150PF is therefore the least viscous polymers, while 450PF the most viscous. PEK HP3 has a value between the results of the two PEEK grades. The findings were found to be in agreement with the viscosity values provided by the materials manufacturer (Victrex, UK [2]). As discussed in chapter 2.2, material viscosity is known for playing a key role in particle sintering, particularly in LS. A low material viscosity is considered beneficial but if it is too low it becomes detrimental for part definition. Controversially, higher molecular weight and therefore higher viscosity has been proved to be responsible for higher mechanical performance of the laser sintered components [77, 192]. On the basis of these considerations, there is a smaller MFI difference between PEK HP3 and PEEK 450PF (9) than between PEK HP3 and PEEK 150PF (17). This finding could indicate that PEEK 450PF is more suitable than PEEK 150PF for optimisation in HT-LS for the case where the mechanical performance are required to be as high as possible. However, this is a preliminary result and further validation is provided in the following chapter of this research project (chapter 5.3).

The MFI test was carried out in order to check the viscosity of the material under test and in order to compare them against the established HT-LS grade PEK HP3. The MFI test also represents also a well-accepted industry viscosity tests.

4.2 Particle size distributions

The PSDs of the LS powders (HP3 PEK, virgin PA 2200 and 50/50 virgin/used PA 2200) and the PEEK grades (PEEK 450PF and 150PF) are reported in Figure 24.
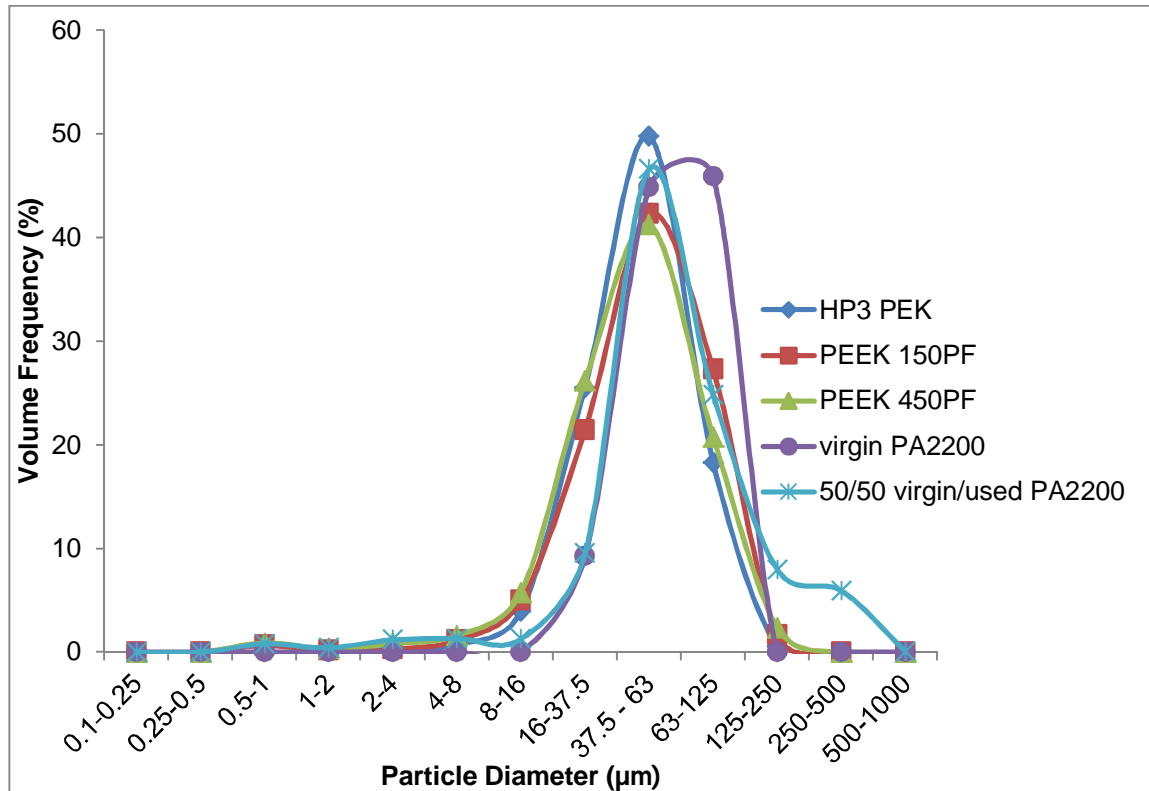
Figure 24. PSD of LS polymers and PEEK grades

PEK HP3 and both PEEK grades exhibit fairly similar PSDs, approximately covering the same diameter range. However, PEK HP3 shows a higher content of particles having a diameter in the 37.5-63 µm range. The PA 2200 curve is slightly shifted to the right (peak in the 63-125 µm range), indicating the presence of particles with larger diameters than the other grades. The PSD of 50/50 virgin/used PA 2200 was similar to that of the PAEK powders. PSD data for fillers used with PEEK 450PF are shown in Figure 25.
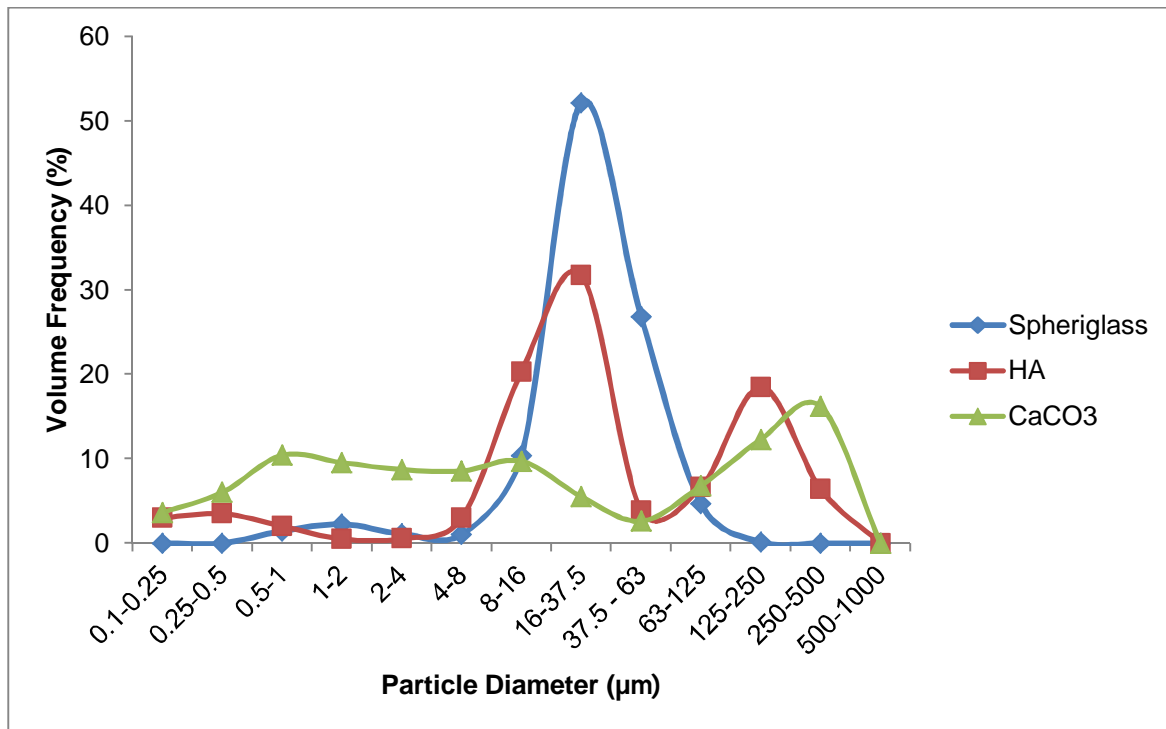
Figure 25. PSD of the filler materials

The powders show very different size distributions. Calcium carbonate ($CaCO_3$) shows fairly constant amount of particles along all the particle diameters. HA exhibits a bimodal distribution with peaks for diameters at which PEK and PEEK grades have a fewer amounts of particles. Spheriglass presents a similar PSD to those of PEEK materials, but with a higher content of smaller particles: this could be an advantageous property as a wider particle size range might allow a better compaction of the powder during the spreading stage in the LS process. Although the PSD test based on laser diffraction is largely used in the LS community, this technique hypothesises that the particles under test are spherical or nearly spherical. This condition is not necessarily true for new powdered materials. Therefore the results obtained with this method should be coupled with other analytical techniques such as optical imaging and flow characterisation tests.

4.3   Angle of repose

The Angle Of Repose (AOR) values of already optimised LS grades and PEEK powders are reported in Table 6.

Material	AOR (°)
Spheriglass 2000	23.6 ± 1.3
PA 2200	33.1 ± 1.5
PA 2200 50/50 used/virgin	38.4 ± 0.8
PEK HP3	42.4 ± 1.1
PEEK 150PF	47.4 ± 0.7
PEEK 450PF	52.8 ± 0.9

Table 6. AOR values (average and standard deviations) of LS optimised powders and PEEK grades

Spheriglass and PA 2220 exhibit the smallest values of AOR indicating a better flow performance. This is not surprising as Spheriglass was known to be composed by round particles having smooth surfaces, and PA 2200 has been already been optimised for LS. The AOR of the PA 2200 50/50 used/virgin, one of the most common PA refreshed blends currently used in LS manufacturing, was found to decrease slightly, indicating a reduction of the flow performance. This was an interesting finding for two reasons. Firstly, it allowed to broaden the values of AOR still leading to good flow behaviour. Secondly, it demonstrated that although the flowability decreased slightly, the powder retains good material properties that allows manufacture of good products used on market. Interestingly, the AOR test can distinguish virgin PA 2200 from blends containing a recycled fraction of powder. Hence this method could help to support in monitoring and managing powders within laboratories.

4.3.1 AOR of PEEK and fillers

Several studies [91, 125, 127-129] on new powders for LS discuss the incorporation of additives and fillers in order to improve the flow performance. In most cases, the addition of small quantities of fillers or additives seems to improve the overall flowability of the material blend under test. However, the mechanisms leading to such an improvement are not clearly discussed and no results are presented to justify the addition of a filler or an additive. With the aim to understand the role of

filler particles on the flowability of a powder material, three fillers have been added by dry mixing to PEEK 450PF, the grade exhibiting the lowest flow performance. It was believed that in this way the effect of fillers would have been more prominent than in already good-flowing materials such as PA 2200.

The blends under test and the results of the AOR are listed in Table 7.

Material	AOR (°)
PEEK 450PF+ 20% HA	49.2 ± 1.0
PEEK 450PF + 30% HA	50.4 ± 0.7
PEEK 450PF + 10% $CaCO_3$	50.3 ± 1.0
PEEK 450PF + 20% $CaCO_3$	49.4 ± 0.7
PEEK 450PF + 30% $CaCO_3$	48.2 ± 1.0
PEEK 450PF + 10% Spheriglass 2000	51.8 ± 0.8
PEEK 450PF + 20% Spheriglass 2000	50.0 ± 0.9
PEEK 450PF + 30% Spheriglass 2000	48.6 ± 1.7

Table 7. AOR (average values and corresponding standard deviations) of the blends of PEEK 450PF containing fillers at increasing concentrations by weight.

It was noticed (Table 7) that the incorporation of fillers helped the flow, although not very significantly. This effect is not only due to the type of particles added, but also to their concentrations. The overall flow improved with increasing amounts of calcium carbonate and Spheriglass in the blends. Higher contents of HA particles instead did not lead to better flow performance.

It is believed that, depending on the particle size, the fillers can enhance the flow performance of the PEEK 450PF in two ways. Firstly, when the additive particles have a similar particle size as the host powder but rounder shapes and smoother surfaces, the host polymeric powder can flow better thanks to the presence of these additional particles that trigger the flow. Secondly, when the fillers instead exhibit such small particles that they can fill in the spaces between the superficial flakes and fibrils and the main body of the host particles, the additive particles make the host particles overall rounder and therefore can flow better.

Adding the Spheriglass particles to PEEK 450PF caused a slight decrease in the AOR value and therefore an increase of the flowability. Similarly, the addition of HA particles to PEEK 450PF improved the flow property only at the lowest concentration (20%). This could be due to the complex surface structure of the HA particles, which instead of facilitating reciprocal sliding of the particles caused more inter-particle mechanical locking due to high surface roughness. In both cases, glass and hydroxyapatite, it was surprising to see that these particles although round do not necessary help the flow in spite of their high concentrations in the mix. Interestingly, the addition of $CaCO_3$ powder makes the polymeric powder flow best. It is then possible to say that both the adjoining smooth and round particles (Spheriglass) but with size comparable to the one of the PEEK 450PF and the incorporation of smaller and rounder particle (HA and $CaCO_3$) slightly improved the flow.

4.4   SEM imaging

The results of the SEM imaging have been divided into well-established LS grades, new potential PEEK grades and PEEK blends.

4.4.1   SEM of the LS optimised grades

The particle morphology of virgin PA 2200 and PA 2200 50/50 virgin/used at increasing magnifications are reported in Figure 26 and Figure 27, respectively. In both grades, the particles look circular or slightly elongated. The surfaces are significantly smooth, however a high magnification allowed to show the presence of cracks. As these superficial fractures were found in both grades, PA 2200 virgin and 50/50 virgin/used PA 2200, they were not considered detrimental. PA 2200 represents a well-established LS material, therefore its morphology was used as one of the benchmark materials for the potential HT PEEK powders.
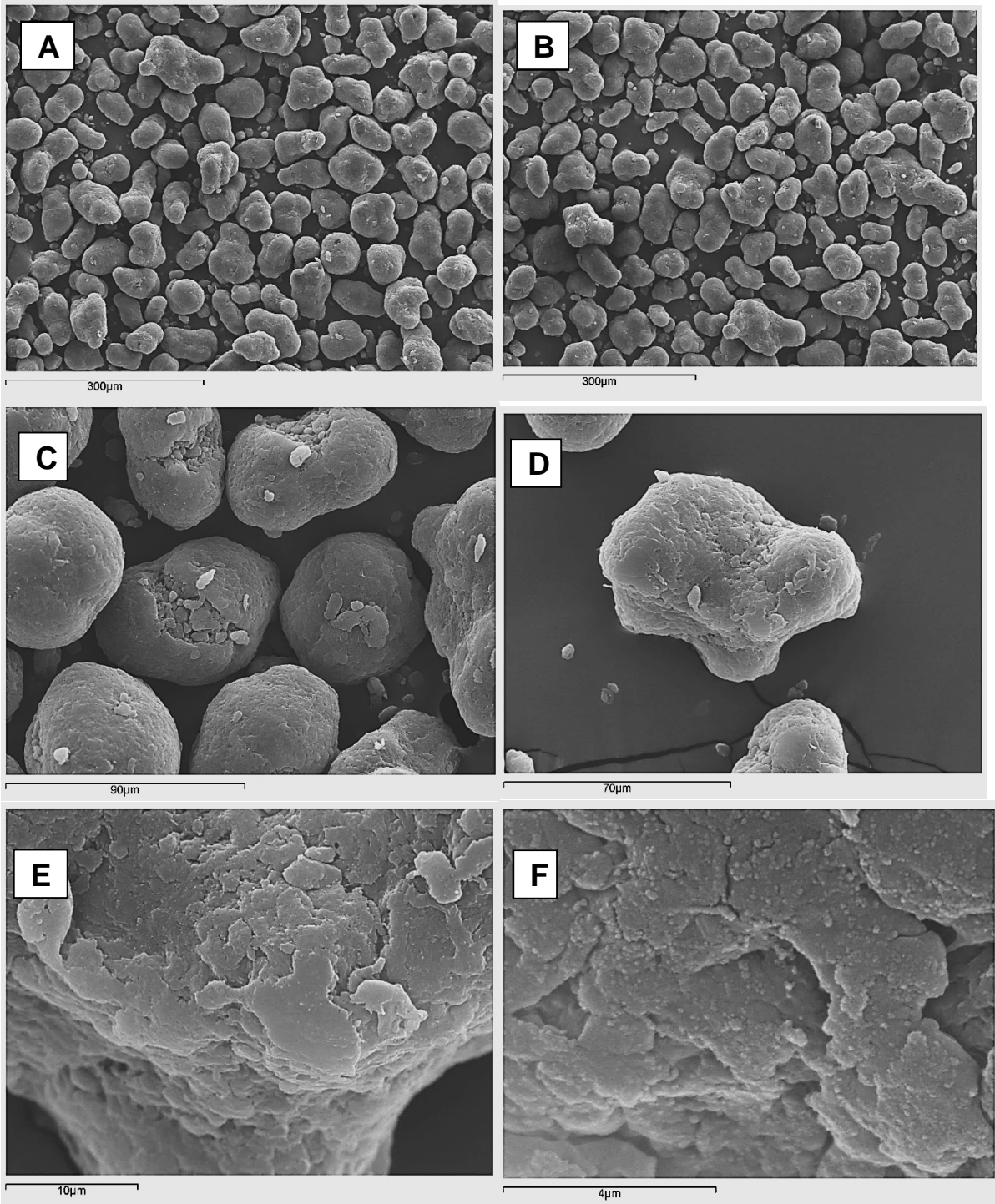
Figure 26. SEM images of virgin PA 2200 particles, at increasing magnification
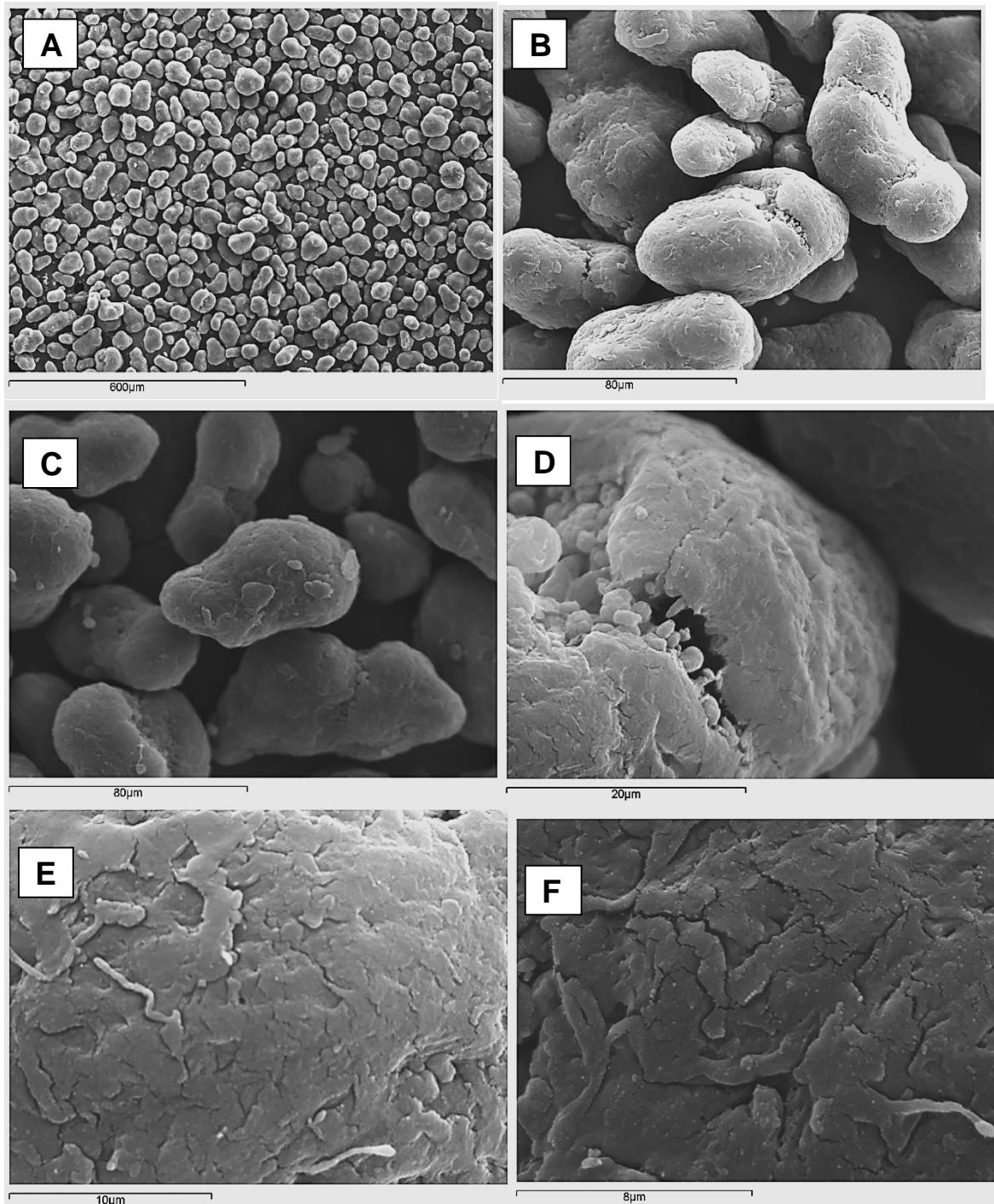
Figure 27. SEM images of PA 2200 50/50 virgin/used particles, at increasing magnification

The particles of the only commercial HT-LS optimised grade PEK HP3 are shown in Figure 28. The particles are not as round as the particles of both virgin PA 2200 and PA 2200 50/50 used/virgin grades. However, they exhibit smooth surfaces and fully dense structures at high magnification.
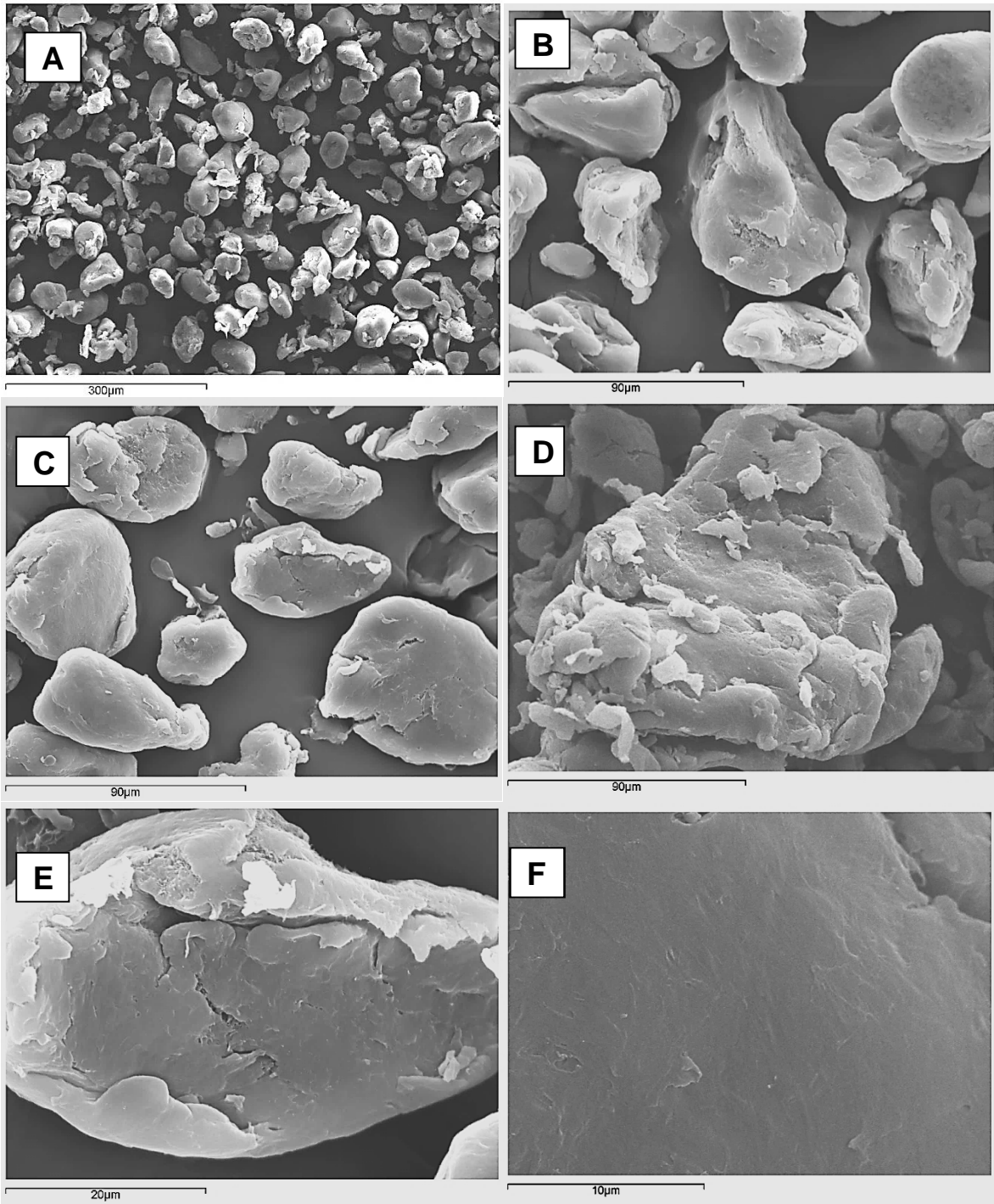
Figure 28. SEM images of PEK HP3 particles, at increasing magnification

4.4.2 SEM of new potential HT-LS PEEK grades

Particles of both PEEK grades (150PF and 450PF) are shown from Figure 29 to Figure 31.
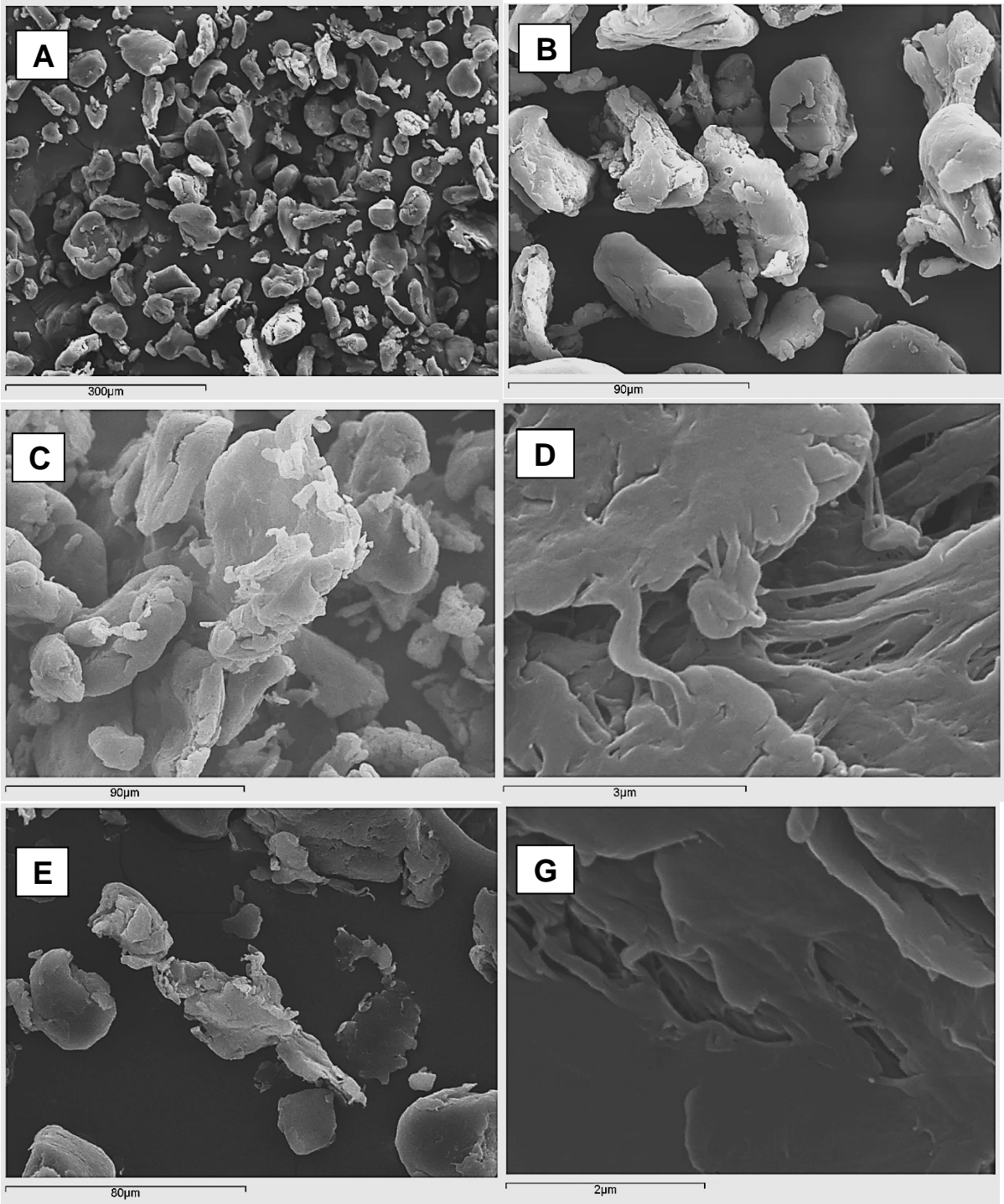
Figure 29. SEM images of PEEK 450PF at increasing magnification [193, 194]
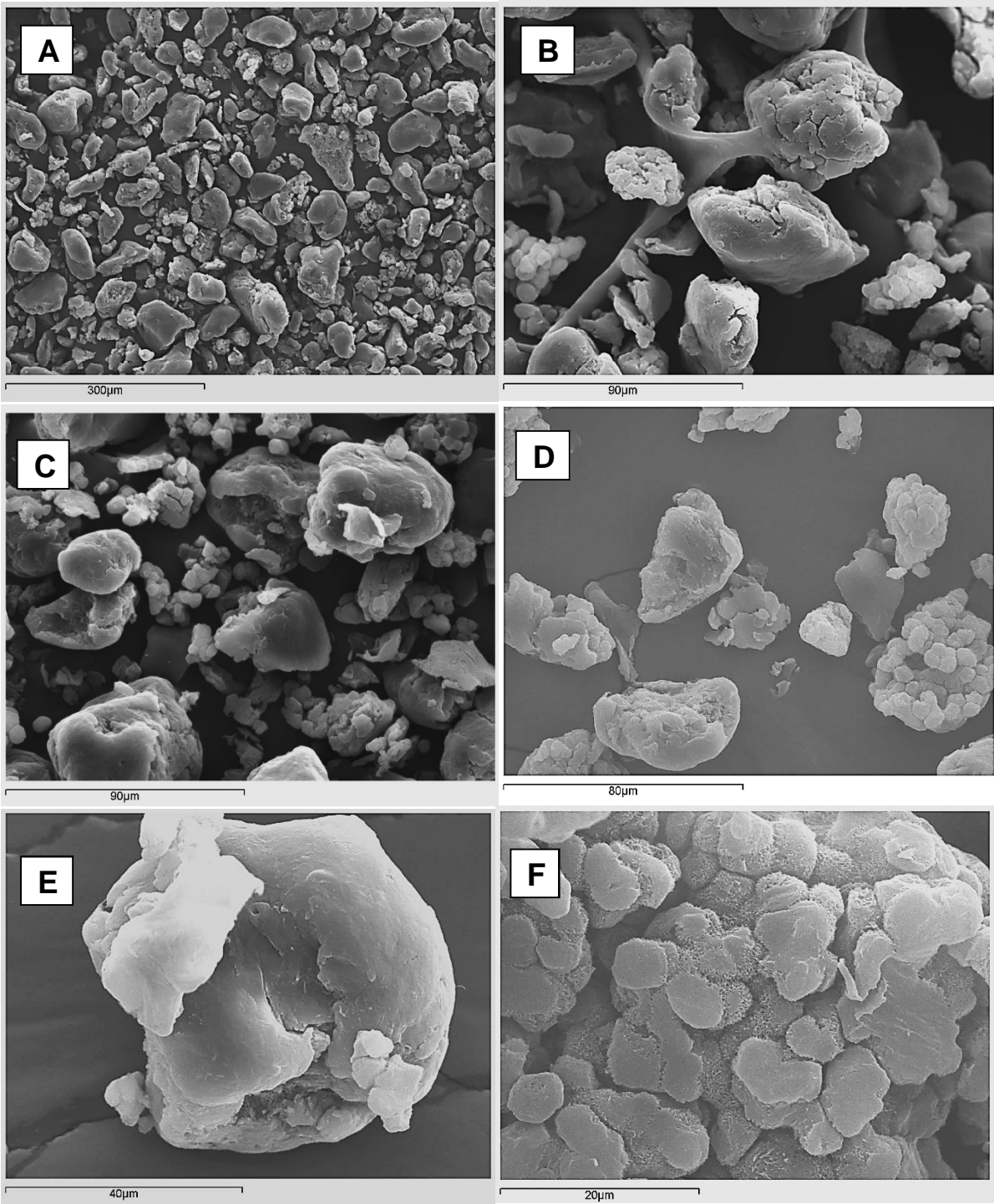
Figure 30. SEM images of PEEK 150PF particles, at increasing magnification. A-F
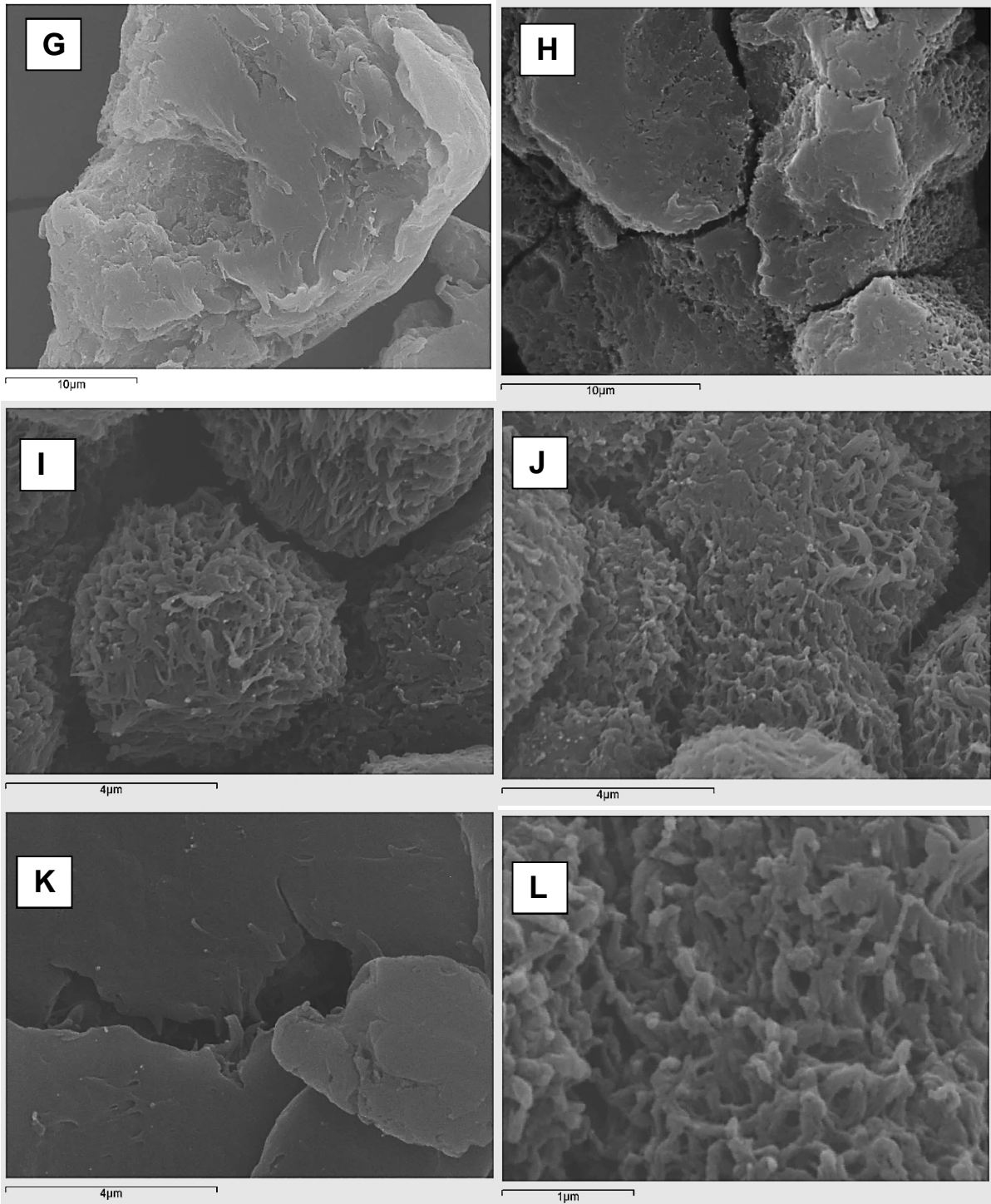
Figure 31. SEM images of PEEK 150PF particles, at increasing magnification. G-L

Figure 29 shows the particles of the PEEK 450PF grade. The particles exhibit an angular shape and are characterised by the presence of highly irregular flaky structures on the surfaces. These structures could cause mechanical interlocking between the particles in a flow scenario and therefore they could be the reason why

450PF showed the highest value of AOR. Interestingly, the location of these flakes and fibrils in respect to the main core of the particles might affect to some extent the evaluation of the shape descriptors used in the particle shape analysis and described in chapter 3.1.5. In other words, these surface irregularities might not be fully detected during the particle shape analysis in the case they do not lie on the external profile of the particles under test. An illustration of this test limitation is shown in Figure 32.
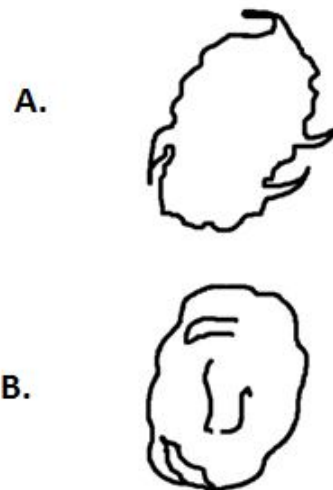
Figure 32. Particle surface features in SEM imaging and shape analysis: flakes that affect the shape descriptors (A) and flakes that do not affect the shape descriptors (B).While SEM imaging allowed fully detection of these surface irregularities, the shape analysis is limited by the outlining of the 2D external profiles of the particles

Furthermore, PEEK 450PF particles do not appear fully dense at high SEM magnification (Figure 29).

Figure 30 and Figure 31 show the particles of PEEK 150PF. It is interesting to note that this material includes two types of structures: the structure A, which is similar to the flaky particles (Figure 30 E) found in PEEK 450PF; and a structure B which is characterised by round protuberances composed by sub-structural fibrils (Figure 30 F). It is reasonable to believe that as the structure B appears rounder in shape at a larger scale, it is responsible for the better flow performance of PEEK 150PF when compared to PEEK 450PF, as outlined in the AOR results.

4.4.3 SEM of fillers

The SEM images of the particles of Spheriglass 2000 are shown in Figure 33. As expected, the particles were very round and presented highly smooth surfaces. It is not surprising why the AOR of this material was very low, indicating high free-flowing characteristics.
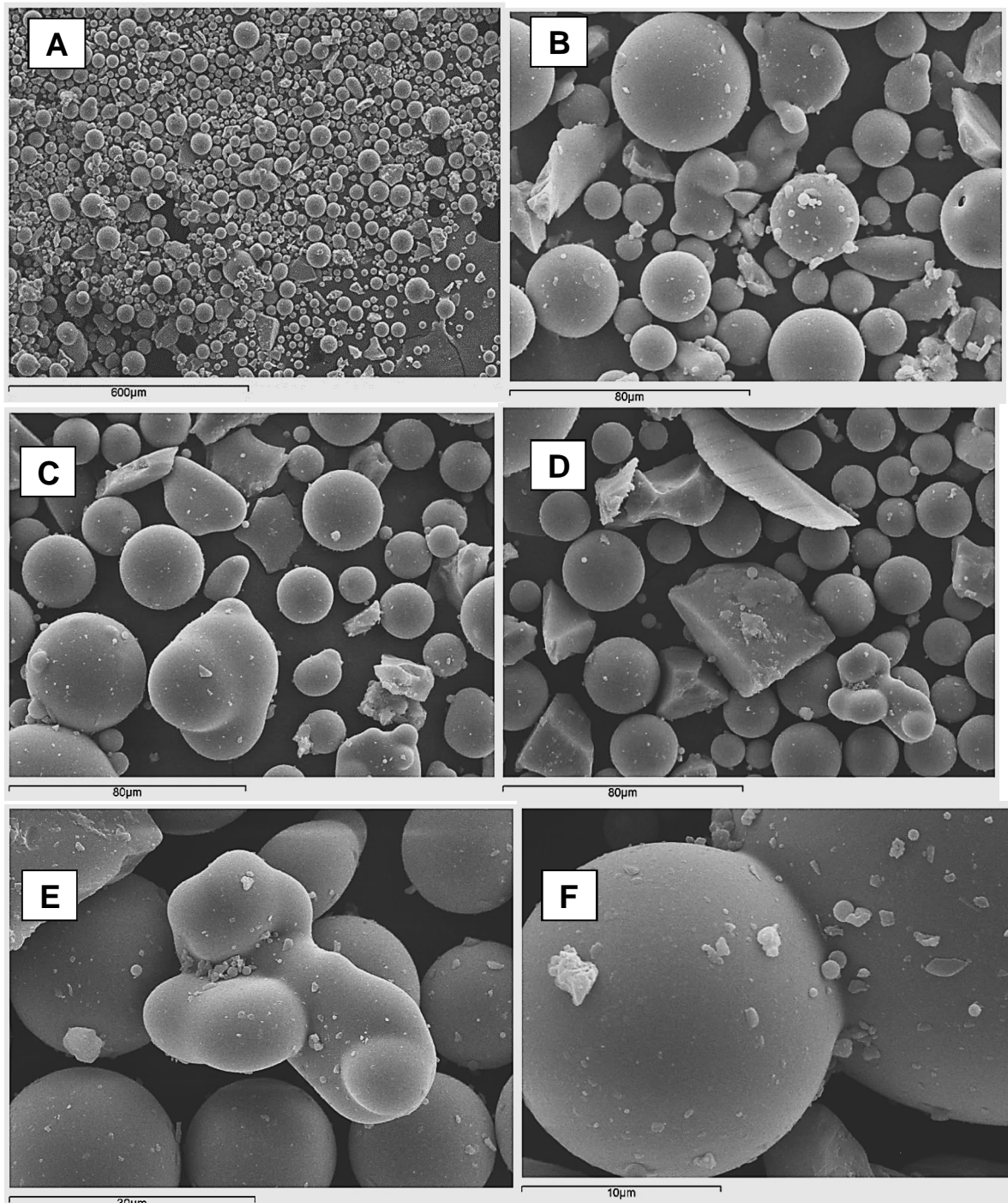
Figure 33. SEM images of Spheriglass 2000 particles, at increasing magnification

SEM images of the CaCO$_3$ particles are shown in Figure 34. The particles appear smaller than PEEK 450PF particles and exhibit complex surfaces at high SEM magnification. Interestingly, their overall shape is acceptably round.
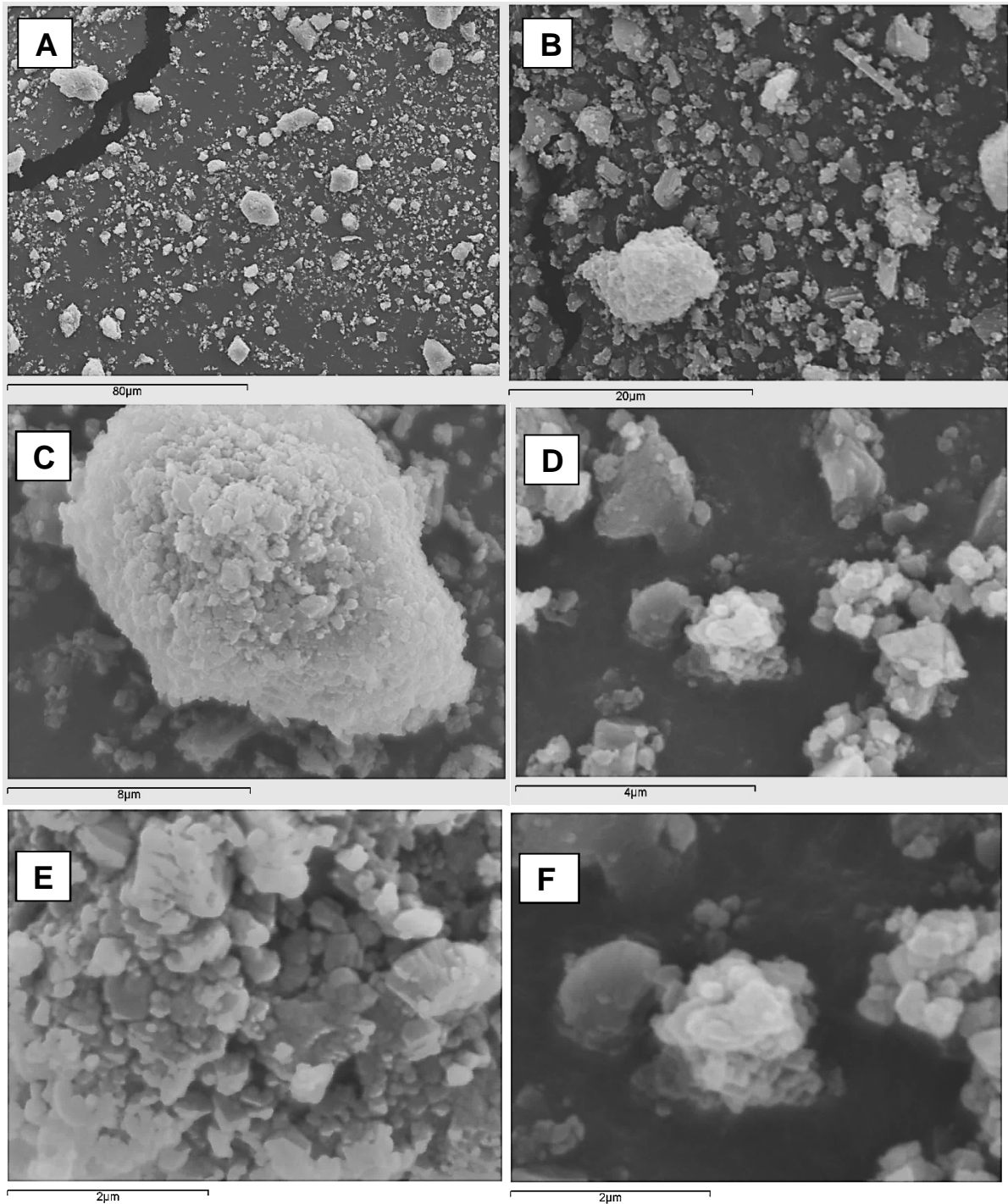
Figure 34. SEM images of CaCO$_3$ particles, at increasing magnification

The SEM images of the HA particles are shown in Figure 35. HA particles are round with complex Nano-structures and similar size of PEEK particles.
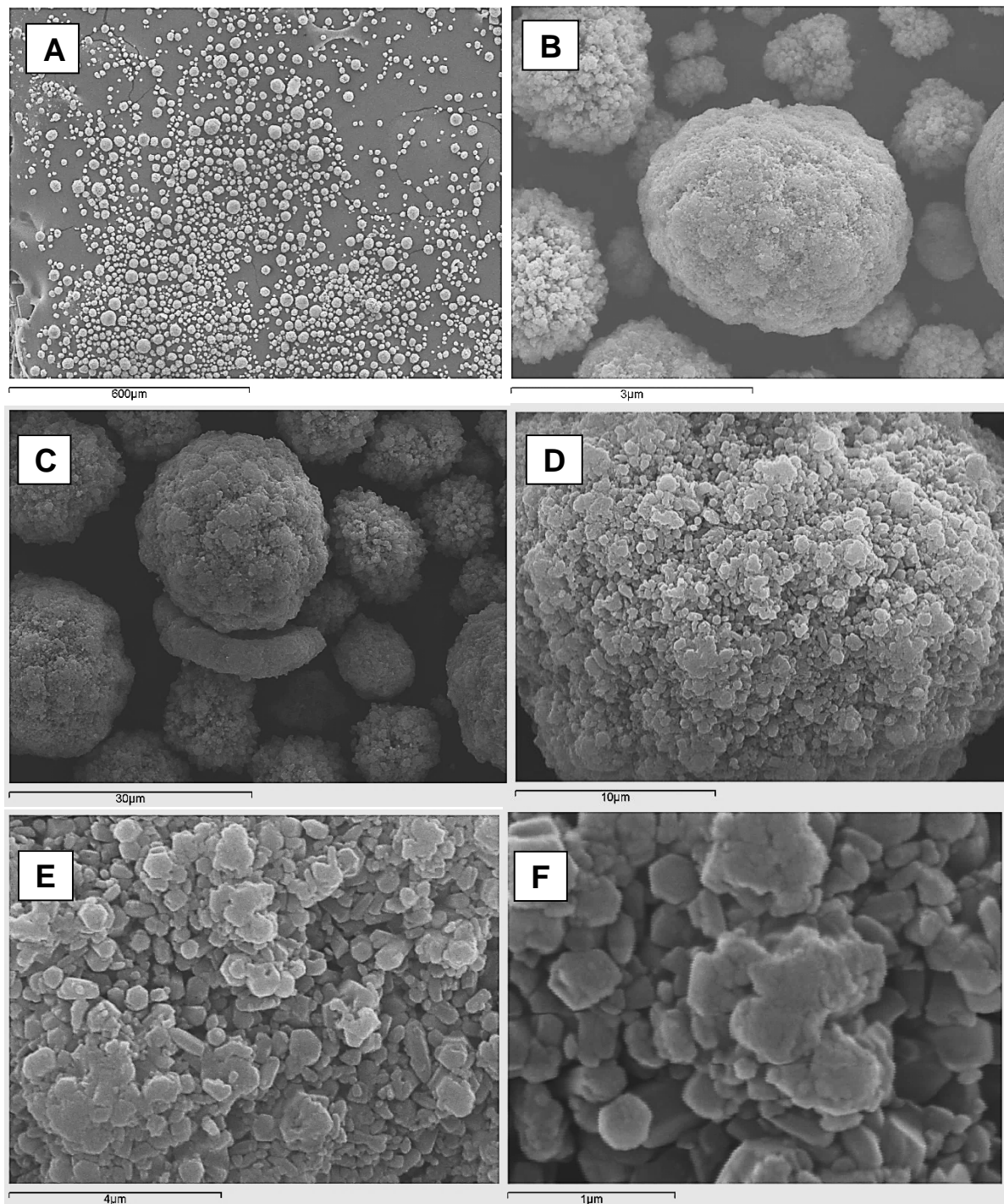
Figure 35. SEM images of HA particles, at increasing magnification

4.4.4 SEM of PEEK blends

Images of the blends of PEEK 450PF with HA, CaCO$_3$ and Spheriglass are shown from Figure 36 to Figure 38, respectively. HA particles appear round and of similar size of PEEK 450PF. Therefore the blend PEEK-HA allowed isolating the effect of the different particle shape on the overall flow performance.
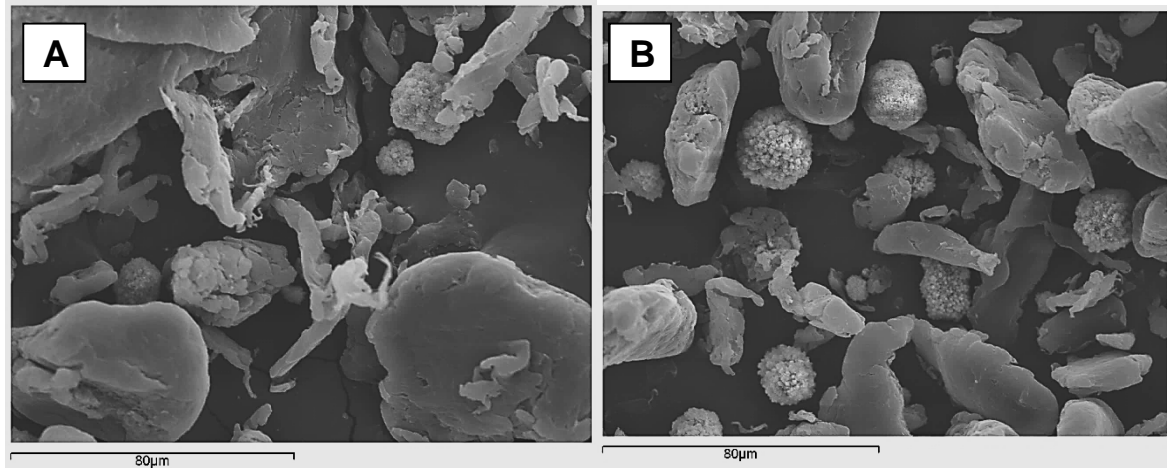
Figure 36. SEM images of HA-PEEK 450PF, at increasing magnification

Figure 36 shows round HA particles between PEEK particles. As seen in the AOR results, the presence of HA particles help the flow of the overall PEEK blend. HA particles seem to trigger the flow of the angular PEEK units, overcoming to some extent the mechanical interlocking occurring when there are PEEK 450PF particles only.

The CaCO$_3$ particles with the PEEK 450PF particles are shown in Figure 37. Clearly the CaCO$_3$ particles are considerably smaller than the PEEK 450PF elements. This property allowed isolating the effect of the size on the flow performance of a blend.
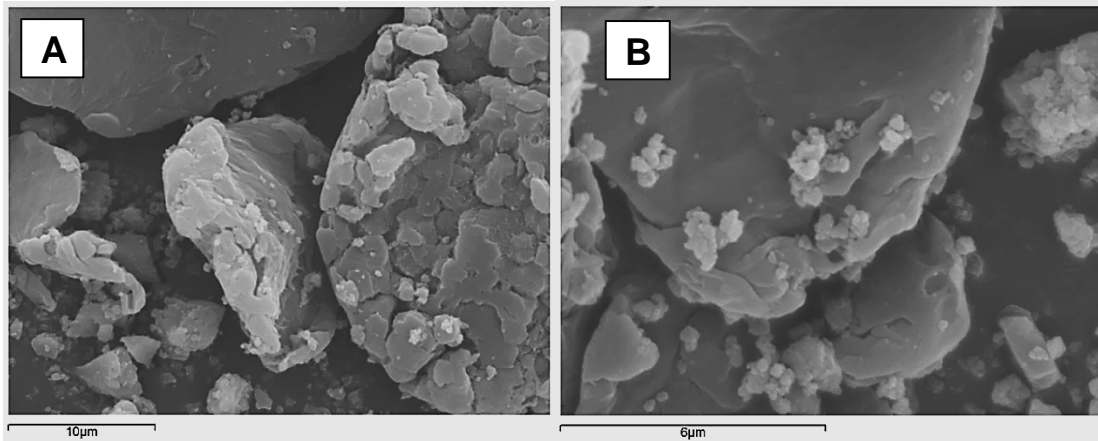
Figure 37. SEM images of CaCO$_3$-PEEK 450PF, at increasing magnification

Interestingly, the smaller particles of CaCO$_3$ are located in the empty spaces created by the flakes on the surfaces of the PEEK 450PF particles, filling in the gaps. Filling gaps of the PEEK particles might make the PEEK particles rounder overall, which then tend to flow better as seen in the results of the AOR test. The Spheriglass particles mixed with PEEK 450PF particles are shown in Figure 38.
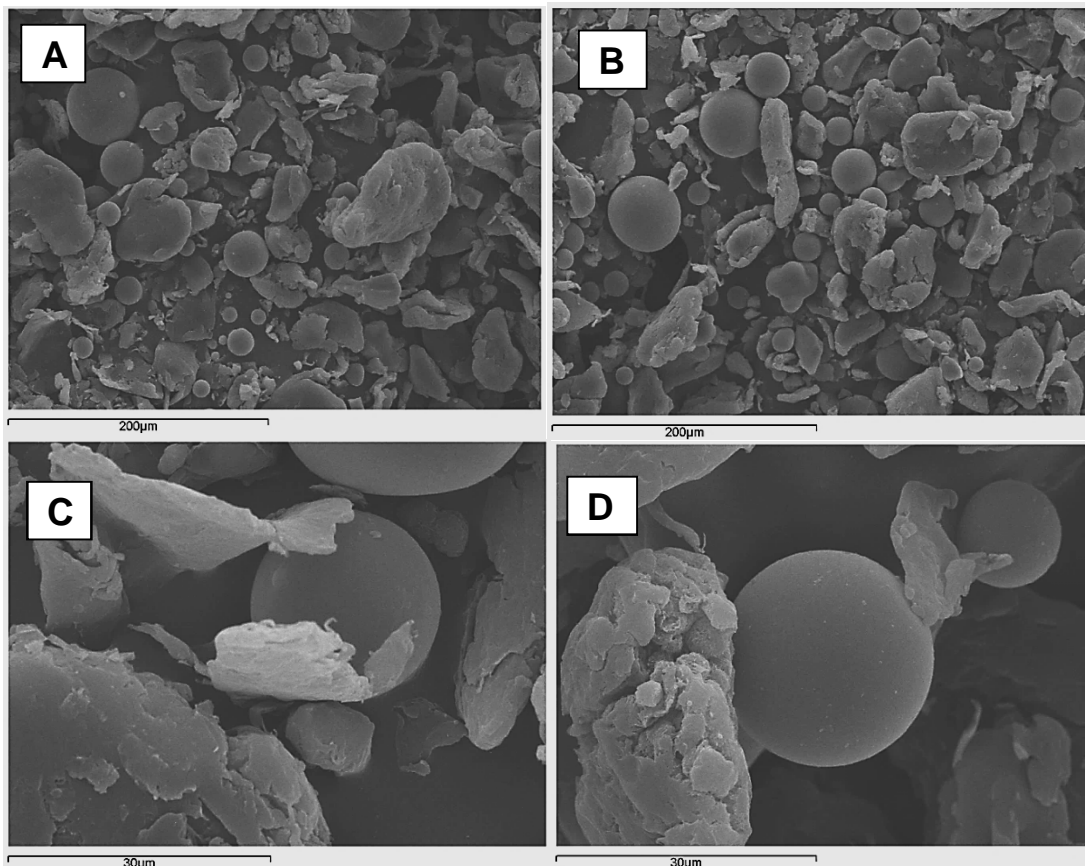
Figure 38. SEM images of Spheriglass 2000 - PEEK 450PF, at increasing magnification

Spheriglass particles and PEEK 450PF particles appeared of similar size. Also in the case of PEEK 450PF- Spheriglass blend the AOR showed a decrease, a sign of improved flow behaviour. This mechanism could be explained by observing Figure 38 C-D. The round Spheriglass particle with smooth surface is located between two irregular and fairly sharp PEEK 450PF particles, acting as interspacing. This condition could help the flow behaviour by triggering the overall blend flow and reducing particle interlocking between the PEEK particles.

4.5 Particle shape analysis

The particle shape descriptors of circularity, roundness, AR and solidity have been evaluated for virgin PA 2200, 50/50 virgin/used PA 2200, HP3 PEK, PEEK 450PF and 150PF. The mean values obtained and their standards deviations are reported in Table 8.

Material	Circularity	AR	Roundness	Solidity
PA 2200 virgin	0.77 ± 0.11	1.51 ± 0.33	0.69 ± 0.14	0.93 ± 0.03
PA 2200 50/50 virgin/used	0.81 ± 0.11	1.54 ± 0.35	0.68 ± 0.14	0.94 ± 0.03
PEK HP3	0.61 ± 0.18	1.82 ± 0.73	0.61 ± 0.18	0.86 ± 0.09
PEEK 450PF	0.53 ± 0.19	2.00 ± 0.84	0.57 ± 0.18	0.83 ± 0.10
PEEK 150PF	0.60 ± 0.19	1.72 ± 0.61	0.63 ± 0.17	0.86 ± 0.09

Table 8. Particle shape descriptors: average values and standard deviations

Both grades of PA 2200 show the highest values of circularity, roundness and solidity and smallest value of AR, suggesting that the particles from this grades are round, circular, fairly equiaxial and regular (not equipped with flakes and fibrils on their surfaces). PEK HP3 and PEEK 150PF exhibit similar values of circularity, roundness and solidity, which are all lower in comparison with the values of PA 2200. Therefore, PEK HP3 and PEEK 150PF powders comprise slightly less round, less circular and less regular particles than the PA 2200 grades. The lowest values of circularity, roundness, solidity and the highest value of AR occur for PEEK 450PF, implying then the presence of sharper, elongated and irregular particles.

The graph showing circularity values plotted (Y axis) against roundness values (X axis) is often used in the particle technology community in order to understand the relationship between these two descriptors and better visualise the particles under test. This graph is shown in chapter 3.1.5 in Figure 11. The graph of circularity plotted against roundness allows identifying more easily: round and spherical particles (simultaneous high values of circularity and roundness), nearly elliptical particles (low values of circularity and high values of roundness), sharp overall circular shapes (high value of circularity and low value of roundness) and sharp and elongated shapes (low values of both circularity and roundness).

The circularity-roundness diagram obtained after the application of the Mahalanobis distance (chapter 3.1.6) for the virgin PA 2200 and PA 2200 50/50 virgin/used materials is shown in Figure 39.
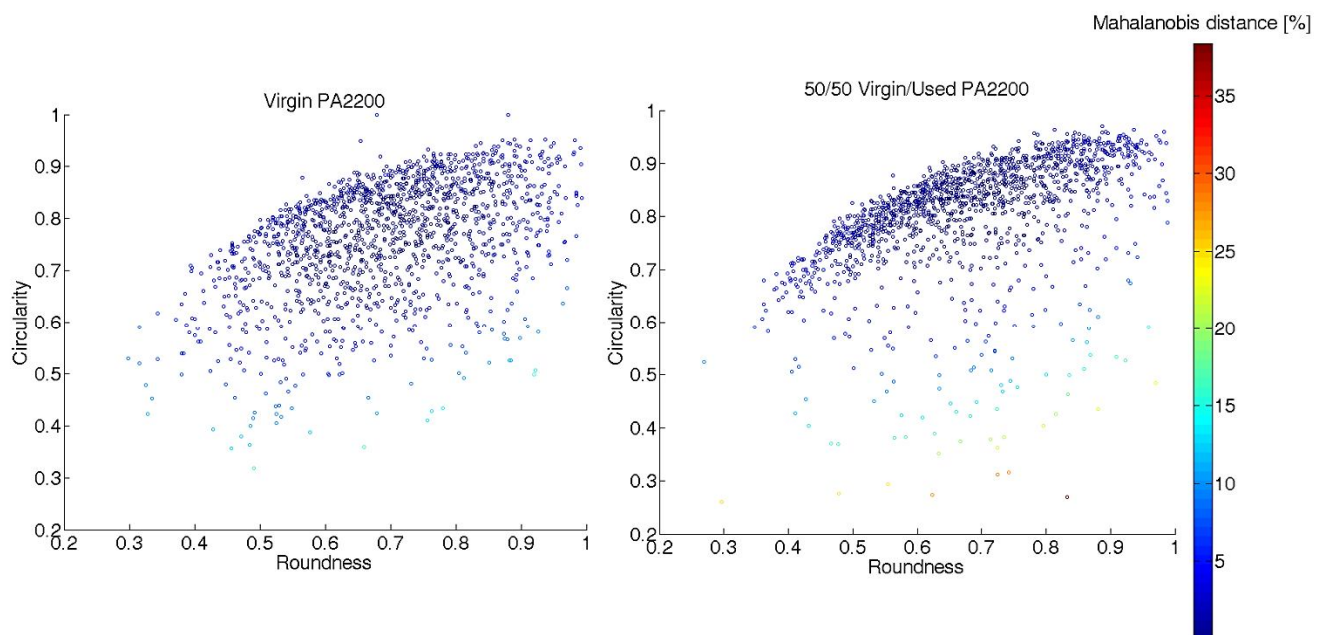
Figure 39. Roundness and circularity of the PA 2200 powders with the application of the distance descriptor Mahalanobis distance

Virgin PA 2200 and 50/50 virgin/used PA 2200 exhibit datasets centred at high simultaneous values of circularity and roundness. Therefore most particles are confirmed to be round and nearly spherical. It is interesting to notice that particles in the 50/50 virgin/used PA 2200 are less widespread than in the virgin PA 2200 virgin,

indicating a higher circularity and roundness of the particles of the recycled blend. In other words, the 50/50 virgin/used PA 2200 has better powder morphology qualities.
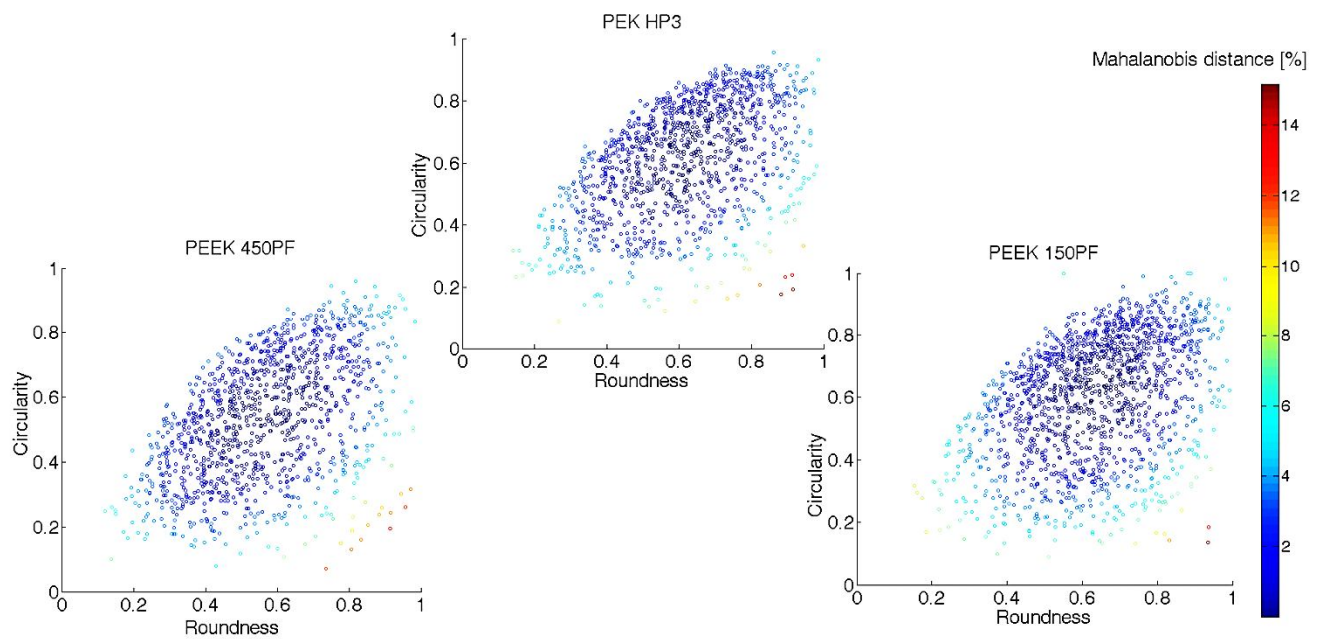
Figure 40. Circularity and roundness diagram of PAEK grades with application of the distance descriptor, Mahalanobis distance.

The circularity-roundness diagram obtained for the PAEK polymers after the application of the Mahalanobis distance is shown in Figure 40. The HP3 PEK dataset is centred at middle high values of roundness and circularity, though the data appears more spread towards lower values than in PA 2200 grades. PEEK 150PF shows similar results, but slightly shifted towards lower values of circularity. PEEK 450PF shows a data distribution centred just over middle high values of roundness and circularity, indicating a smaller proportion of particles with high values of roundness and circularity compared to PEK HP3 and PEEK 150PF. In order to outline the findings obtained with the Mahalanobis distance, the centroids of the distributions of each material are reported in Figure 41.
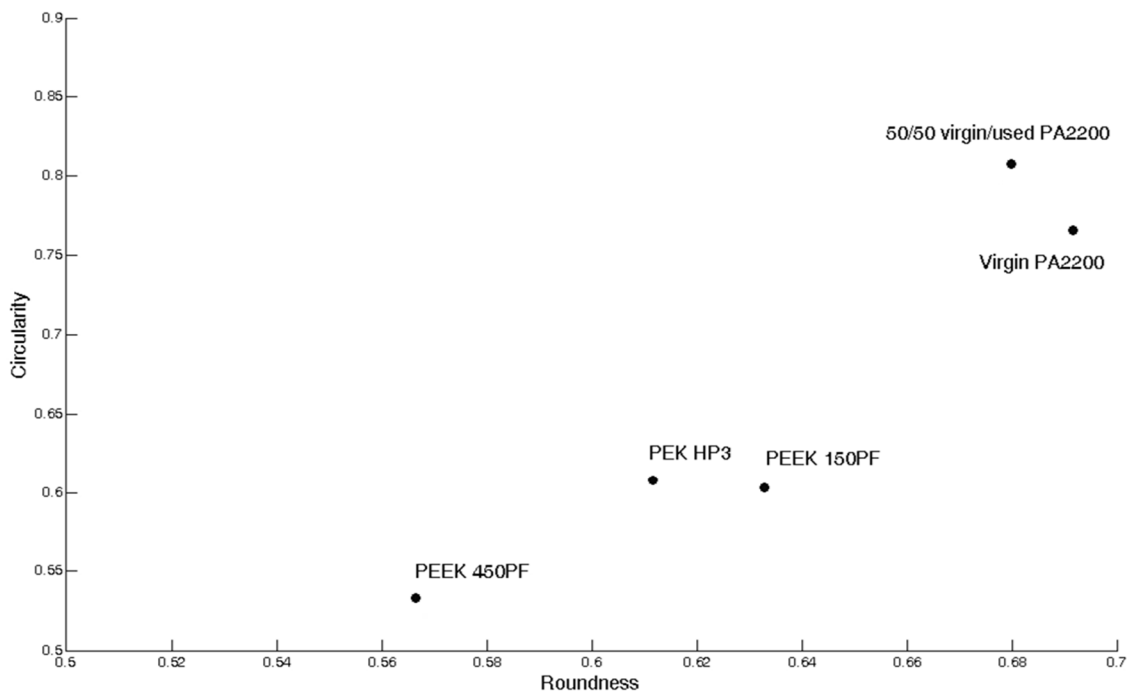
Figure 41. Circularity-roundness diagram of the centroids of the datasets of: virgin PA 2200, 50/50 virgin/used PA 2200, PEK HP3, PEEK 150PF and PEEK 450PF. Centroids evaluated by application of the Mahalanobis distance

The particles of the 50/50 virgin/used PA 2200 and the virgin PA 2200 are the most circular and round and have centres above circularity of 0.7 and roundness of 0.69. The centres of PEK HP3 and PEEK 150PF are located above 0.6 for both circularity and roundness, while the centre of the PEEK 450PF particles is at approximately 0.56 for both circularity and roundness. PEK HP3 and 150PF are fairly round and spherical. PEEK 450PF particles, as seen in the SEM results, are more elongated and sharp than the particles of all the other grades.

Data distributions of the AR of the LS grades and PEE K powders are reported in Figure 42 and Figure 43.
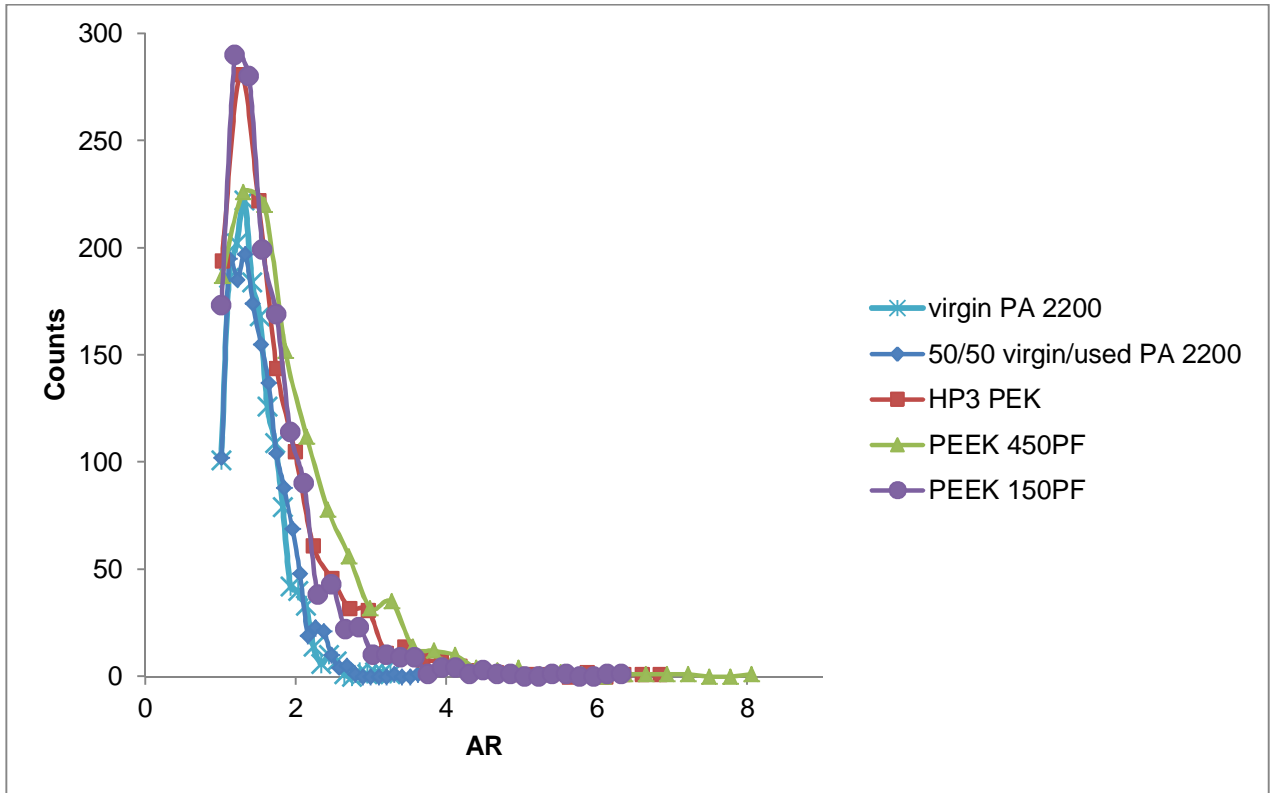
Figure 42. Shape descriptor AR of LS grades and PEEK powders
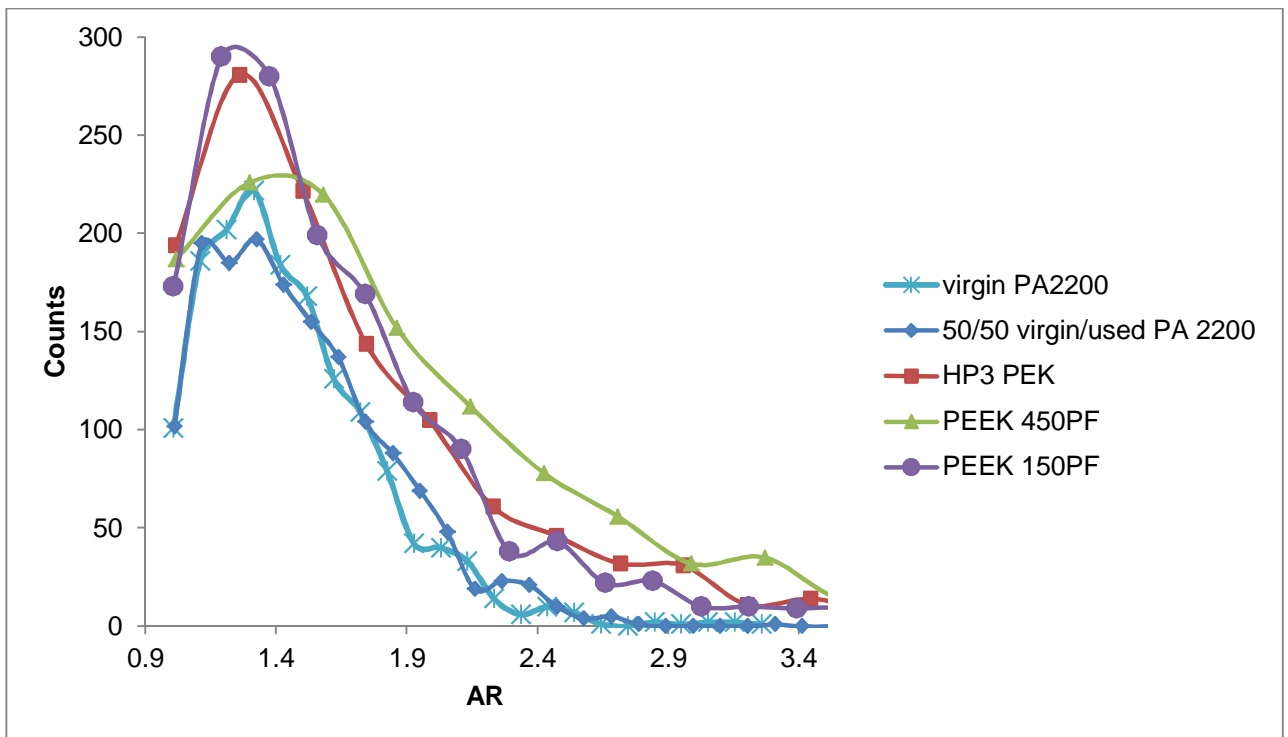
Figure 43. Shape descriptor AR of LS grades and PEEK powders - zoom in

Both PA 2200 grades exhibit the narrowest AR distribution among all the materials with values spread between 1.2 and 3.6. More precisely, the highest frequency is slightly over 1.3 indicating that the majority of the particles are circular or slightly elongated. HP3 and PEEK particles show fairly similar distributions, with higher aspect ratio than the PA 2200 grades. PEEK 450PF powder covers higher values of AR, up to 8 (Figure 42), indication the presence of highly elongated particles.

The experimental results of the descriptor solidity of the LS materials and PEEK grades are shown in Figure 44.
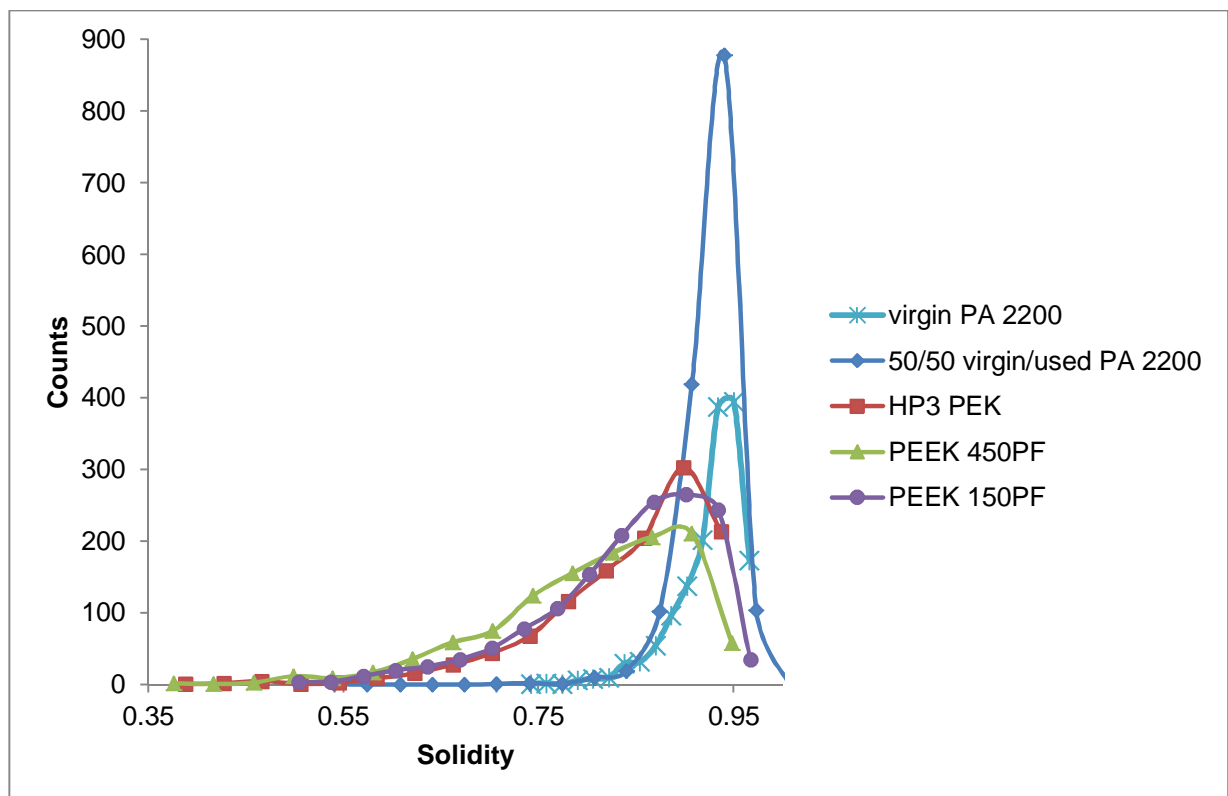
Figure 44. The shape descriptor solidity for LS materials and PEEK powders

Again the PA 2200 grades exhibit the narrowest distribution located at higher values of solidity, followed by PEK HP3, PEEK 150PF and PEEK 450PF. This is not surprising considering the morphological characteristics noticed in 4.4.2. The PEEK and PEK particles are rougher, less round and less circular. It is interesting to notice

that 50/50 virgin/used PA 2200 used shows higher values of solidity, confirming again the better particle morphology of this material over the virgin PA 2200 grade.

4.6   Hamaker constant evaluations

The Hamaker constant (A) is a parameter that evaluates the entity of attractive forces between particles by taking into consideration the chemo-physical properties and sizes of the particles under test. The lower the Hamaker constant, the smaller the inter-particle forces and in this specific case the better the particles will flow. The values of the refractive indices and dielectric constants used for the evaluation of the Hamaker constant were found in the literature and are reported in chapter 3.1.7. The results obtained for the pure materials and PEEK 450PF blends are reported in Table 9 and Table 10, respectively.

Materials (in air)	A (J)
PEEK-PEEK	1.26 E-19
PA 12 - PA 12	7.65 E-20
Spheriglass -Spheriglass	7.44 E-20

Table 9. Hamaker constant of pure materials [193]

Mixtures (in air)	A (J)
HA - PEEK	1.18 E-19
CaCO$_3$ - PEEK	1.06 E-19
Spheriglass – PEEK	9.67 E-20

Table 10. Hamaker constant of powder blends [193]

Spheriglass and PA 2200 show the lowest value of Hamaker constant indicating better flow performance (smaller inter-particle interactions), confirming the findings found in the AOR test. Considering the blends, Spheriglass and PEEK exhibit the smallest A value, followed by CaCO$_3$-PEEK and HA-PEEK. These results are also in agreement with the findings of the AOR test.

The effect of viscosity (PEEK 150PF and 450PF have different melt viscosity characteristics) on the dielectric constants and refractive indices measurements has not been considered here, one literature value [165, 168] has been used for the calculation of the Hamaker constants for PEEK and PEEK blends.

The evaluation of the Hamaker constant aimed to explain some of the differences found in the powder flow behaviour on the basis of the materials' chemical and physical properties. The effect of an increasing temperature, as experienced during LS processing, on the dielectric constant values and the refractive indices was then not considered in this analysis. In other words, dielectric constant values and refractive indices might change with the material's temperature and the testing temperature. However, this was not one of the reasons of the evaluation of the Hamaker constant. The calculation of this parameter was carried out in order to understand the role of intrinsic material properties on the powder flow behaviour and the differences found in the AOR results at room temperature.

4.7   Spreading test

The flow performance of powder material is a property that is affected by wide range of factors that not only include material properties and testing environment but also the testing technique and the final application set up. In order to final asses the performance of the materials in real LS equipment conditions, spreading tests in two LS systems were carried out using two powder spreading devices, an counter-rotating roller and a double blade recoater.

4.7.1   Spreading test of PAEK materials at room temperature

The results of the tests of PAEK powders carried out in the PA LS system Sinterstation 2000 (3D Systems, US [124]) and in the HT-LS system, EOSINT P 800 (EOS, Germany [1]) are shown, layer per layer and for each material, from Figure 45 to Figure 48 (see Appendix 9.1 for layers 3-5 and 7-9). As explained in chapter 3.1.8, the two systems are equipped with a different spreading device: a counter-rotating roller in the Sinterstation 2000 and a double blade recoater in the EOSINT P 800. The purpose of this experimental test was to assess the effect of the spreading

device on the spreading performance of the HT polymeric powders in the real LS equipment. PAEK powders were spread over a base composed of used PAEK powder (15 mm thick) as indicated in the EOS guidelines for HT-LS manufacturing. The PAEKs powders are pale yellow or nearly white in colour and were spread over a powder base which is of darker colour. The description of this test is explained in chapter 3.1.8.

EOSINT P 800

PEK HP3   PEEK 450PF   PEEK 150PF

SINTERSTATION 2000

Figure 45. Spreading test of HT PAEK polymers PEK HP3, PEEK 150PF and 450PF, within the Sinterstation 2000 (spreading tool: counter-rotating roller) and the EOSINT P 800 (spreading tool: double blade recoater) at room temperature. Layer 1

Figure 45 shows the first layer of all the powders (PEK HP3, PEEK 150PF and PEEK 450PF) over the powder base. This first layer appears not uniform for all the materials under test and in both systems, EOSINT P 800 and Sinterstation 2000. In particularly, PEEK 450PF shows deep scratches (see arrows) in the powder bed. PEEK 450PF particles were found to exhibit the lowest values of circularity, roundness and solidity, and the highest values of AR than the other powders

(chapter 4.5). The findings of the powder morphology analysis affect therefore both AOR behaviour and spreading performance in the LS systems.

Figure 46. Spreading test of HT PAEK polymers, within the Sinterstation 2000 and the EOSINT P 800 at room temperature. Layer 2

Figure 46 shows the second layer of fresh powders spread over the powder base for all materials in both systems. Both PEEK 150PF and 450PF exhibit deep lines in the powder bed when spread within the EOSINT P 800 system (see arrows). The materials start to cover a bigger area of the powder bed when spread in the Sinterstation 2000. This result indicates a higher spreading performance of the powders in the Sinterstation 2000 system, likely due to the counter-rotating roller device. This spreading tool might lead to higher spreading performance by applying a pressure on the powder bed when depositing a new layer of powder. This action could, to some extent, reduce the irregularities in the powder bed introduced by the elongated and interlocked particles.

PEK HP3   PEEK 450PF   PEEK 150PF

SINTERSTATION 2000

Figure 47. Spreading test of HT PAEK polymers within the Sinterstation 2000 and the EOSINT P 800) at room temperature. Layer 6

In Figure 47, PEK HP3 shows a uniform and homogenous spreading performance over the powder bed in both EOSINT P 800 and Sinterstation 2000 systems. Similarly to PEK HP3, PEEK 150PF exhibits good spreading performance in the Sinterstation 2000 and EOSINT P 800, while PEEK 450PF still does not appear uniformly spread in both systems. Both PEEK 150PF and 450PF still shows scratches in the powder bed within the EOSINT P 800 system.
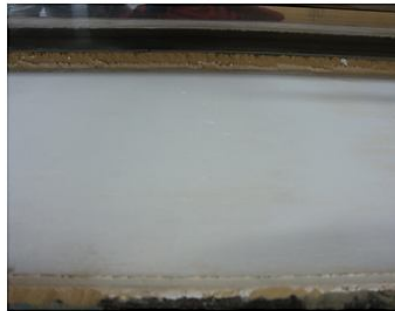
Figure 48. Spreading test of HT PAEK polymers within the Sinterstation 2000 (spreading tool: counter-rotating roller) and the EOSINT P 800 (spreading tool: double blade recoater) at room temperature. Layer 10

Figure 48 represents the last layer (10th layer) analysed in this test. All the material show good spreading performance within the Sinterstation 2000. Good spreading results are also shown by the PEK HP3 and the 150PF grades within the EOSINT P 800 system. However, PEEK 450PF still presents scratches and lines in the powder bed.

In summary, all the materials performed well in the Sinterstation 2000 system, where the roller spreading device allows reaching homogenous and even layers of powder regardless the particle characteristics of the materials under test. The differences found between PEK HP3 and PEEK grades in the AOR test and in the shape analysis do not significantly affect the spreading conditions when an counter-rotating roller device is used. This fact could be explained by analysing the functioning of the counter-rotating roller. When the roller spreads a new layer of powder, it applies a certain amount of pressure on the powder bed and on the new layer itself. This leads

to a more compact powder bed and overcomes the inter-particle locking due to the particle morphology of the material in exam, that otherwise would be responsible for deep line along the powder bed. This behaviour is clear in the PEEK 450PF grade.

When the same test is instead carried out in the EOSINT P 800 system by means of the double blade recoater, the PEEK grades exhibit more detrimental spreading behaviour, confirming the lower flowability shown in the AOR test. This result could be a consequence of the lack of pressure applied by the double blade recoater on the new layer of powder and on the powder bed underneath. It could also be explained by hypothesising a less efficient rotating dynamics of the powder particles within the double blade recoater than in the counter-rotating roller. Irregular particles could mechanically interlock together within the double blade recoater device and remained locked because of the lack of an external pressure able to remove these particle arrangements and allow the particles to rotate and be spread. Either hypotheses or the combination of the two could explain why the spreading performance of the PEEK particles in the EOSINT P 800 was difficult to achieve.

It seems therefore that the characteristics of the particles play are a more prominent role in the double blade recoating than in the in the counter-rotating roller device. However, the LS system Sinterstation 2000 was developed for the processing of low temperature polymers such as PA and therefore is unable to process PEK and PEEK polymers. It must be noticed also that for intellectual property reasons, a counter-rotating roller device patented by the University of Texas and sold to 3D systems, the machine manufacturer of the Sinterstation 2000, cannot be mounted and commercially used within an EOS manufactured LS system such as the EOSINT P 800.

4.7.2 Spreading tests of PAEK materials at processing temperature

The temperature at which the powder is kept just before the laser exposure and the consolidation of selected areas in the powder bed in a LS building process is called "part bed temperature". Other processing temperatures are set in a LS system during a real LS build operation (chapter 5.2.4). For simplicity reasons, processing temperature here indicates only the part bed temperature.

Spreading conditions of the PAEK materials were also carried out at a processing temperature in order to evaluate the effect of the testing temperature on the spreading performance of the powders within the EOSINT P 800 system (Figure 49). The testing temperature of the HP3 PEK material was 365 °C as indicated in the EOSINT P 800 manual [118], while the processing temperatures for PEEK 150PF and 450PF were set at 334 °C and 339 °C, respectively.
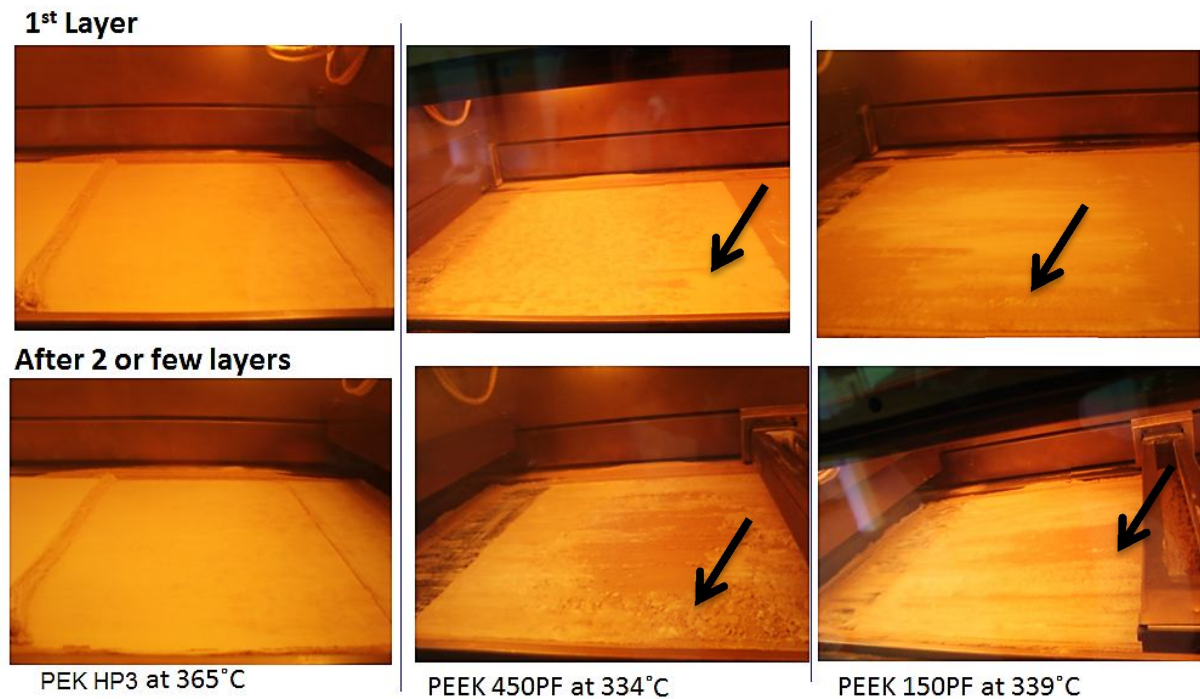
Figure 49. Spreading tests of PEK HP3 and PEEK powders at processing temperature within the EOSINT P 800 system

The temperatures used for testing the PEEK grades were chosen on the basis of the thermal properties of the powders (chapter 3.1.9) and application of the first derivative method (chapter 6.1.3) by using DSC analysis. The first derivative method was used at this stage of the investigation because it was found to be an accurate prediction of the EOS recommended processing temperature of the PEK HP3 material. It therefore afforded a quick early stage estimate of the processing temperatures for the two PEEK grades, which were also found to be in agreement to the processing temperatures used in previous research work on PEEK LS within in-lab modified LS systems as discussed in chapter 2.3.1. It is important to outline that this test aimed to investigate the spreading performance of new HT grades in the

EOSINT P 800 at a temperature reasonably close to the final optimised processing temperature. An ad-hoc calibration of the processing temperatures of PEEK 150PF and 450PF was carried out according to EOS guidelines is provided in chapter 5.

The PEEK grades showed poor test performance at the processing temperatures. This could be seen by darker areas of the powder base that are not covered by the lighter fresh powder (see arrows). This result was not surprising as poor spreading was also noticed in the PEEK grades at room temperature and the reasons were found to be a consequence of the flowability and particle morphology of these powders. However, the spreading is even worse at higher temperature. Several hypotheses can be applied to explain the worsening of the spreading behaviour: thermal expansion of the particles and enhanced inter-particle locking, not ideal processing temperature and lastly, possible particle agglomeration due to water absorption of the powder during storage. Powder thermal expansion is unavoidable in LS processing. The combination of particle properties and higher testing temperature can lead to a higher degree of inter-particles locking, which in turn caused very low to impossible spreading. To this regard, Amado et al. [102] showed that flowability of one of the most optimised LS grades, PA 12, indeed changed when tested above its glass transition temperature. Another explanation could be the non-optimal value of the chosen processing temperature. It could be possible that a too high test temperature might have triggered melting of the particles that caused them to become sticky and therefore difficult to spread. In this regard the same test was carried out at a lower testing temperature, 250 °C, which is above the glass transition of the PEEK materials, and this is described in chapter 4.8.1.2. An increased particle agglomeration of the powder particles due to water absorption in the shelf life (although the materials have always been stored at controlled temperature and humidity) was also considered. This suggestion was the reason why dried and sieved PEK HP3 and PEEK powders were tested again. The corresponding results are provided in chapter 4.8.1.2.

Interestingly, even the HP3 PEK material did not present a perfectly homogenous first layer, a condition that is achieved only after two layers. This is a surprising result, provided that PEK HP3 is an established HT-LS optimised material ad-hoc designed for use in the EOSINT P 800 system.

4.8 Strategies to improve the spreading performance of PEEK polymers

In order to improve the flow behaviour of the PEEK materials and their spreading performance within the EOSINT P 800 system, three strategies have been applied:

- Drying and sieving of the PEEK powders in order to eliminate potential water absorption during material storage
- Addition of the flow aid Aerosil Pharma 200
- Thermal conditioning of the PEEK powders.

4.8.1 Drying and sieving of the HT polymeric powders

PEEK 150PF and 450PF were dried and sieved as described in chapter 3. The materials were tested again in terms of AOR and spreading performance within the EOSINT P 800.

4.8.1.1 AOR of dried and sieved PAEK powders

The results of the AOR of dried and sieved PEEK 150PF, PEEK 450PF and PEK HP3 are reported in Table 11.

Material	AOR (°)
PEK HP3	42.4 ± 1.1
PEEK 150PF	47.4 ± 0.7
PEEK 450PF	52.8 ± 0.9
Dried PEK HP3	40.1 ± 0.7
Dried PEEK 450PF	51.6 ± 1.0
Dried PEEK 150PF	45.0 ± 0.9
Sieved PEK HP3	41.3 ± 0.6
Sieved PEEK 450PF	50.3 ± 1.1
Sieved PEEK 150PF	44.9 ± 1.1

Table 11. AOR average values and standard deviations of sieved and dried PEEK powders. For clarity the AOR results of the undried grades have been reported again

Both sieving and drying operations slightly helped the flow; however the standard deviations of the AOR values remained high, suggesting that these strategies may not be very effective.

4.8.1.2 Spreading test at 250 ˚C within the EOSINT P 800

The role of water absorption on the spreading ability of the PAEK materials was also investigated. PEEK powders and HP3 PEK were dried in air ventilated air-oven at 150 ˚C for 2 hours before the test, according to PEEK material processing guide [147] as described in chapter 3.2.1 and sieved. In order to guarantee the elimination of any absorption effect in the powder within the P 800 system, a testing temperature of 250 ˚C was set. This temperature was also chosen because it both assured o eliminate water absorption and it was above the glass transition temperature of PEEK, condition that according to Amado et al. [102] affect the flowability at least for PA based LS grades. Dried powders of PEK HP3, PEEK 150PF and 450PF were tested at this temperature according to the tests description in 3.1.8. PEK HP3 was also tested under the same conditions and used as a reference. The results are shown in Figure 50.
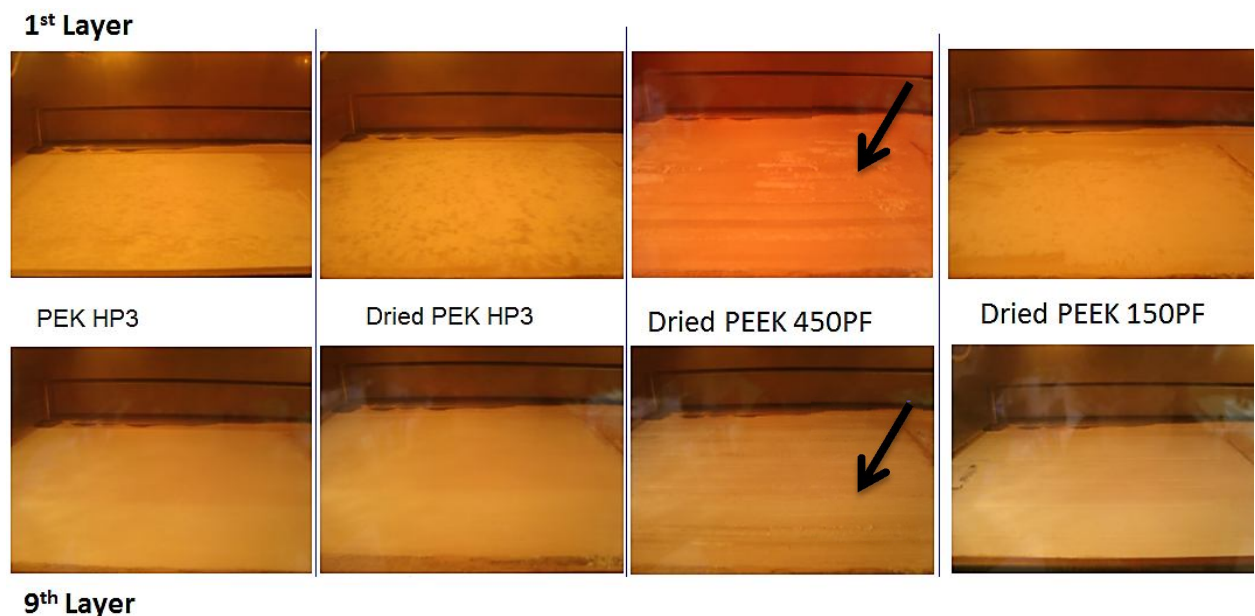
Figure 50. Spreading tests at 250 ˚C in the EOSINT P 800 for dried PEEK grades and PEK HP3

Both dried and undried PEK HP3 performed well, while the spreading performance of PEEK 150PF and 450PF did not seem to improve after the drying and sieving procedure. The layers were still far from uniform and the deep lines (see arrows in Figure 50) still occurred. Poor spreading behaviour of the PEEK grades was considered not due to water adsorption phenomena during the material storage or testing.

4.8.2 Aerosil Pharma 200

Aerosil 200 Pharma [126] is Nano metric flow aid powder. The mixtures PEEK 450PF /Aerosil (99:1) and 150PF/Aerosil (99:1) (by weight) were mixed by using a high speed mixer and then sieved. The blends were investigated in terms of: morphology using SEM imaging, AOR flow behaviour, inter-particle forces with the evaluation of the Hamaker constant and spreading performance at room temperature in the EOSINT P 800.

4.8.2.1 SEM of Aerosil Pharma 200-PEEK

Images of Aerosil Pharma 200, Aerosil-PEEK 150PF and Aerosil-PEEK 450PF blends are shown from Figure 51 to Figure 53, respectively.
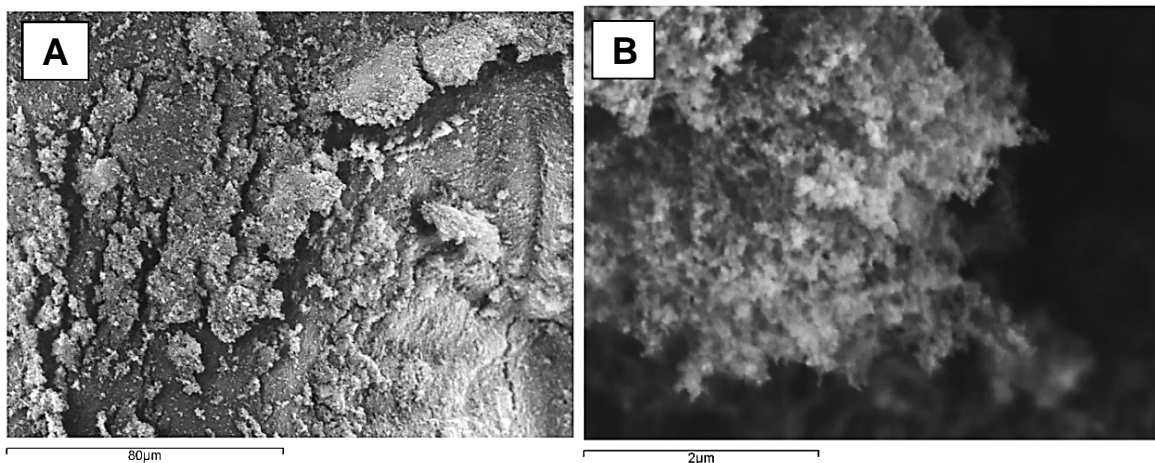
Figure 51. SEM images of Aerosil Pharma 200, at increasing magnification
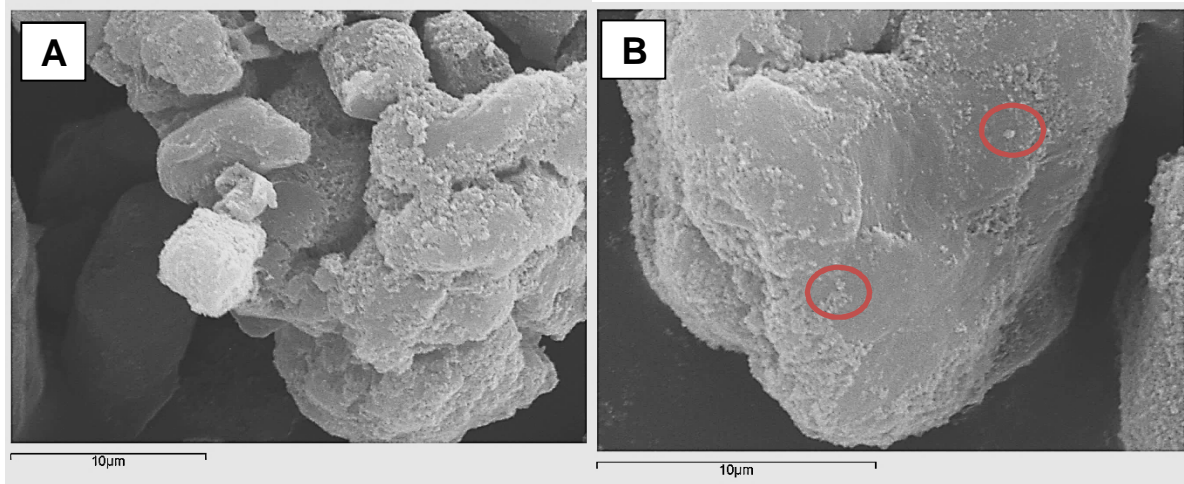
Figure 52. SEM images of Aerosil Pharma 200-PEEK 150PF. The red circles indicate Aerosil particles on the surface of PEEK 150PF particles
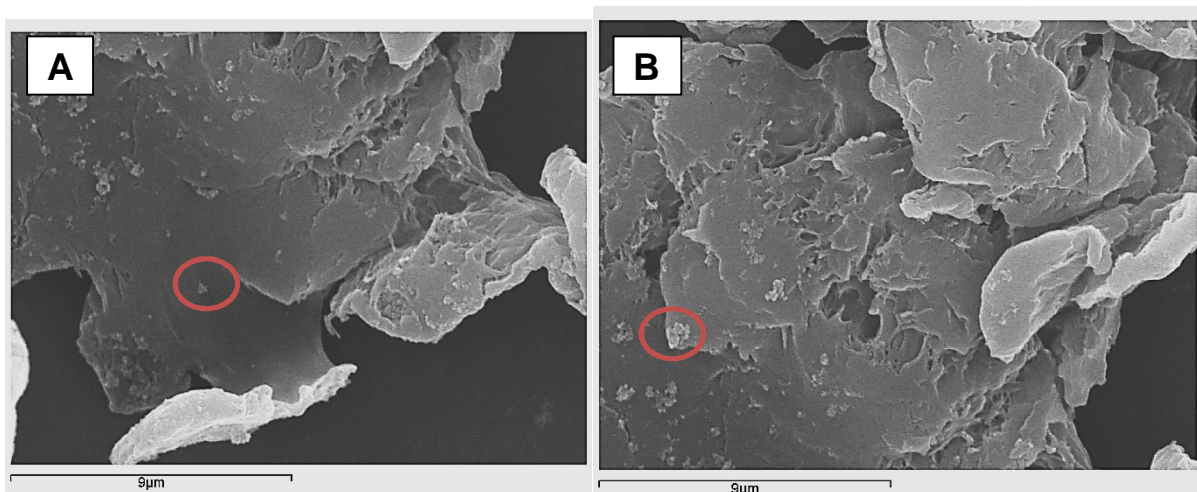
Figure 53. SEM images of Aerosil Pharma 200-PEEK 450PF. The red circles indicate Aerosil particles on the surface of PEEK 450PF particles

It is possible to notice that the Aerosil nanoparticles seem to cover the PEEK particles homogenously in both grades.

4.8.2.2 AOR of Aerosil Pharma 200-PEEK blends

The role of the Aerosil additive on the flow behaviour of the PEEK blends has been investigated by carrying out the AOR test. The results are listed in Table 12.

156

Material	AOR (°)
PEEK 150PF	47.4 ± 0.7
PEEK 450PF	52.8 ± 0.9
PEEK 450PF + 1% Aerosil Pharma 200	43.0 ± 0.4
PEEK 150PF + 1% Aerosil Pharma 200	36.4 ± 0.5

Table 12. AOR average values and standard deviations of Aerosil Pharma 200 and PEEK grades blends. For clarity, the AOR results of the pure PEEK grades have been showed again

Aerosil Pharma 200 improves significantly the flow performance of the PEEK powders by reducing the value of the AOR by 10 °. This result can be explained by considering the inter-particle forces between PEEK particles and Aerosil and therefore the Hamaker constant of the blend was evaluated.

4.8.2.3 Hamaker constant of Aerosil Pharma 200-PEEK

The role of the Aerosil flow additive on the inter-particle forces has also been analysed. The evaluation of the Hamaker constant between PEEK particles and Aerosil is shown in Table 13 along with the Hamaker constant value calculated for the PEEK particles only.

Mixture (in air)	A (J)
PEEK-PEEK	1.26 E-19
Aerosil Pharma 200 - PEEK	8.67 E-20

Table 13. Hamaker constant for PEEK and PEEK + 1% Aerosil Pharm 200 (average values and standard deviations)

The evaluation of the Hamaker constant outlines that Aerosil Pharma 200 allows to reduce the entity of the inter-particle attractive forces, thus explaining the significant decrease of the AOR.

4.8.2.4 Spreading performance of Aerosil Pharma 200-PEEK

The spreading performance of the mixtures PEEK 150PF + 1% Aerosil and PEEK 450PF + 1% Aerosil were tested at room temperature within the system EOSINT P 800 as described in chapter 3.1.8. The results of PEEK 150PF + 1% Aerosil are shown from Figure 54 to Figure 56, while Figure 57 to Figure 59 show the results obtained for the PEEK 450PF + 1% Aerosil Pharma 200 blend.

1st Layer

2nd Layer

3rd Layer

4th Layer
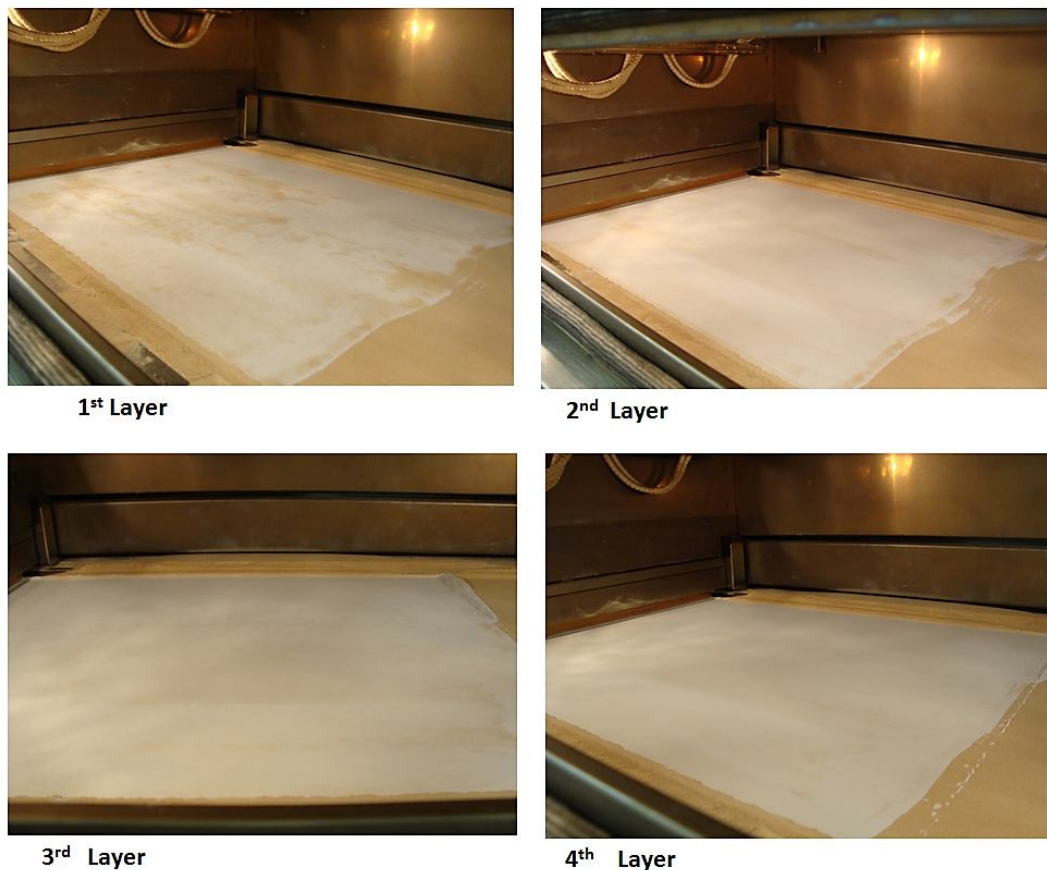
Figure 54. Spreading test of PEEK 150PF + 1% Aerosil Pharma 200 at room temperature within the EOSINT P 800 system. Layers 1-4

Figure 54 shows the first four layers of PEEK 150PF + 1% Aerosil Pharma 200. The layers appear significantly improved compared to the first four layers of PEEK 150PF only (Figure 45 to Figure 48). Yet, they are still not completely uniform.

Figure 55. Spreading test of PEEK 150PF + 1% Aerosil Pharma 200 at room temperature within the EOSINT P 800 system. Layers 5-8

Figure 56. Spreading test of PEEK 150PF + 1% Aerosil Pharma 200 at room temperature within the EOSINT P 800 system. Layers 9 and 10

Figure 55 and Figure 56 show the remaining layers analysed in this test (5th to 10th). It is possible to notice that these layers exhibit a uniform distribution of PEEK 150PF

159

powder with no signs or area of the powder base left exposed. Therefore, the addition of Aerosil Pharma 200 to PEEK 150PF could be a good strategy for an acceptable spreading performance within the EOSINT P 800 system.

1st Layer

2nd Layer

3rd Layer

4th Layer
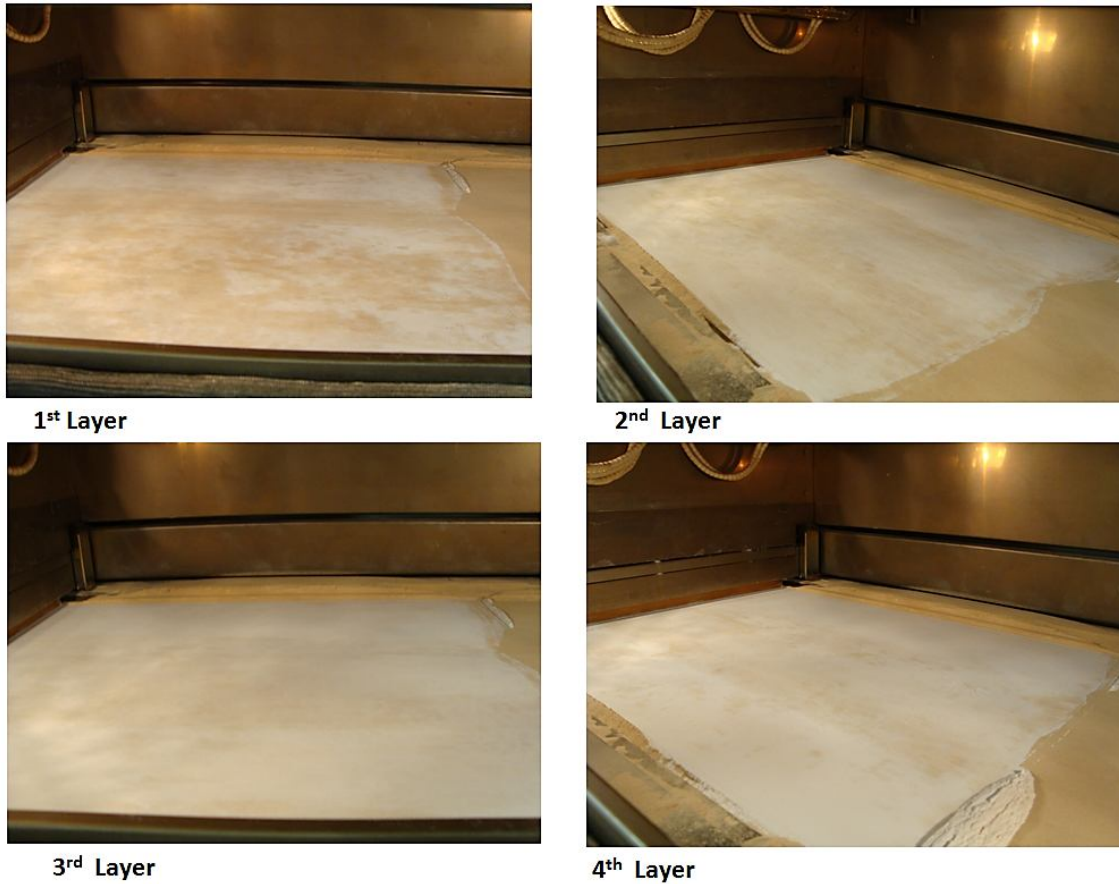
Figure 57. Spreading test of PEEK 450PF + 1% Aerosil Pharma 200 at room temperature within the EOSINT P 800 system. Layers 1-4

Figure 57 presents the first four layers of PEEK 450PF + 1% Aerosil Pharma 200. Darker areas of the powder base are visible, indicating a non-optimal spreading performance, yet significantly improved to that of PEEK 450PF alone (Figure 45 to Figure 48).

5th Layer

6th Layer

7th Layer

8th Layer

Figure 58. Spreading test of PEEK 450PF + 1% Aerosil Pharma 200 at room temperature within the EOSINT P 800 system. Layers 5-8

9th Layer

10th Layer

Figure 59. Spreading test of PEEK 450PF + 1% Aerosil Pharma 200 at room temperature within the EOSINT P 800 system. Layers 9, 10

Figure 58 and Figure 59 show layer 5 to layer 10 of PEEK 450PF + 1% Aerosil Pharma 200. The layers appear homogenous with no deep lines or areas of powder base left exposed. The spreading performance of the 450PF grade has significantly improved with the addition of Aerosil Pharma 200, making the overall blend suitable for further optimisation in the HT-LS process.

4.9   Thermal conditioning of PEEK 150PF and 450PF

The last strategy applied in this research work for the improvement of the spreading behaviour of the PEEK particles has been a thermal conditioning. The thermal conditioning, described in chapter 3.2.2, consisted of the exposure of the material at 250 °C for 24 hours in an air-ventilating oven and then left it to cool down to room temperature. This procedure was inspired by the patent "PAEK powder, in particular for the use in a method for a layer-wise manufacturing of a three-dimensional object, as well as method for producing it" [148], owned by EOS [1]. In this patent, a limited number of PAEK grades, which could be related to PEEK 150PF and 450PF, are thermally and mechanically treated under varied conditions of temperatures, duration and applied force. The purpose of the patent is to increase the bulk density of the materials under test. The effect of this procedure on the powder flow, particle morphology and spreading performance was not directly investigated and therefore was analysed in this research project. Thermally conditioned PEEK 150PF and 450PF were analysed in terms of SEM imaging, viscosity, shape characteristics, AOR performance and spreading ability.

4.9.1   SEM of thermally conditioned PEEK grades

The particles of thermally conditioned PEEK 150PF and 450PF analysed with SEM imaging are shown in Figure 60 and Figure 61, respectively.
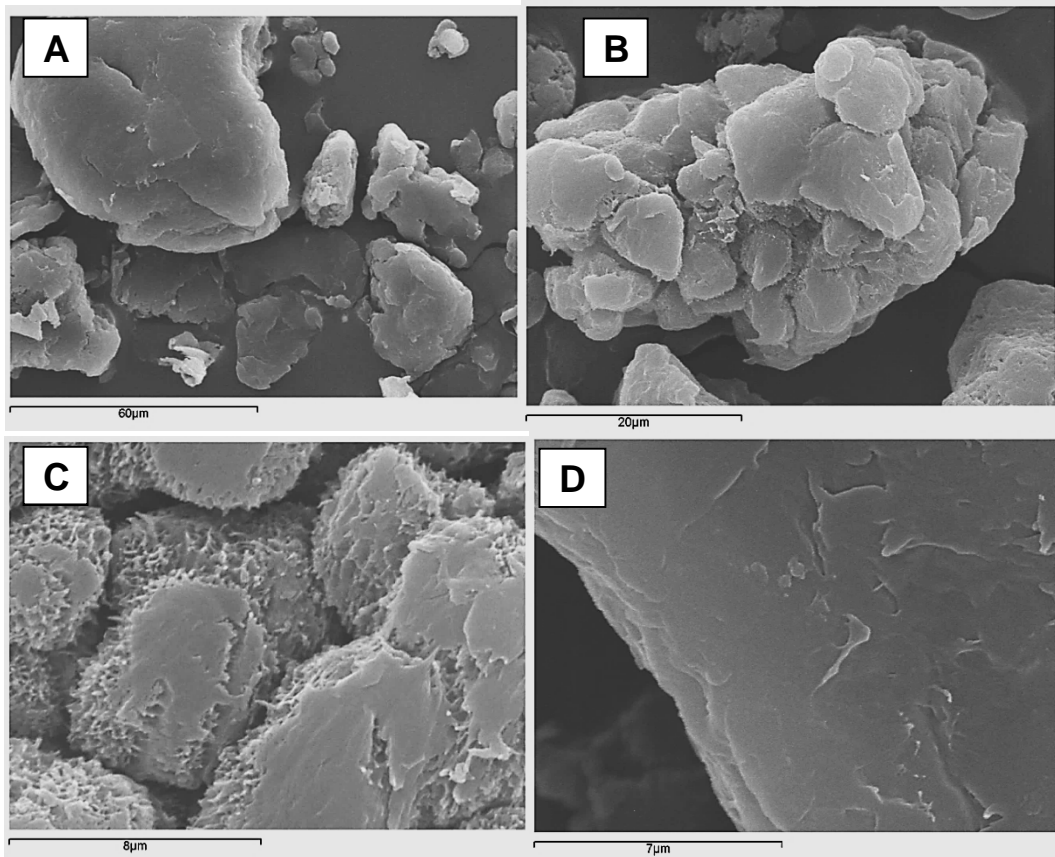
Figure 60. SEM images of thermally conditioned PEEK 150PF, at increasing magnification

Figure 60 shows thermally conditioned PEEK 150PF particles having smoother surface than the particles of the corresponding unconditioned grade (Figure 30 and Figure 31). It seems that the structures constituting the PEEK 150PF particles melt and solidify into a uniform and highly smooth surface. This characteristic could occur as consequence of a partial re-melting of the particle surface during the thermal conditioning process.
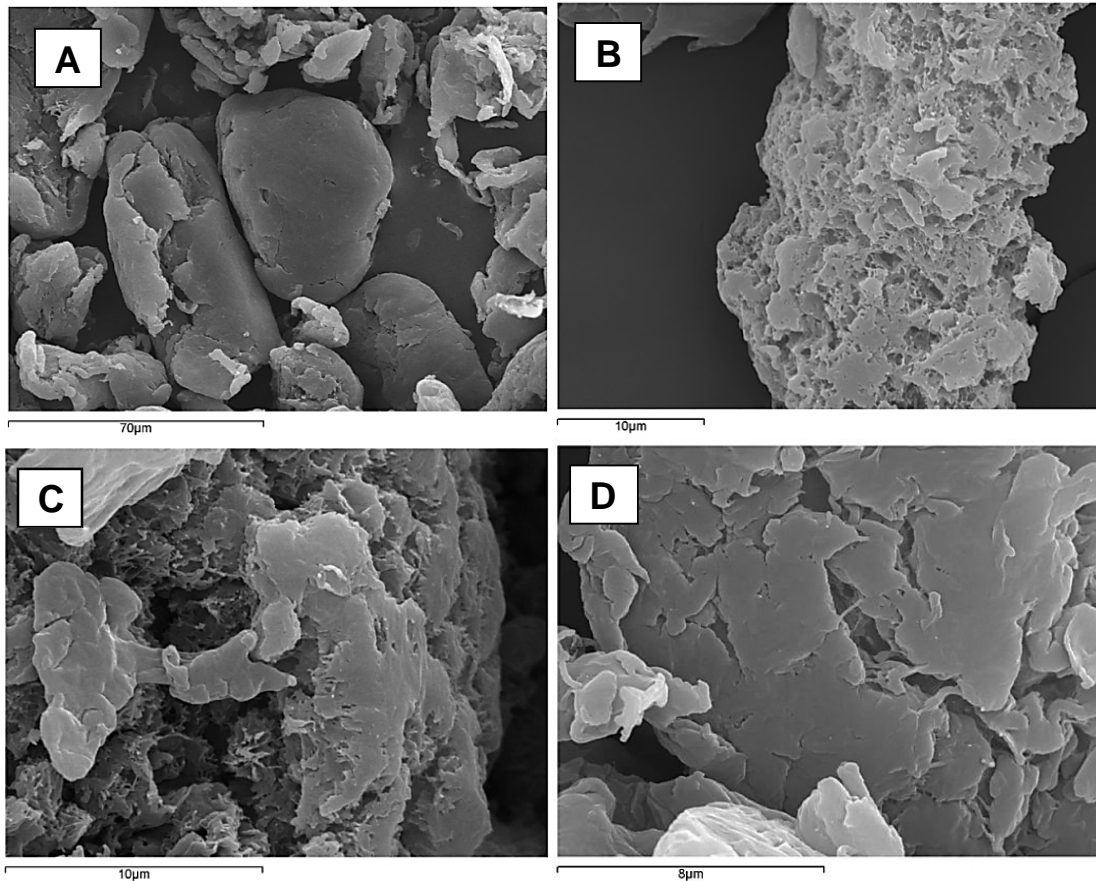
Figure 61. SEM images of thermally conditioned PEEK 450PF particles, at increasing magnification

Figure 61 shows the particles of thermally conditioned PEEK 450PF. The particles look rounder with smoother surfaces overall. As seen in Figure 60, the particle surfaces seem to have been subjected to partial re-melting and solidification in a smoother arrangement during the thermal conditioning process.

Clearly, the thermal conditioning smoothed the surface of the particles, which appeared to be less irregular and flaky overall in both grades when compared to the untreated corresponding powders (Figure 29 to Figure 31). Especially for those particles having a fairly porous structure with high surface area (Figure 60 C and Figure 61B-D), the thermal conditioning seemed responsible to have caused a partial re-melting of the surface leading to a more regular particle surface.

Similar effects were also noted by Nelson et al. [74] during the development, modelling and optimisation of a Bisphenol A-polycarbonate material for LS.

According to the authors the particles changed shape, from oblate to more spherical, after a heat treatment of 10 minutes above the glass transition of the polymer. This alteration of the particle shape was considered by the authors the cause of a reduction in the surface energy of the particles, which in turns facilitated viscous sintering during LS manufacturing. Although the authors did not measure quantitatively the shape alterations of the powder elements, a considerable powder bed expansion due to spherical particles was noted in the powder bed of the LS apparatus used.

4.9.2 Shape analysis of thermally conditioned PEEK 450PF

In order to assess the shape modifications due to thermal conditioning, 1201 particles of thermally conditioned PEEK 450PF were analysed with the shape analysis procedure (chapter 3.1.5). The average results of the shape descriptors circularity, roundness, AR and solidity and their standard deviations are listed in Table 14 in parallel with the corresponding values of the unconditioned PEEK 450PF. Only the thermally conditioned PEEK 450PF grade was analysed; it is believed to better highlight the effect of the thermal conditioning on the shape descriptors for the material exhibiting the least performing values.

Material	Circularity	AR	Roundness	Solidity
PEEK 450PF	0.53 ± 0.19	2 ± 0.84	0.57 ± 0.18	0.83 ± 0.10
PEEK 450PF thermally conditioned	0.65 ± 0.17	1.81 ± 0.65	0.61 ± 0.17	0.88 ± 0.08

Table 14. Shape descriptors of non-thermally conditioned PEEK 450PF and thermally conditioned PEEK 450PF. Average values and standard deviations.

All the values of the shape descriptors improved in the thermally conditioned material: circularity, roundness and solidity increased, while the AR decreased. These findings imply the presence of more circular, less elongated particles with rounder edges and more fully solid shapes in the thermally conditioned PEEK 450PF.

The distribution of the descriptors circularity and roundness are shown in Figure 62 and Figure 63. To better visualize the presence of particles having simultaneously round edges and circular profiles, circularity and roundness distributions have been plotted as described in 3.1.5 with application of the Mahalanobis distance 3.1.6. The diagram is shown in Figure 64.
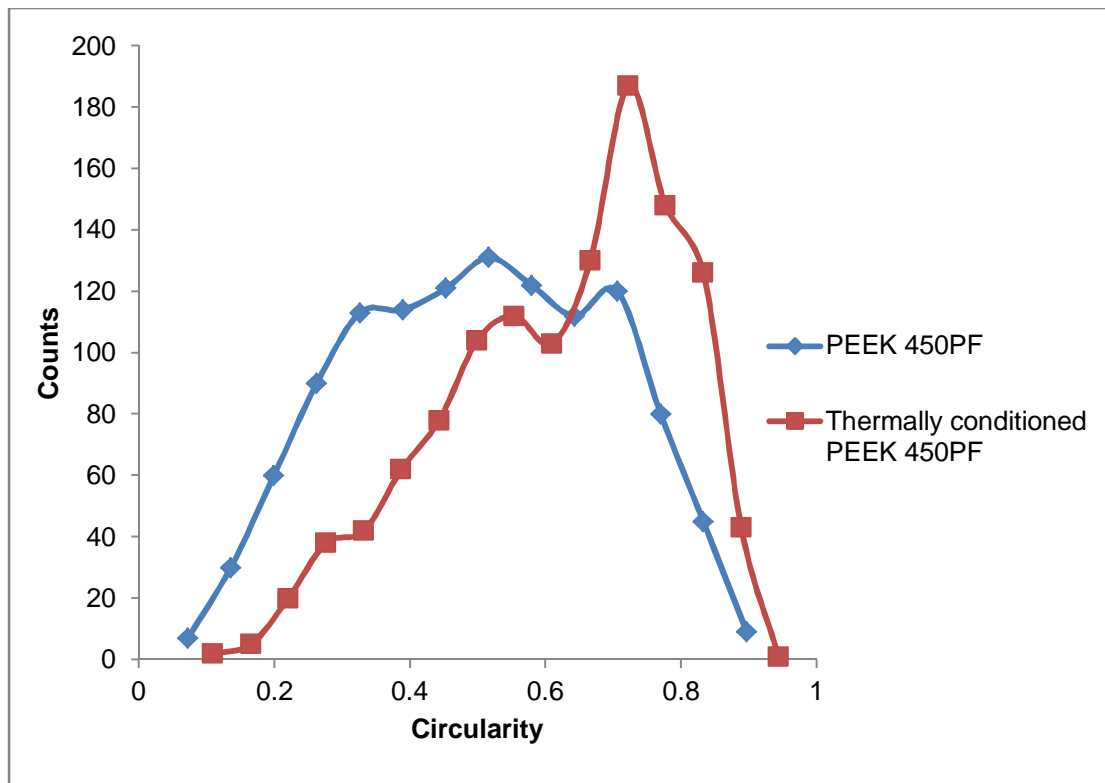
Figure 62. Data distribution of the shape descriptor circularity for PEEK 450PF and thermally conditioned PEEK 450PF
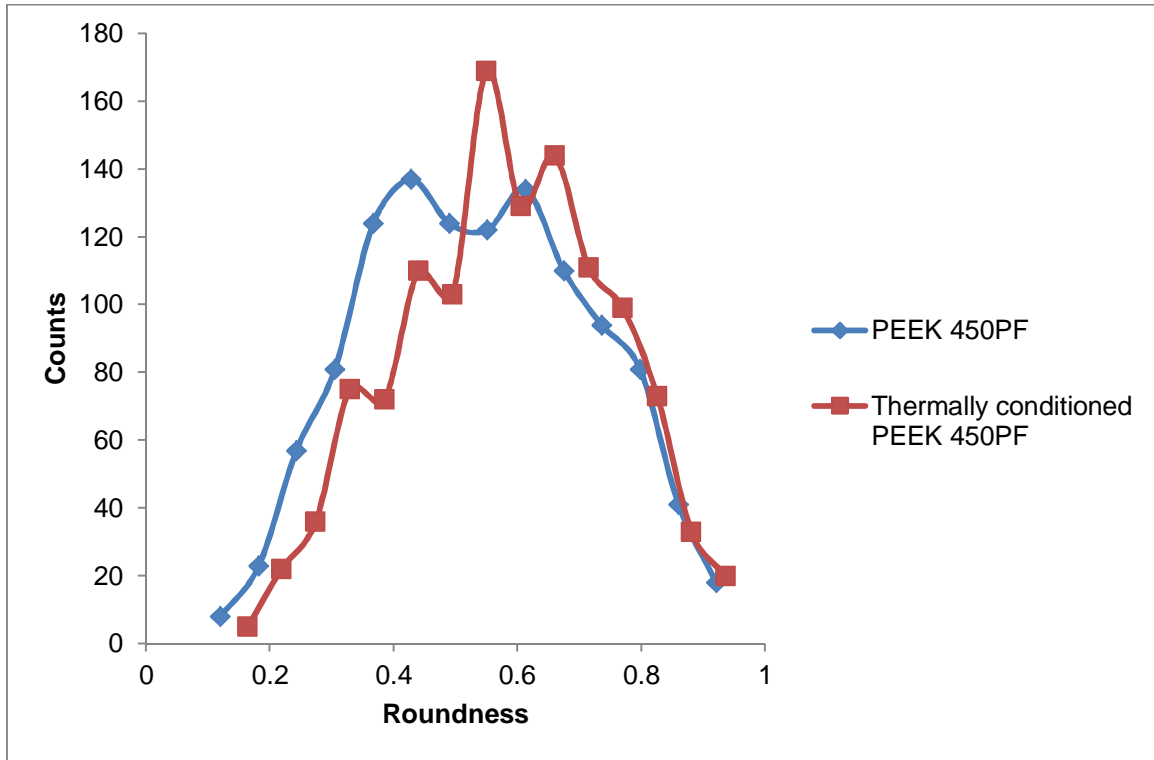
Figure 63. Data distribution of the shape descriptor roundness for PEEK 450PF and thermally conditioned PEEK 450PF
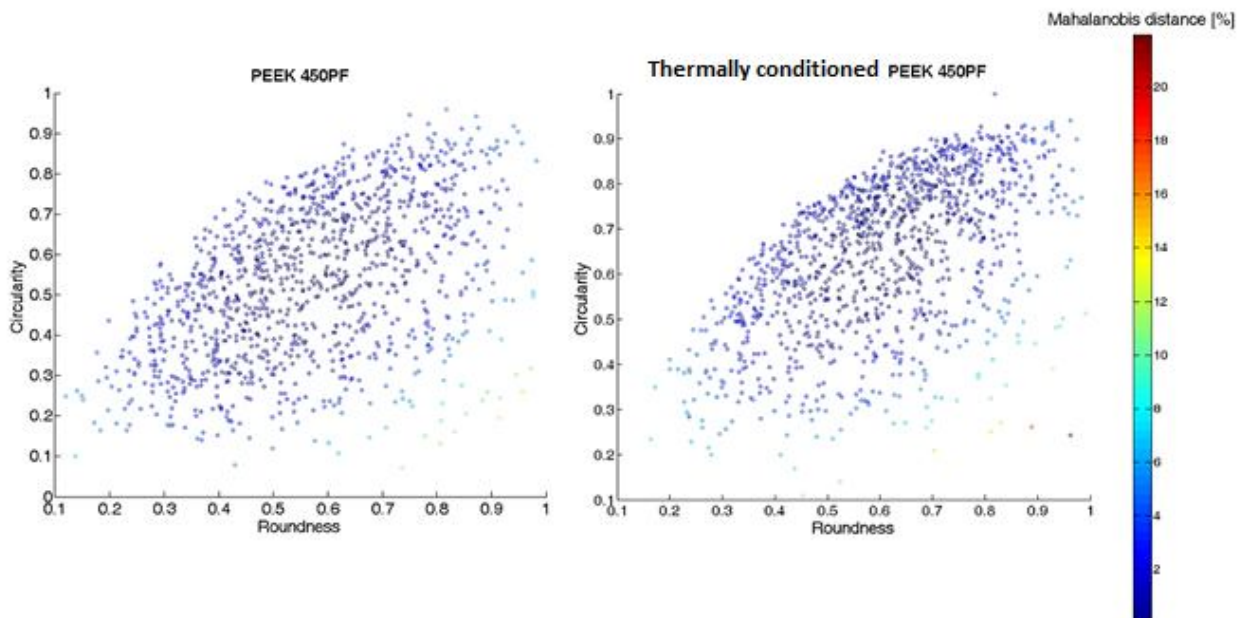
Figure 64. Circularity and roundness of PEEK 450PF and thermally conditioned PEEK 450PF

Figure 62 and Figure 63 show a shift of the shape descriptors to higher values of circularity and roundness. This result indicates that the thermally conditioned PEEK 450PF particles have softer edges and more circular shapes. This improvement is even clearer in Figure 64. After the thermal conditioning, the circularity-roundness diagram shows a dataset shifted toward simultaneous higher values of circularity and roundness. Additionally, the data dispersion is lower than in the corresponding unconditioned grade, indicating a higher presence of particles with more common performing shape properties.

The shape descriptors AR and solidity are shown in Figure 65 and Figure 66, respectively.
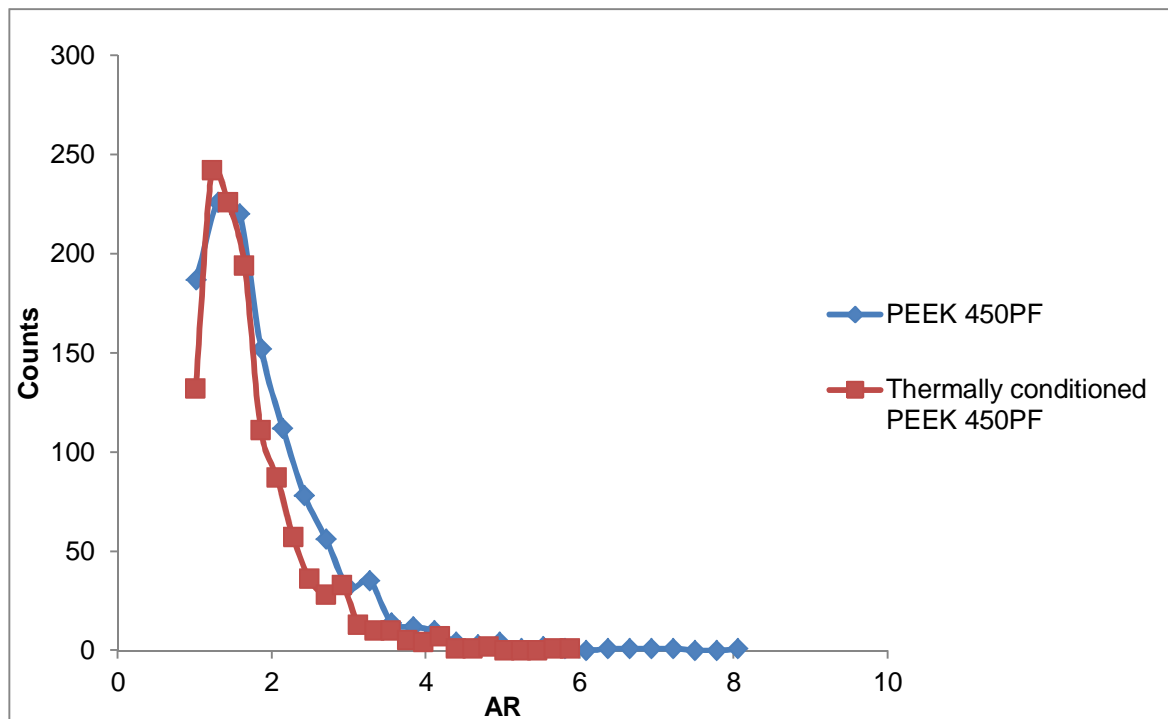
Figure 65. Data distribution of the shape descriptor AR for PEEK 450PF and thermally conditioned PEEK 450PF
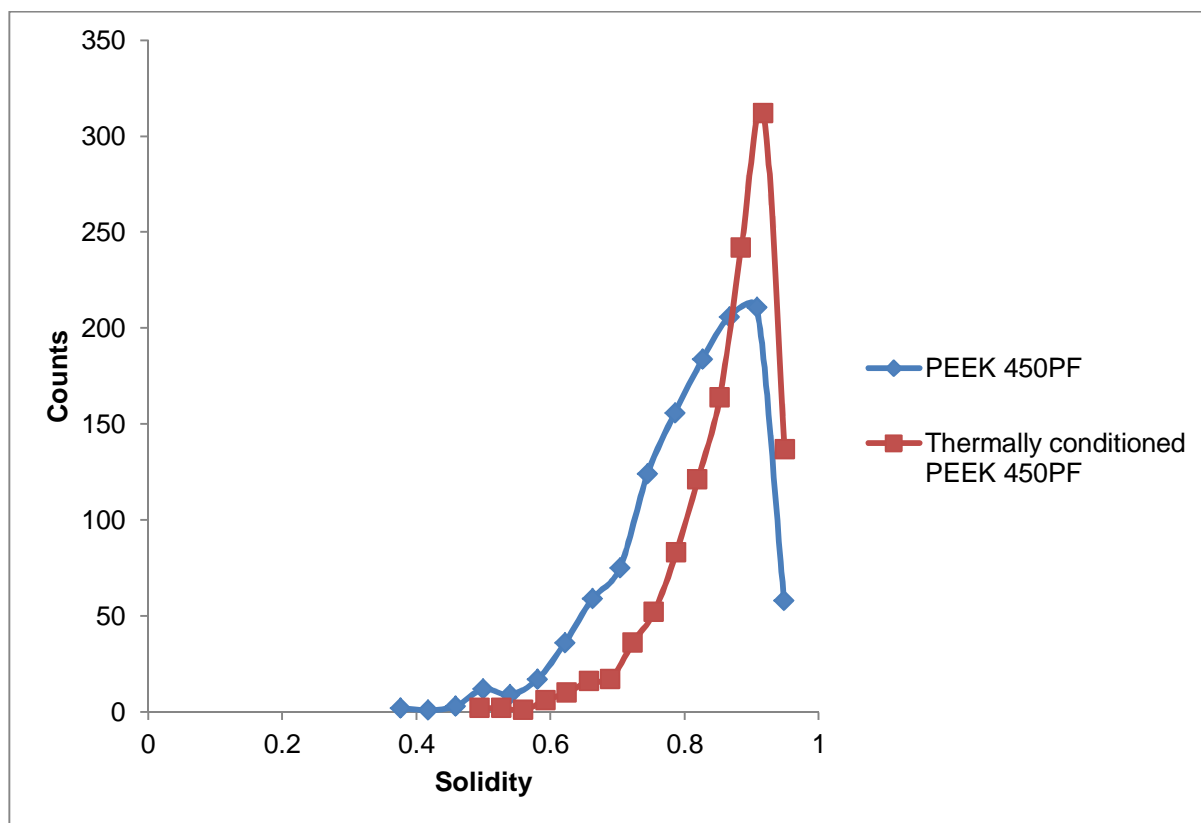
Figure 66. Data distribution of the shape descriptor solidity for PEEK 450PF and thermally conditioned PEEK 450PF

The shape descriptors AR and solidity respectively decrease and increase after thermal conditioning of the PEEK 450PF powders. These results imply that the PEEK 450PF particles change into less elongated and more solid shapes after the conditioning, thus improving overall.

Seemingly, the thermal conditioning makes the surface of the particles smoother, but also changes their shape. An explanation of the effect of the thermal conditioning is represented in Figure 67. The flakes and the irregularities located on the surface of the powder elements re-arrange by folding towards the main core of the particles during the thermal conditioning that takes place at above the glass transition temperature but below the onset of the melting region. When these protuberances and irregularities fold back inwards, the shape of the particle becomes rounder, more circular, less elongated and more solid as seen in the results of the shape analysis of thermally conditioned PEEK 450PF.
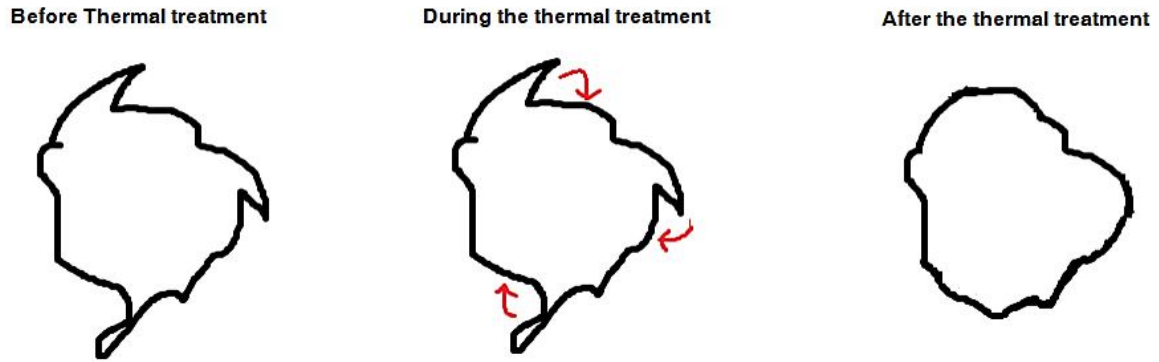
Figure 67. Effect of the thermal conditioning on the morphology of PEEK particles

4.9.3 AOR of thermally conditioned PEEK grades

The results of the AOR measurements for thermally conditioned PEEK 450PF and 150PF are reported in Table 15.

Material	AOR (°)
PEEK 150PF	47.4 ± 0.7
PEEK 450PF	52.8 ± 0.9
PEEK 450PF thermally conditioned at 250 °C 24 hours	45.8 ± 0.8
PEEK 150PF thermally conditioned at 250 °C 24 hours	39.9 ± 0.7

Table 15. AOR results of unconditioned and thermally conditioned PEEK 450PF and 150PF. Average values and standard deviations

The AOR of both thermally conditioned PEEK grades significantly improved after the thermal conditioning. The results are in agreement with the findings obtained by SEM imaging and particle shape analysis. The flow behaviour of the powder was then positively affected by the change of the surfaces of the particles and the alteration of their shapes, both due to thermal conditioning.

4.9.4 Spreading test of thermally conditioned PEEK grades at room temperature

Thermally conditioned PEEK 150PF and 450PF were lastly tested in terms of spreading performance within the P 800 system at room temperature. A poor spreading performance at room temperature would have been indication of unsuitability of the materials under test for LS processing at higher temperatures. Figure 68 to Figure 70 show the spreading results obtained for thermally conditioned PEEK 150PF, while the spreading behaviour of the thermally conditioned of PEEK 450PF grade is reported from Figure 71 to Figure 73.

Figure 68. Spreading test of thermally conditioned PEEK 150PF at room temperature within the EOSINT P 800. Layers 1-4

Figure 68 shows the first four layer of thermally conditioned PEEK 10PF spread within the EOSINT P 800 system. The first layer is not homogenous, a result also noticed for the HT-LS established PEK HP3 grade. For this reason, this result was considered acceptable. However, the next layers appear uniform with fresh powder evenly distributed across the powder bed.

5th Layer

6th Layer

7th Layer

8th Layer

Figure 69. Spreading test of thermally conditioned PEEK 150PF at room temperature within the EOSINT P 800. Layers 5-8

9th Layer   10th Layer

Figure 70. Spreading test of thermally conditioned PEEK 150PF at room temperature within the EOSINT P 800. Layers 9-10

Figure 69 and Figure 70 show the remaining layers of thermally conditioned PEEK 150PF under test (5th to 10th). All the layers seem highly homogenous. These findings indicate that the thermal conditioning of PEEK 150PF makes the spreading within the EOSINT P 800 possible and the material can then be a suitable candidate for the HT-LS process.

173
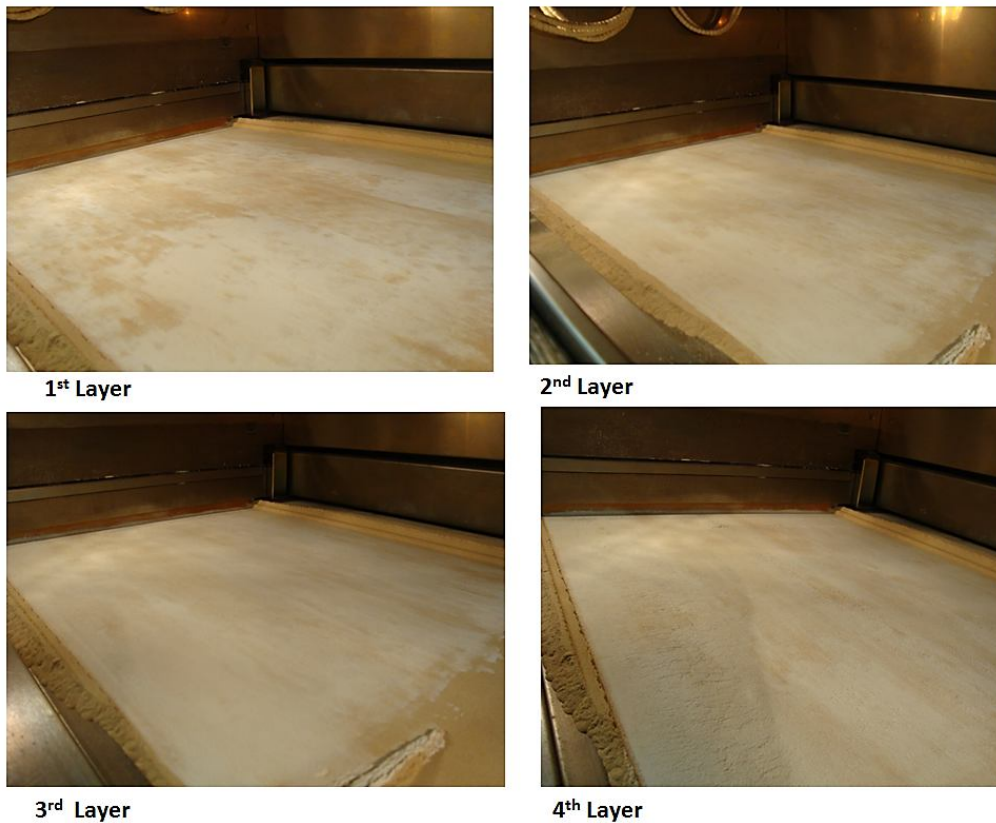
Figure 71. Spreading test of thermally conditioned PEEK 450PF at room temperature within the EOSINT P 800. Layers 1-4

Figure 71 shows the first four layers of thermally conditioned PEEK 450PF spread in the EOSINT P 800 at room temperature. The layers improved significantly in respect to the first four layers of unconditioned PEEK 450PF (Figure 45 to Figure 48). No deep lines or regions of the powder base are evidently visible. However, these four layers are still not fully uniform.

5th Layer

6th Layer

7th Layer

8th Layer

Figure 72. Spreading test of thermally conditioned PEEK 450PF at room temperature within the EOSINT P 800. Layers 5-8

9th Layer

10th Layer

Figure 73. Spreading test of thermally conditioned PEEK 450PF at room temperature within the EOSINT P 800. Layers 9, 10

Figure 72 and Figure 73 present the remaining layers (5th to 10th) of thermally conditioned PEEK 450PF examined in this test. These layers appear uniform,

175

suggesting that also thermally conditioned PEEK 450PF is suitable for optimisation in the HT-LS technology.

In summary, the spreading of PEEK 150PF is significantly improved after the thermal conditioning. This could be seen by homogenous and uniform layers of lighter powders over the darker powder base. No scratch lines have been noticed in any of the spread layers. This improvement in the spreading performance confirms the results found in the SEM imaging and AOR test. Similarly, also thermally conditioned PEEK 450PF exhibited a good spreading performance, thus indicating a significant improvement of the flow performance. Also this result was found to be in agreement with SEM, AOR and particle shape analysis data.

Interestingly, Figure 74 shows an effect found for the PEEK 450PF grade in the powder bed.

Figure 74. Imperfections in the powder bed of the EOSINT P 800 system. Material: thermally conditioned PEEK 450PF

Figure 74 shows a defect found powder bed of the EOSINT P 800 system for thermally treated PEEK 450PF. Although the thermally conditioned PEEK 450PF powder layers are acceptably homogenous they are still not fully homogenous as

certain areas are not still fully flat and even. An investigation of the thermal conditioning under different conditions could then provide more optimal conditions.

4.10 Conclusions

Well established LS grades such PA 2200 grades and PEK HP3 have been in-depth investigated in parallel with new potential HT polymeric PEEK powder for their implementation and optimisation in the HT-LS process.

The AOR for the commercial LS grades was found to be between 33° and 42°, whereas the non-LS grades gave higher AOR values. The SEM analysis showed morphological differences between all the grades analysed and explained the differences in the AOR results. Although the presence of fillers slightly improved the AOR, the Nano-sized additive improved the flowability significantly. The shape analysis outlined that high values of roundness and circularity, coupled with high values of solidity and low values of AR are characteristic of the commercial LS materials such as PA 2200 and PEK HP3.

The evaluation of the Hamaker constants agreed with the experimental data found for the AOR: the materials with higher values of AOR showed greater values of Hamaker constant, thus indicating grater inter-particle attractive forces and lower flowability. Additionally, the same order of performance across the materials is confirmed in the Hamaker constants. These findings proved that it is not only the combination of particle size and powder morphology responsible for good flowing performance, but also the physicochemical nature of the powder materials have a significant impact on the powder flow behaviour.

Spreading tests in different conditions and in different LS systems have also been carried out in order to asses flow performance in real LS scenarios. PEK HP3, the only HT powder grade at present commercially available, performed well in all the spreading tests with both spreading devices, counter-rotating roller and double blade recoater, at every temperature. Interestingly, even the first PEK HP3 fresh layer is not uniform. The PEEK material exhibit acceptable spreading performance when the counter-rotating roller tool was utilised. This results was likely due to the effect of a pressure applied by the counter-rotating roller when depositing and levelling layers of

new powder. However, when a double blade recoater was used, the effect of the irregular shape of the PEEK particles became prominent. The spreading appeared very difficult, up to a limit where it was completely unachievable for all temperatures investigated: room temperature, 250 °C and similar-processing temperatures. Although the roller mechanism could provide a simple solution for LS processing of the PEEK grades, patents limitations do not allow the installation of an counter-rotating roller device developed by 3D Systems [124] on a EOS [1] LS system such as the EOSINT P 800.

Three strategies have been applied to the PEEK grades in order to improve their flow behaviour within the EOSINT P 800. The addition of a flow aid additive and the thermal conditioning of the raw particles, significantly improved the powders flow behaviour. This performance was confirmed by AOR tests and spreading tests in the EOSINT P 800.

All data provided here constitute a starting point in a quantitative characterisation and understanding of powder materials for LS and could contribute to the creation of a database for the benchmark of new suitable LS materials. The study showed that the non-commercial PEEK grades require optimisation that can be achieved through thermal conditioning methods and incorporation of Nano metric additives. However, powder characteristics and optimisation treatments cannot be considered in isolation; further investigation into spreading and processability of the powders in the actual LS system has to be carried out for a full assessment of a specific material.

5 High temperature laser sintering of PEEK

HT-LS of PEEK components, their characterisation and the optimisation of the processing parameters carried out within the HT-LS system EOSINT P 800 are described in this chapter. The investigation of the role of variable size building chamber and post sintering time, characteristics unique of the P 800 system, on HT laser sintered PEEK structures is also provided here.

5.1 The EOSINT P 800

The EOSINT P 800 system is the only commercial HT-LS system currently available. The system has a central building chamber size of 700 x 380 x 560 mm, two side powder feed hoppers (dispensers or feeders) at the top and two side overflow powder collector bins at the bottom. Facing the top surface of the building chamber there are: two CO_2 lasers, four infrared radiant heaters, an optical pyrometer and a double blade recoater for the spreading of the powder materials during the HT-LS process. Heaters are also incorporated within the walls and the platform of the building chamber in order to ensure accurate thermal control of the whole unit. The EOSINT P 800 located at the University of Exeter is shown in Figure 75, while Figure 76 shows the internal structure of the system.

Figure 75. The EOSINT P 800 system
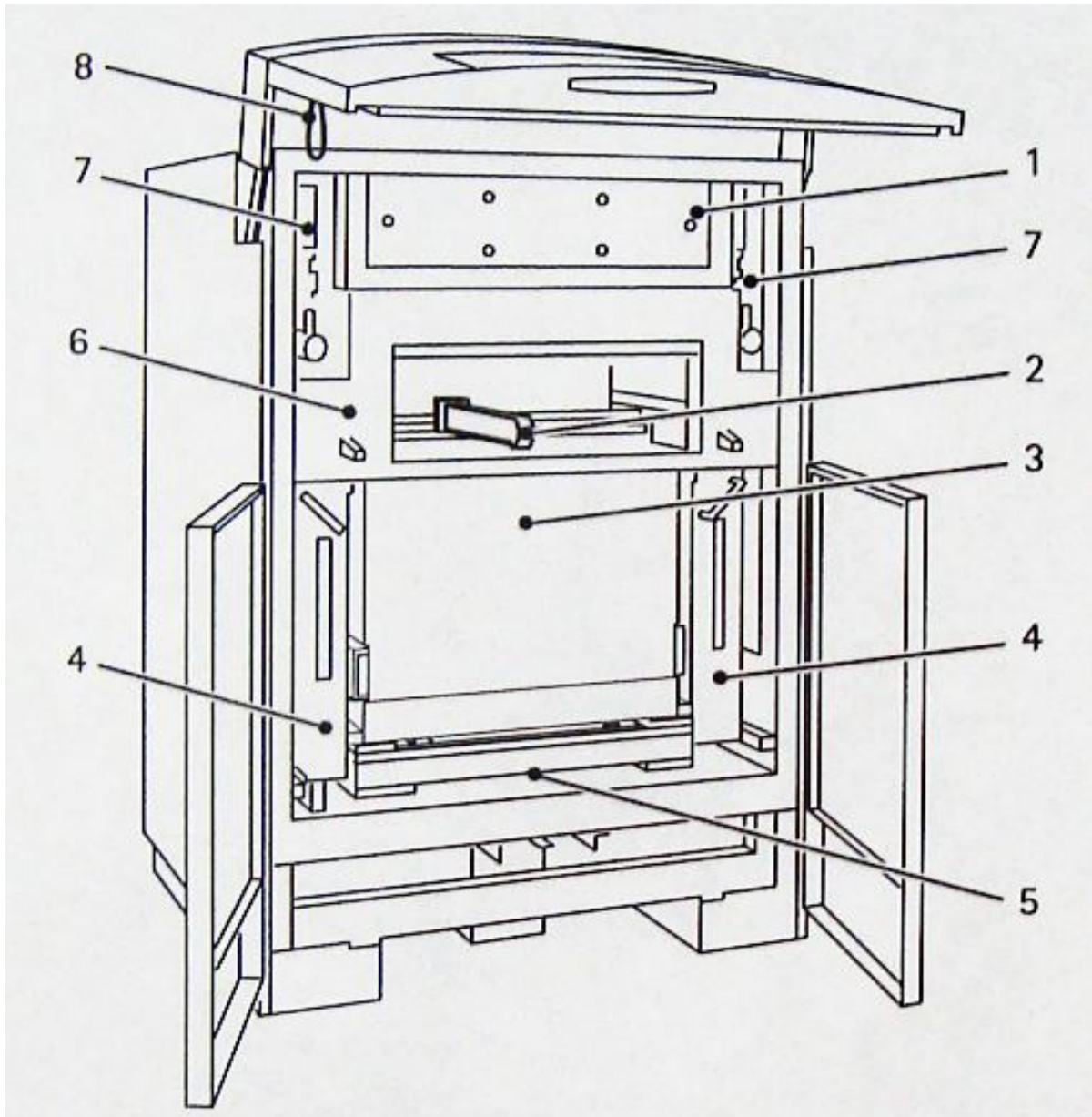
Figure 76. Front view of the EOSINT P 800 system: 1 Optics chamber cover, 2 Recoater, 3 Exchangeable frame with building platform, 4 Collector bin, 5 Exchangeable frame lifting system, 6 Process chamber, 7 Dispenser, 8 Rubber strap [118]

5.2 A HT-LS building process

A HT-LS building process is constituted of a software and a hardware stage. In the software stage, the 3D designs of the components are grouped in terms of orientation and position in a configuration that represents the actual characteristics and dimensions of the building chamber within the EOSINT P 800 system that will be used. This stage is performed by using the software package Materialise Magics RP v18 [190], programme that also allows detecting mesh errors and correcting potential

part clashes. The output file is an STL file that still contains the information about the design, the location and the orientation of the component to build. An example of build data preparation carried out in Magics RP for a full build chamber mode building process in the EOSINT P 800 system is shown in Figure 77.
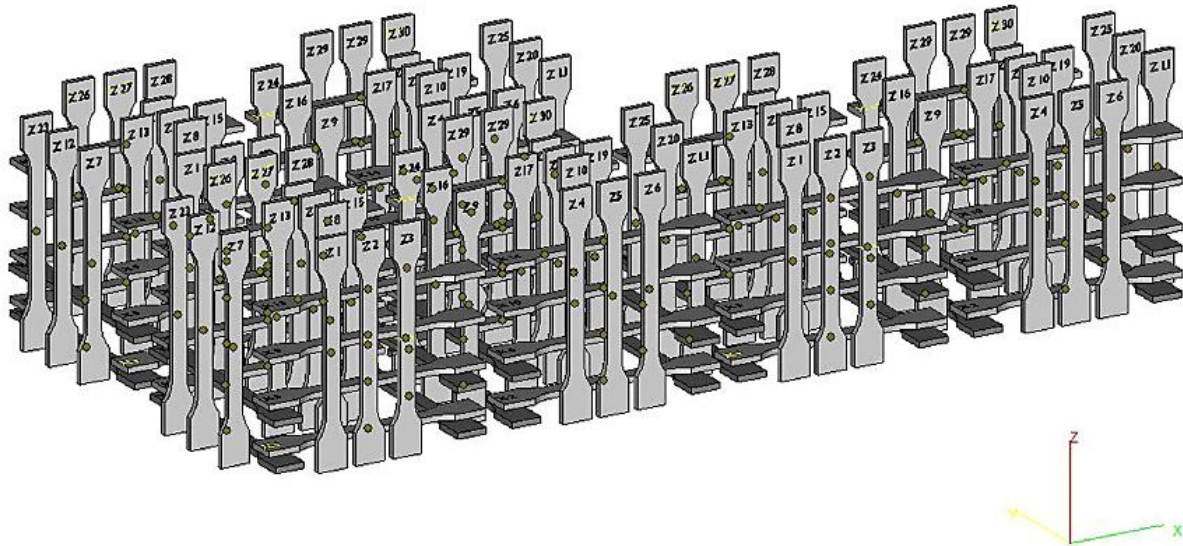
Figure 77. Example of component grouping in Materialise Magics RP v18 [116]

The component STL file is then converted into a new file format (SLI) where part design, part orientation and part positioning are arranged into cross-sectional data corresponding to a layer of the building process. This operation, generally called "slicing", is carried out using the software package RPTools [195], that generates SLI files specific for the EOS machines. The SLI files are lastly checked and fixed in case the slicing generated mesh or line discontinuities in the components' design.

The physical building process (hardware stage) comprises three phases: warm up, component building and cooling. During the warm up phase, layers of fresh powder are deposited across the building chamber while the temperature is gradually increased up to the user defined processing temperatures. Three temperatures (chapter 5.2.4), corresponding to the process chamber, the removable frame slide heaters and the base of the building chamber, are set in every building process. The building phase starts when the three temperatures are reached. A layer of fresh powder (thickness 120 µm) is spread across the bed (powder bed or building area)

from the feeder bins using a double blade recoater device. When the temperature of the deposited material is stable, the laser scans the areas corresponding to the cross section of the desired parts, inducing the consolidation of the powder particles. Once the laser exposure is completed, the infrared heaters provide an additional heating period, called "Post Sintering" (PS) that aims to ensure homogeneous melt of the exposed regions across the chamber independently of which part was scanned first and last. When the PS is completed, the powder bed is lowered by 120 μm, a new layer of powder is deposited, the layer is heated, the exposure is repeated and the PS is applied. These steps are repeated until all the components are fully built. At that point, a controlled cooling procedure starts. The heating elements of the P 800 system control the cooling phase down to a temperature of approximately 180 °C and then the system is left to cool naturally.

The whole process takes place in inert atmosphere (positive pressure nitrogen atmosphere) and the temperature, at which the powder is kept, before the laser exposure, is such that the laser supplies only the surplus of energy necessary to induce the solidification of some areas. In this way the fusion of unwanted regions is avoided and the unsintered powder acts, throughout the manufacturing operation, as supporting structure for the fabricated parts.

When the temperature of the building chamber has reached 120 °C it can be removed from the system [118]. However, the parts can be extracted from the powder cake only when the temperature of the powder cake is less than 80 °C. The reasons for these thermal limits are either to avoid thermal distortion of the components and to guarantee safe handling. A good practice that ensures to follow these guidelines is to wait at least 24 hours before removal of the building chamber from the EOSINT P 800 system. Once the parts are removed from the powder bed (Figure 78), they are cleaned with sand blasting.

Figure 78. Powder cake and removal of HT laser sintered PEEK parts (tensile testing bars) from the powder bed

A discrete number of parameters are involved in a HT-LS building process and will be discussed in the following paragraph. For clarity, a schematic illustration is provided in Figure 79.
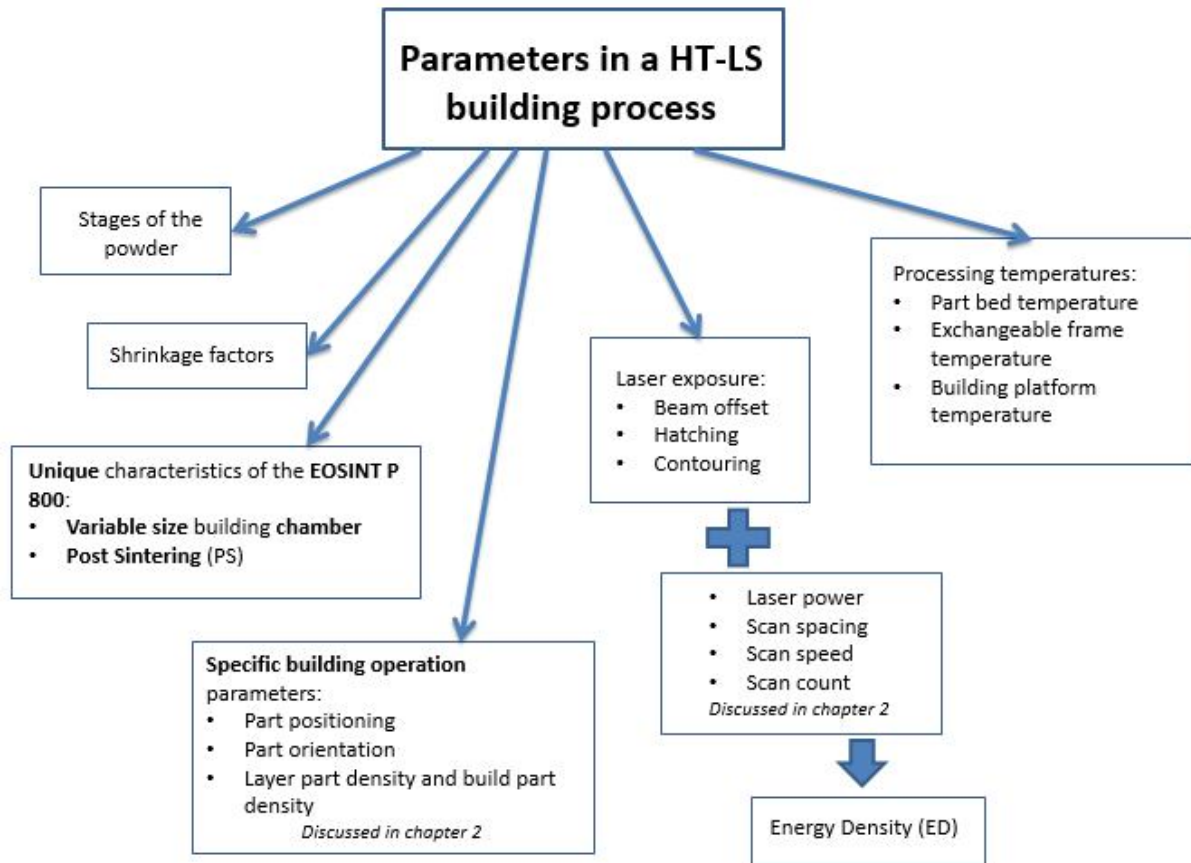
Figure 79. Parameters involved in a HT-LS building process

5.2.1 The stages of the powder

The powder material within a HT-LS system can experience different levels of thermal conditioning during a building process and is therefore classified as: fresh, overflow and used. When a powder has never been used in a LS process is classified as "fresh"; if instead it has been through a whole manufacturing process, acting as supporting material, it becomes "used". "Overflow" is the surplus of powder during the spreading of layers throughout a manufacturing LS process. The overflow powder experiences exposure to the processing temperature for a short period of time before being discarded into the overflow bin collectors.

5.2.2 Unique characteristics of the P 800 system

5.2.2.1 Variable size building chamber

Unlike others LS machines, the EOSINT P 800 allows to build components in full, half and reduced building chamber configurations. The half-build chamber is approximately half of the size of the full build chamber, while the reduced-build chamber is approximately a third of the size of the full building chamber. Interestingly, both reduced- and half-build chamber modes are achieved without the presence of physical frames, a condition that is believed to be a consequence of the particle properties of the PAEK materials.

Once PAEK particles are exposed to high temperatures for a relatively long amount of time, they retain a consolidated powder bed arrangement without requiring a physical frame. This behaviour could be due to the combination of thermal expansion and particle morphology that increases inter-particle mechanical locking and therefore the retaining of a vertical arrangement. Alternatively, it could be explained by hypothesising the formation of bonds between the unsintered particles of the powder bed that are later annulled during the operations of removal of the components from the powder cake and powder sieving. To this regard, Ghita et al. [134] have though shown that the PSD of used PEK HP3 powder shifted towards higher particle diameter values than the PSD of the original PEK HP3 powder, thus indicating an overall size increase of the used PEK HP3 particles potentially due to particle coalescence of the unsintered particles during HT-LS.

The size of half- and reduced- build chambers in respect to the full build chamber is shown in Figure 80, while the powder bed of the reduced building chamber mode during a building process is displayed in Figure 81.
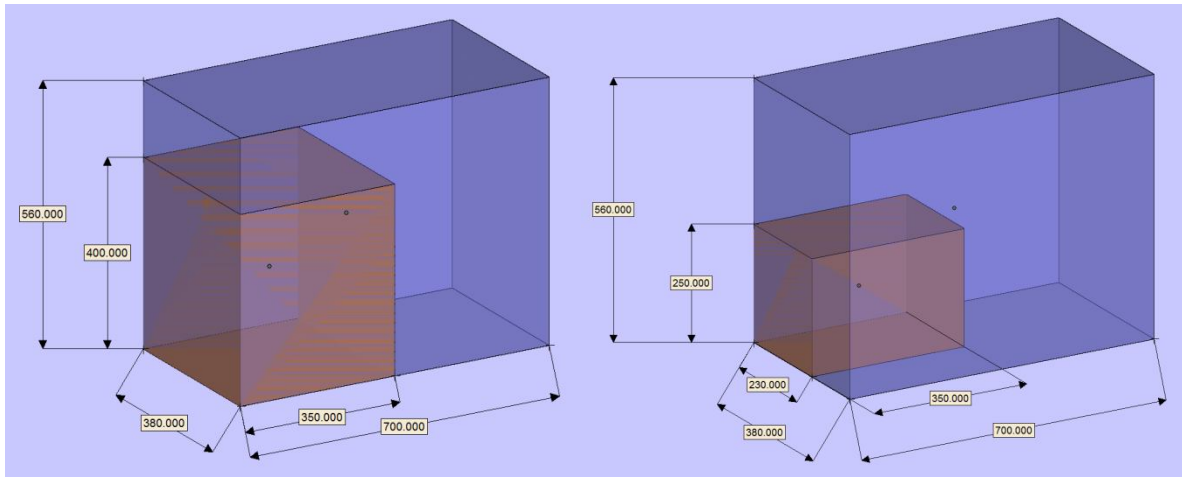
Figure 80. From the left, half and reduced build chambers within the full build chamber of the EOSINT P 800 system (measurements in mm)
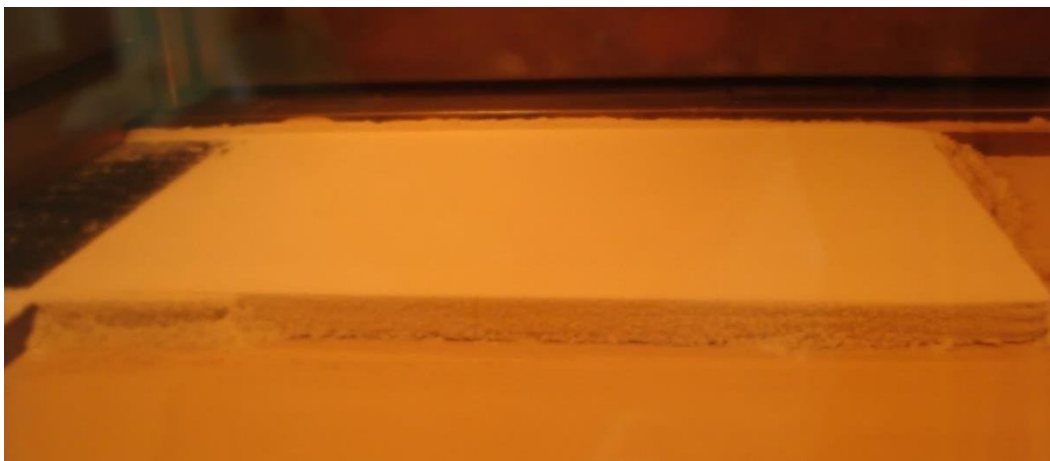
Figure 81. EOSINT P 800 powder bed in reduced build chamber mode. PAEK particles retain the powder bed arrangement without a physical frame

A few mechanical adjustments such as the change of the internal structure of the double blade recoater and consequentially of the feeder bin in order to match the geometry of the new recoater, modification of the orientation of the infrared heaters and activation of a physical switch on the system are required in order to change the P 800 system between the three building configurations. Additionally, parameters such as dispensing factor and part bed temperature also need to be appropriately modified. Although these changes are provided by the machine manufacturer [118],

187

orientation of the infrared heaters, alteration of the part bed temperature and modification of the dispensing factor are worth of discussion.

Infrared heaters are located above the building chamber along each side. Four in total, they provide for the powder bed temperature of new layers of powder during a building process. When the EOSINT P 800 is switched from full build mode to half or reduced modes, the reduction is applied from the right end side of the chamber towards the left end side (Figure 80), leaving the right end of the new powder bed (half and reduced) far away from the infrared heater fixed on the left end of the P 800 system. In order to still provide for the part bed temperature, this infrared heater is moved forward along its jig and its angle in respect with Z axis increased. The angle of the full build mode (41˚) is changed into a new value equal to 45˚. A scheme of these changes is illustrated in Figure 82.
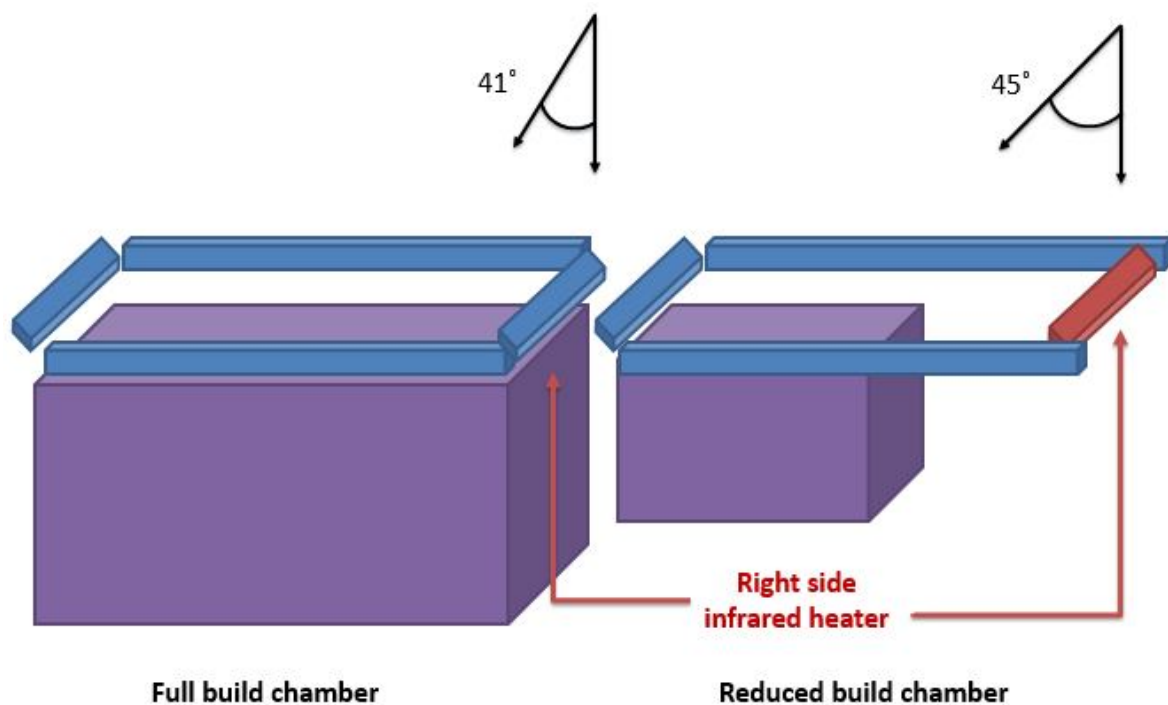
Figure 82. Variable build size chamber in the EOSINT P 800: position and orientation changes of the infrared heater on the right side of the system

When the P 800 system is switched instead from half or reduced building chamber mode to full building chamber mode, the part bed temperature has to be raised by 2 ˚C. No explanations of such a change are provided by the machine manufacturer.

Possibly, this modification is related to the considerable large size of the full building mode (700 mm x 380 mm) of the EOSINT P 800 system. Thermal gradients between sintered and unsintered material and thermal gradients between distant areas of the powder bed might be more likely to occur in a larger powder bed than in the powder bed of a smaller LS system, where laser sintered regions, unsintered powder and heating elements are closer. Therefore, the 2 °C temperature increase in the EOSINT P 800 system in full chamber build mode might help to minimise the occurrence of these detrimental thermal gradients in the powder bed.

The dispensing factor is a parameter that controls the amount of powder dosed into the double blade recoater prior to spreading. With value between 0 and 1, it has to provide enough fresh powder to cover the building area. If the EOSINT P 800 is used in reduced building mode, rather than in full or half building mode, this factor must to be changed accordingly, following the EOSINT P 800 manual guidelines [118]. It must be also outlined that an evaluation of this parameter should be carried out in case of any building mode with a new material. This adjustment will avoid encountering signs of poor recoating in the laser sintered parts as shown in Figure 83. Unfortunately, at present this evaluation could only be assessed by trial and error.
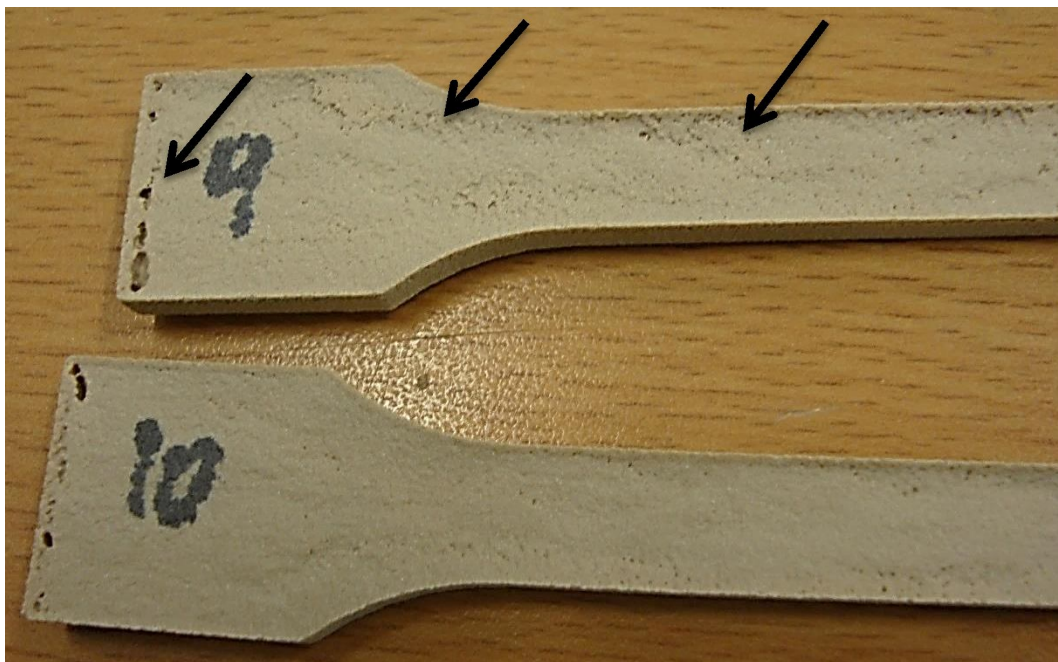
Figure 83. Examples of poor spreading due to inaccurate dispensing factor

Inaccurate values of the dispensing factor (Figure 83) lead to large depressions and cavities through the laser sintered parts and geometrical instability across the parts. The holes at edges were possibly originated by the lack of fresh powder during the hatching and contouring laser exposures (chapter 5.2.5). The lack of powder through the cross section of the part (hatching) can be seen by depressions and part geometrical loss indicated in the parts.

The analysis on the effect of the build chamber mode on the mechanical properties of HT laser sintered PEEK components is provided in chapter 5.4.

5.2.2.2 Post sintering

The Post Sintering (PS) is an additional heating phase applied to every layer during a building process. This phase is provided by the infrared heaters facing the powder bed when the laser exposure is completed, and before the powder bed is lowered and a new layer is deposited [118]. According to EOS [118], the PS allows to reach uniform melt between the areas exposed first and last in the same layer. The PS time is set to 12 s for PEK HP3 regardless of the building chamber mode. However, this parameter can be used defined.

The role of the PS time on the mechanical properties and microstructure of HT laser sintered PEEK specimens will be described in chapter 5.5.

5.2.3 Shrinkage factors

The shrinkage factors consist of a set of compensation values applied to the STL files in X, Y and Z directions in order to fend for the nominal dimensions of the components. These parameters are machine and material specific. Machine specific means that machines from different manufacturers may have different thermal distribution across the building areas and therefore require different thermal compensation factors. It can also mean that machines of different size (and therefore different powder bed size) have different thermal distributions and hence require ad-hoc compensation shrinkage factors. Material specific means that theoretically every material has its own shrinkage coefficients which should be considered during LS

manufacturing. In case of processing PEK HP3 in the EOSINT P 800 system, the standard EOS shrinkage factor values are: 5% in the X and Y directions and 5.4% in z direction [118].

5.2.4 Processing temperatures

When a material is processed in the EOSINT P 800 system, three temperatures are configured in every build. These temperatures, shown in Figure 84, are applied to different locations in the building chamber within the HT-LS system.

The part bed processing temperature (or simply part bed temperature) is the temperature of the material at the top of the building chamber as read by the optical pyrometer and corresponds to the actual temperature at which the LS takes place. In other words, it is the temperature at which the powder is kept before the laser exposure. Ideally, this temperature should set in order to achieve the best LS conditions by being not too high to cause over melt of the powder and not too low to trigger curling of the parts just after the laser exposure.

The exchangeable frame temperature is the temperature applied to the walls of the building chamber and it refers to the middle height of the building chamber.

Lastly, the building platform temperature is the temperature of the base of the building chamber. Exchangeable frame temperature and building platform temperature should match the ideal temperature gradient for the best cooling and crystallisation conditions of the material in use.

While EOS provides a procedure for the evaluation of the part bed temperature, no indications are available for the setting of the exchangeable frame temperature and the building platform temperature.
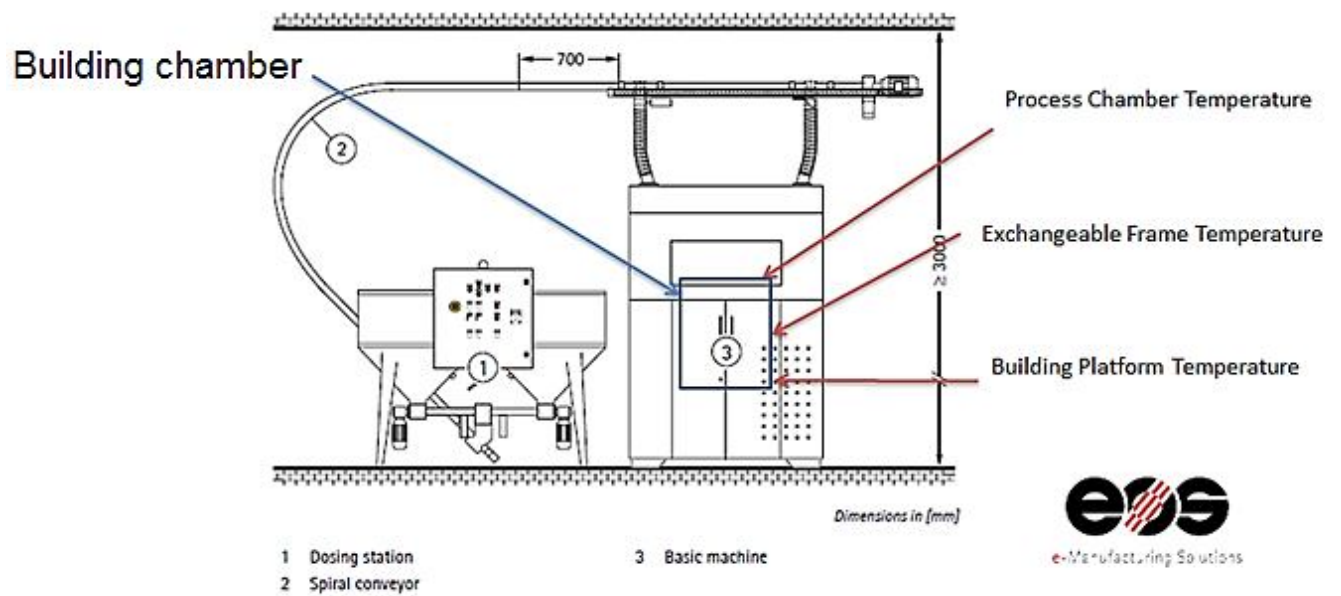
Figure 84. Processing temperatures applied to building chamber in the EOSINT P 800 [118]

5.2.5 Laser exposure

The laser exposure represents the strategy with which a part is consolidated by the laser. Contour exposure, hatch exposure and beam offset are the parameters that determine the final exposure of laser sintered part.

5.2.5.1 Hatching and contouring

The laser exposure strategy of a part is typically the sum of two contributions: contour exposure and hatch exposure. In the contour exposure, the laser induces the melt of the material particles that will form the outer edge/boundary of a component. In the hatch exposure the laser sinters the cross section of the parts. In order to ensure structural homogeneity in the solidification of the inner regions, hatching is alternated in the X and Y axes every layer.

An example of hatching and contouring is shown in Figure 85, where the red line represents the nominal dimension of the part, the blue line is the contour and green lines are the hatch lines.

192
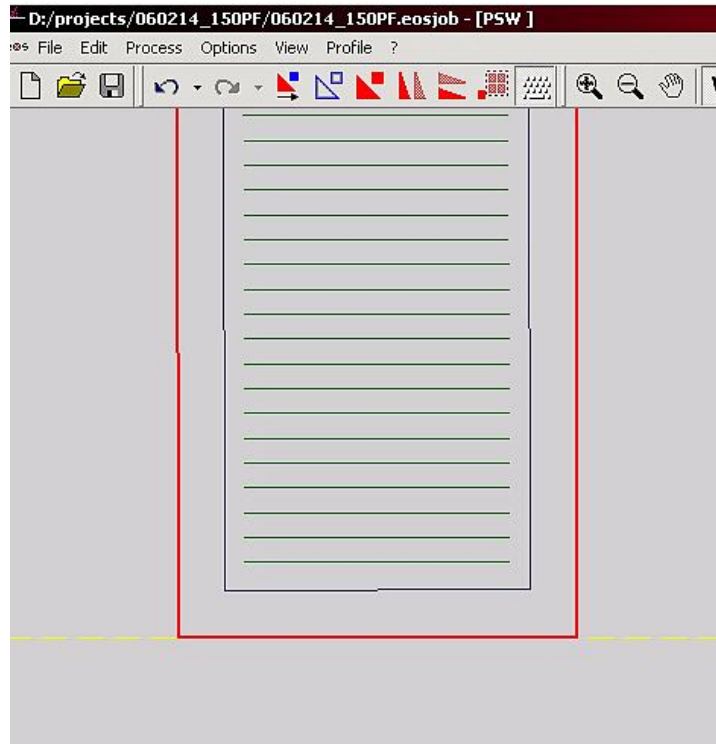
Figure 85. Hatching and contouring in LS

Hatching and contouring can be user defined. Parameters such as laser power, scan speed (laser speed during the exposure), scan count (number of times a vectors is scanned by the laser, generally equal to 1) and scan spacing (distance between two adjacent lines of hatching), described in chapter 2.2.2.1, can be set in the laser exposure profile for hatch and contour. For example, they can be appositely adjusted for the LS of sharp or very round edges and rough surfaces according to information generally provided in the LS manuals.

5.2.5.2 Beam offset

The beam offset is a correction of the laser path which aims to ensure that the nominal contour of a part will be equal to the actual contour of the part [118]. An illustration on the role of the beam offset in provided in Figure 86.
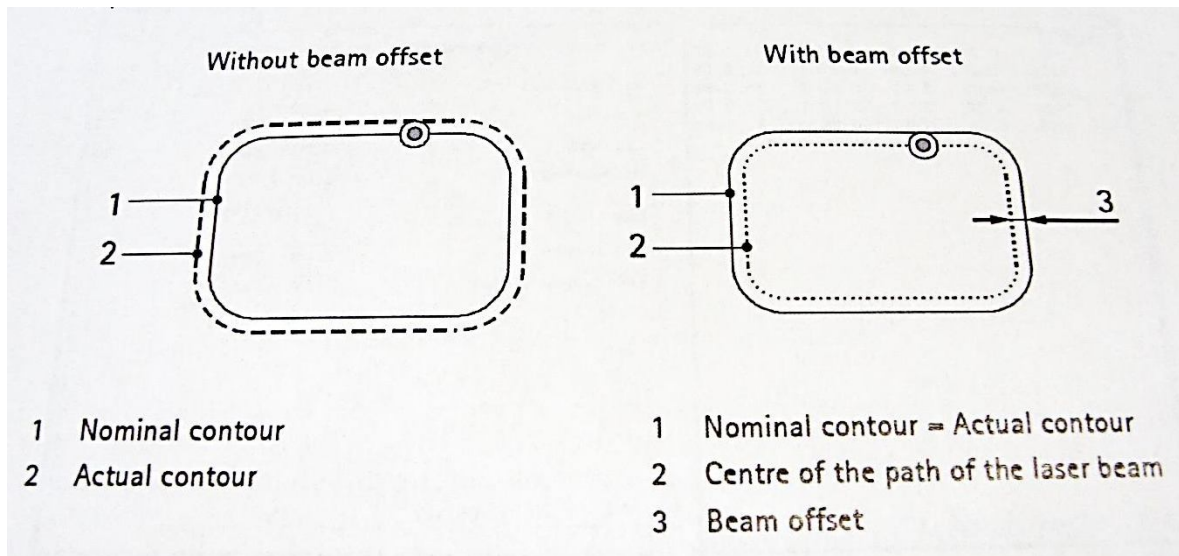
Figure 86. Beam offset [118]

5.3 HT-LS PEEK processing temperatures

EOS [118] provides a method for the evaluation of the optimum part bed temperature of PEK HP3 (EOS method). This technique is based on the visual inspection of the powder bed and is supplied in the manual of the EOSINT P 800 for the calibration of the part bed temperature over time.

In this project, the same procedure has been applied to thermally conditioned PEEK grades 150 PF and 450PF. The steps of the EOS method for finding the optimum part bed temperature are the following:

- Set the part bed processing temperature at 320 °C;
- Deposit layers as per normal operation;
- Pause build process, increase the part bed temperature by 5 °C, deposit one layer and wait for the heater power to drop below 40%;
- Increase the part bed temperature by 5 °C to 330 °C, deposit one layer and wait for the heater power to drop below 50%;
- Increase the part bed temperature in 2 °C increments, deposit one layer for each increment until the surface starts to discolour showing hotspots (melt of the material);

194

- Reduce the temperature from this transition temperature, in 1-2 °C stages, deposit one layer for each increment until the hot spots stop to occur.

PEK HP3 exhibits discolouring patches, indicators of material melt, at 374-375 ˚C. An approximately 9 °C reduction is required to obtain a stable powder bed.

In both thermally conditioned PEEK grades hotspots appear at approximately 340 ˚C, a 2 °C reduction to 338 °C and a reduction of 8 ˚C to 332 ˚C has been found for thermally treated PEEK 150PF and 450PF, respectively before the powder bed was thermally stable, i.e. without hotspots. These temperature were then found to be the optimal part bed temperatures of the PEEK grades.

Once the part bed temperature was found, tensile bars (chapter 3.2.1) of PEEK 150PF and 450PF were laser sintered along the X axis of the referencing system of the EOSINT P 800 system. A 20% decrease of the standard PEK HP3 laser exposure settings was used in both builds. The lowered laser energy allowed the building process to be carried out without the risk of over melt to the materials or damage to the system. More precisely, the building parameters were: laser speed of 2550 mm/s, scan spacing of 0.2 mm, laser power of 12 W for an overall energy density equal to 0.024 J/mm².

The HT laser sintered samples of both materials were compared in terms of tensile strength as described in chapter 3.2.1. PEEK 450PF exhibited higher tensile performance than PEEK 150PF and was therefore chosen to be the material to further optimise in the process. The different mechanical behaviour between the two materials can be explained by considering their melt viscosities. PEEK 450PF presents a higher melt viscosity than PEEK 150PF, as shown in chapter 4.1, which leads to a stronger material microstructure and ultimately a higher tensile strength than PEEK 150PF. Similar results were also found per ultra-high-molecular-weight polyethylene of different viscosity by Rimell et al. [192].

The tensile data for PEEK 150PF were determined as part of a parallel industrial project and results for this material cannot be reported in this thesis due to intellectual property reasons.

The optimisation of the part bed temperature in the HT-LS process was carried out on the thermally conditioned PEEK grades only. The reason for such a choice is

related to one of the industrial application areas that could strongly make use of HT-LS of PEEK, i.e. the medical sector. The addition of the Aerosil additive to the equivalent medical grades of PEEK 150PF or 450PF would have compromised the biocompatibility certification of the PEEK material overall, thus making the findings of this research project significantly less worthwhile for the medical device industry.

5.4 HT-LS optimisation according to variable build chamber size

The EOSINT P 800 system offers variable building chamber size. A standard low temperature (like PA) powder bed of a LS system operates by spreading layers of powder across the entire bed chamber. The top of the powder bed is thermally controlled by infrared heaters located above the building chamber, while the rest of the powder bed is uniformly regulated by heaters incorporated in the frame of the building chamber. This setup should guarantee a uniform temperature distribution. However, previous research showed the presence of small thermal gradients in the building area [115, 116]. Temperature discrepancies lead to part shrinkage, which, in turn, alters density and ultimately the mechanical behaviour of the laser sintered components.

Varying the building mode in the EOSINT P 800 system means varying this condition of direct contact between the frame heating elements and powder bed. While in full-chamber all sides of the powder bed are in contact with heaters, half chamber mode presents only three sides directly heated and one fully exposed to the building environment atmosphere. Reduced chamber presents even less direct heating control as only two sides are directly heated and two sides are left exposed. It appeared therefore essential to investigate the effect of the building mode on the HT laser sintered part properties.

Standard tensile testing bars (chapter 3.2.1) were built with the same building orientation in all the three building modes and tested in terms of tensile strength. More precisely, 20 samples were produced in reduced-building chamber mode, 32 in half-building mode and 64 in full-building chamber mode. The three builds were set with the following processing parameters: laser power of 6.8 W, scan speed of 1000 mm/s for contour and laser power of 12 W, scan speed of 2550 mm/s and scan spacing of 0.2 mm for hatching. The three builds carried out to analyse the effect of

the variable build size on the mechanical performance of HT laser sintered PEEK components are shown in Figure 87.
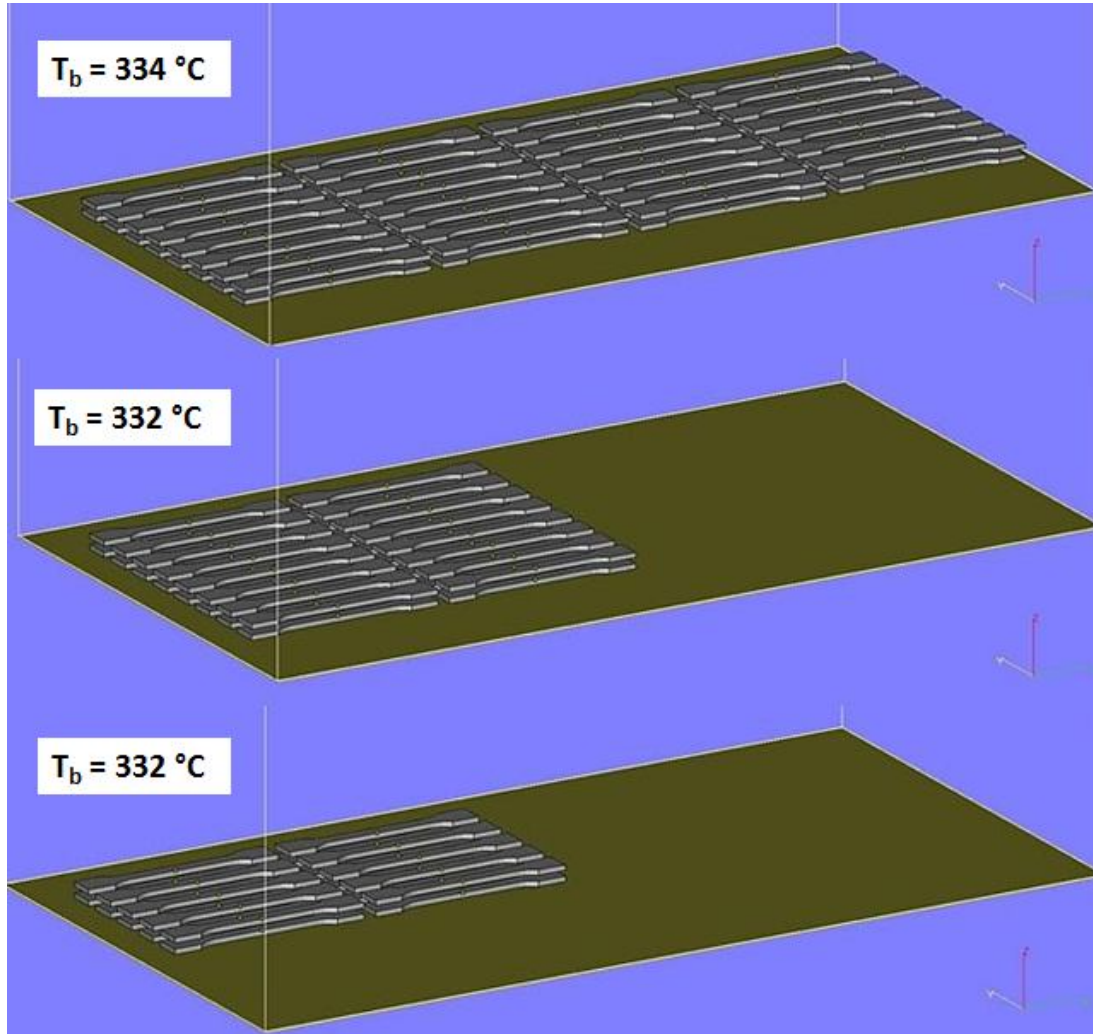
Figure 87. Manufacture of tensile bars carried out in the three building conditions: full-, half- and reduced-chamber

5.4.1 Variable build size chamber and tensile strength

The tensile strength values (average value and standard deviation) of the samples built in reduced-, half- and full-building chamber mode are reported in Figure 88, while the results of the statistics ANOVA analysis (chapter 3.2.7) are listed in Table 16.
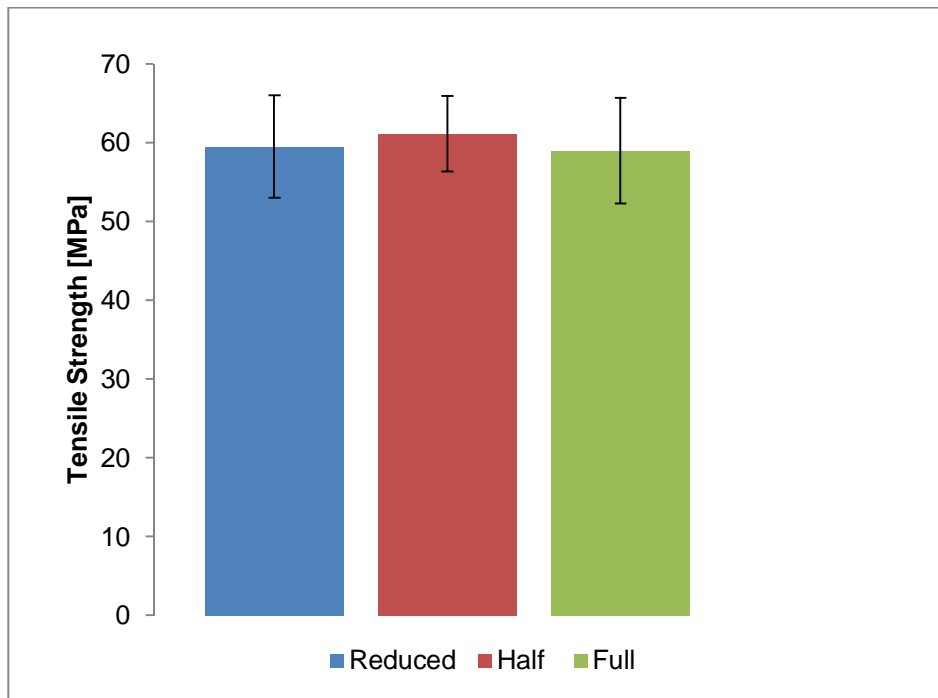
Figure 88. Tensile strength of the HT laser sintered PEEK 450PF samples built in full-, half- and reduced-chamber modes

Groups	P	Conclusion
Reduced chamber - Half chamber	0.733	*Not different*
Reduced chamber – Full chamber	0.987	*Not different*
Half chamber- Full chamber	0.228	*Not different*

Table 16. ANOVA results for the tensile strength values of the samples built in full-, half- and reduced- building configurations

The results displayed in Figure 88 clearly show that the tensile strength values of the samples manufactured in the three configurations are similar and independent of the building chamber mode when the builds are relatively shallow. The ANOVA results (Table 16) confirm as expected, the lack of significant difference between the tensile strength values of the specimens from the three builds.

Build height can affect the mechanical and surface properties of LS components (chapter 2.2.1.2). The greater the height, the longer the parts will stay in the building chamber of a LS system, before the cooling phase starts. In addition, certain building heights can more favour homogenous thermal distributions than others, i.e. parts built in the at mid height and in the central position will be more thermally shielded by the surrounding components and unsintered powder than parts more close to sides. Effects of these manufacturing conditions can be controversial.

Gibson and Shi [63] analysed the role of part orientation and part location on laser sintered PA specimens and found that samples built at central height of the building chamber were therefore exhibited higher tensile properties than parts built elsewhere. The authors suggested that the more performing specimens underwent better sintering because of a better thermal distribution condition due to the building location. Parts, for example, built close to the sides of the building chamber were less performing because thermal gradients might have potentially influenced structure and ultimately mechanical properties of these specimens.

However, Ghita et al. [116] found different levels of superficial colour change in PEK HP3 samples built at different heights within the building chamber of the EOSINT P 800. The skin of samples built at the bottom of the building chamber appeared darker and was found to have a lower onset material degradation temperature than the core of the same samples, indicating therefore the occurrence of thermo-oxidative phenomena on the surface of the sample during the cooling phase of the HT-LS building process. In the same work, the authors also found that the central building position and height led to more shrinkage in the HT laser sintered components.

It appears clear then the same parts built in a shallow build and in deep build might exhibit a few differences. Therefore, it is important to specify that the results found here are fully valid for shallow build (approximately 15-20 cm), but It would be good practice to check part performance in case of required higher build or full build manufacture.

The tensile strength results show that the energy supplied by the top infrared heaters is significantly higher and more prominent in the process than the energy provided by the frame heaters and the powder bed. This is an important finding for real

manufacturing processes and applications where repeatability and accuracy are key parameters in the future uptake of a technology. These findings also allowed the author to carry out the optimisation of the processing parameters in terms of ED and PS time by using the reduced-chamber building mode.

Lastly, it must be outlined that one of the differences between building in full building chamber and half- or reduced- is the number of spreading stages that each layer is subjected to. In half- and reduced- chamber, as the double blade recoater is reloaded with fresh of powder only on the left side of the HT-LS system, it recoats every layer twice. In case of full building chamber instead the recoater can be refilled on both sides, therefore every layer is recoated only once. This aspect becomes important when the spreading of the powder is still not optimal. One layer spreading might not overcome the irregularities introduced in the powder bed by the shape of irregular particles, but it might instead be strongly reduced with double spreading.

5.5 HT-LS optimisation of PEEK versus energy density

The ED is the amount of energy applied by the laser to the powder materials in order to induce the consolidation of material particles in specific areas across the powder bed inside a LS system. ED is a function of laser power (P), scan speed (v) , scan spacing (SS) and scan count (SC) [63]. For clarity the ED formula is shown again in Equation 21.

$$ED = \frac{P \times SC}{v \times SS}$$

Equation 21. ED formula

As it can be seen in Equation 21, if the laser power raises while the scan speed and scan spacing are kept constant, the overall ED increases and vice versa. Similarly, if the scan speed is lowered and the others two parameters are kept constant, the ED will increase again and vice versa.

During the laser exposure of a specific area, hatching and contouring have different ED values. The contouring interest only the outer surface of a part and has effect on surface finishing, while the ED related to the hatch phase is responsible for changes in the microstructure and mechanical performance of a LS component. For this reason only the role of the ED value related to the hatch stage is generally examined on the mechanical performance of laser sintered structures and so will it be applied here.

5.5.1 Testable samples

A build of specimens with individual settings of laser exposure (and therefore individual values of ED) was carried out in order to investigate the range of processing parameters leading to the manufacture of specimens that could be tested. Test samples were tensile bars built as described in chapter 3.2.1.

The processing parameters such as scan count and scan spacing were kept constant: scan count of 1 for both contour and hatch, scan spacing of 0.2 mm for hatch. It must be specified that when ED is calculated for the contour, the scan spacing is equal to 1. The varied processing parameters are listed in Table 17 (P=laser power and v = scan speed). The samples are ordered for increasing values of ED. Only the ED value related to the hatch stage will be considered against the mechanical properties of the corresponding HT laser sintered PEEK components.

Sample	Varied Parameter	Hatching: P (W)	Hatching: v (mm/s)	Hatch: ED (Jmm^{-2})	Contour: P (W)	Contouring: v (mm/s)	Contouring: ED (J/mm²)
A	P 10%	1.5	2550	0.0029	0.85	1000	0.0008
B	P 20%	3	2550	0.0059	1.7	1000	0.0017
C	P 30%	4.5	2550	0.0088	2.6	1000	0.0026
D	P 40%	6	2550	0.0118	3.4	1000	0.0034
E	P 50%	7.5	2550	0.0147	4.2	1000	0.0046
F	P 60%	9	2550	0.0176	5.1	1000	0.0051
G	P 70%	10.5	2550	0.0206	5.9	1000	0.0060
H	P 80%	12	2550	0.0235	6.8	1000	0.0068
I	P 90%	13.5	2550	0.0265	7.6	1000	0.0077
J	P 100%	15	2550	0.0294	8.5	1000	0.0085
K	P 110%	16.5	2550	0.0324	9.4	1000	0.0093
L	v 90%	15	2295	0.0327	8.5	900	0.0094
M	v 80%	15	2040	0.0368	8.5	800	0.0106
N	v 70%	15	1785	0.0420	8.5	700	0.0121
O	v 60%	15	1530	0.0490	8.5	600	0.0142

Table 17. Processing parameters and ED values for individual tensile bars (P = Laser power, v = Scan speed)

Images of the samples manufactured with individual ED values during the HT-LS process are shown in Figure 89 and Figure 90.

Figure 89. Build for testable samples. Each tensile bar was sintered with individual values of laser exposure corresponding to individual values of ED.
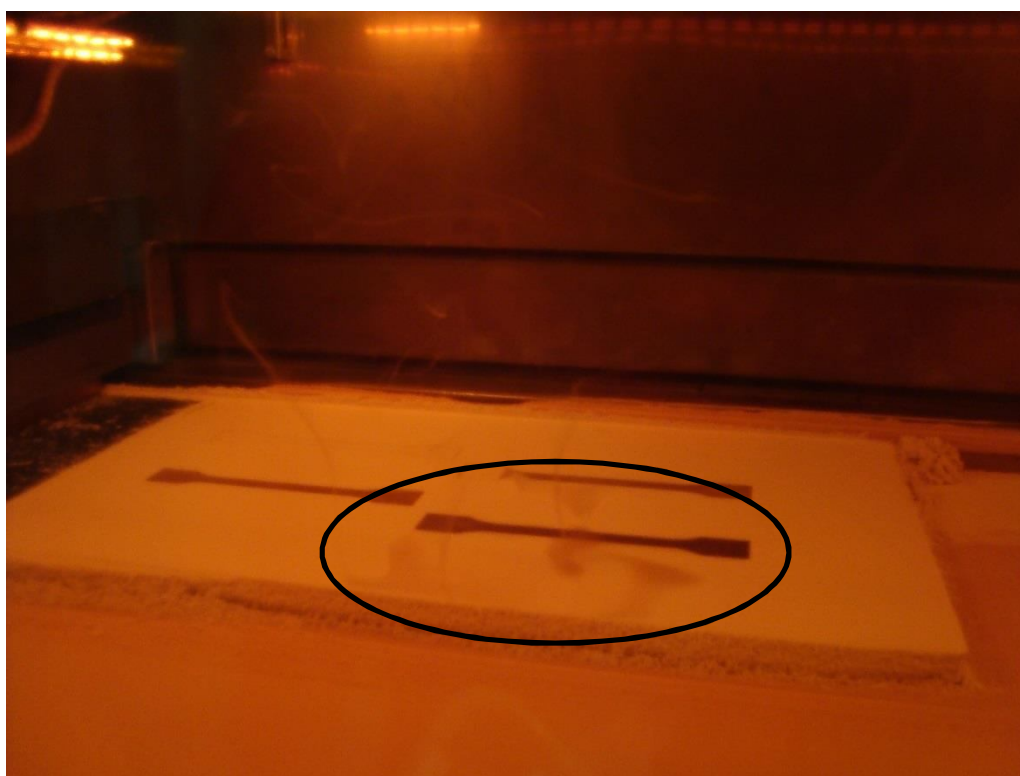
Figure 90. Smoke in the building chamber for the HT laser sintered PEEK samples manufactured at too high values of ED

Figure 89 shows different HT laser sintered tensile bars during the building operation. The samples exhibit different colours due, in this context, to the varied ED values chosen for their manufacture. Paler colours indicate lower ED, while darker colours indicate a more advanced melting status of the powder particles and correspond to higher ED values.

Figure 90 shows the samples built with the highest values of ED. The samples appear darker because of the more fully melting status of the powder and significant amount of smoke was originated in the building chamber because of the high ED applied.

The HT laser sintered samples manufactured with individual ED values were examined by qualitative observation. The individual samples are shown from Figure 91 to Figure 105.

It is important to outline that all the samples will present two set of numbers. The number of one or two figures was applied by the author during the removal of the specimens from the powder cake in order to keep track of part positioning in the HT-LS manufacturing process. The other number is a percentage number related to the ED manufacturing value. More precisely, the percentages are in respect to the standard EOS ED for the PEK HP3 material, whose conditions of laser exposure strategy are the following: laser power 15 W; hatching beam speed 2550 mm/s; scan spacing 0.2 mm; overall ED of 0.029 J/mm² (Equation 21).

The individual ED values are reported in Table 17 and were chosen in order to apply a systematic reduction or increase to the EOS standard settings (Figure 91 to Figure 105).

Figure 91. Build for testable HT laser sintered PEEK samples: sample A, manufactured at 10% laser power in respect to the standard EOS laser exposure settings

The sample manufactured with the lowest ED value is shown in Figure 91. The ED value was so low that the particles were not consolidated during the laser exposure and the sample broke when removed from the powder bed. Clearly, this sample had no part definition.

Figure 92. Build for testable HT laser sintered PEEK samples: sample B, manufactured at 20% laser power in respect to the standard EOS laser exposure settings

Figure 92 shows a sample built with a low value of ED. Although the sample did not break during the removal from the powder bed, it appears highly porous which will likely lead to very low mechanical properties.

Figure 93. Build for testable HT laser sintered PEEK samples: sample C, manufactured at 30% laser power in respect to the standard EOS laser exposure settings

Figure 93 shows another sample where the ED applied did not lead to an acceptable dense structure. The surface is rough and full of cavities.

Figure 94. Build for testable HT laser sintered PEEK samples: sample D, manufactured at 40% laser power in respect to the standard EOS laser exposure settings

Also in sample D (Figure 94), the surface is rough and highly irregular, signs of low processing parameters during the laser exposure.

Figure 95. Build for testable HT laser sintered PEEK samples: sample E, manufactured at 50% laser power in respect to the standard EOS laser exposure settings

Figure 95 shows a tensile sample built at a value of ED that is half of the standard ED used for PEK HP3 HT-LS. The surface of the specimen appears smoother than in the previous samples and therefore this manufacturing conditions were considered the lower limit of the processing parameters leading to the manufacture of testable samples.

Figure 96. Build for testable HT laser sintered PEEK samples: sample F, manufactured at 60% laser power in respect to the standard EOS laser exposure settings

Figure 97. Build for testable HT laser sintered PEEK samples: sample G, manufactured at 70% laser power in respect to the standard EOS laser exposure settings

Figure 98. Build for testable HT laser sintered PEEK samples: sample H, manufactured at 80% laser power in respect to the standard EOS laser exposure settings
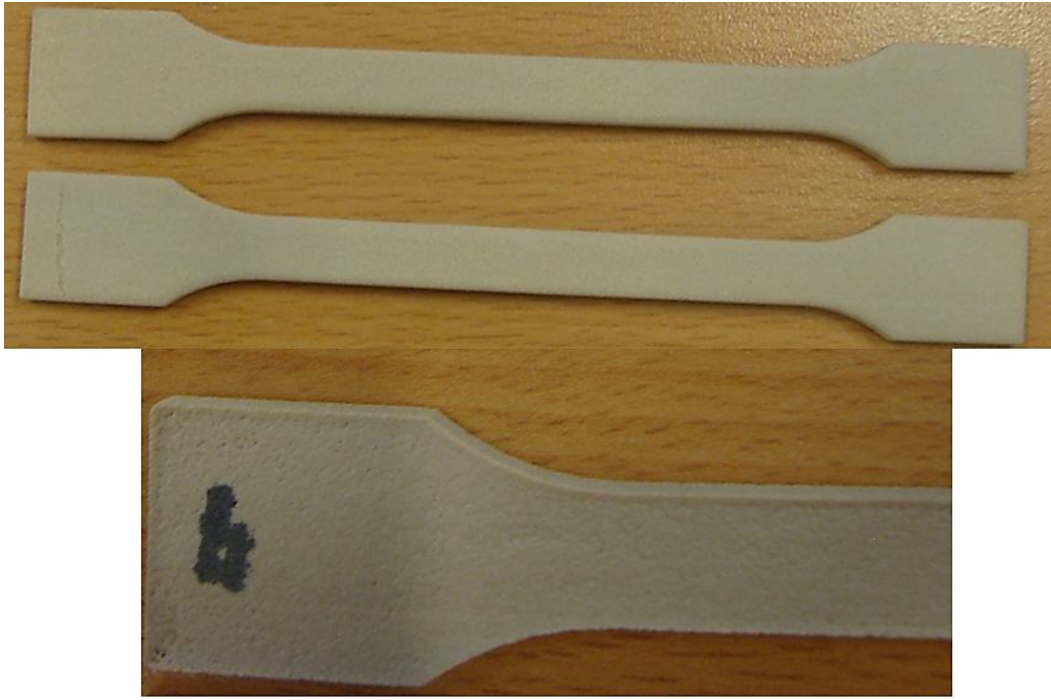
Figure 99. Build for testable HT laser sintered PEEK samples: sample I, manufactured at 90% laser power in respect to the standard EOS laser exposure settings
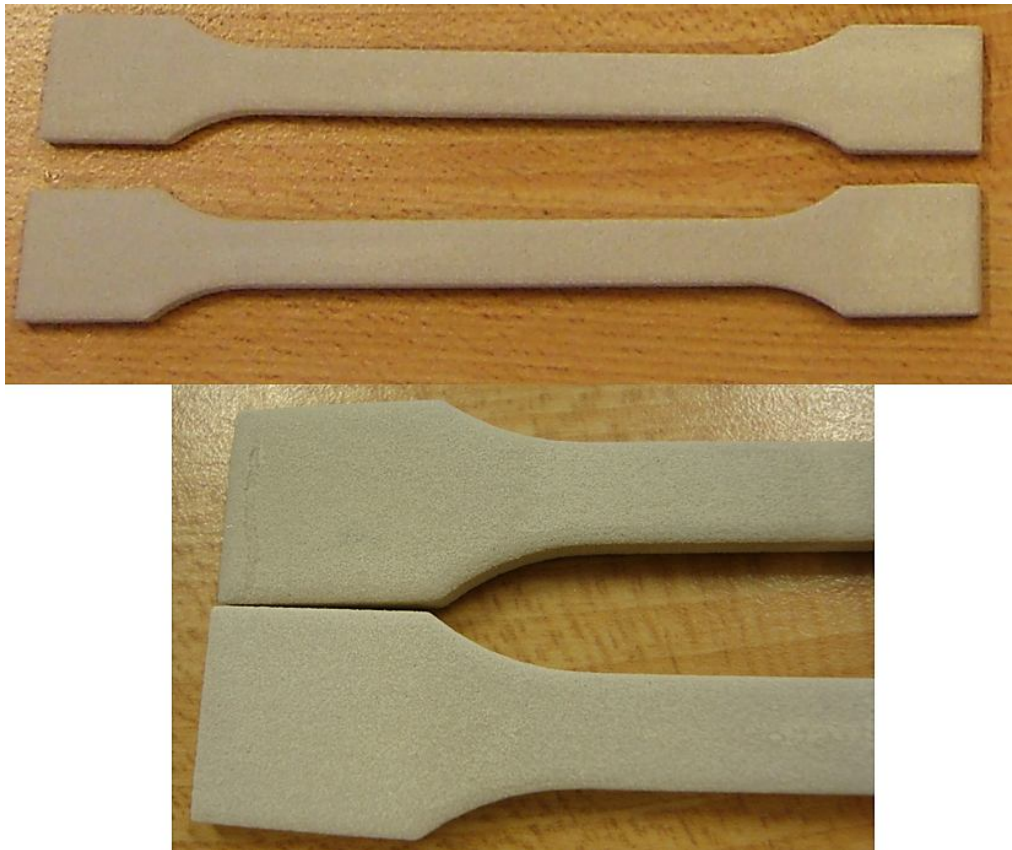
Figure 100. Build for testable HT laser sintered PEEK samples: sample J, manufactured at (100% laser power) at the standard EOS laser exposure settings

The specimens shown from Figure 96 to Figure 101 have been fabricated with increasing values of ED. All these samples showed denser structures and therefore the corresponding settings were used in later builds for the manufacture of test samples. In Figure 99 to Figure 101 the samples exhibited a line on one of the ends of the tensile bars. When a build of 30 tensile samples was performed with these ED values (chapter 5.5.2), only a minority of the samples showed this defect. As this line was always located at the edge and not across the gauge length of the samples, the specimens could still be used for tensile testing.
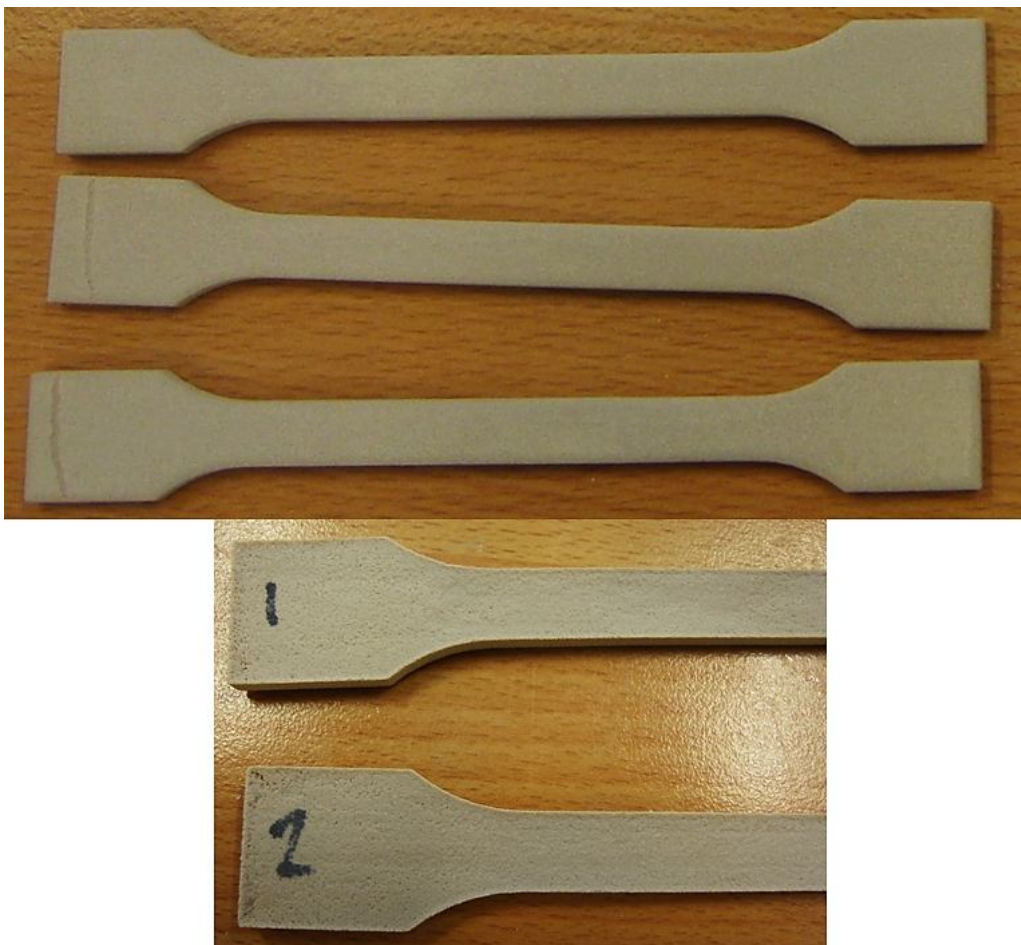
Figure 101. Build for testable HT laser sintered PEEK samples: sample K, manufactured at 110% laser power in respect to the standard EOS laser exposure settings
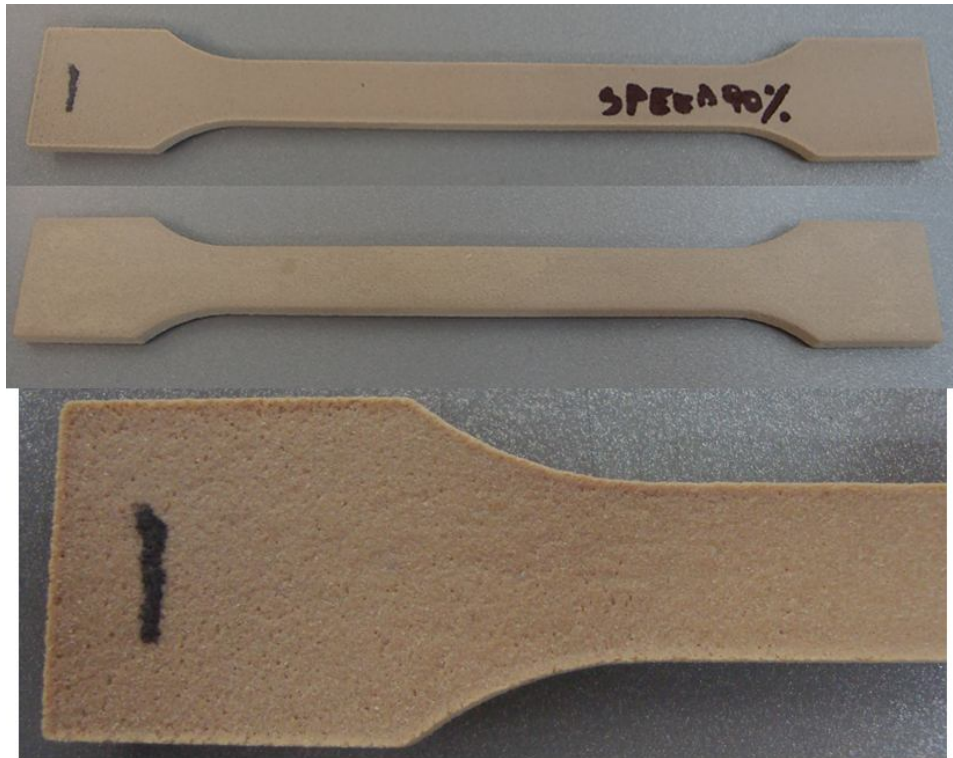
Figure 102. Build for testable HT laser sintered PEEK samples: sample L, manufactured at 90% scan speed in respect to the standard EOS laser exposure settings

Figure 103. Build for testable HT laser sintered PEEK samples: sample M, manufactured at 80% scan speed in respect to the standard EOS laser exposure settings

Figure 104. Build for testable HT laser sintered PEEK samples: sample N, manufactured at 70% scan speed in respect to the standard EOS laser exposure settings Sample N

Figure 105. Build for testable HT laser sintered PEEK samples: sample O, manufactured at 60% scan speed in respect to the standard EOS laser exposure settings

The samples from Figure 102 to Figure 105 were built with higher values of ED by decreasing the scan speed. These samples exhibited black speckles. These spots were considered signs of degradation of the polymer during the laser exposure. This was not surprising as a significant amount of smoke was generated during the laser consolidation of these samples (Figure 90).

Test samples were in summary those samples that were not too fragile to break only by handling during removal from the powder cake and not build at such high ED values that signs of material degradation (black spots) or loss of the geometrical stability of the component occurred.

5.5.2 ED optimisation

In order to optimise the HT-LS process for PEEK, an identical build (the same number of parts, in the same configuration and same orientation) was performed at different values of ED in reduced chamber mode. The values of ED were chosen after the analysis carried out in chapter 5.5.1. The ED range was of 0.0147-0.0324 J/mm² (Table 17). This *modus operandi* has allowed to isolate the role of the ED on the mechanical performance of the HT laser sintered PEEK parts. The build is shown in Figure 106.
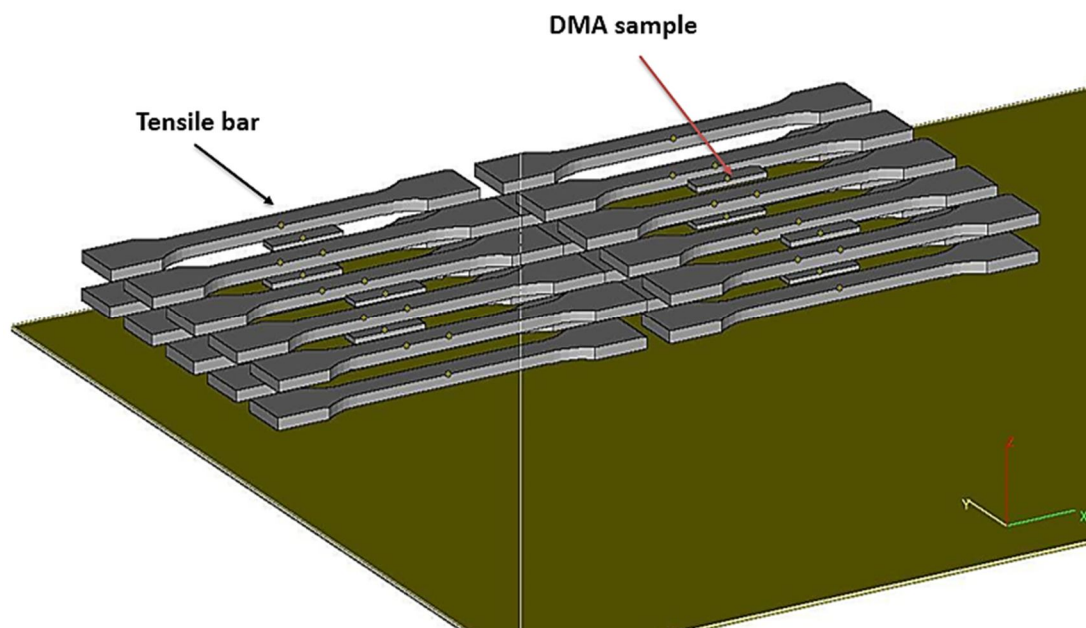
Figure 106. HT-LS PEEK build performed at increasing values of ED

The manufacturing parameters and the ED values calculated according to Equation 21 are listed in Table 18. Laser speed and scan distance were not varied and kept constant at 2550 mm/s and 0.2 mm for the hatch and at 1000 mm/s and 1 mm for the contour, respectively. A minimum of 20 tensile samples (chapter 3.2.1) and 4 DMA samples (chapter 3.2.4) were produced and tested for every build.

Processing parameters profile name	Hatch		Contour	
	v = 2550 mm/s SS = 0.2 mm P (W)	ED $[\frac{J}{mm^2}]$	v = 1000 mm/s SS = 1 mm P (w)	ED $[\frac{J}{mm^2}]$
1	7.5	0.015	4.3	0.004
2	9.0	0.018	5.1	0.005
3	12.0	0.024	6.8	0.007
4	13.5	0.026	7.7	0.008
5	15.0	0.029	8.5	0.009
6	16.5	0.032	9.4	0.009

Table 18. Processing parameters and ED

5.5.2.1 ED and tensile strength results

The tensile strength values of the same build manufactured at different ED is reported in Figure 107.
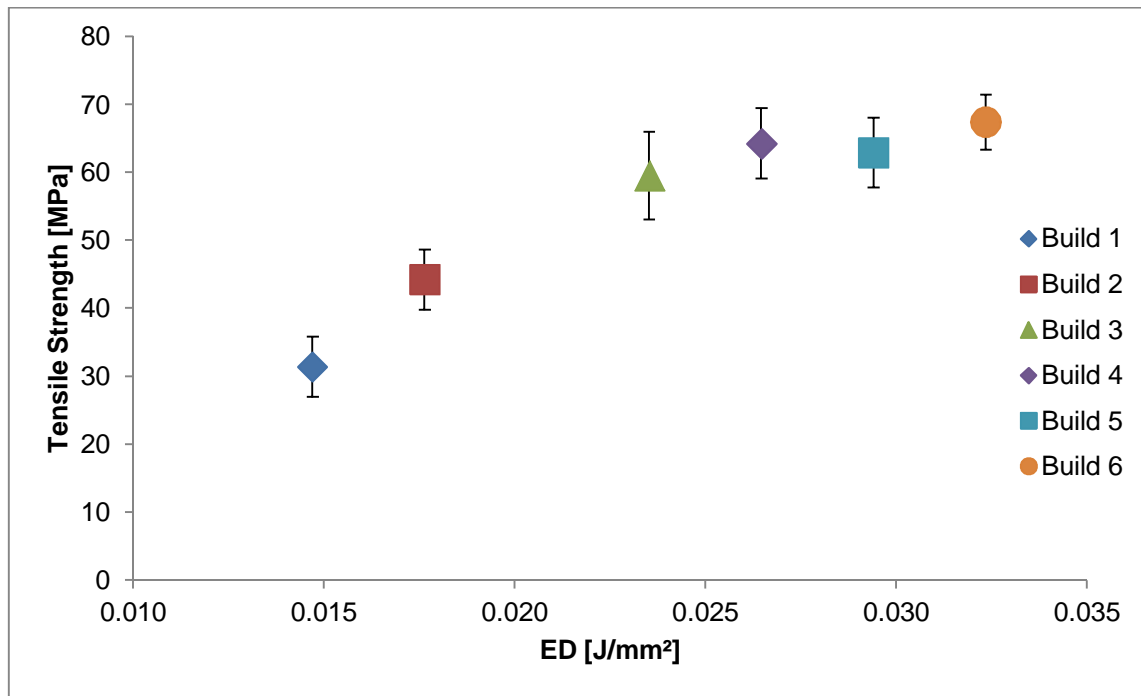
Figure 107. A plot showing the tensile strength of HT laser sintered PEEK samples manufactured at increasing ED values

As expected, the tensile strength values increased with higher ED. This was not unforeseen as similar results were exhaustively investigated for laser sintered PA based components [63, 85, 104, 121]. The results of the ANOVA analysis (chapter 3.2.7) are shown in Table 19. It is interesting to note that the tensile strength values corresponding to the energy densities of 0.026, 0.029 and 0.032 J/mm² are not significantly (statistically) different, which means that these three energy densities led to the similar mechanical performance in the samples. This is not surprising as similar results were found also in laser sintering of PA12 [121]. Higher laser energy densities lead to higher mechanical performance until a plateau in the mechanical properties is reached.

The parameters of build 5 corresponding to the ED of 0.029 J/mm², located in the central area of the tensile strength values plateau in Figure 107, were considered the optimal set of PEEK HT-LS processing parameters and therefore used in the next builds of this work.

Groups	P	Conclusion	Groups	P	Conclusion
1 - 2	0	*Different*	2 – 6	0	*Different*
1 - 3	0	*Different*	3 – 4	0.152	*Not different*
1 - 4	0	*Different*	3 – 5	0.614	*Not different*
1 - 5	0	*Different*	3 -6	0.001	*Different*
1 - 6	0	*Different*	4 – 5	0.997	*Not different*
2 - 3	0	*Different*	4 – 6	0.185	*Not different*
2 – 4	0	*Different*	5 - 6	0.008	*Not different*
2 – 5	0	*Different*			

Table 19. ANOVA results and ED optimisation of tensile strength of HT laser sintered PEEK components

In Figure 108, the optimised tensile strength value found for HT laser sintered PEEK 450PF samples (build 5) has been plotted for comparison with the tensile strength value of HT laser sintered PEK HP3 components [12]. Additionally, the literature values found for injection moulded PEEK 450PF and injection moulded PEK (trading name "HT P22PF" [2]) are shown. As expected, injection moulded samples showed higher values of tensile strength because of the pressure applied to the materials during the injection moulding process. The tensile strength of HT laser sintered PEEK 450PF is approximately 20 MPa lower than HT laser sintered PEK HP3, but can be still acceptable for a wide range of engineering applications [22]. Although HT laser sintered PEEK samples present lower tensile performance than PEK HP3 samples, HT laser sintered PEEK parts still retain the same high operating temperature of PEK components (250-260 ˚C) [23]. In addition, PEEK provides a melting temperature which is 20-30 ˚C lower than PEK. This property could lead to less degradation of the unsintered particles during HT-LS manufacturing and therefore higher potential for the recycle of the PEEK material.
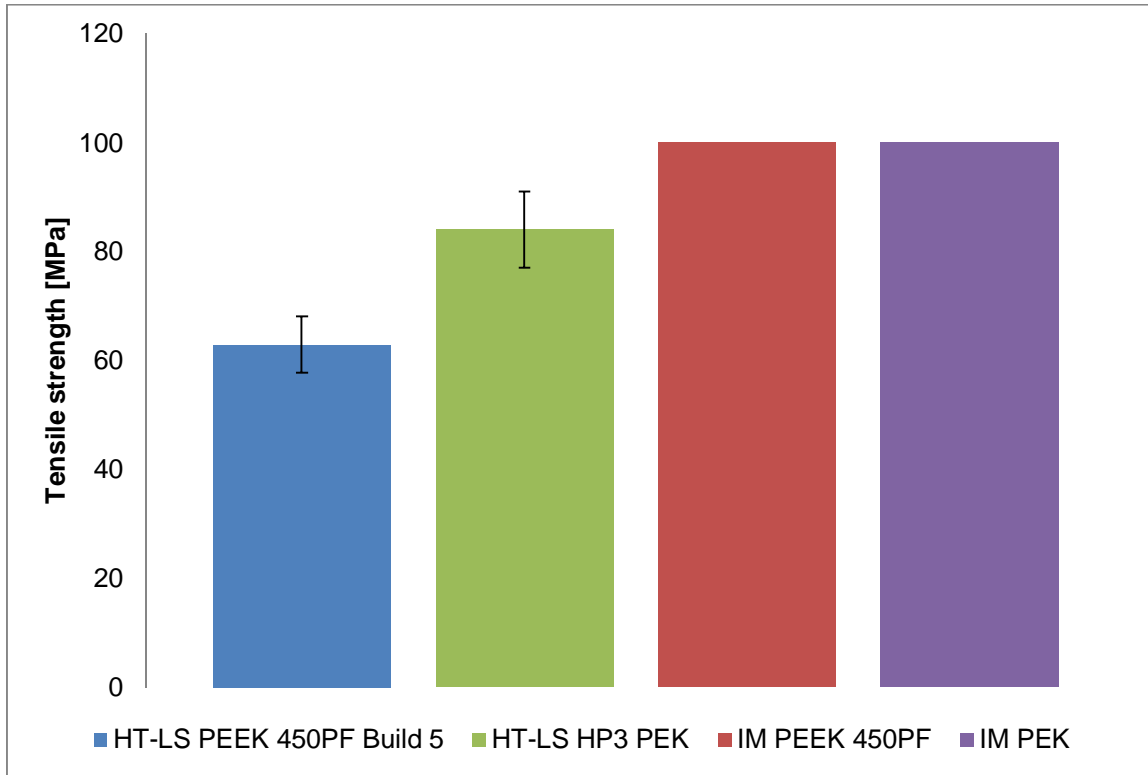
Figure 108. Tensile strength of HT laser sintered and Injection Moulded (IM)

PEEK 450PF and PEK HP3 [134]

5.5.2.2 Post-treatment of HT laser sintered samples build 6

With the aim to push the limits of the tensile strength of HT laser sintered samples, an additional build according to the parameters of build 6 was repeated and the sintered samples were subjected to a post treatment after their LS manufacturing as described in chapter 3.2.2. The samples were tested and compared with the tensile test results of the samples from build 6. The tensile strength results (average values and standard deviations) are listed in Table 20.

Sample	Tensile Strength (MPa)
Build 6	67 ± 4
Build 6 + Post-treatment	69 ± 5

Table 20. Tensile strength of post-treated build 6 samples

The tensile strength results of the two sets of samples showed no significant increase in the tensile properties. However, black spots appeared on the tensile bars after the post-processing treatment (Figure 109), indicating the occurrence of thermal degradation in the samples.

Figure 109. Post-treated build 6 samples

5.5.2.3 *Micro-CT analysis of HT laser sintered PEEK samples*

The micro-CT imaging analysis carried out for all the PEEK samples manufactured at different ED is reported from Figure 110 to Figure 132.

The purpose of this analysis was to examine the microstructure of HT laser sintered PEEK samples manufactured at increasing ED overall, not necessarily the bonding between layers. Therefore, it was not kept track of the building orientation of the samples during the micro-CT scanning.

A sample was measured as described in chapter 3.2.6 for each set of manufacturing parameters listed in Table 18. A 3D image of each ED sample with the indication of the planes of cross-sections (XY, YZ and XZ) is followed by the corresponding cross sectional images, an example of pore size and material density evaluation.

Figure 110 shows the micro-CT scan of the sample fabricated according the settings of build 1. The three planes identify the locations of the cross sections reported in the following figure (Figure 111). The 3D image resulting from the evaluation of the material density is shown in Figure 113.

Figure 110. Micro-CT scan of the sample from build 1

Figure 111. Micro-CT scan of the sample from build 1: cross sections

219

Figure 112. Micro-CT scan of the sample from build 1: example of pore size, 0.39 mm

The sample of build 1 (Table 18) shows a high level of porosity (Figure 111). The layer effect, which is typical of LS manufacturing, is clearly visible in both XY and XZ cross sections of Figure 111. This characteristic indicates the lack of good melting between successive layers during the LS process, due to the low ED set for this HT-LS build. An example of 0.39 mm pore size found in the sample is shown in Figure 112.
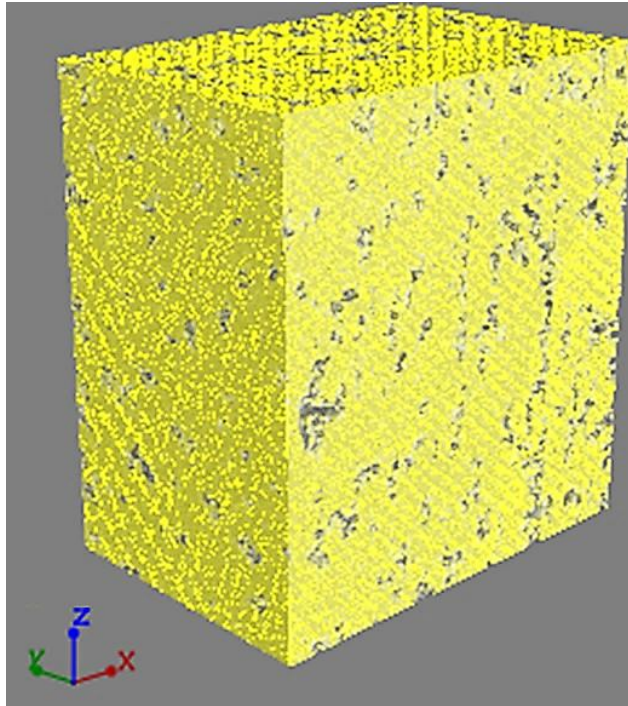
Figure 113. Micro-CT scan of the sample from build 1: material density

Figure 114 represents the sample built according the parameters of build 2 (Table 18) and the corresponding cross sections are shown in Figure 115. Figure 116 and Figure 117 show an example of pore size and material density, respectively.
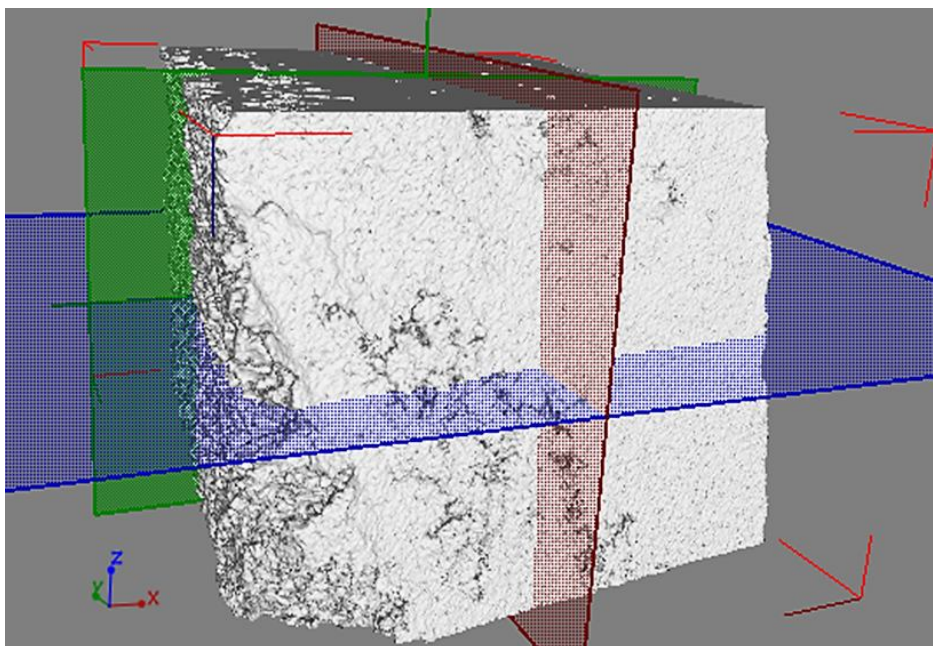
Figure 114. Micro-CT scan of the sample from build 2
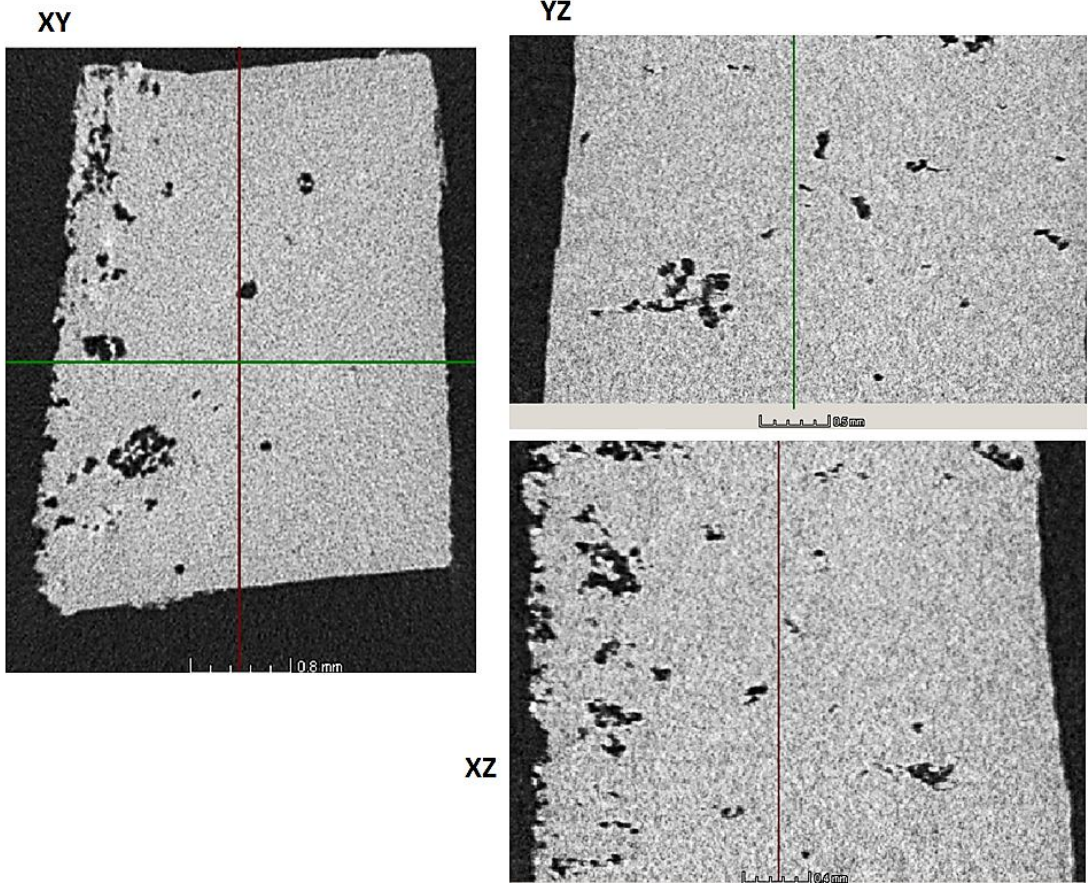
Figure 115. Micro-CT scan of the sample from build 2: cross sections
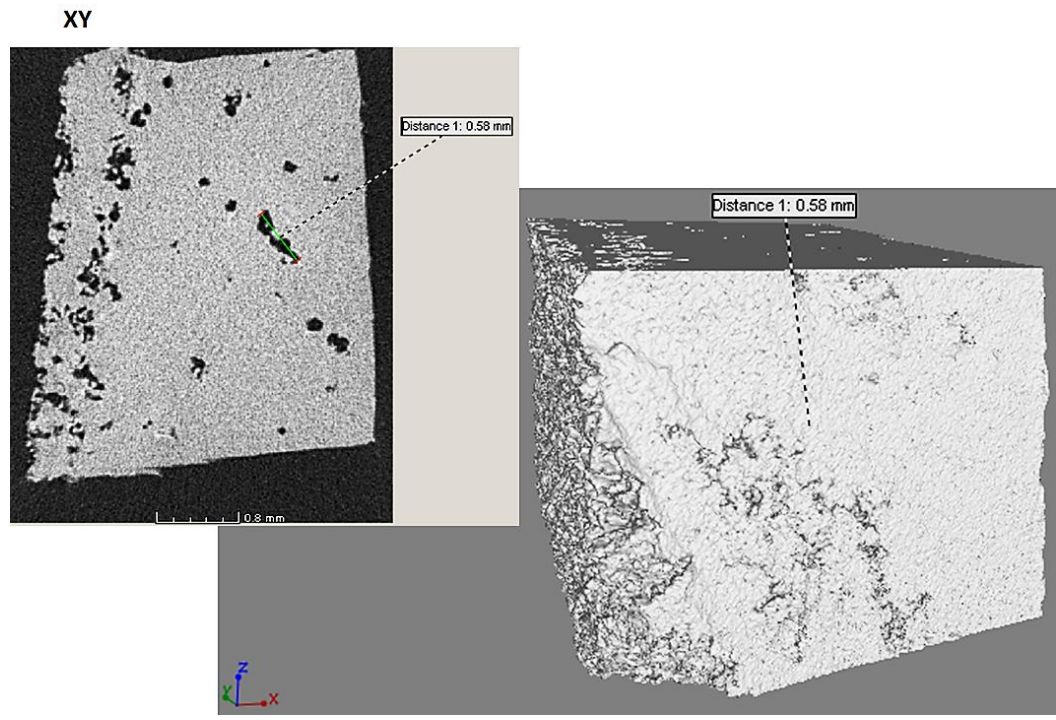
Figure 116. Micro-CT scan of the sample from build 2: example of pore size, 0.58 mm
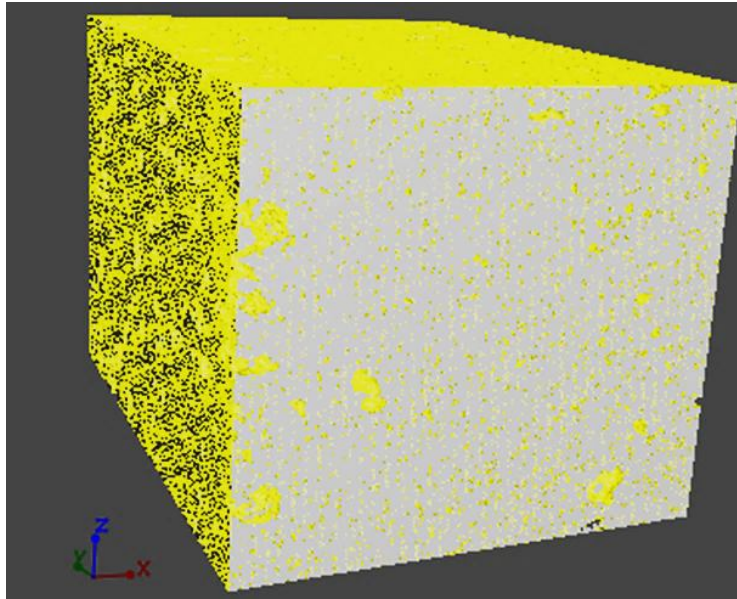
Figure 117. Micro-CT scan of the sample from build 2: material density

Porosity and pores of 0.58 mm (Figure 116) are clearly visible in the sample as the result of low energy density used in this build. However, when compared to build 1, the increase of the ED led to two main effects: the smaller number of cavities when compared to build 1 and a denser structure where the layer effect is no longer visible. The sample from build 3 with corresponding cross section images and example of pore size is shown from Figure 118 to Figure 120, respectively.
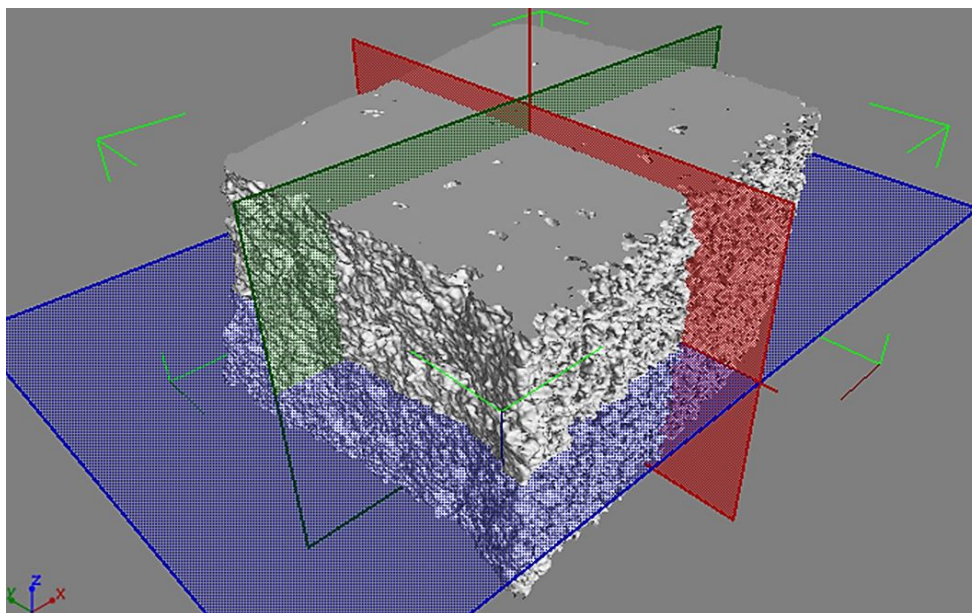
Figure 118. Micro-CT scan of the sample from build 3
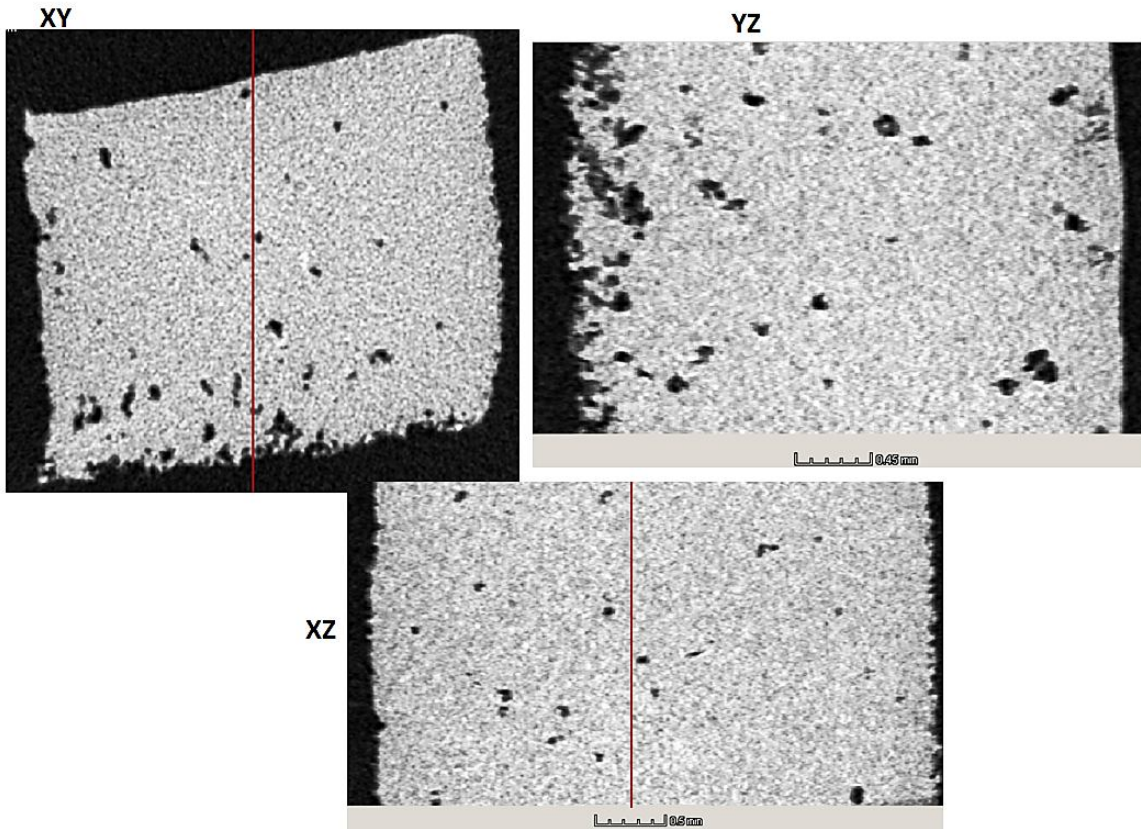
Figure 119. Micro-CT scan of the sample from build 3: cross sections
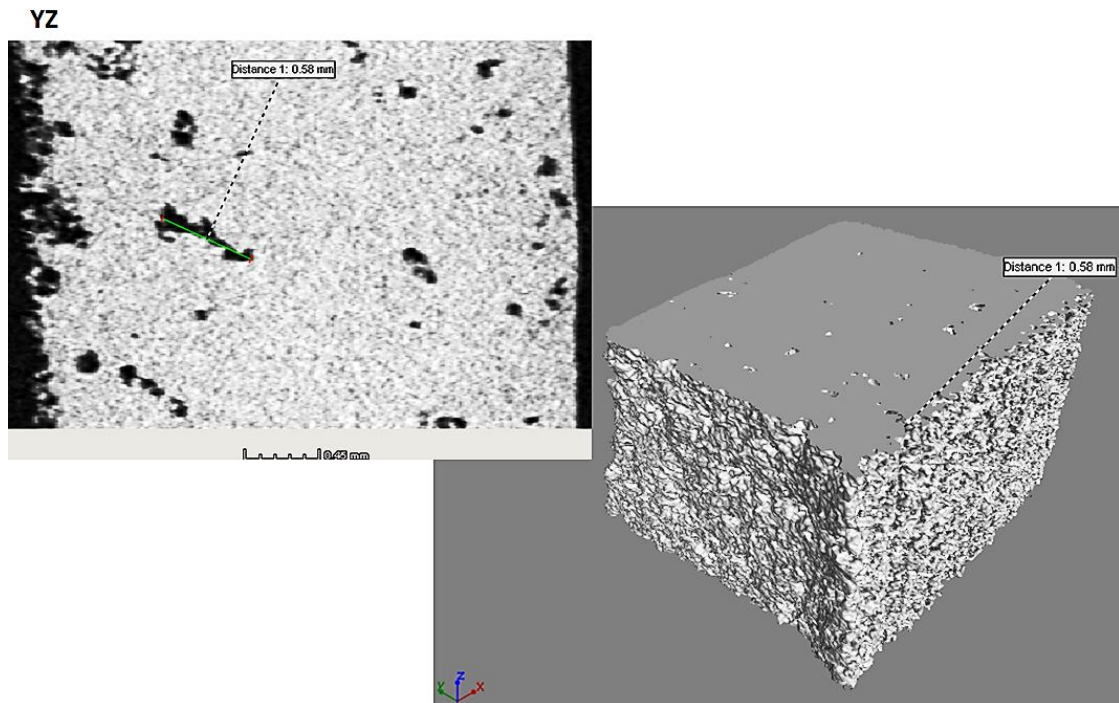
Figure 120. Micro-CT scan of the sample from build 3: example of pore size, 0.58 mm
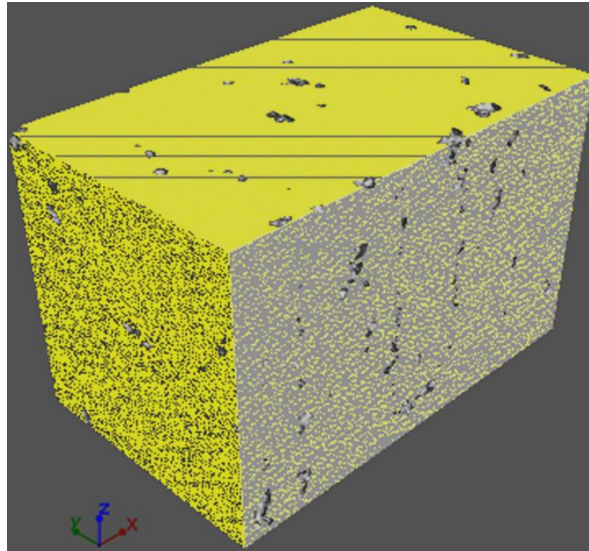
Figure 121. Micro-CT scan of the sample from build 3: material density

The sample from build 3 shows similar characteristics of the sample from build 2. The layer effect is not clearly visible; however pores are still present with size up to 0.58 mm. These large pores of size of 0.58 mm are considerably large when compared to the layer thickness of 120 µm used in the HT-LS process. In other words, if these cavities were developed along the building direction of the HT-LS process, this pore size could indicate that the pore was developed through at least 5 layers. However, as specified before it was not kept track of the building orientation of the samples during the micro-CT scanning, and therefore these pores might instead had developed only across one layer (one XY plane) as results of low ED and particle arrangement. The increase of 10% between the ED of build 2 and build 3 did not cause a significant density improvement in the microstructure (Figure 121), contrary to the results found in the tensile test (chapter 5.5.2). The result of the material density evaluation is shown in Figure 121. Figure 122 shows the sample from build 4 with corresponding cross sections shown in Figure 123. The analysis of the material density is shown in Figure 125.
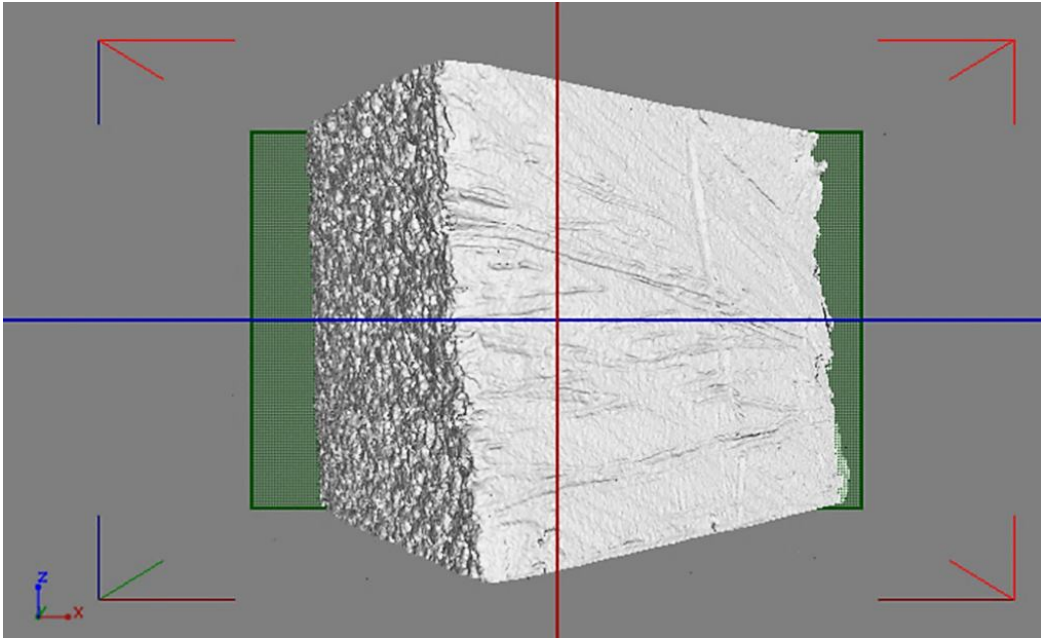
Figure 122. Micro-CT scan of the sample from build 4
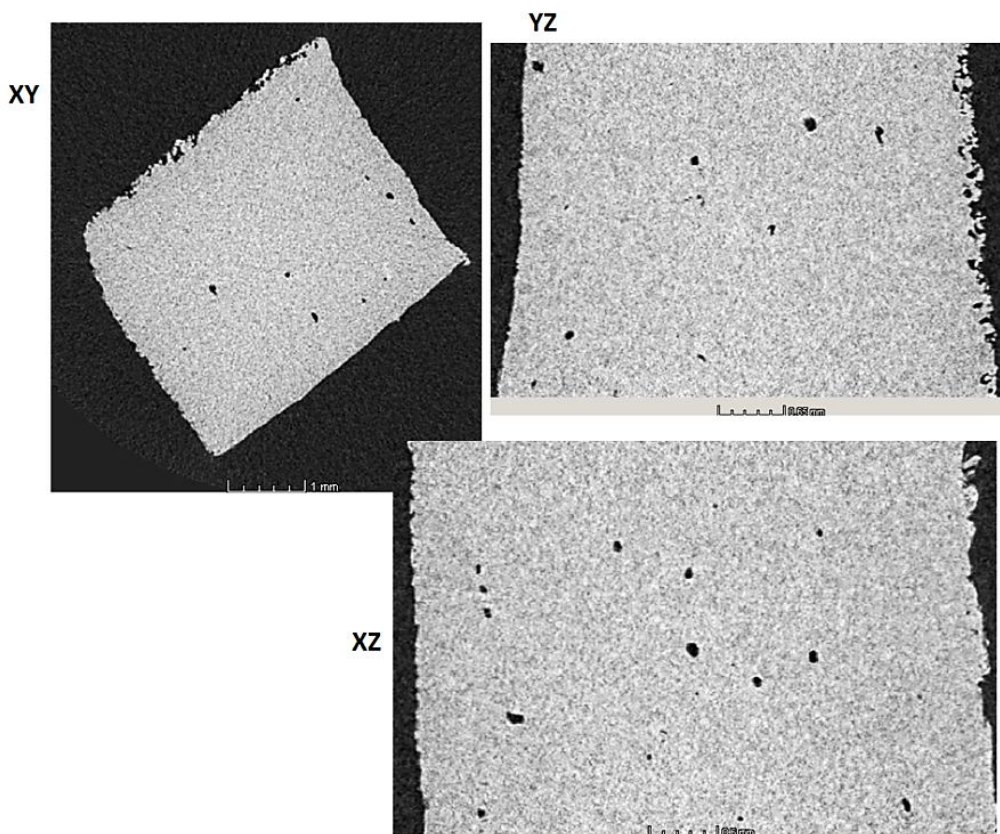
Figure 123. Micro-CT scan of the sample from build 4: cross sections
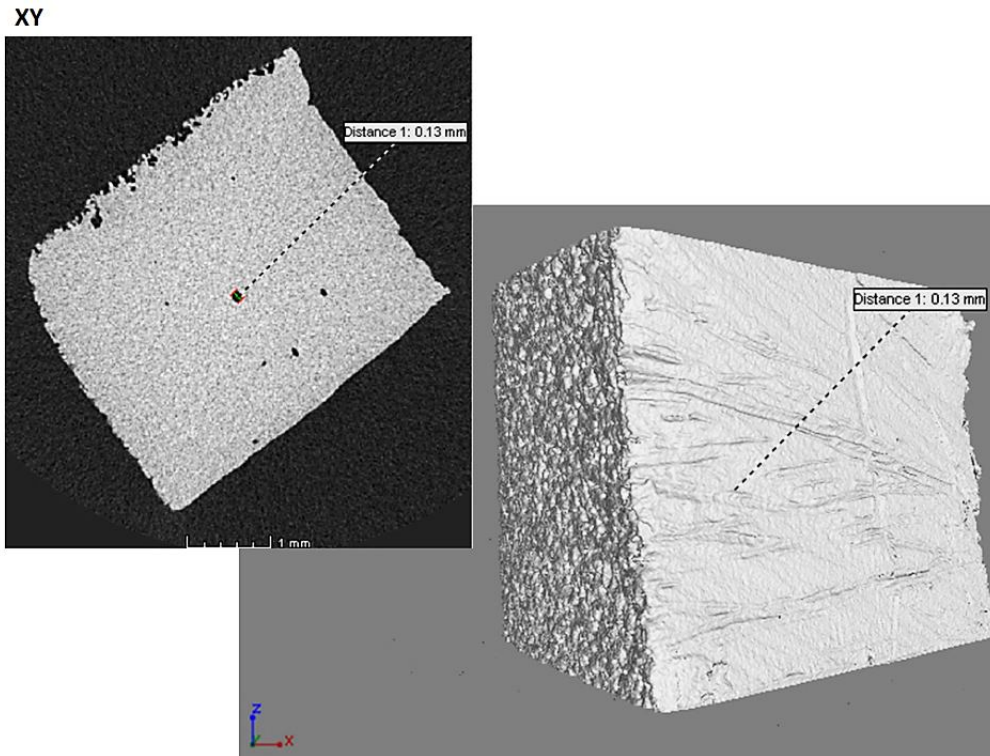
Figure 124. Micro-CT scan of the sample from build 4: example of pore size, 0.13 mm

The microstructure from the sample from build 4 appears less porous and the size of the pores is smaller (size of 0.13 mm for the pore shown in Figure 124). This finding can indicate a more advanced consolidation stage of the particles during the HT-LS process carried out with these processing parameters.
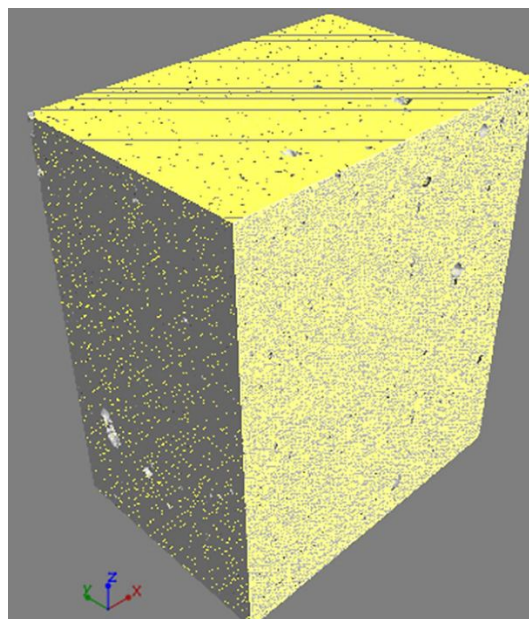
Figure 125. Micro-CT scan of the sample from build 4: material density

The sample manufactured according the setting of build 5 is shown in Figure 126. Cross sections are reported in Figure 127 and an example of pore size is displayed in Figure 128.
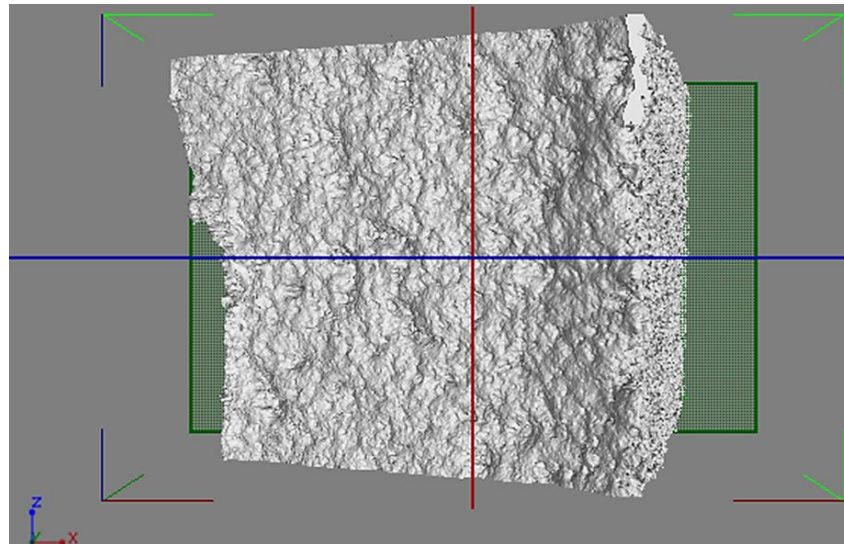
Figure 126. Micro-CT scan of the sample from build 5
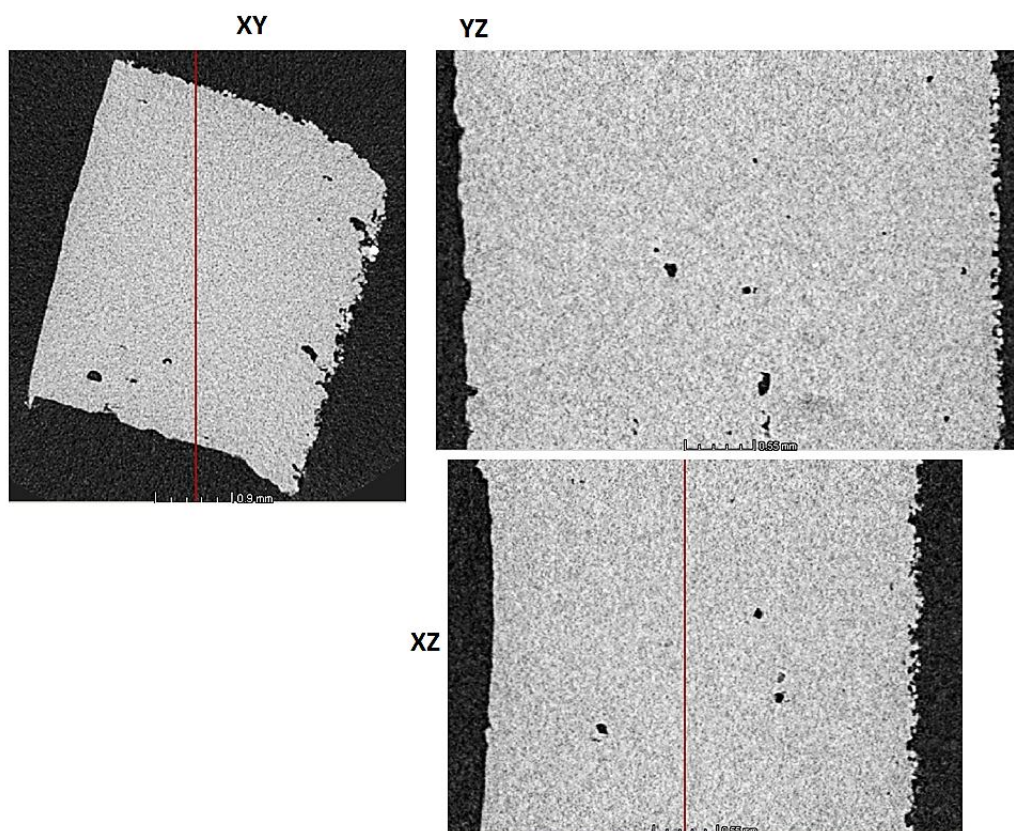
Figure 127. Micro-CT scan of the sample from build 5: cross sections
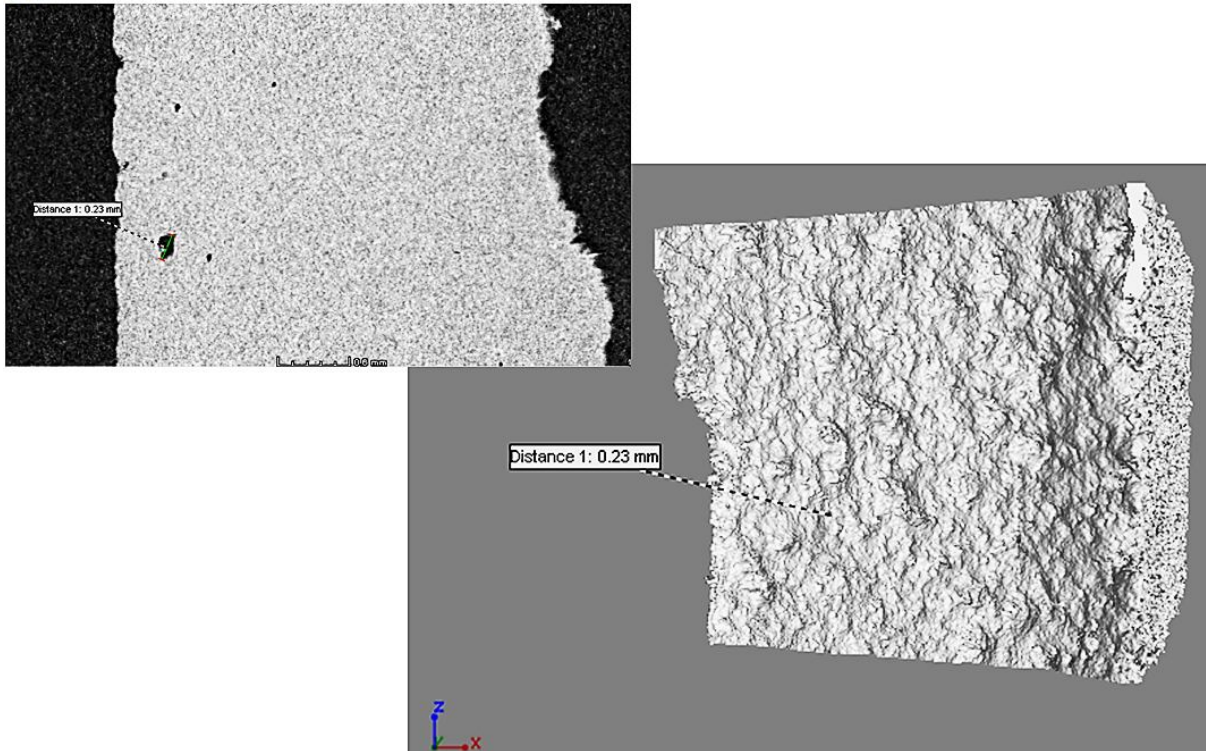
Figure 128. Micro-CT scan of the sample from build 5: example of pore size, 0.23 mm

Sample 5 exhibits a dense microstructure with a few pores of size up to 0.23 mm (Figure 128). This result confirms what was found in the tensile test results (5.5.2) where build 5 was chosen as the set of optimal processing parameters for the next HT-LS PEEK builds. The evaluation of the material density is shown in Figure 129. The samples appear fairly dense with only few small visible pores.
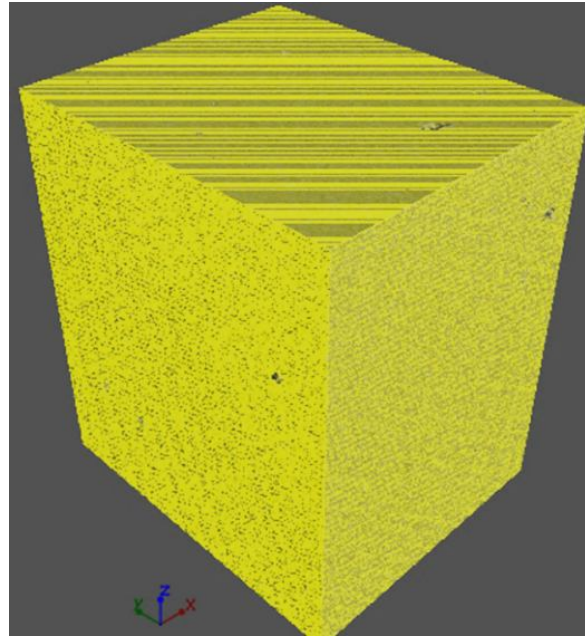
Figure 129. Micro-CT scan of the sample from build 5: material density

The sample manufactured according to build 6 parameters is shown in Figure 130, while cross sections, example of pore size and density are shown in Figure 131 to Figure 133, respectively.
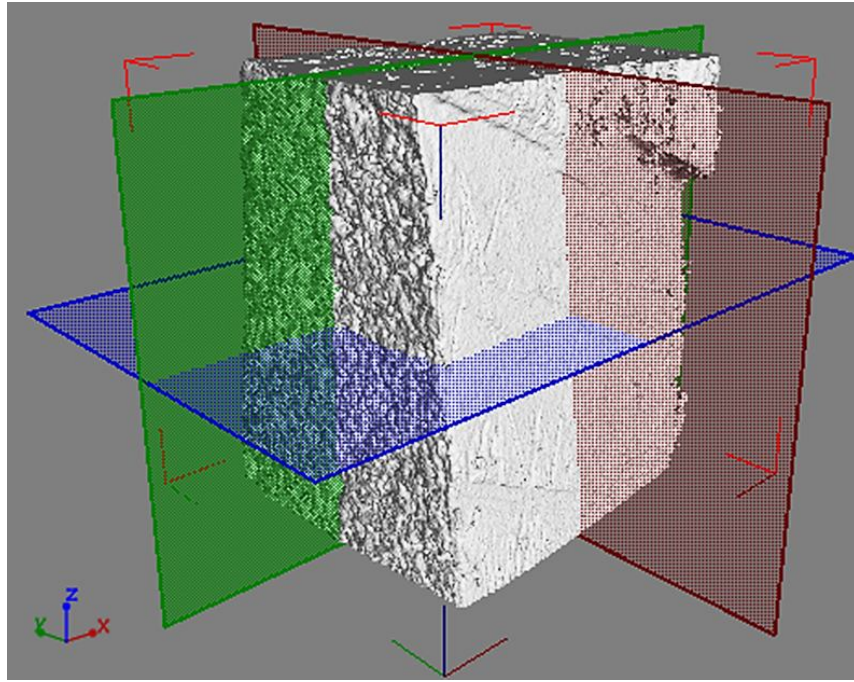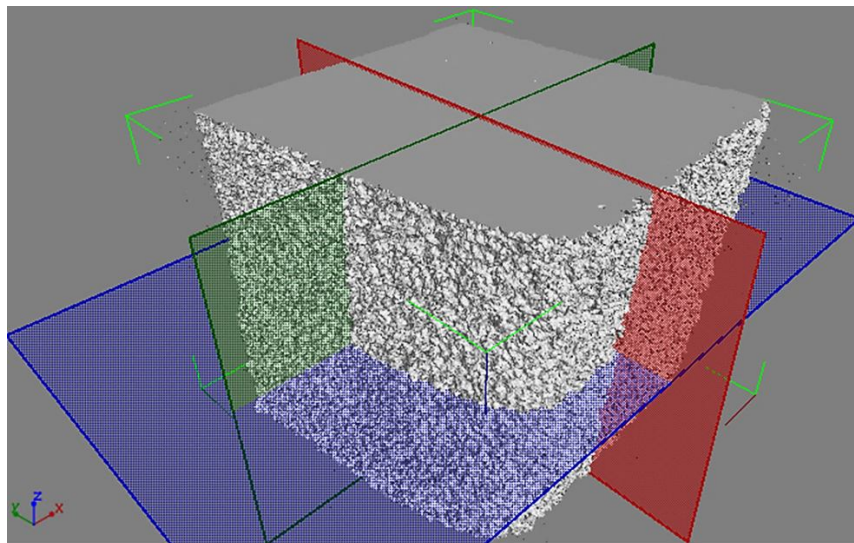

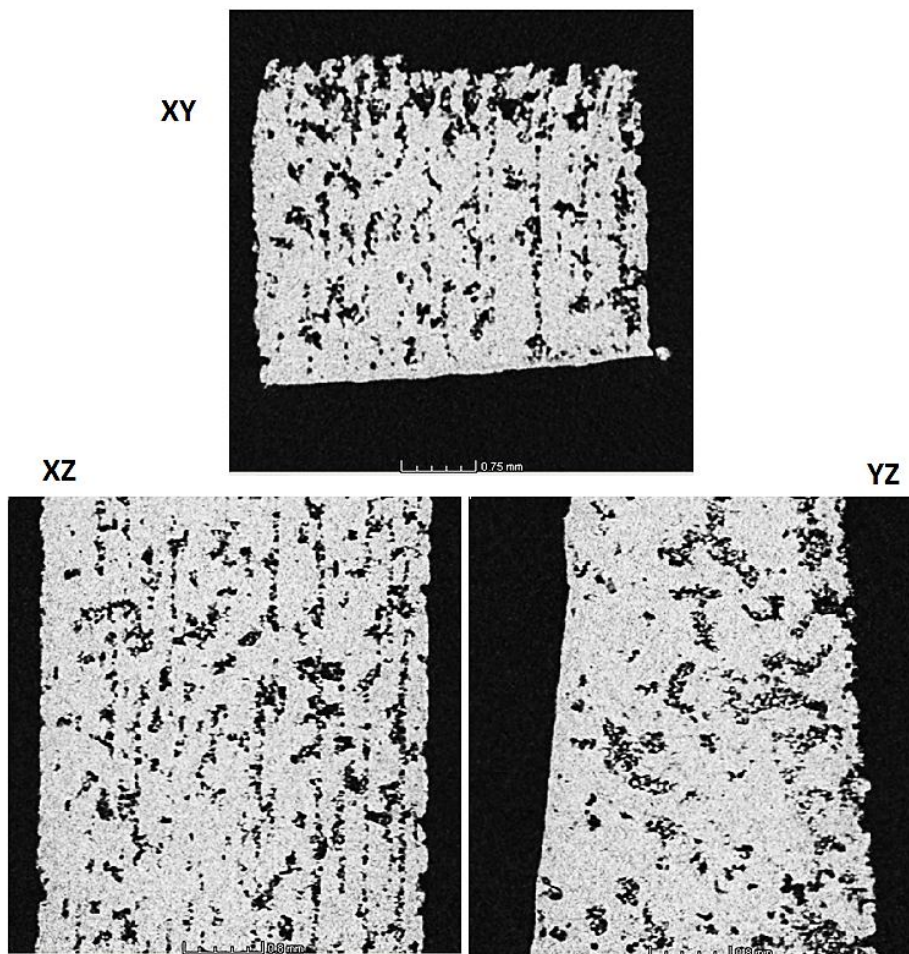**Figure 130.** Micro-CT scan of the sample from build 6

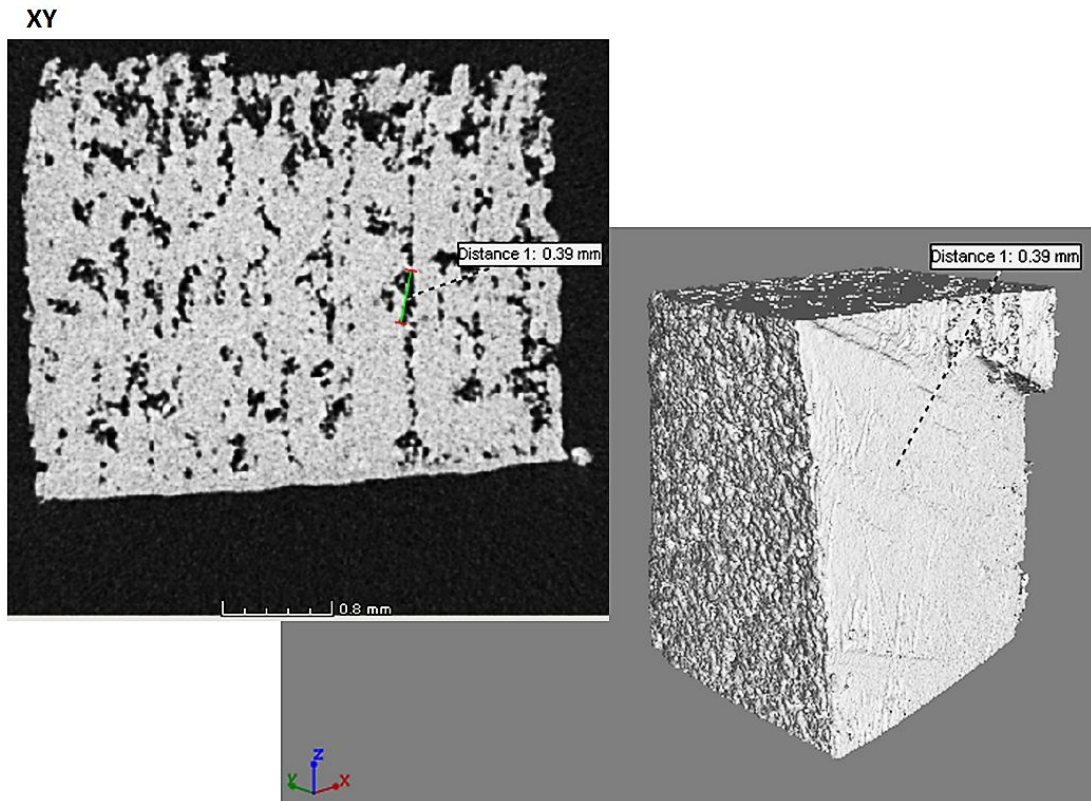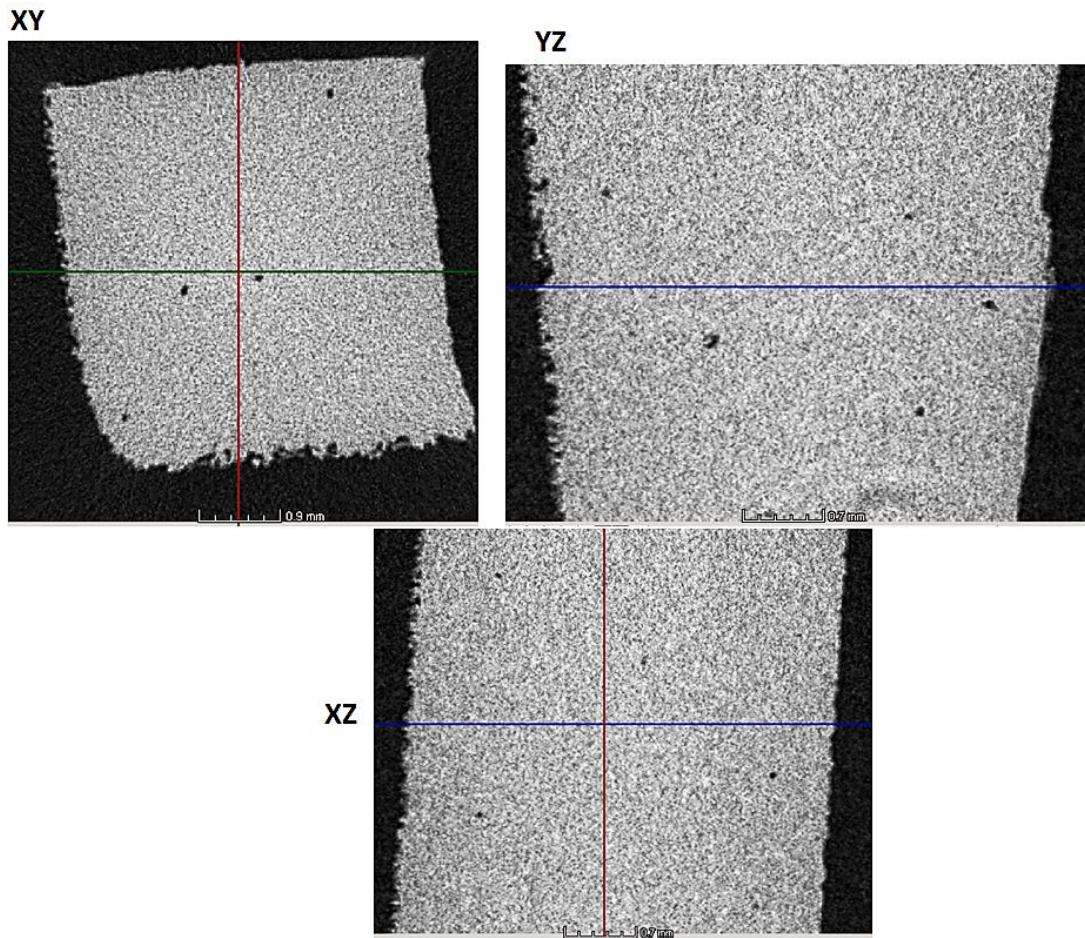**Figure 131.** Micro-CT scan of the sample from build 6: cross sections
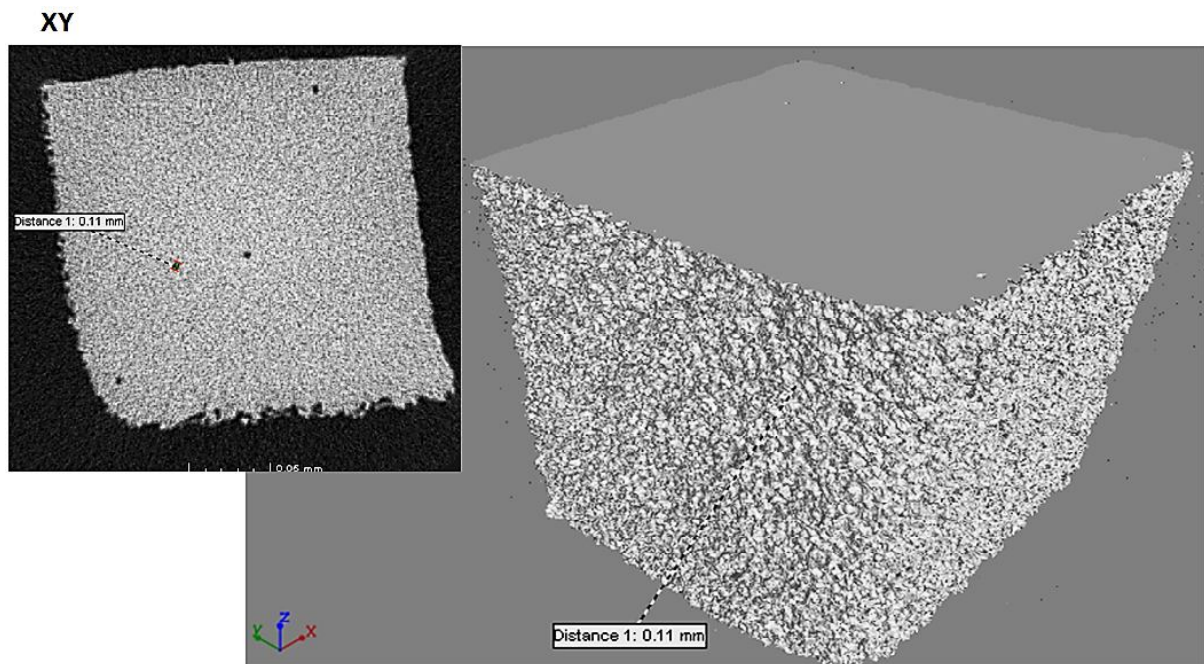
Figure 132. Micro-CT scan of the sample from build 6: example of pore size, 0.11 mm

231

Also the sample from build 6 shows a dense microstructure and only a few small pores with size up to 0.11 mm.
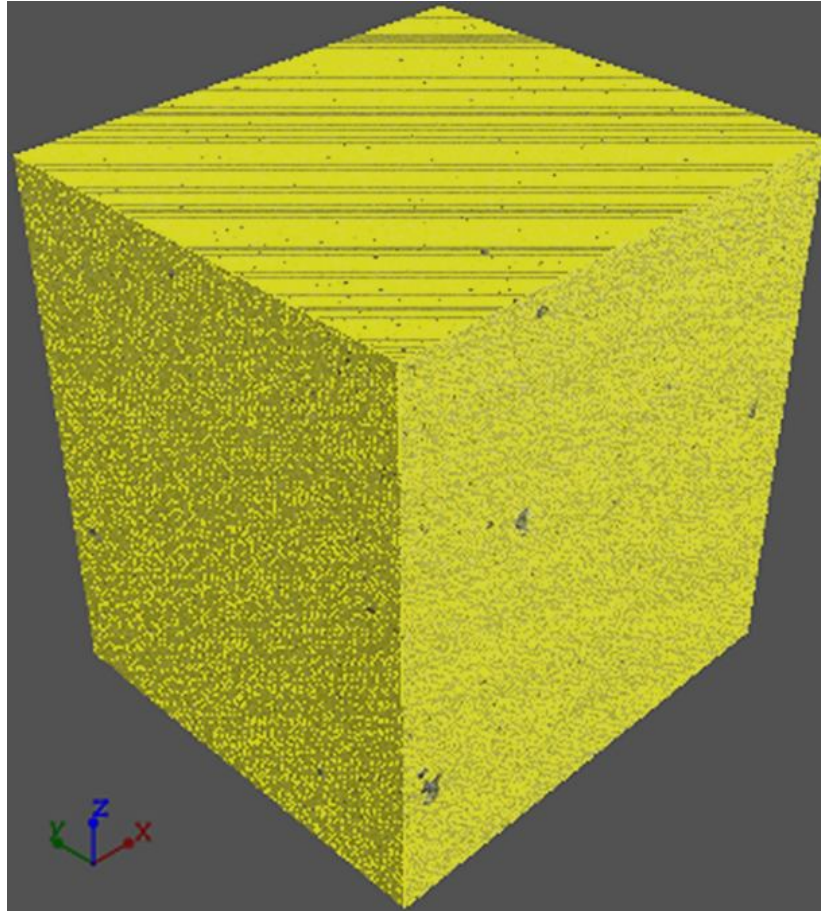
Figure 133. Micro-CT scan of the sample from build 6: material density

The sample from build 6 (Figure 133) appears very similar to the sample build 5 (Figure 129). Both specimens exhibit a high level of material density and only few visible pores, indicating therefore a significant decrease of the porosity content. Although the structure from build 6 appears fairly dense, the presence of a few pores of size 0.11 mm is still noticeable.

The estimates of the material densities of all the samples, measured as described in chapter 3.2.6, built at increasing ED are listed in Table 21.

Processing parameters profile	ED $[\frac{J}{mm^2}]$	Material density [%]
Build 1	0.015	82.63
Build 2	0.018	96.88
Build 3	0.024	97.96
Build 4	0.026	95.37
Build 5	0.029	99.65
Build 6	0.032	97.91

Table 21. Material densities of the HT laser sintered PEEK samples built at increasing ED values

The material density results have plotted against the ED values used in the manufacture of the corresponding HT laser sintered PEEK components in Figure 134.
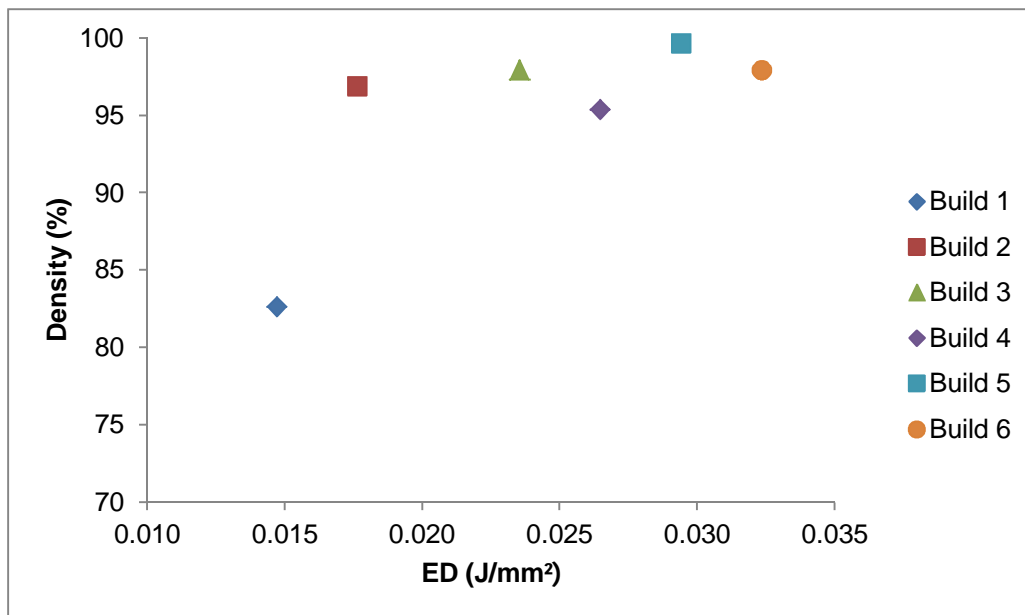
Figure 134. ED and density of the HT laser sintered PEEK components built at increasing ED

As seen in the tensile test, the increase of the ED induced a denser microstructure and therefore a higher material density, especially for builds 5 and 6 (Figure 134).

5.5.2.4 Micro-CT analysis of the post-treated HT laser sintered PEEK sample

As described in 3.2.2, samples built according the processing parameters of build 6 have been thermally treated after the HT-LS process in order to enhance the mechanical properties of the components. Although the thermal conditioning did not significantly improve the tensile strength of the HT laser sintered samples, the microstructure of the samples was investigated. The 3D scan with the corresponding cross sections and an example of pore size are reported from Figure 135 to Figure 137 , respectively. The evaluation of the sample density is shown in Figure 138.
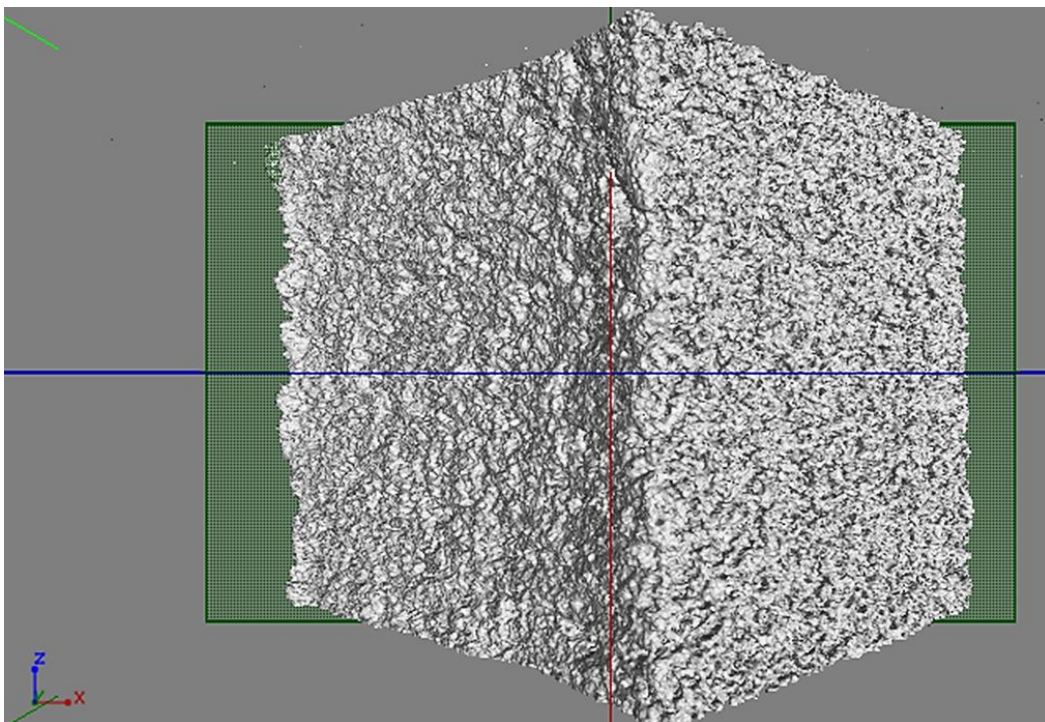
Figure 135. Micro-CT scan of the post treated sample from build 6
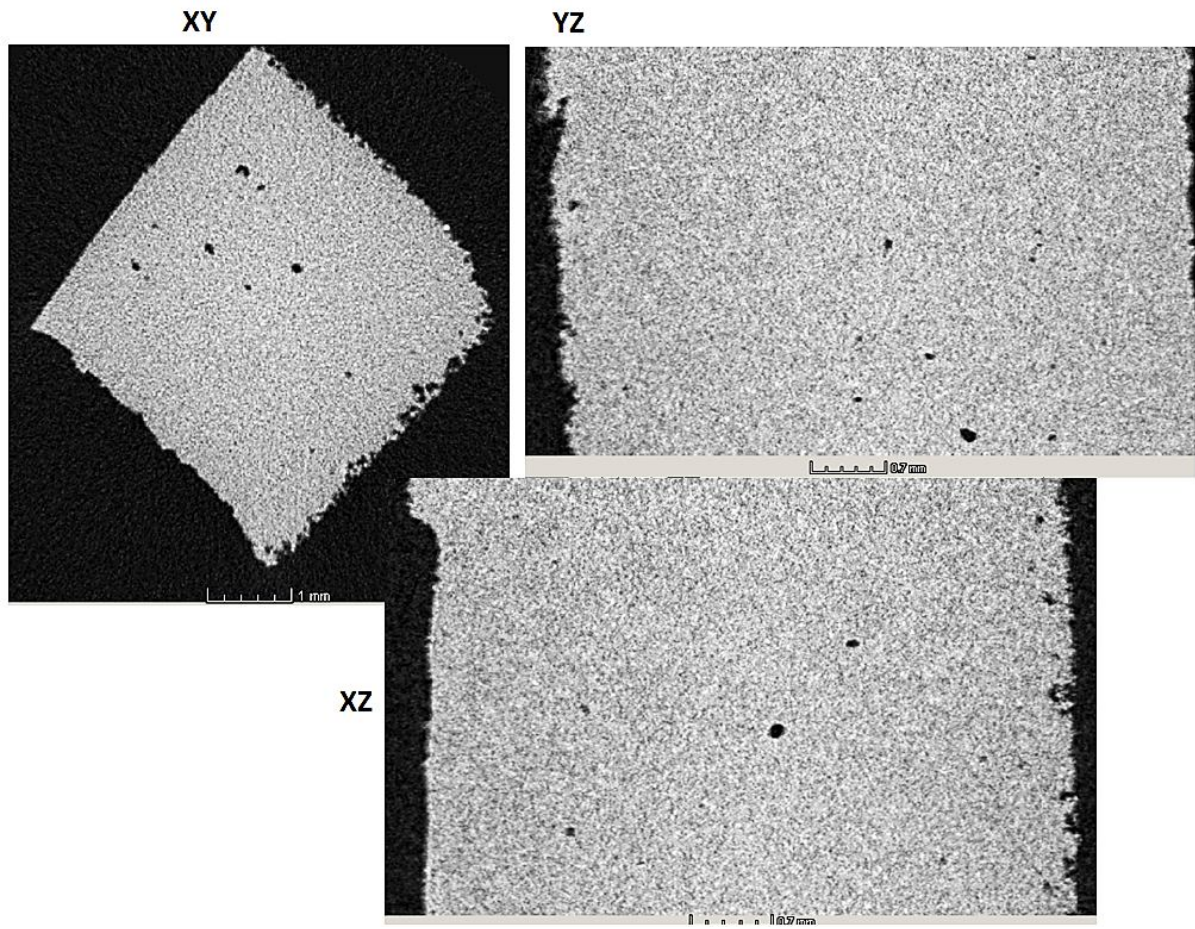
Figure 136. Micro-CT scan of the post treated sample from build 6: cross sections
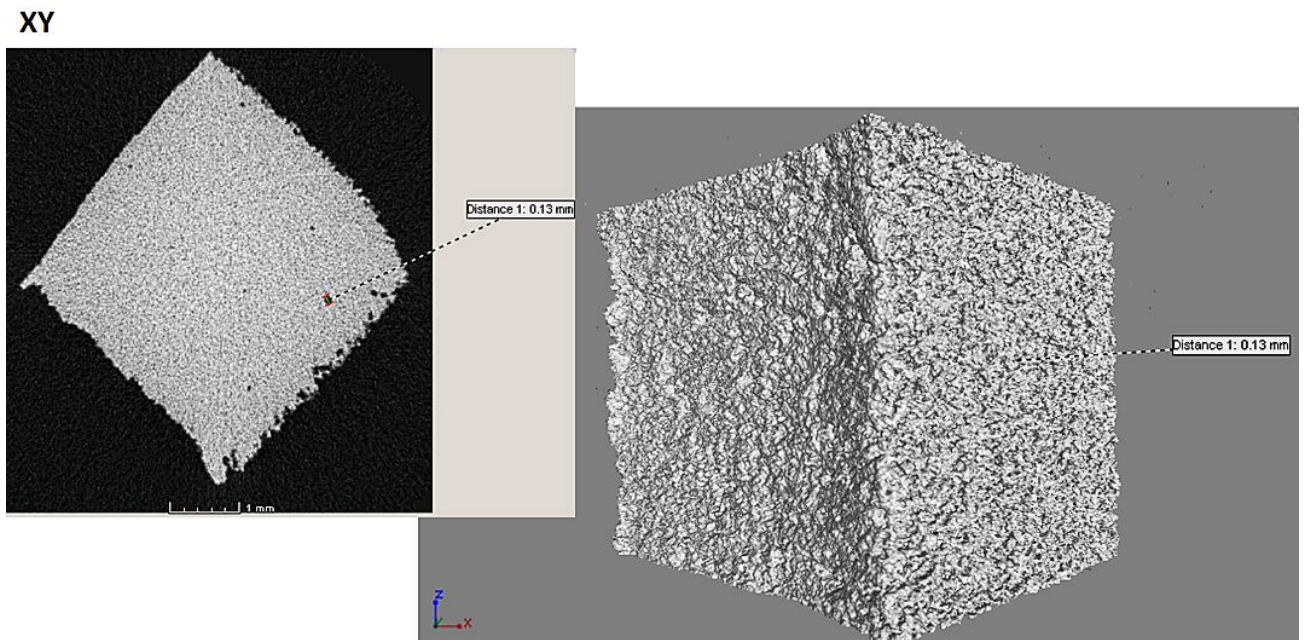
Figure 137. Micro-CT scan of the post treated sample from build 6: example of pore size, 0.13 mm

.
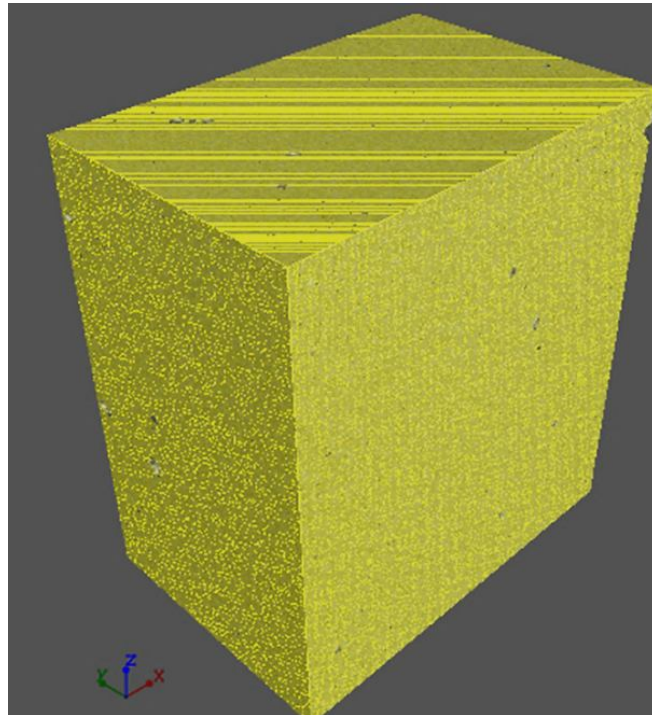
Figure 138. Micro-CT scan of the post treated sample from build 6: material density

The post treated sample did not show significant difference to the samples from builds 5 and 6 shown in 5.5.2.3. The post treated specimen shows a nearly fully dense structure with only few small pores of size above 0.10 mm, as seen in the samples from build 5 (Figure 126 to Figure 129) and 6 (Figure 130 to Figure 133).

5.5.2.5 DMA of HT laser sintered PEEK

Storage modulus, loss modulus and tan δ of HT laser sintered PEEK samples built at increasing ED are presented from Figure 139 to Figure 142 in parallel with the corresponding results of HT laser sintered PEK HP3.
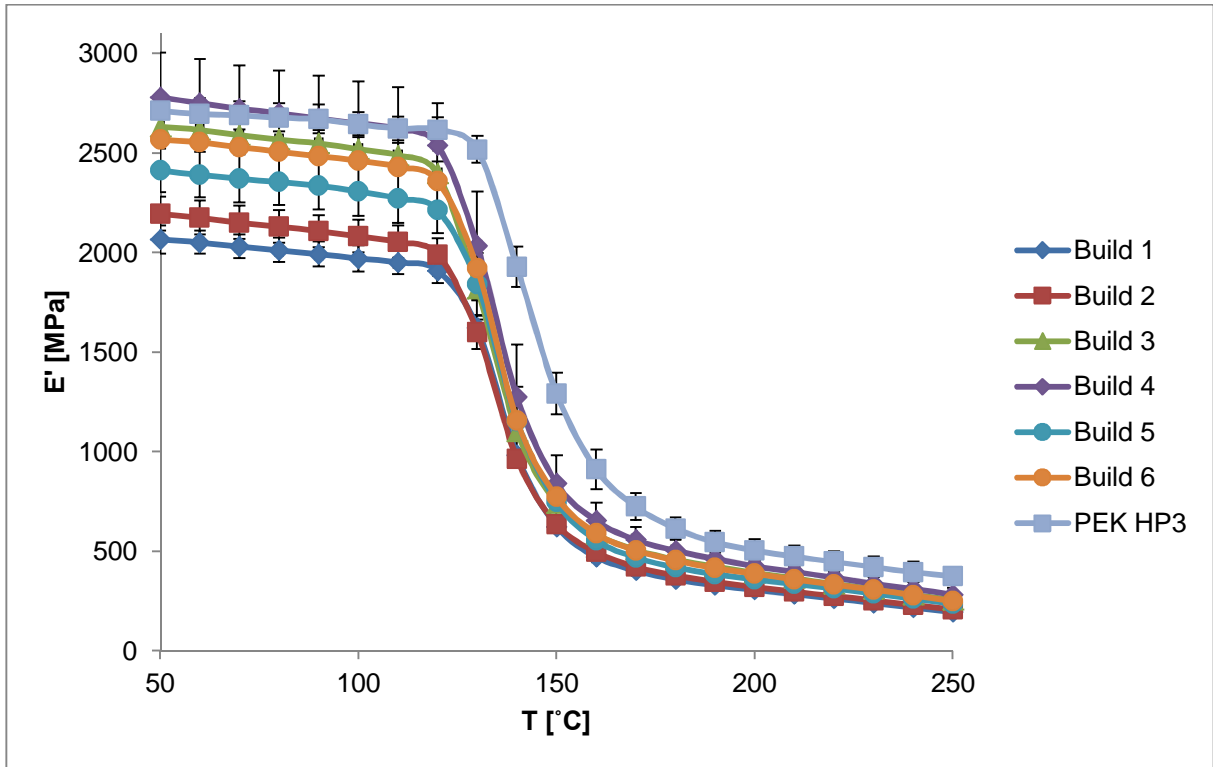
Figure 139. Storage moduli of HT laser sintered PEEK 450PF and HP3 PEK samples
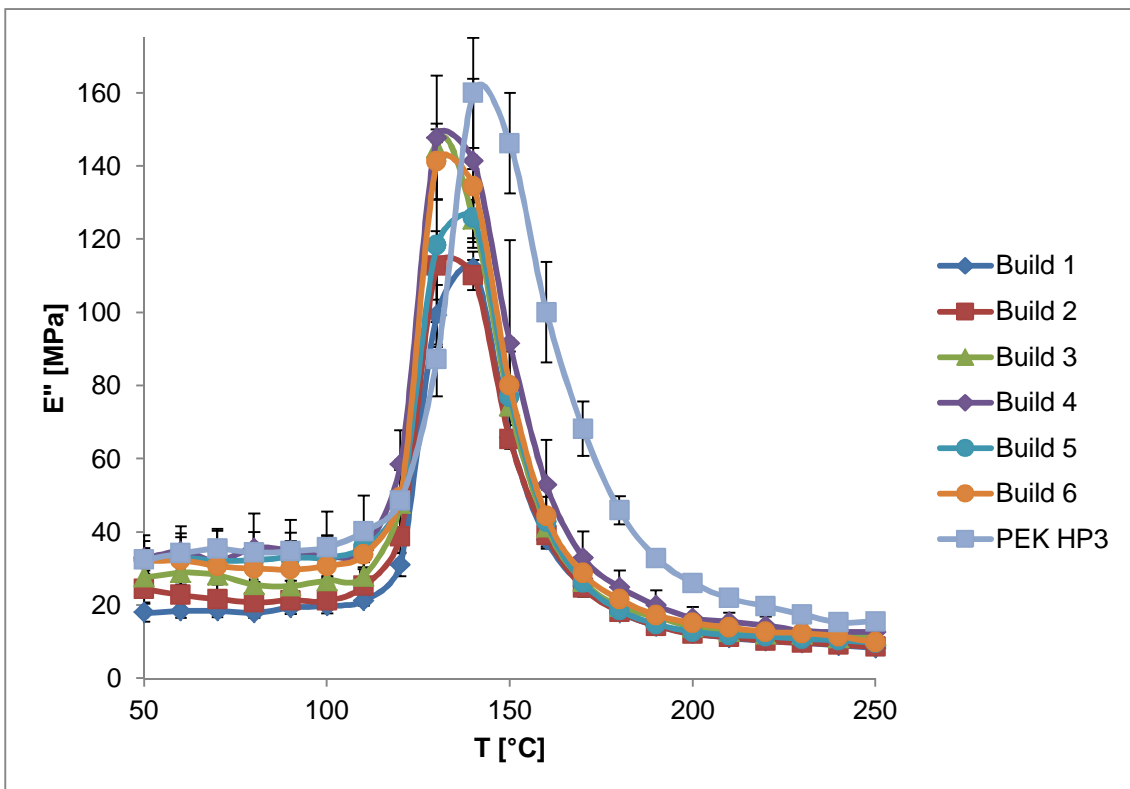
Figure 140. Loss moduli of HT laser sintered PEEK 450PF and PEK HP3 samples
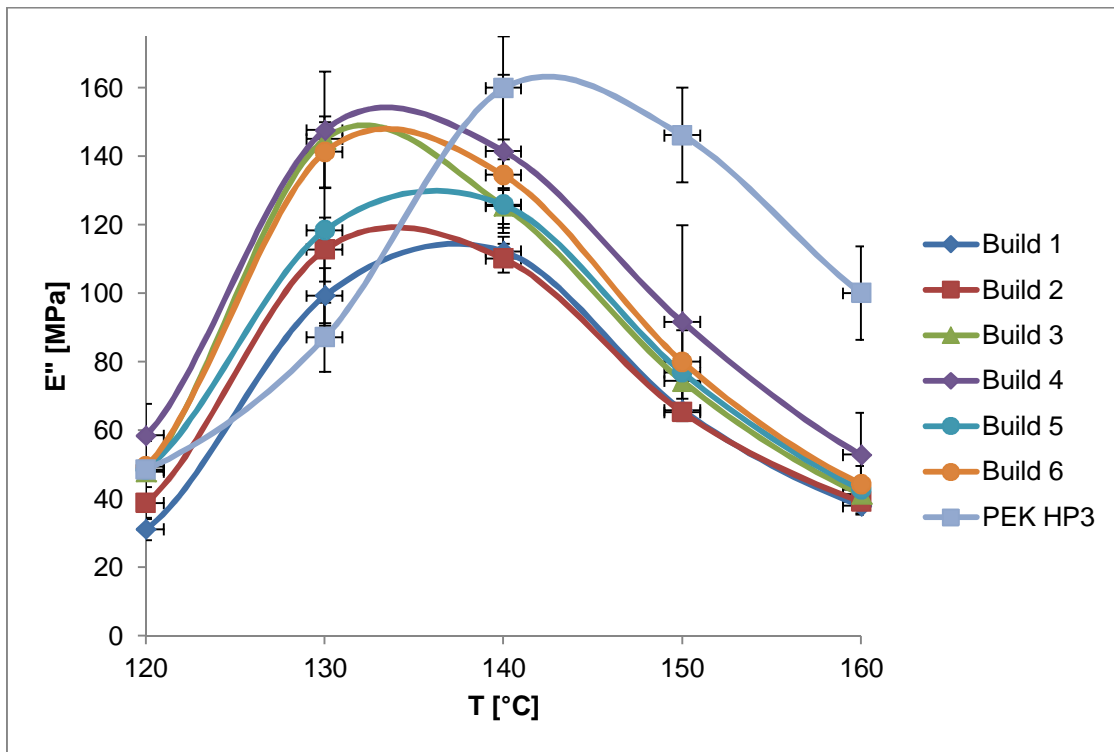
Figure 141. Loss moduli of HT laser sintered PEEK 450PF and PEK HP3 samples (zoom in)
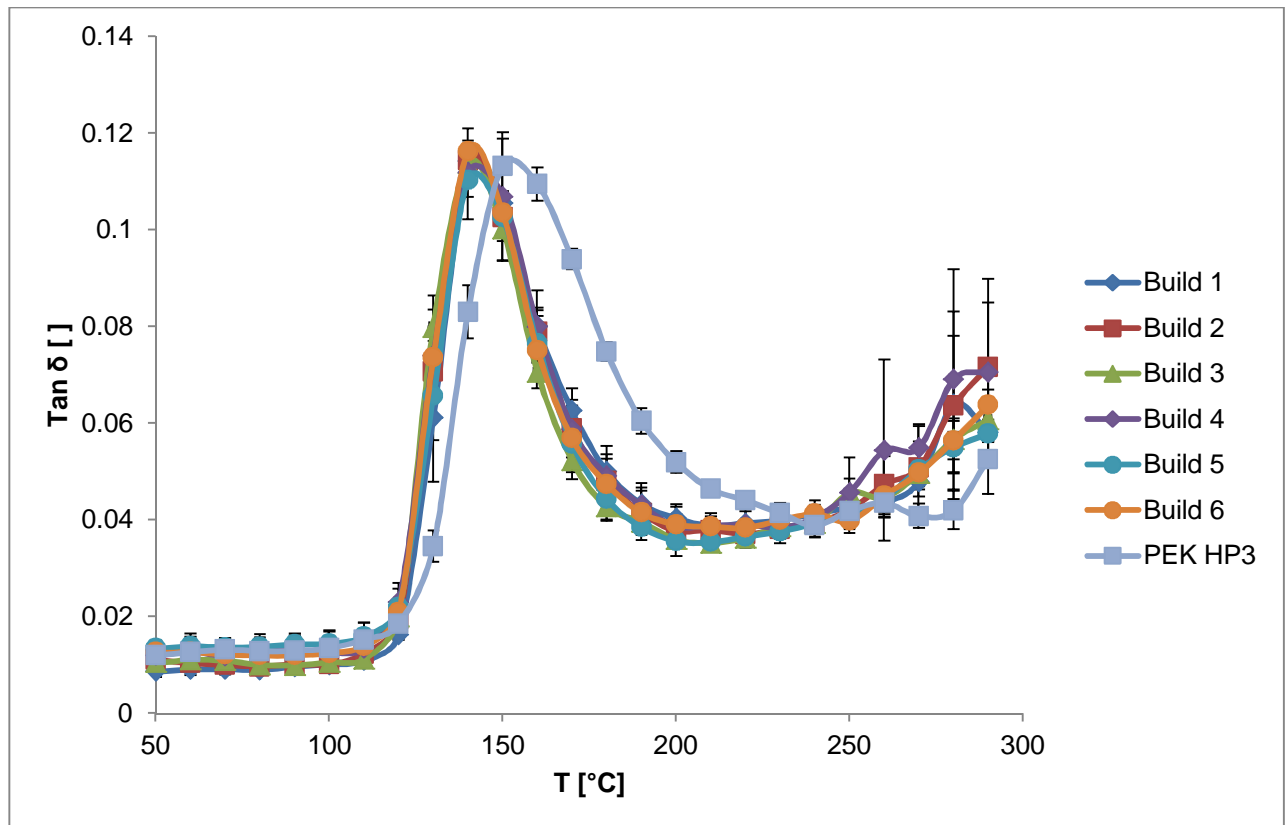
Figure 142. Tan δ of laser sintered PEEK 450PF and PEK HP3 samples

The storage modulus of HT laser sintered PEEK samples, equal to 2000-2800 MPa in the temperature range 30-110 °C, falls drastically in proximity of the glass transition temperature (140 °C) and stabilizes above 100 MPa for temperatures higher than 200 °C. As seen in the tensile test results, the storage modulus seems to improve with increasing values of ED, especially between builds 1-3 and build 4-6. These results indicates that HT laser sintered PEEK structures become slightly stiffer at increasing ED, thus confirming the tensile strength and samples density improvements seen in the previous analyses (chapter 5.5.2.1 and 5.5.2.3). It is possible to notice that HT laser sintered PEEK and PEK samples present the same storage profile and values, with PEK only exhibiting higher glass transition temperature. This is not a surprising result, as similar findings were found by Tregub et al. [23] when studying the storage modulus of compression moulded PEEK and PEK samples. PEEK and PEK have different ketone content (Table 1, PEEK 33% and PEK 50%). According to the authors, the contribution of the immobile amorphous phase of these polymers on the viscoelastic behaviour is more dominant, and therefore the contribution of the ketone content that counts is negligible.

The loss modulus of HT laser sintered PEEK samples was found to be equal to 20-40 MPa in the temperature range 30-100 °C, jumps above 150 MPa in the glass transition region (110-170 °C) and levels off at 10-20 MPa for higher temperatures. It seems that the samples manufactured at high ED (build 4, 5 and 6) exhibit slightly higher peak height of the loss modulus, possibly showing more damping. The HP3 PEK samples exhibit similar loss modulus profile, only slightly shifted at higher temperatures and higher peak height.

Both storage and loss moduli of HT laser sintered PEEK and PEK samples exhibited high standard deviations. This behaviour could be due to the combination of building orientation of the samples (X axis, Figure 106) and testing orientation of the samples (Z axis). It is well known in the LS community that the mechanical properties of a laser sintered part are lower along the building direction (Z). This is an effect of the formation of weaker bonds between than the layers (Z axis) than across the layers (X and Y axes). These weaker bonds therefore might introduce in the DMA test more variations and ultimately larger standard deviations.

5.6 Post sintering optimisation

The PS (chapter 5.2.2.2) is an additional heating phase applied to each layer during HT-LS processing. Although set to 12 s for PEK HP3 [118], it can be user defined. It is unclear how this standard 12 s PS has been optimised for PEK HP3 and therefore which value should be instead be optimal for PEEK 450PF. For this reason tensile testing and DMA PEEK 450PF specimens were HT laser sintered with PS of 6, 9 and 15 s according to build 5 processing parameters in reduced building chamber mode and tested. The specimens built according to build 5 processing parameters and standard PS time of 12 s were available from previous investigation (optimisation of the ED, chapter 5.5.2.1, 5.5.2.3 and 5.5.2.5).

PEEK one and ten layers specimens (chapter 3.2.3) were also HT laser sintered and analysed in terms of for microstructure and surface roughness as described in chapter 3.2.3. One and ten layers specimens of PEK HP3 were also produced in the same condition with the standard PS time of 12 s and used as benchmark.

5.6.1 SEM of one and ten layer specimens

The top surface (XY cross section, chapter 3.2.3) of one layer and ten layer HT laser sintered samples was analysed using SEM. The results of the one layer PEEK specimens for 6 and 12 s PS time are shown in Figure 143 and Figure 144, respectively. The PEEK samples with PS of 12 s were compared with the samples of 6 s PS time (half standard PS time) to best highlight the effects due of the PS phase and possibly the importance of this step within the HT-LS process. Both PEEK samples were also compared against PEK HP3 samples manufactured with standard PS of 12 s.
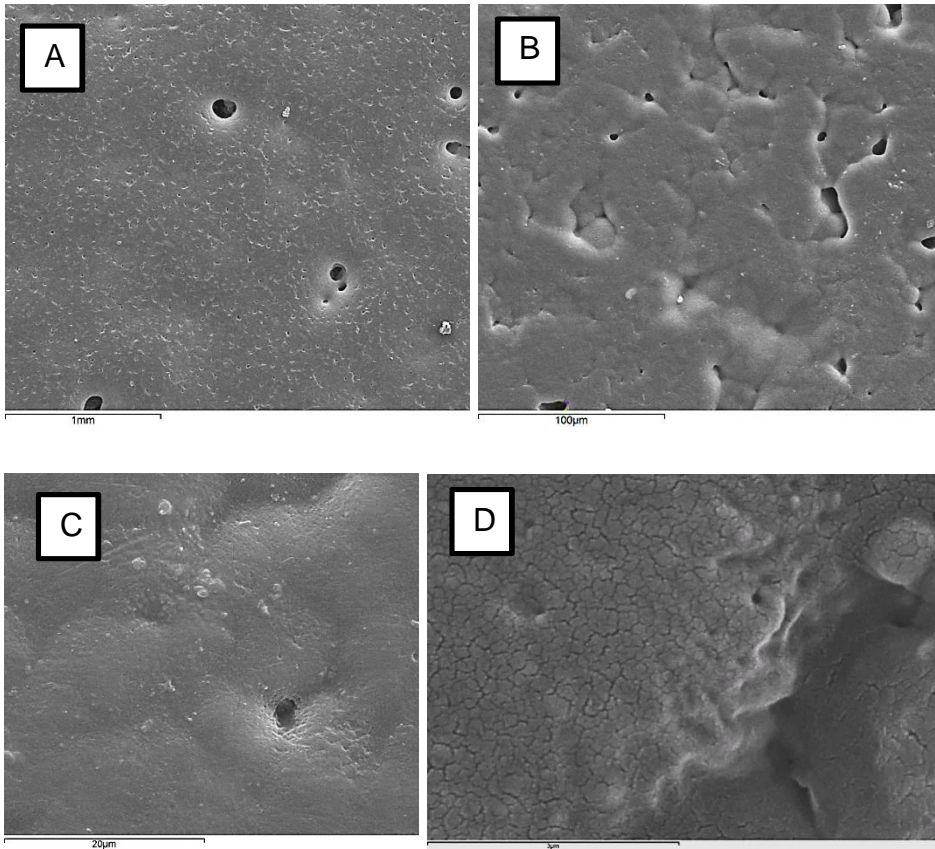
Figure 143. PEEK one layer specimen PS = 6 s, at increasing magnification
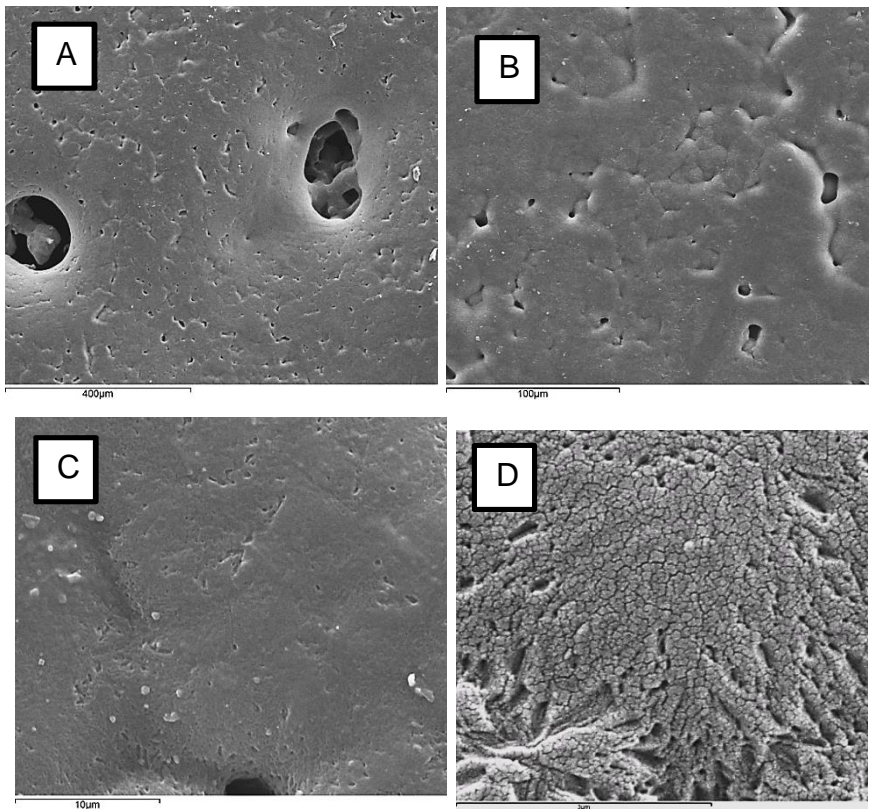
Figure 144. PEEK one layer specimens PS = 12 s, at increasing magnification
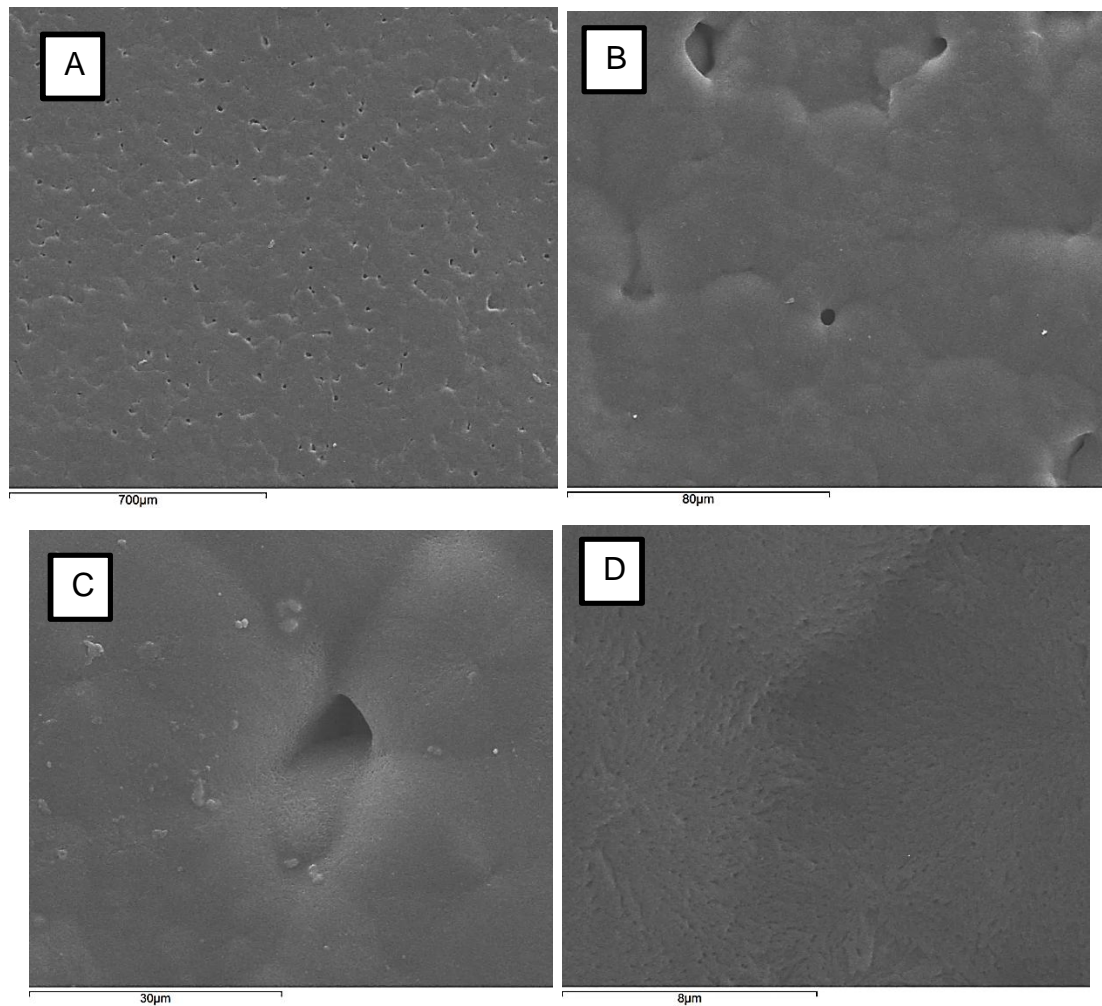
Figure 145. PEK HP3 one layer specimen PS = 12 s, at increasing magnification

The one layer PEEK specimens (Figure 143 and Figure 144) with PS of 6 and 12 s do not seem to show significant distinctions. Both samples exhibit the presence of cavities of similar size. Similar surface irregularities were also found by Ho et al. [119] when optimising the LS process for use of a polycarbonate powder. The authors laser sintered one layer specimens in order to define the optimum ED, expecting that a uniform layer is related to a good degree of sintering. However, the laser sintered layers were presenting the same type of surface blemishes even when the laser power was set at the value leading to the highest mechanical properties in the corresponding tensile samples. It seems therefore that the presence of these irregularities will appear even at optimal processing conditions. The examination at higher orders of magnification (Figure 143 D, Figure 144 D) outlines in both cases

the presence of micro cracks. This is likely to be due to the rapid cooling as the process for producing these samples was disrupted and forced to cool.

Also one layer specimens of PEK HP3 (Figure 145) did not show a homogenous molten film. However, the cavities were smaller than those noticed for one layer PEEK samples. It is possible that the LS of just one layer is not enough to remove the irregularities related with the particles arrangement of the powder bed underneath.

For these reasons, ten layer samples were created and analysed. SEM captures of the ten layer specimens with PS time equal to 6 and 12 s are shown in Figure 146 and Figure 147, respectively. The PEK HP3 sample used as benchmark is shown in Figure 148.
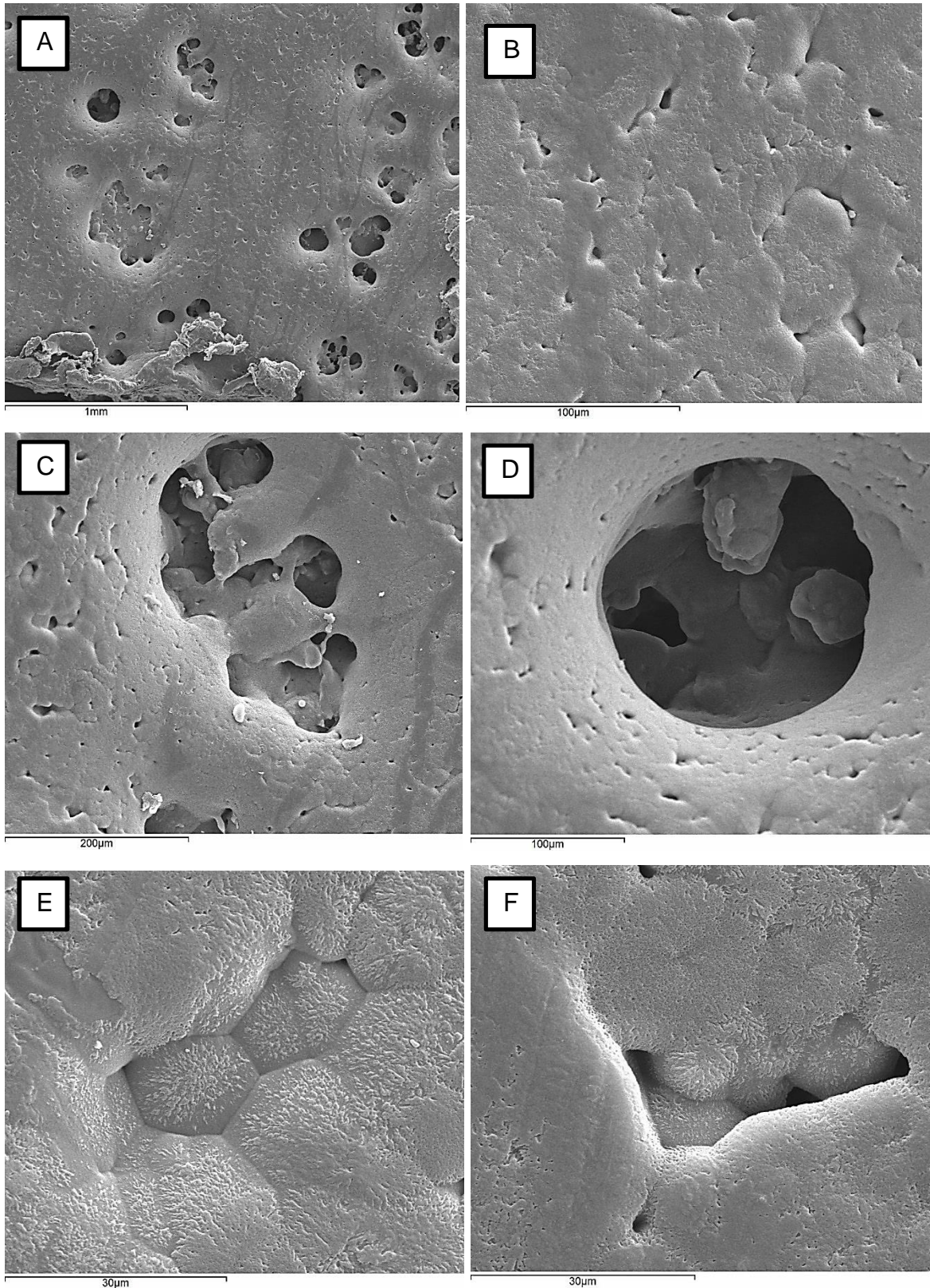
Figure 146. PEEK ten layer specimen, PS = 6 s, at increasing magnification

244
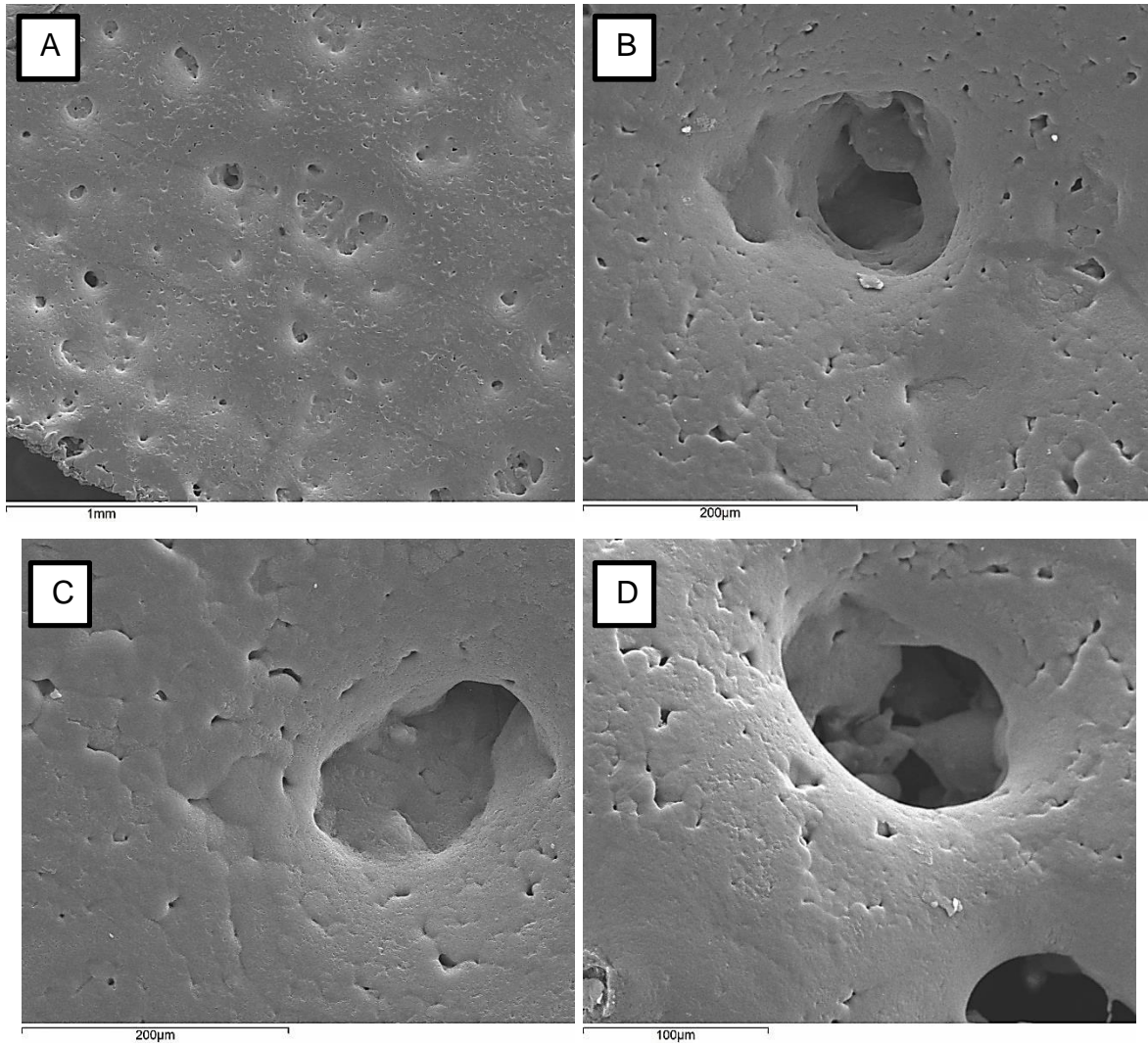
Figure 147. PEEK ten layer specimen PS = 12 s, at increasing magnification
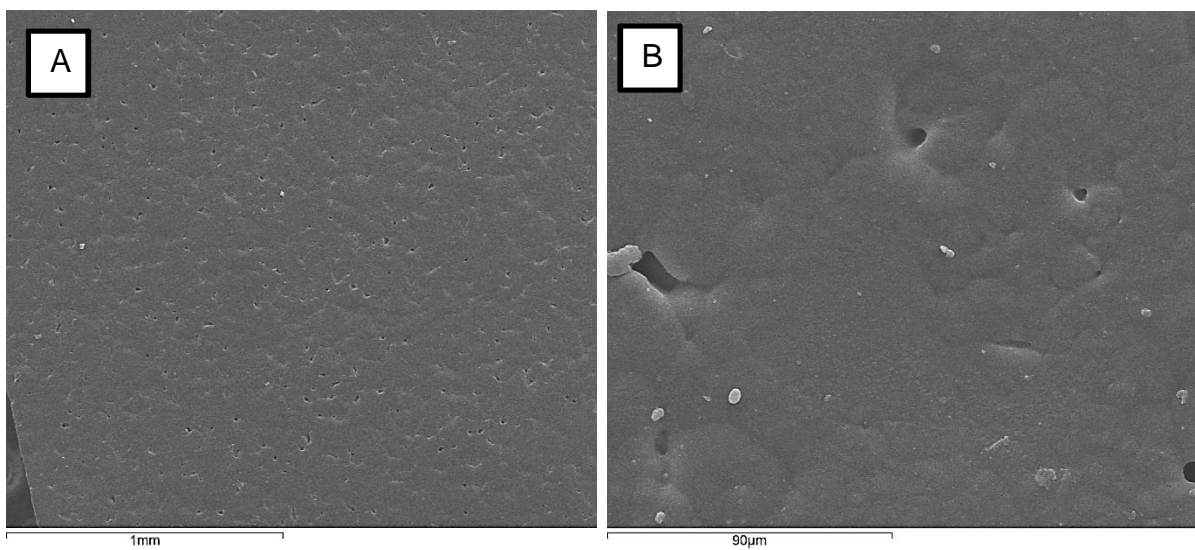
Figure 148. PEK HP3 ten layer specimen PS = 12 s, at increasing magnification

Irregularities and cavities can be clearly identified for both one and ten layer PEEK specimens manufactured with PS time of 6 and 12 s, hence indicating the lack of a uniform molten layer and potentially fully dense parts. PEK HP3 samples (Figure 148) showed more uniform layers than PEEK, with only a few very small cavities. The cavities in the PEEK samples are fairly deep and seem to transfer from one layer to the other, although it is expected they would fill up with fresh powder. The presence of these cavities is an interesting effect that can explain some of the porosity noticed in the HT laser sintered parts. It is not clear at this stage whether the presence of the PS phase helps or actually creates larger and deeper cavities in PEEK samples. However, these cavities could also be originated by the particle morphology and particle arrangement in the powder bed. The particle morphology significantly affects the flow behaviour of LS materials [193], the spreading of layers and the achievement of a dense powder bed (chapter 4.8). The SEM examination of the PS PEEK samples has shown that the shape of the powder particles in use can also strongly influence the formation of voids and uneven layers in the powder bed, causing cavities through successive layers of a HT laser sintered component.

The fracture surfaces of the ten layer samples of PEEK produced with increasing PS times (Figure 149 to Figure 152) and PEK HP3 (Figure 153) were also analysed with SEM in order to qualitatively assess the effect of the PS on the layer bonding properties across the cross-section of the samples.
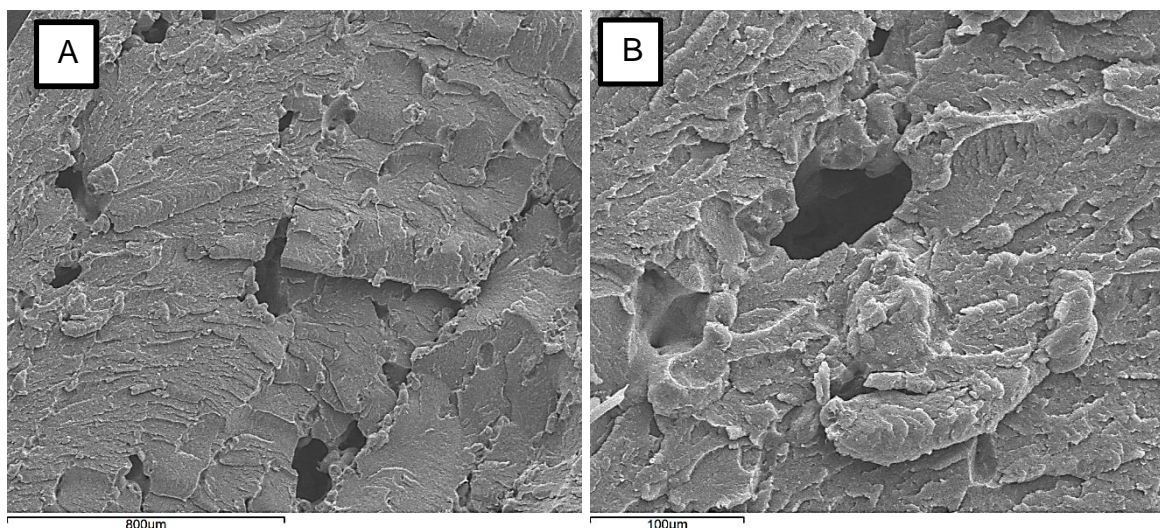
Figure 149. Fracture surface of PEEK ten layer specimen, PS = 6 s, at increasing magnification
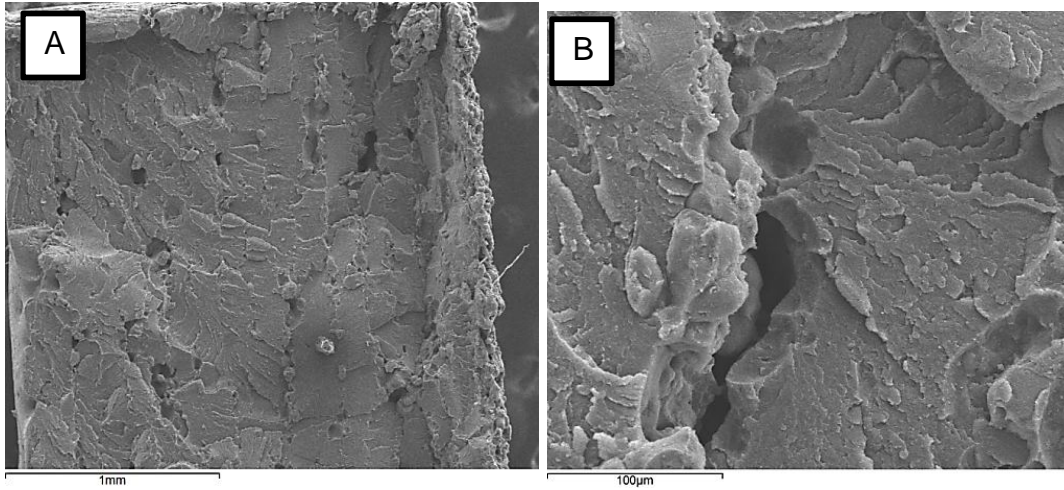
Figure 150. Fracture surface of PEEK ten layer specimen, PS = 9 s, at increasing magnification
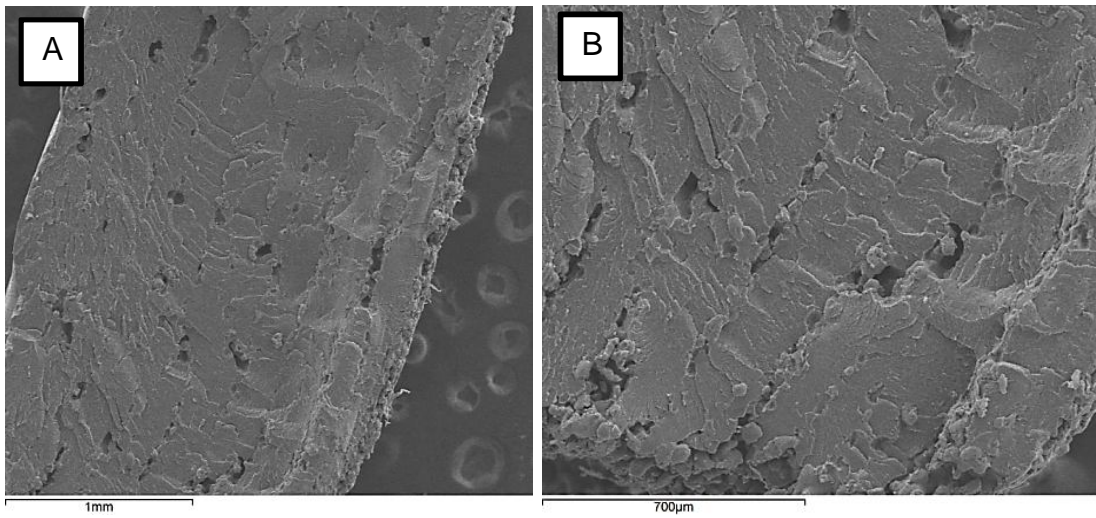
Figure 151. Fracture surface of PEEK ten layer specimen, PS = 12 s, at increasing magnification
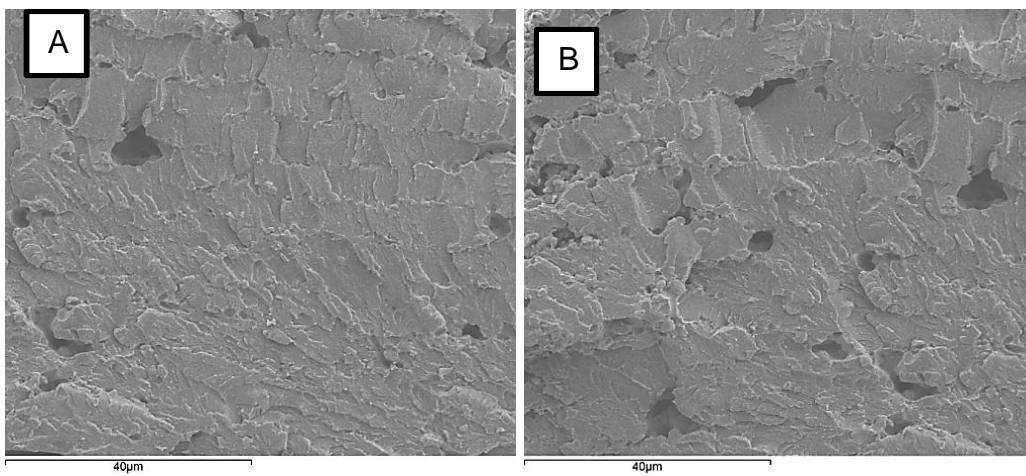
Figure 152. Fracture surface of PEEK ten layer specimen, PS = 15 s, at increasing magnification

247
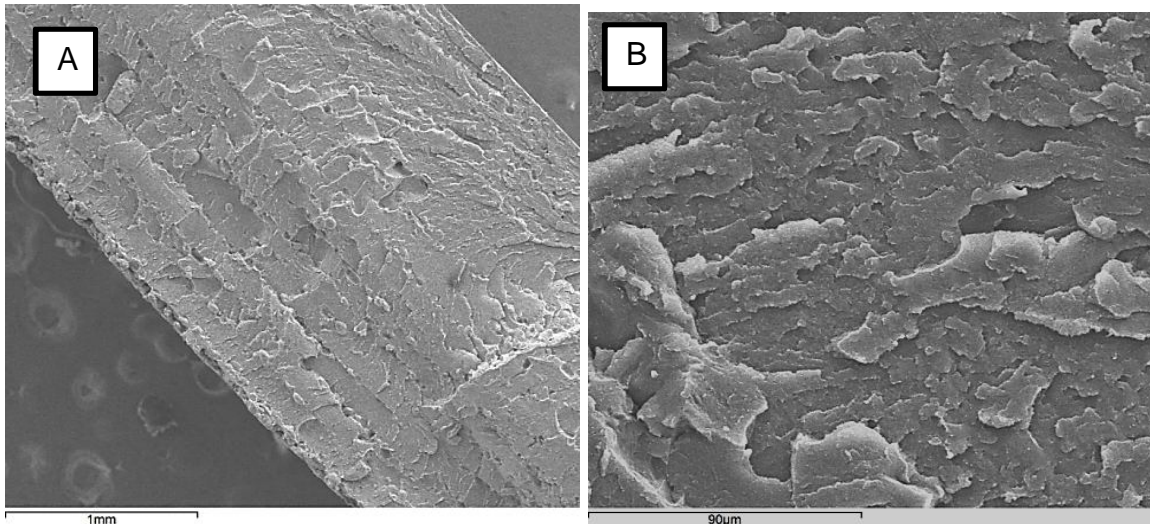
Figure 153. Fracture surface of PEK HP3 ten layer specimen (benchmark), PS = 12 s, at increasing magnification

All the samples exhibited the layer structure typical of the LS manufacturing process. While the PEEK samples with PS time of 6 s (Figure 149) and 9 s (Figure 150) showed large cavities, the samples with higher PS seemed to show better bonding properties between the layers (Figure 151 and Figure 152). Interestingly, also the benchmark sample manufactured using PEK HP3 showed the presence of small cavities across the layers although of smaller size and smaller depth when compared to those of PEEK. This result helps to understand the differences found in the tensile properties of HT laser sintered PEEK and PEK HP3 samples.

5.6.2 Surface roughness of one and ten layer specimens

The one and ten layer PEEK specimens manufactured with PS times of 6, 9, 12 and 15 s as described in chapter 3.2.3 were also examined in terms of the surface roughness parameter S_a [196]. The results of the one and ten layer PEEK samples were compared to those of the one and ten layer PEK HP3 specimens used as benchmark and produced with the standard EOS 12 s PS time.

The surface profile of the one and ten layer PEEK sample manufactured with PS time of 6, 9, 12 and 15 s are shown from Figure 154 to Figure 161. Figure 162 and Figure 163 exhibit the results obtained for PEK HP3 samples.

248
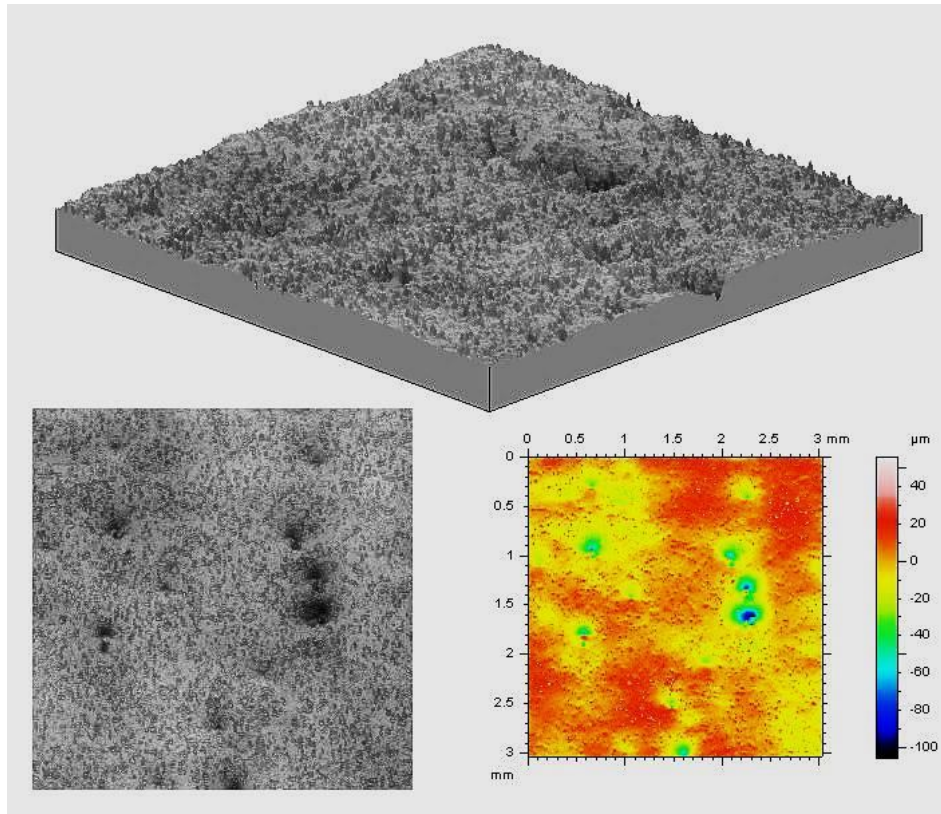
Figure 154. Surface roughness measurement of PEEK one layer specimen, PS = 6 s
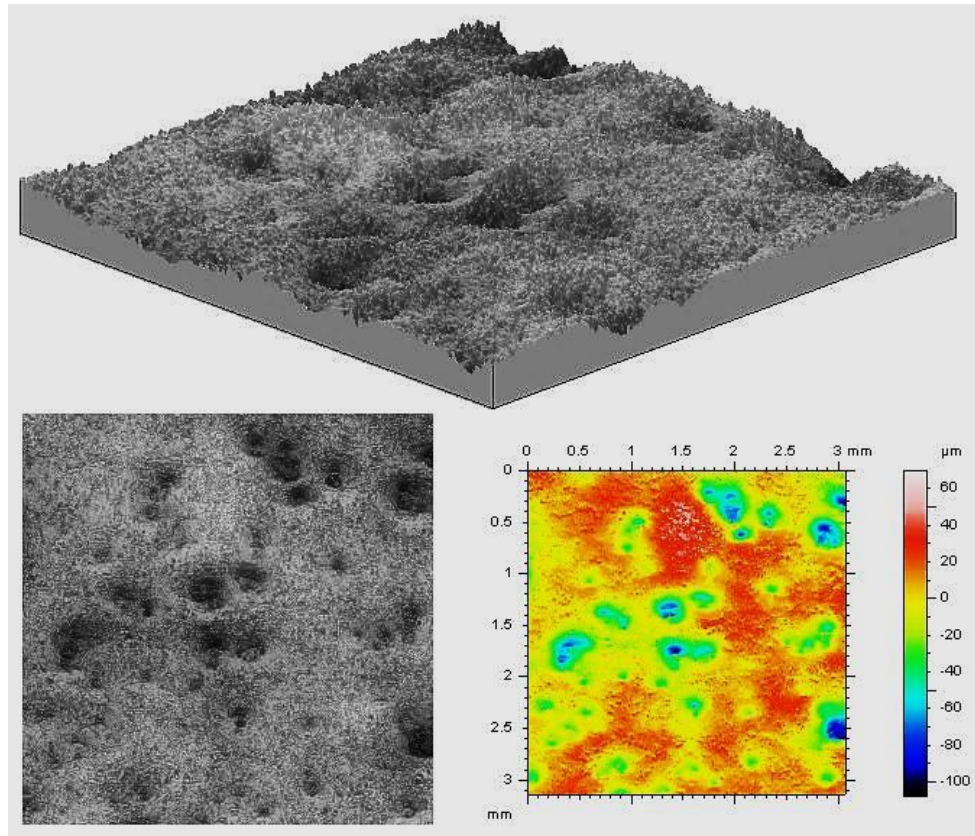
Figure 155. Surface roughness measurement of PEEK ten layer specimen, PS = 6 s

249
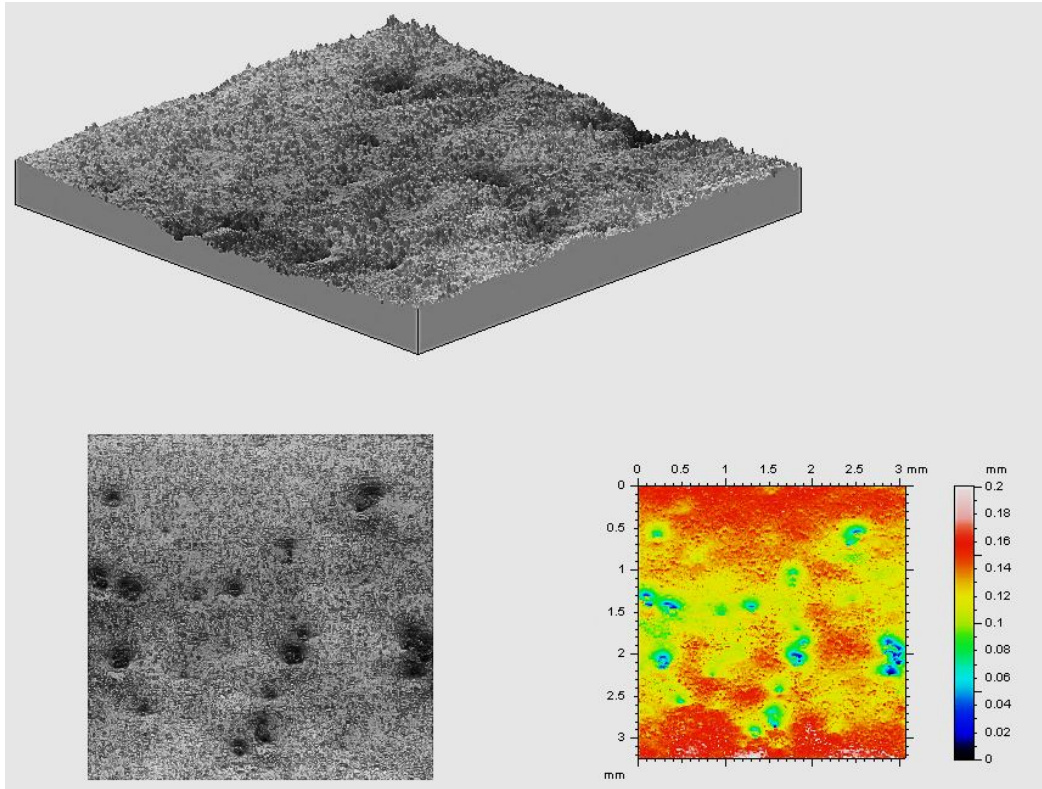
Figure 156. Surface roughness measurement of PEEK one layer, PS = 9 s
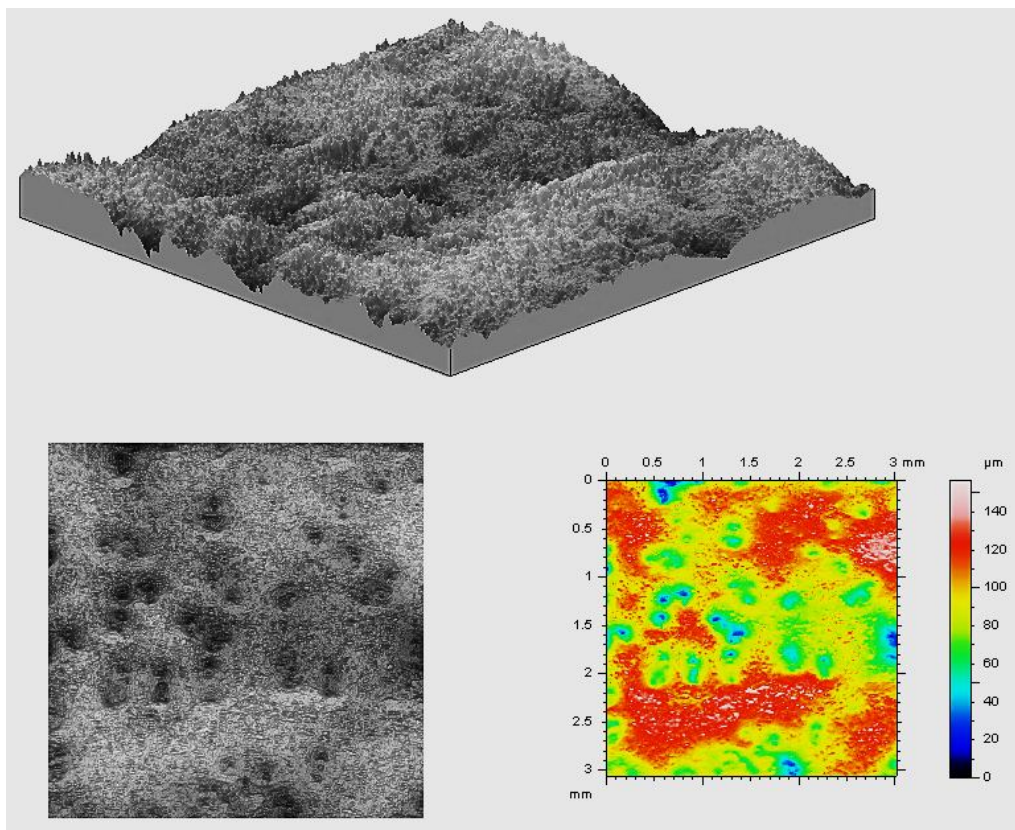
Figure 157. Surface roughness measurement of PEEK ten layer specimen, PS = 9 s
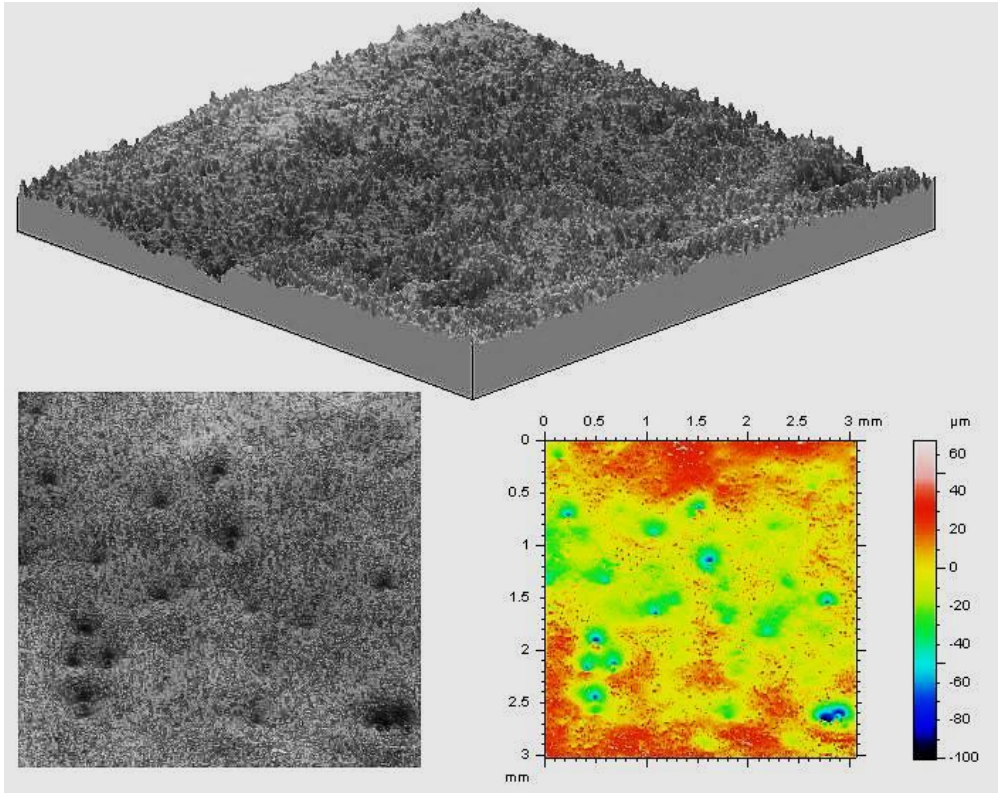
Figure 158. Surface roughness measurement of PEEK one layer specimen, PS = 12 s
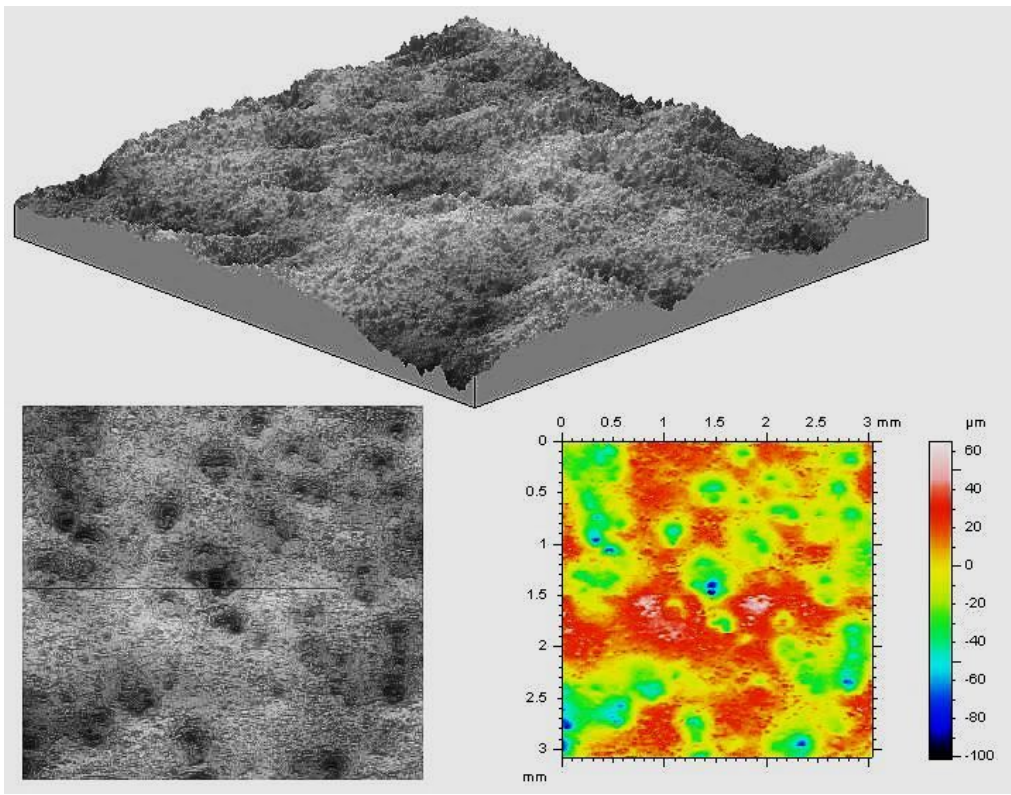
Figure 159. Surface roughness measurement of PEEK ten layer specimen, PS = 12 s
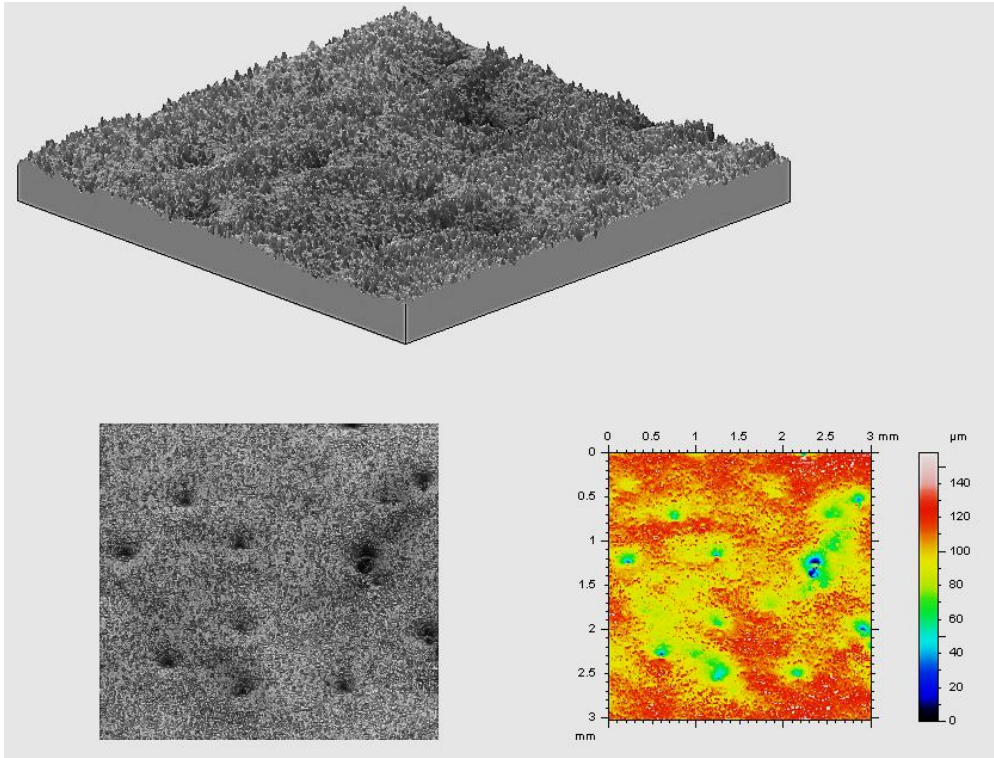
Figure 160. Surface roughness measurement of PEEK one layer specimen, PS = 15 s
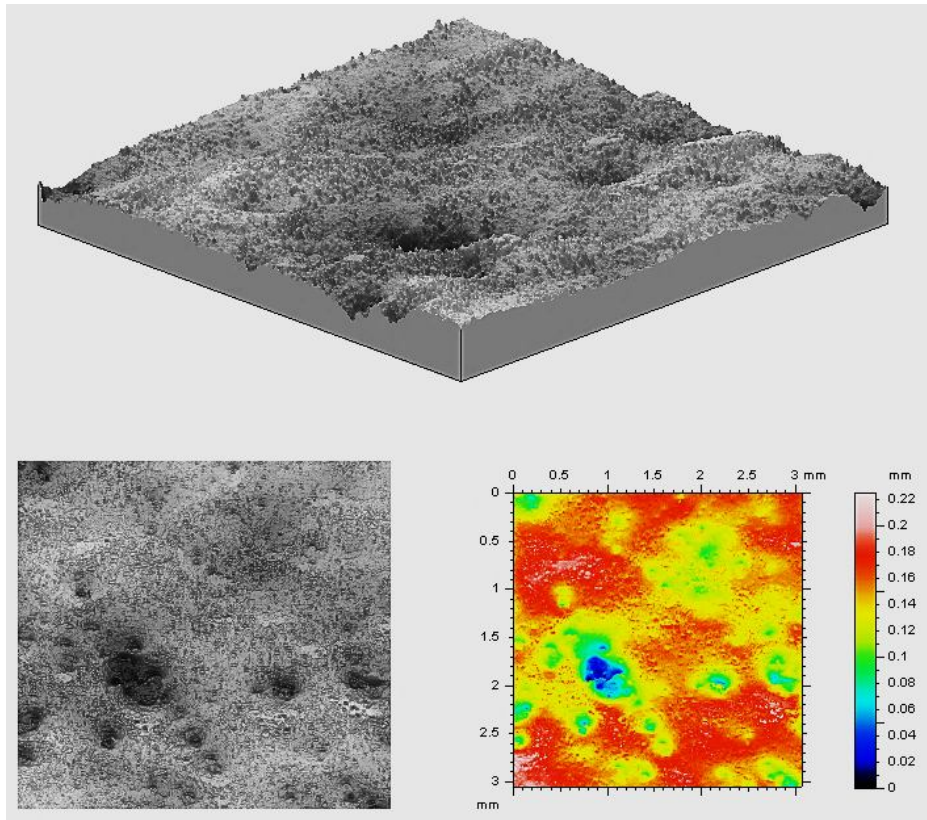
Figure 161. Surface roughness measurement of PEEK ten layer specimen, PS = 15 s
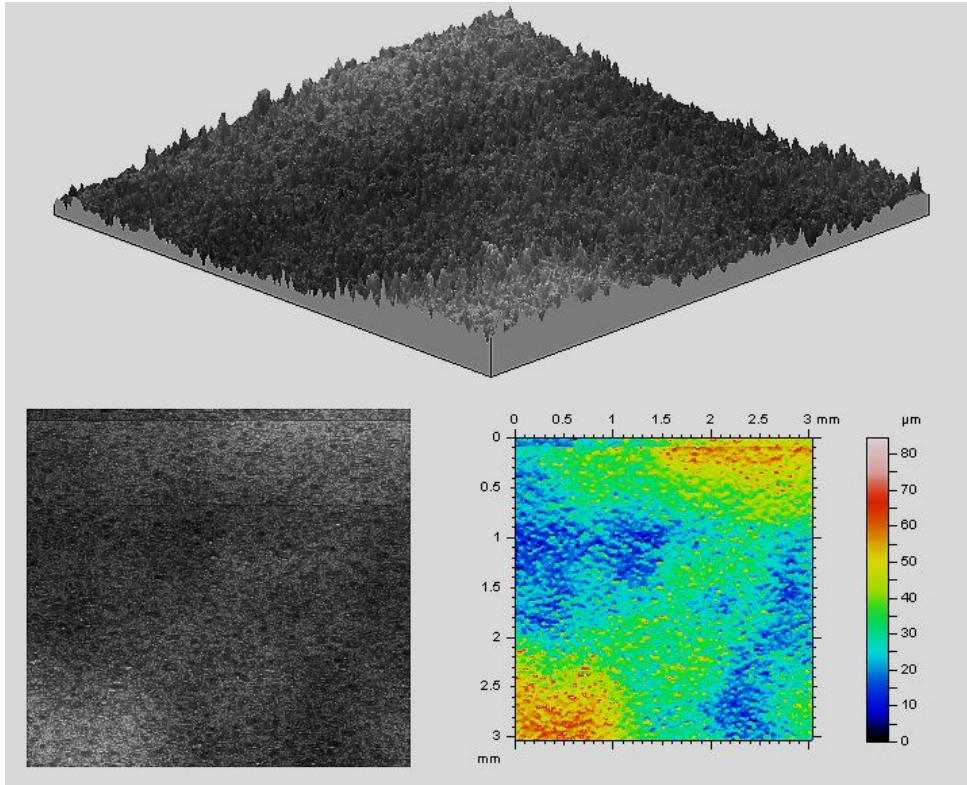
Figure 162. Surface roughness measurement of PEK HP3 one layer specimen, PS = 12 s
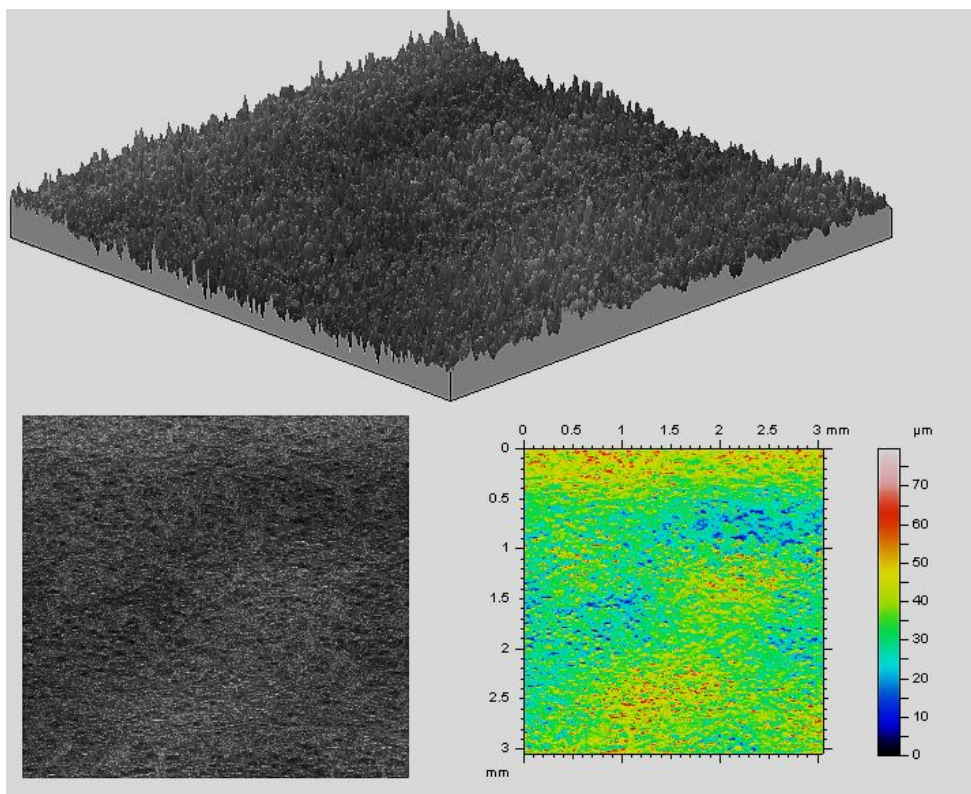
Figure 163. Surface roughness measurement of PEK HP3 ten layer specimen, PS = 12 s

For all the samples, the surface roughness profiles outlined the presence of cavities in the one and ten layer specimens as previously noticed with the SEM imaging. The S_a results are reported in Table 22 and Table 23.

One layer specimen	S_a [μm]
PEEK 450 PF – 6 s	8.7
PEEK 450 PF – 9 s	9.27
PEEK 450 PF – 12 s	12.8
PEEK 450 PF – 15 s	10.9
Benchmark: PEK HP3 – 12 s	9.24

Table 22. Surface roughness values of the one layer samples

Ten layer specimen	S_a [μm]
PEEK 450 PF – 6 s	15.1
PEEK 450 PF – 9 s	16.9
PEEK 450 PF – 12 s	16.5
PEEK 450 PF – 15 s	19.4
Benchmark : PEK HP3 – 12 s	6.9

Table 23. Surface roughness values of the ten layer samples

The surface roughness of the one layer specimens seems to increase up to 12 s PS time, where it levels off. This result could be possibly explained by considering the morphology of the powder particles constituting the powder bed underneath the one layer samples.

When a layer of powder particles is melted as effect of the laser exposure, a molten polymeric film is created over a particle bed arrangement. The molten material can flow over the underneath particles and solidify along the profile created by those particles. If the particle arrangement underneath is fairly compact and dense because constituted of highly round and circular particles, the molten layer will solidify according to the profile created by these regular particles and it will appear

254

acceptably flat, smooth and homogenous. If however the particle bed arrangement is highly porous because composed of highly elongated and sharp particles, the molten polymer will solidify following the profile created by these irregular particles. The new layer will then exhibit peaks and cavities, looking highly rough overall. A longer PS phase can further melt the polymeric film and so further decrease the viscosity of this molten polymeric film to its minimum value, thus allowing easier flow of the molten polymer amongst the particles, but it might still be an effect not dominant enough to overcome the irregular profile created by highly porous particles bed arrangements. A graphical explanation for this hypothesis is shown in Figure 164.

Figure 164. Surface roughness of the one layer samples and particle morphology in the powder bed

The continuous line represents the molten layer of particles as consequence of the laser exposure. The black units with different shape and size represent the particles in the powder bed. In case A, the powder bed is constituted of nearly spherical particles which form a dense arrangement. During the PS the just molten polymer flows over this powder arrangement and solidifies along the significantly flat profile created by the regular particles. The new layer will then result flat and smooth overall. In case B instead, the particles constituting the powder bed are significantly more irregular than those of case A and when the molten polymer flows over them, it solidifies following the rough profile created by these irregular particles.

The PS phase aims to create a homogenous molten film by possibly providing the additional energy necessary to create a polymeric film with constant viscosity all over the laser exposed area. The longer the PS time, the more likely the molten polymeric film reaches the minimum viscosity allowed by its molecular weight. More simply, the longer the PS time, the lower the polymer viscosity and the more the molten polymer flows over the profile created by the particles underneath, creating a new smooth or

highly rough layer according to the condition of the powder bed underneath. This mechanism might enhance the irregularities of the powder packing instead of creating a smoother surface. When comparing the results of the PEEK one layer samples to PEK HP3 it can be noted that the PEEK sample with 9 s PS time seems to better match the HP3 surface morphology.

It can be noticed that ten layer PEEK specimens are rougher than one layer PEEK specimens. These results could be explained with similar mechanism to the one described above. The viscosity of the just molten polymeric film is lower than the viscosity of the layers underneath that have presumably already started to solidify. The polymer can then easily flow over the layer arrangements underneath. If the previous layers were acceptably flat, the new layer flows over them and solidifies following the same flat profile and hence helping to further smoother the overall area. If instead the layer arrangements underneath are rough with a considerable number of peaks and depressions, the new layer can flows and solidify following the rough profile at times or flow within the irregularities of the below powder arrangements, thus creating new cavities.

Furthermore, the longer the PS time, the lower the viscosity of the polymeric film and the more the new layer flows over and within the structure created from the previous layers.

This mechanism could explain the high values of surface roughness but does not necessarily imply the creation of a significantly low density structure in the HT laser sintered components.

An explanation of this hypothetical mechanism is displayed in Figure 165.

Figure 165. Surface roughness of the ten layer samples and particle morphology in the powder bed

The continuous line represents the molten layer of particles as consequence of the laser exposure. The connected black shapes represent the particles in the powder bed previously molten by laser exposure and assumed in nearly consolidated state.

The ten layer sample of PEK HP3 manufactured with PS time of 12 seconds showed a significant decrease in the surface roughness of the samples, with only small cavities and irregularities. As suggested in previous studies [58] this result could be the consequence of two simultaneous contributions: the particle morphology and melt viscosity. PEK HP3 shows higher values of shape descriptors such as roundness, circularity, aspect ratio and solidity compared to PEEK, leading to higher flowability, therefore higher powder bed density after the layer spreading and ultimately smoother and denser ten layer samples ([193] and chapter 4). In addition, PEEK 450PF and HP3 PEK have different melt viscosities: PEK is less viscous than PEEK 450PF (chapter 4.1). The lower viscosity of the PEK material combined with the better flowability might help the formation of more homogenous and smooth sintered layers than in PEEK.

Figure 166 shows some examples of profiles extracted from the following PEEK samples: (A) one layer specimen with PS = 6 s; (B) ten layer specimen with PS = 6 s; (C) ten layer specimen with PS = 12 s; (D) ten layer specimen with PS = 15 s and (E) the ten layer HP3 PEK sample. In sample A the maximum variation is around 100 μm, while in sample B it is around 120 μm, value equal to the layer thickness set in the EOSINT P 800 system for the manufacture of the samples. This shows thatin the case of one layer specimens cavities are less deep than in ten layer specimens. A variation of 120 μm also proves that the irregularities of the ten layer samples are through the last sintered layer of powder. Samples C and D have respectively maximum deviations of 140 and nearly 200 μm, indicating that with longer PS times cavities and irregularities occur through more than one layer. Lastly, as expected from the results in Table 23, the PEK HP3 sample (E) showed the smallest deviation, sign of a fairly smooth and regular surface.
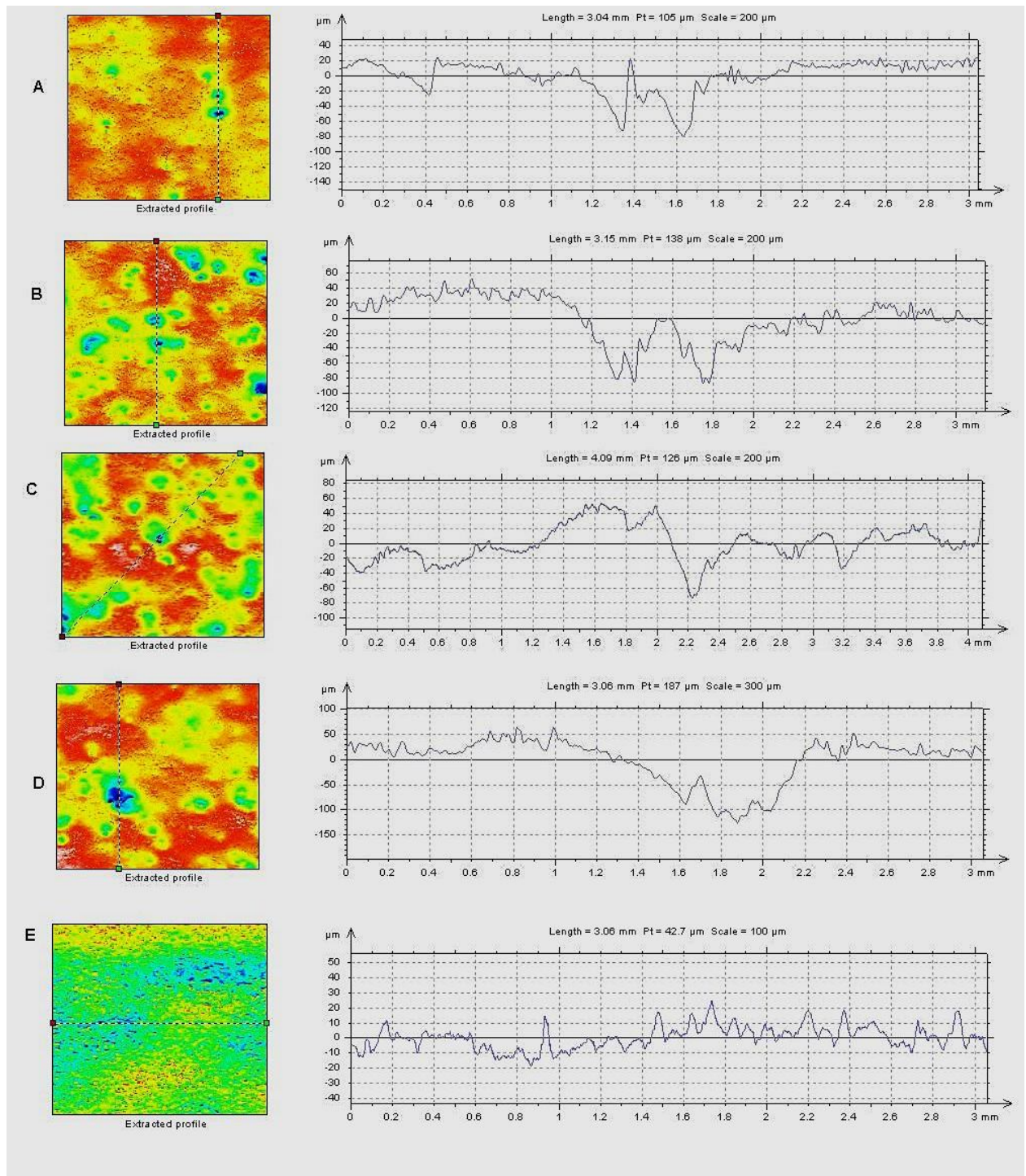
Figure 166. Example of cavities in the profile of one and ten layer specimens: (A) PEEK 450PF one layer, PS = 6 s; (B) PEEK 450PF ten layer, PS = 6 s; (C) PEEK 450PF ten layer, PS = 12 s; (D) PEEK 450PF ten layer, PS = 15 s; (E) PEK HP3 ten layer, PS = 12 s.

5.6.3 Tensile strength results

The performance of the HT laser sintered PEEK tensile samples built according to build 5 (chapter 5.5.2) with different PS times and measured as described in chapters 3.2.1 are shown in Figure 167.
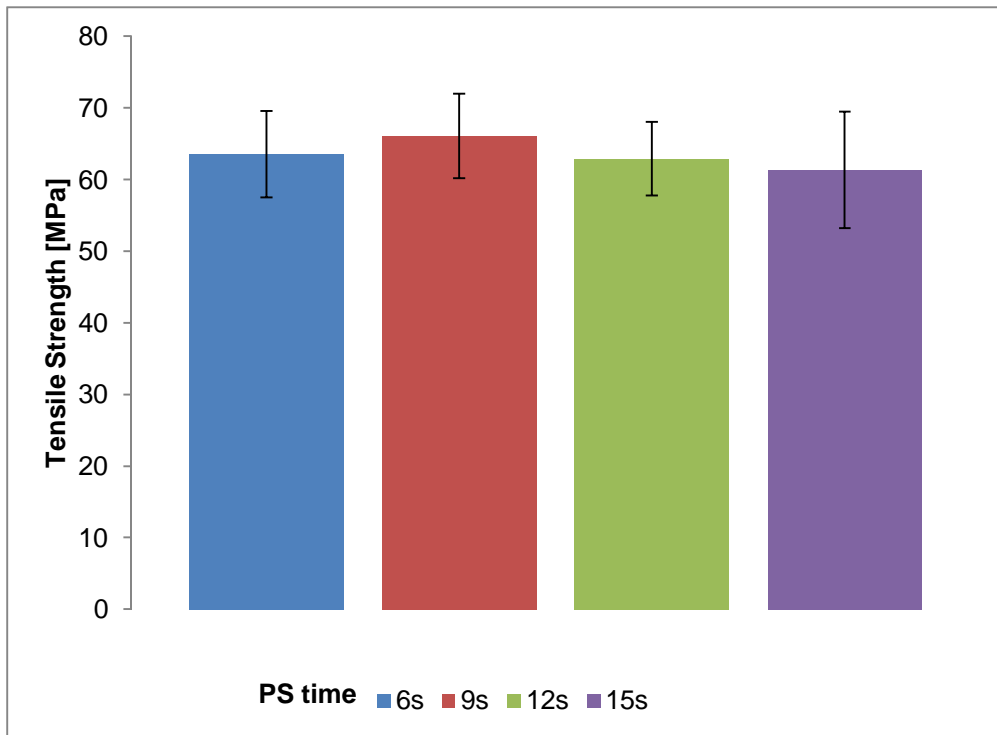
Figure 167. Tensile strength of HT laser sintered PEEK samples built with different PS times (average value and standard deviations)

The tensile strength values of the HT laser sintered PEEK samples manufactured with increasing PS time are similar in the range 6-15 s. The samples, therefore, do not seem to be affected by the PS duration in this time interval. Possibly, the effect due to the variation of the PS time is that small not to impact on the mechanical performance of the specimens.

5.6.4 DMA results

Figure 168 and Figure 169 show the storage and loss moduli of the samples built according to build 5 (chapter 5.5.2) with PS times of 6, 9, 12 and 15 s and measured as described in chapter 3.2.4.
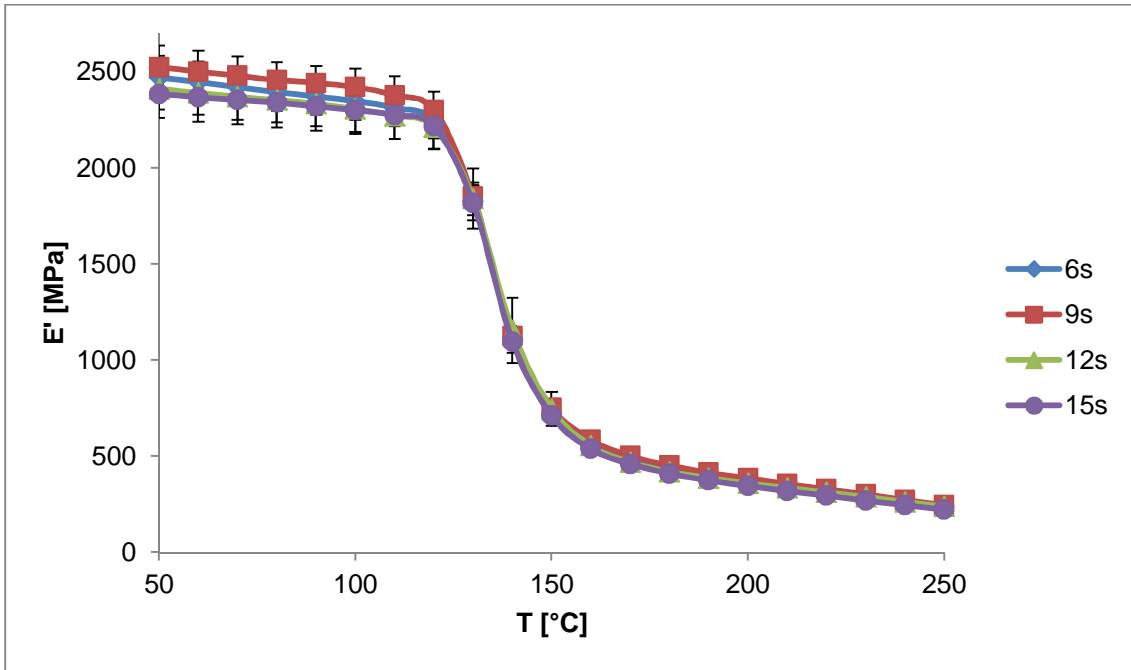
Figure 168. Storage moduli of HT laser sintered PEEK samples built with different PS times
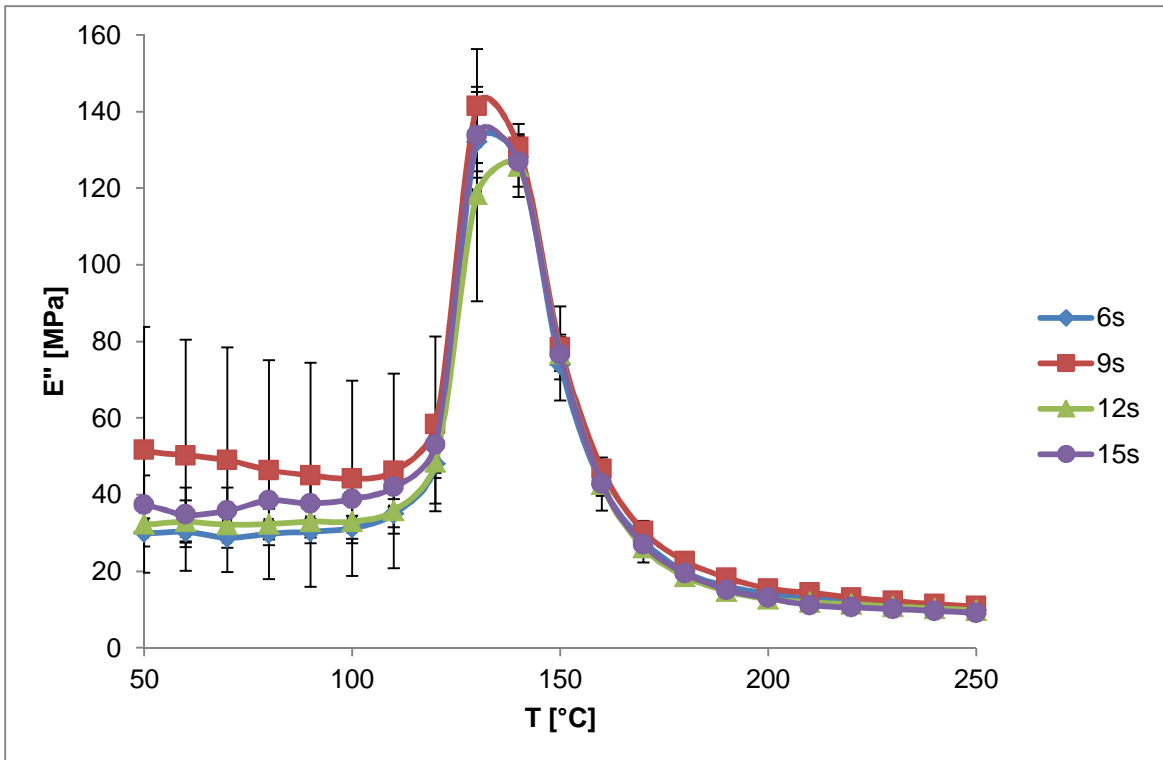
Figure 169. Loss moduli of HT laser sintered PEEK samples built with different PS times

Clearly, both storage and loss moduli are not affected by the PS time, a result found also in the tensile test characterisation.

5.6.5 Micro-CT results

The samples manufactured according build 5 with different PS times have been also examined in terms of microstructure using micro-CT analysis as described in chapter 3.2.6. The planes displayed in the micro-CT scan of every sample indicate the location of the cross sections visualised in the next image. An example of pore size and material density evaluation is also provided for each specimen in exam.

The sample built with PS of 6 s, its cross-sectional characteristics and an example of pore size found in its structure, are shown from Figure 170 to Figure 172, respectively. The result of the specimen density evaluation is shown in Figure 173.
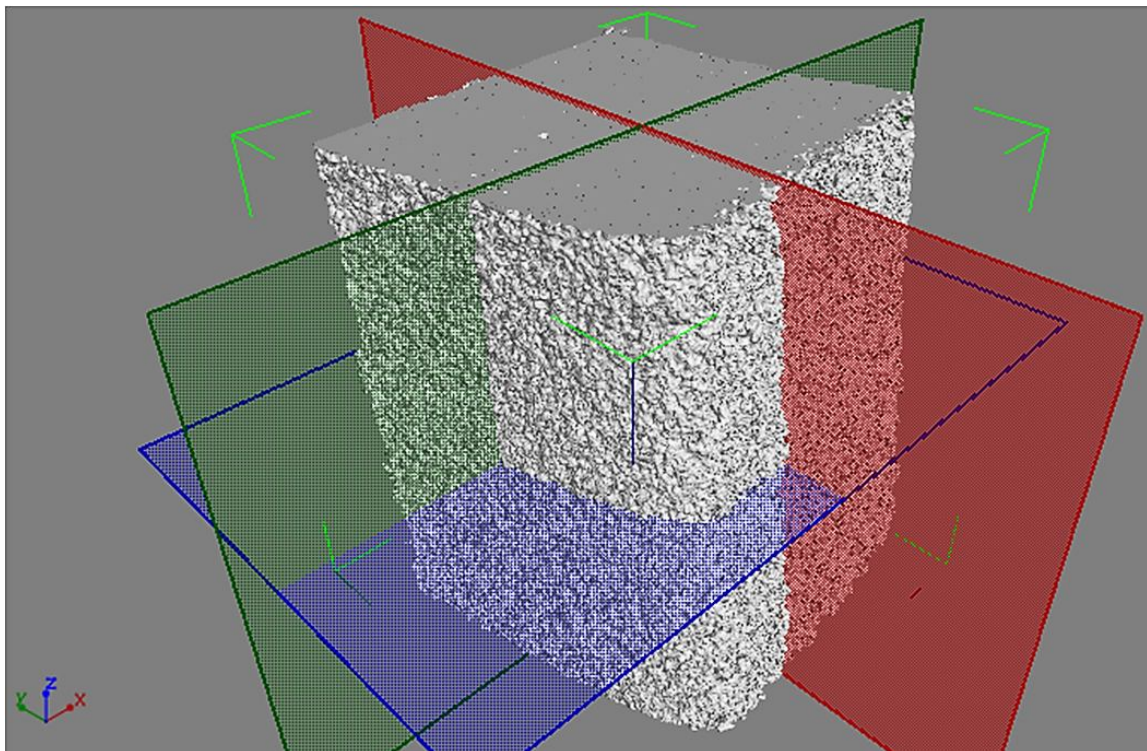
Figure 170. Micro-CT scan of the sample from build 5, PS = 6 s
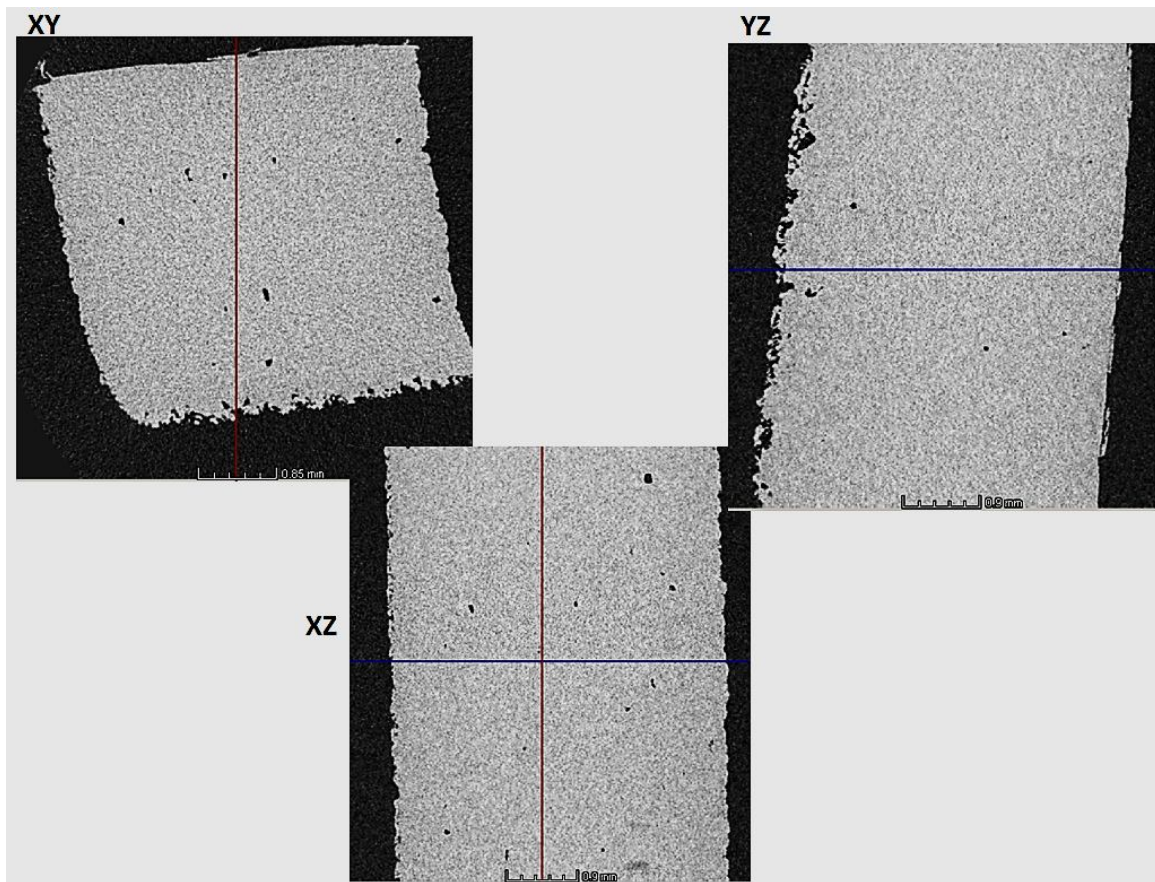
Figure 171. Micro-CT scan of the sample from build 5, PS = 6 s: cross sections
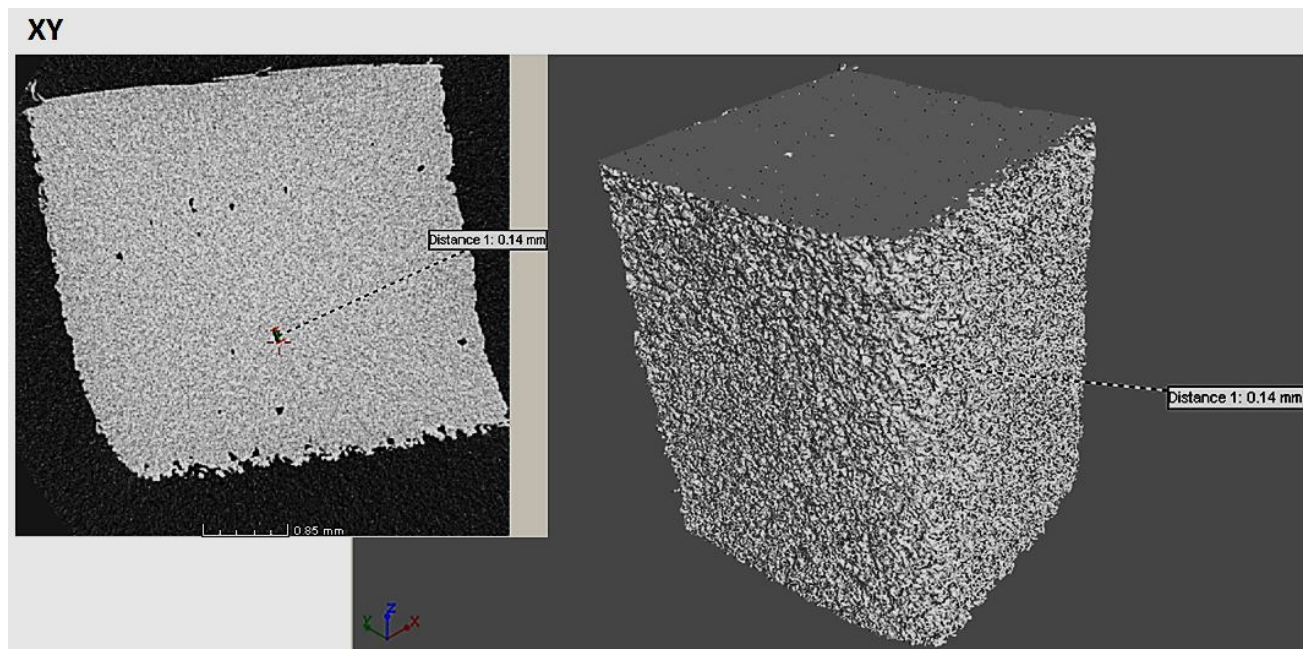
Figure 172. Micro-CT scan of the sample from build 5, PS = 6 s: example of pore size (size = 0.14 mm)
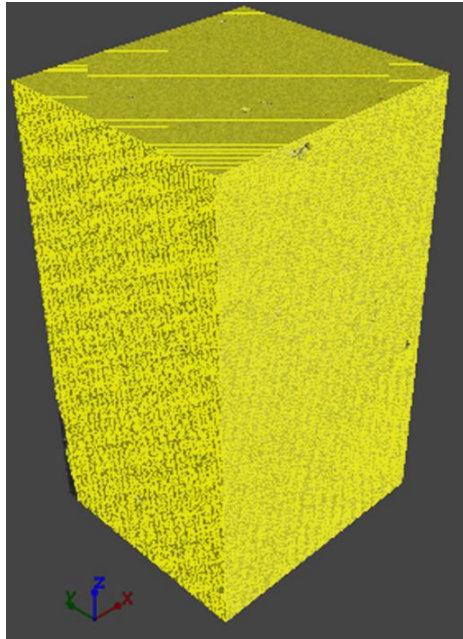
Figure 173. Micro-CT scan of the sample from build 5, PS = 6 s: material density

The sample built with a PS of 6 s shows a fairly dense microstructure (Figure 173) with presence of a few small pores (example of pore size equal to 0.14 mm). Figure 174 and Figure 175 represent the sample and cross sectional images built with a 9 s PS time. Figure 176 is instead an example of pore size found in the specimen. The material density of the 9 s sample is shown in Figure 177.
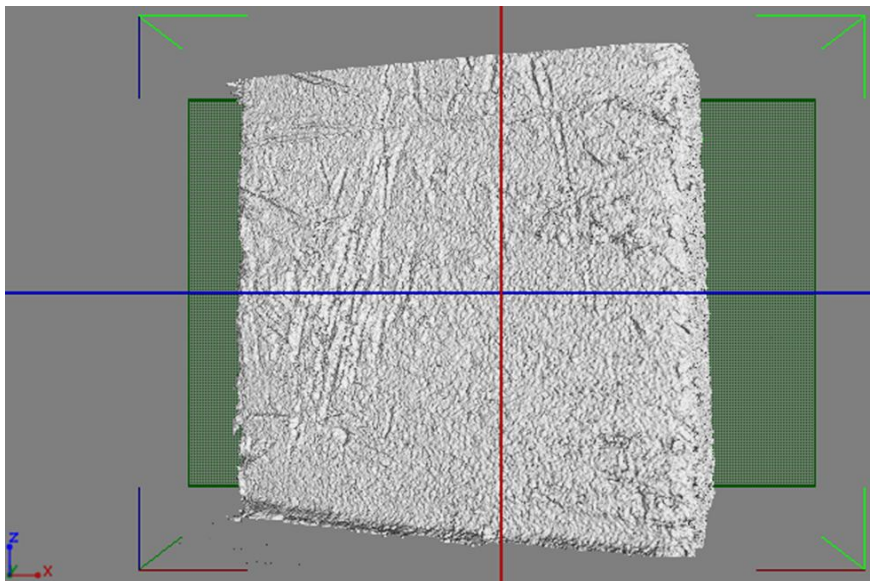
Figure 174. Micro-CT scan of the sample from build 5, PS = 9 s
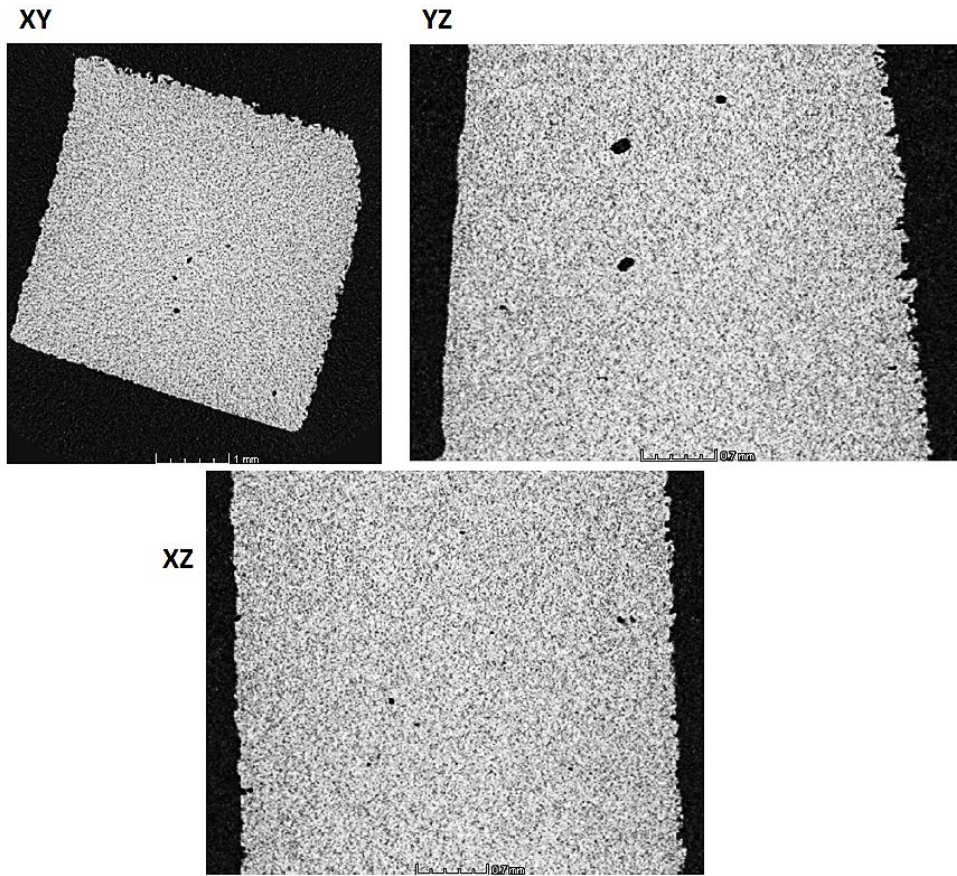
Figure 175. Micro-CT scan of the sample from build 5, PS = 9 s: cross sections
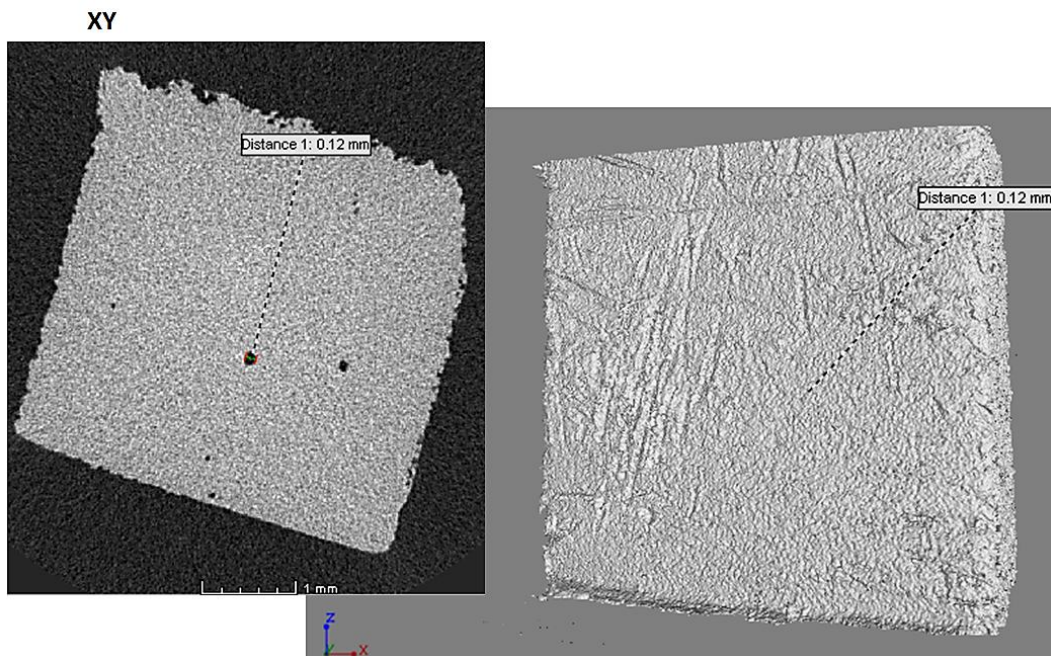
Figure 176. Micro-CT scan of the sample from build 5, PS = 9 s: example of pore size (size = 0.12 mm)
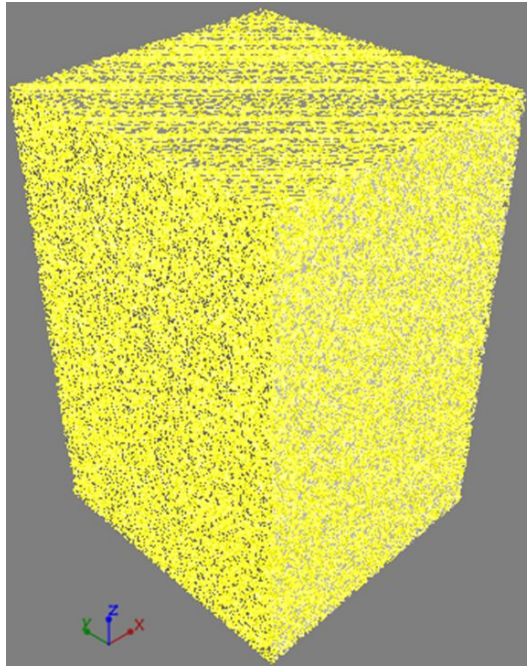
Figure 177. Micro-CT scan of the sample from build 5, PS = 9 s: material density

Again, the sample with 9 s PS does not show significant differences from the samples manufactured with PS of 6 s (Figure 170 to Figure 173) and 12 s (Figure 127 to Figure 129). The specimen appears fully dense with no visible pores (Figure 177), which however were easily detected in the cross sectional images (Figure 175). Lastly, the micro-CT results found of the sample built with a PS time of 15 s are shown from Figure 178 to Figure 180.
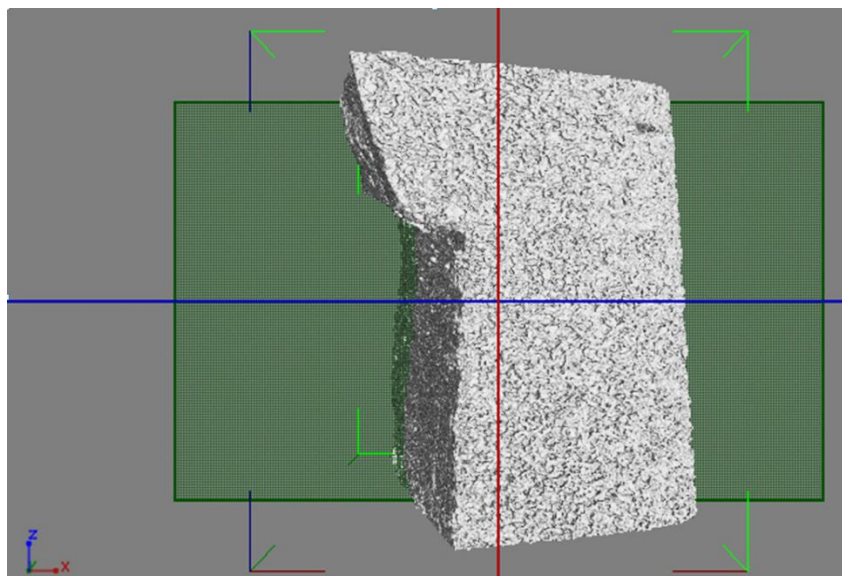
Figure 178. Micro-CT scan of the sample from build 5, PS = 15 s
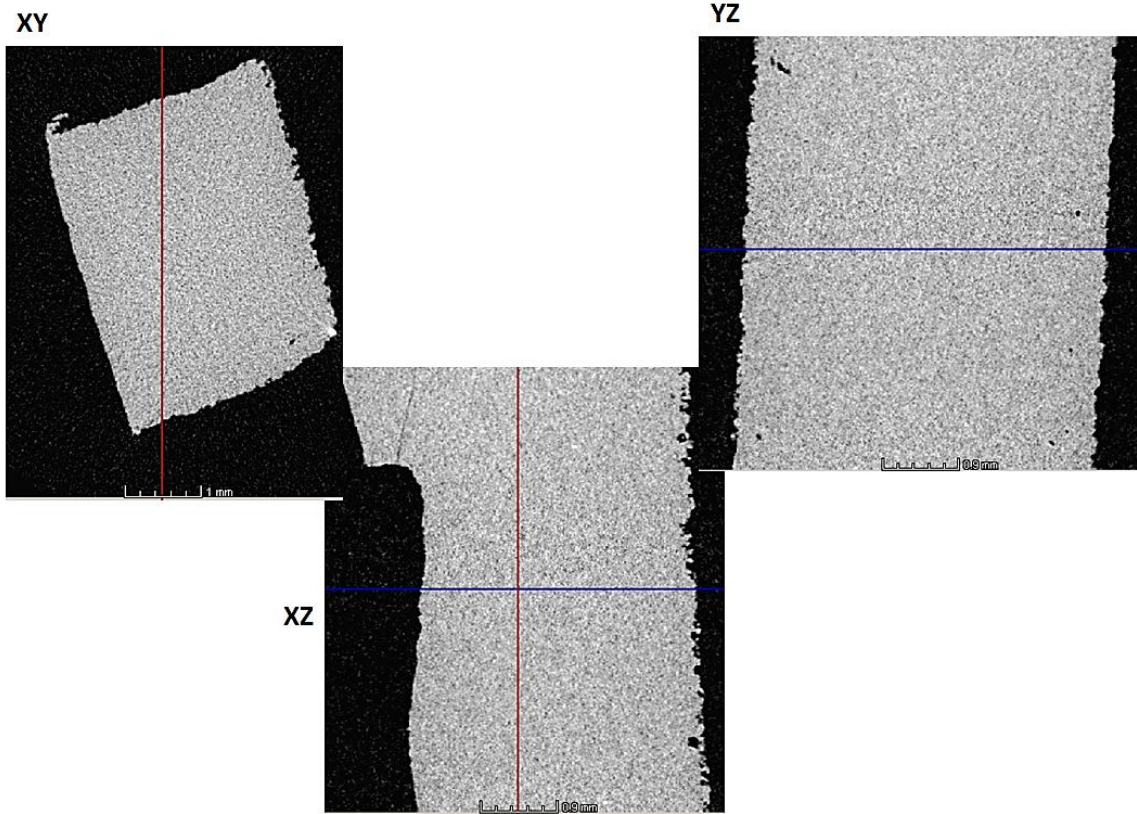
Figure 179. Micro-CT scan of the sample from build 5, PS = 15 s: cross sections
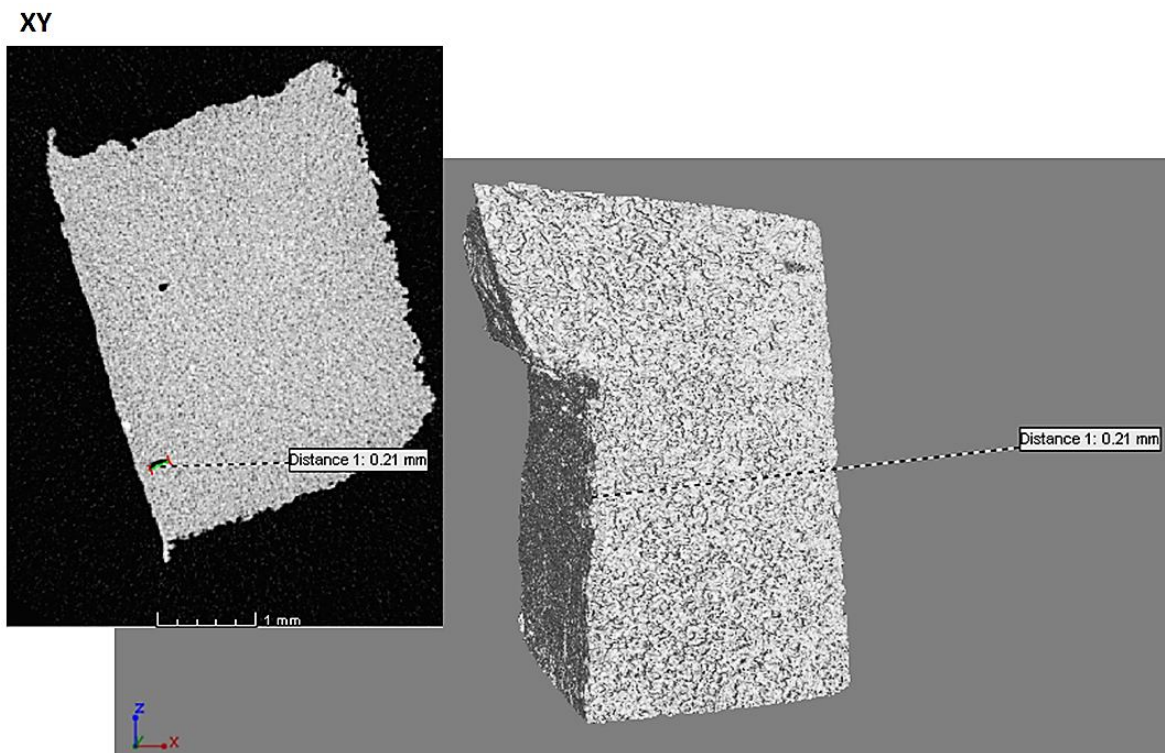
Figure 180. Micro-CT scan of the sample from build 5, PS = 15 s: example of pore size (size = 0.21 mm)

The sample with PS of 15 s exhibits a fairly dense structure and only few pores with size of 0.21 mm. The material density evaluation analysis is displayed in Figure 181.
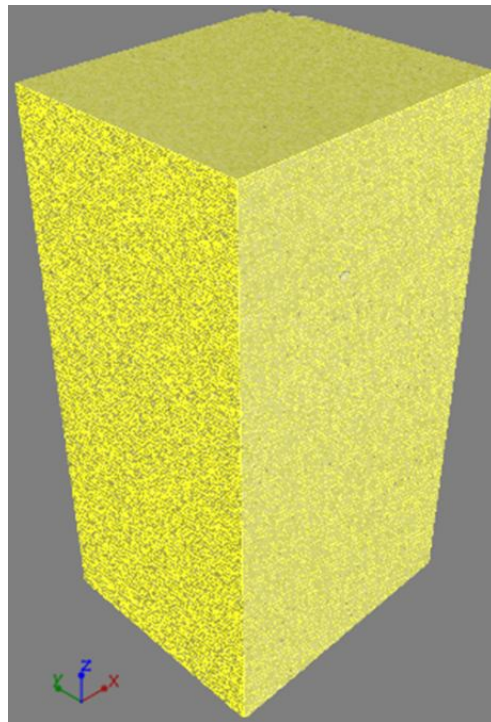
Figure 181. Micro-CT scan of the sample from build 5, PS = 15 s: material density

As seen for the previous samples with different PS times, also this specimen exhibits a high level of material density.

The estimates of the material densities of all the samples, measured as described in chapter 3.2.6, built at increasing ED are listed in Table 24.

Processing parameters profile	Material density [%]
Build 5, PS = 6 s	99.20
Build 5, PS = 9 s	95.52
Build 5, PS = 12 s	99.65
Build 5, PS = 15 s	97.22

Table 24. Material densities of the HT laser sintered PEEK samples with processing parameters from build 5 and increasing PS time

The material density results have plotted against the ED values used in the manufacture of the corresponding HT laser sintered PEEK components in Figure 182.
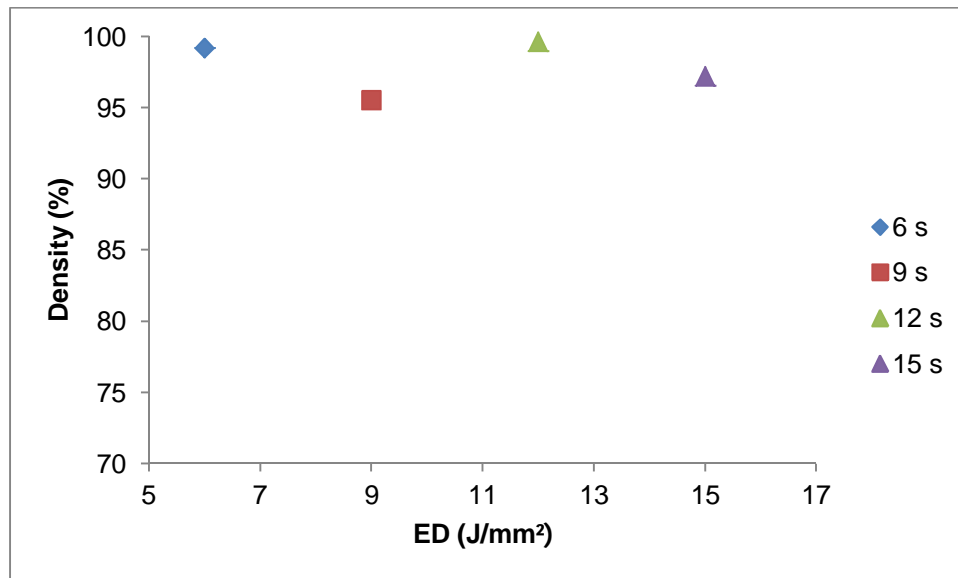
Figure 182. ED and density of the HT laser sintered PEEK components built at increasing PS time

As it can be seen in Figure 182, there is not a clear significant variation in density between the samples manufactured with EOS standard PS time of 12 s and those manufactured with lower and higher PS times.

5.7 Conclusions

This chapter presents the first experimental results on HT-LS of PEEK in a commercial HT-LS system. Processing parameters have been optimised for the manufacturing of testable specimens. The properties of HT laser sintered PEEK samples have been analysed and compared to those of PEK HP3 samples manufactured in standard conditions. Tensile strength, viscous elastic behaviour, microstructure and surface morphology have been analysed.

As found for other LS polymers, the increase of the ED led to an improvement of the tensile strength and microstructure of the HT laser sintered PEEK specimens. The

viscous elastic behaviour, storage modulus, loss modulus and loss factor tan, resulted instead less sensitive to the ED parameter.

Following an optimisation process, the tensile strength of the PEEK components achieved a storage modulus of 2500 MPa and a tensile strength value of 63 MPa, only 20 MPa lower than the current commercial grade HP3 PEK. Additionally, the micro-CT analysis showed a material density of 99% for the sample manufactured with the optimal processing parameters (build 5).

The PS stage, a characteristic unique to HT-LS, does not seem to significantly affect the mechanical properties of HT laser sintered PEEK components in the PS range 6-15 s. Therefore, a time reduction of the overall HT-LS process could be achieved with shorter PS time without altering the mechanical performance of the HT laser sintered PEEK components.

Interestingly, the micro-CT analysis allowed to visualise the layer effect, a characteristic of the LS process, only on the PEEK samples built at low ED (build 1 and build 2), implying good quality of layer bonding for the samples built at higher ED. However, SEM imaging allowed to detect the layer effect on PS ten layer specimens of PEK HP3 and PEEK built at the corresponding optimal processing parameters. This result therefore indicated that the distinction between layers is still visible even for samples built at high ED.

The experimental results of this work can then open the way to the use of PEEK in HT-LS for the manufacture of high performing engineering components. For clarity, a summary of the main findings found in this chapter is shown in Figure 183.
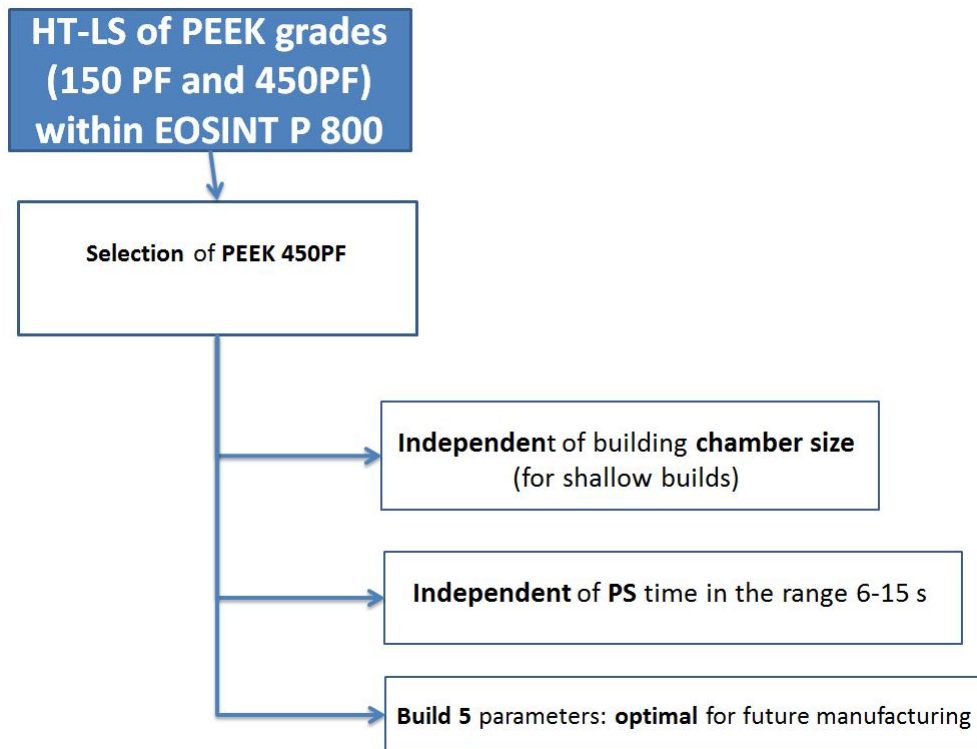
Figure 183. Summary of the main findings of chapter 5 about HT-LS of PEEK grades within the EOSINT P 800

6 Predicting processing parameters in HT-LS

When new materials are to be trialled in the LS process, the general approach for choosing the part bed temperature (described in chapter 5.2.4) is to carry out the procedure explained in chapter 5.3. This *modus operandi* is based on qualitative criteria such as visual inspection of the powder bed and approximate temperature adjustments within the LS system. Although reliable, this procedure could be greatly improved with a more accurate methodology.

The optimisation of the processing parameters for a desired set of properties required on the laser sintered components is instead performed by an iteration of trial and error builds, where one parameter is changed at a time and its effect on the laser sintered part properties is evaluated through experimental testing.

Both strategies – for choosing the part bed temperature and optimising the processing parameters for enhanced part properties – can be highly time consuming and extremely expensive depending on the cost per kg of material being examined and the physical size of the LS equipment available.

It therefore could be beneficial to formulate a method or a small set of experiments that are able to predict the processing temperature of an unknown material and identify the optimal set of processing parameters for a certain application *a priori,* i.e. before physical testing within LS and HT-LS systems.

However, the lack of analytical techniques able to simulate the conditions of the LS process such as high LS heating rate, very long cooling stage, spreading and powder packing conditions have been hindering the formation of a more scientific methodology.

In this chapter a technique to estimate the part bed processing temperature based on the material properties is proposed. The validation of the current methods for the prediction of processing temperatures and parameters available in the LS community - super-cooling window, stable sintering region and EMR, described in chapter 2.2 – are applied to the PEEK grades, especially the thermally conditioned 450PF material, whose optimisation in the HT-LS process was provided in chapter 5.

The structure of this chapter is illustrated in Figure 184.
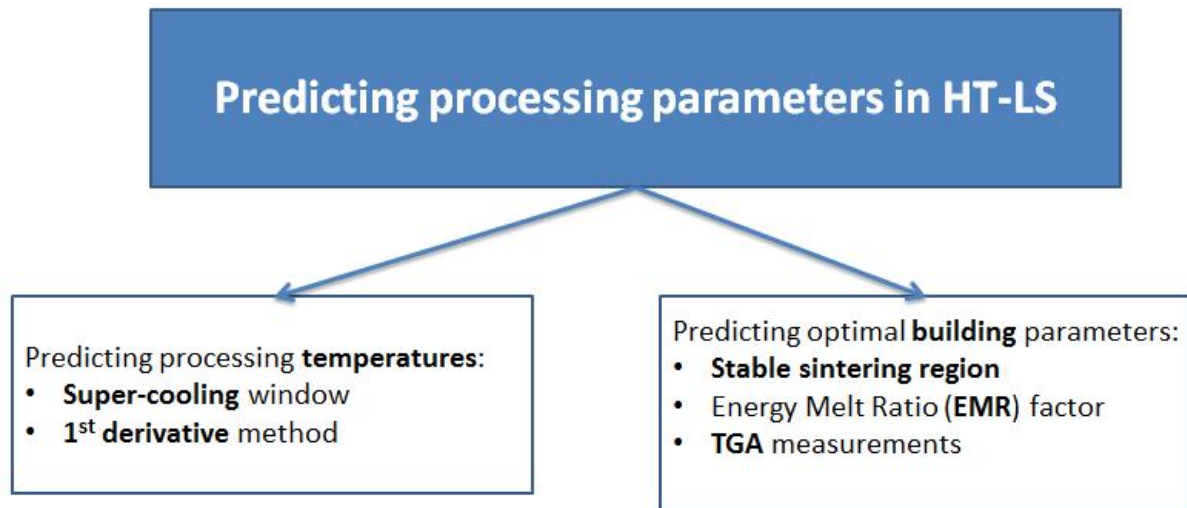
Figure 184. Structure of chapter 6

6.1 Predicting processing temperatures

Two techniques for the prediction of the processing temperatures, especially part bed temperature, during a LS building process are presented here: the established super-cooling window [73] and a new method proposed by the author specifically for HT polymers. Both techniques require the analysis of the thermal properties of the materials under test using DSC.

6.1.1 Thermal properties of established LS powders and PEEK grades

The thermal properties of melting and crystallisation and DSC thermoscans have been evaluated for established LS material such as PA 2200, 50/50 PA 2200, PA 1101 and PEK HP3, and for the new potential HT grades such as PEEK 450PF, thermally conditioned PEEK 450PF, PEEK 150PF and thermally conditioned PEEK 150PF.

The purpose of these analyses was to provide the information required for the application of predicting processing temperature methods. PA based materials and PEK HP3 were used as benchmark materials in the techniques presented. Both unconditioned and thermally conditioned (chapter 3.2.2) PEEK grades have been

272

tested in the predicting methods. As describe in chapter 3.1.1.1, PA 1101 is LS optimised PA 11 powder and was used here as a further benchmark material. The thermal properties measured as described in chapter 3.1.9 are listed in Table 25 and Table 26.

Material	Onset melting (℃)	Melting peak (℃)	Enthalpy of melt (J/g)
PA 2200 virgin	180.6 ± 0.7	185 ± 0.6	104.9 ± 3.6
PA 2200 50/50 used/virgin	179.4 ± 0.2	186.8 ± 0.1	107.3 ± 4.0
PA 1101	197.6 ± 1.0	201.0 ± 0.6	88.9 ± 0.6
PEK HP3	354.2 ± 5.3	372.0 ± 0.2	63.9 ± 0.9
PEEK 150PF	332.6 ± 0.8	346.2 ± 0.5	57.1 ± 1.3
PEEK 150PF thermally conditioned	333.7 ± 5.2	343.6 ± 6.4	57.8 ± 5.8
PEEK 450PF	320.8 ± 1.3	338.9 ± 0.4	57.9 ± 4.5
PEEK 450PF thermally conditioned	320.5 ± 0.4	339.0 ± 0.5	58.6 ± 5.8

Table 25. Thermal properties of melting of LS established grades and PEEK polymers

Material	Onset Crystallisation (℃)	Crystallisation peak (℃)	Enthalpy of crystallisation (J/g)
PA 2200 virgin	151.8 ± 0.3	147.4 ± 0.3	53.6 ± 1.3
PA 2200 50/50 used/virgin	150.6 ± 0.5	146.2 ± 0.2	51.7 ± 1.3
PA 1101	165.8 ± 0.3	163.1 ± 0.3	45.7 ± 1.1
PEK HP3	338.3 ± 0.4	332.2 ± 0.3	49.0 ± 2.7
PEEK 150PF	308.6 ± 0.1	299.1 ± 0.1	51.3 ± 3.3
PEEK 150PF thermally conditioned	313.4 ± 0.2	301.8 ± 0.4	55.6 ± 3.6
PEEK 450PF	298.9 ± 0.1	292.9 ± 0.1	44.8 ± 1.1
PEEK 450PF thermally conditioned	300.2 ± 0.5	295.6 ± 0.6	46.0 ± 0.9

Table 26. Thermal properties of crystallisation of LS established grades and PEEK polymers

The thermal properties of the melting region – onset temperature, peak temperature and enthalpy of melt – are provided in Table 25, while the thermal properties of the crystallisation region – onset temperature, peak temperature and enthalpy of crystallisation – are listed in Table 26.

As expected, the PA grades show lower melting and crystallisation onset and peak temperature than the HT polymers (PEK HP3 and PEEK grades). Interestingly, no significant temperature shift and enthalpy change seem to occur between PA 2200 and 50/50 PA 2200 grades, providing a further indication of the high recyclability of this material. It can be noticed that PA based grades exhibit higher values of melting and crystallisation enthalpies than the HT polymers, due to their chemical structure.

Small changes on the onset and crystallisation peak temperature seem to occur between virgin and thermally conditioned PEEK grades. However, the melting properties - onset temperature, peak temperature and enthalpy of melt- do not seem to vary significantly, implying that the thermal conditioning improved the particle morphology of the two powders without deteriorating the materials. It is not clear at this stage why PEEK 150PF and 450PF showed higher property variations (standard deviations) than the other materials.

The part bed temperature (T_b) (temperature at which the powder is held before the laser exposure during a building process, chapter 5.2.4) of the established LS materials are listed in Table 27 along with the part bed temperatures of the thermally conditioned PEEK grades found by applying the EOS method 5.3. The part bed temperature of the already optimised LS grades were provided by EOS [1].

It must to be outlined that no values of the part bed temperature of virgin PEEK 150PF and 450PF are provided because these material were found impossible to spread across the powder bed, thus hindering any further HT-LS processing (chapter 4.7).

In the EOSINT P 800 a 2 ˚C increase is applied between full building chamber mode and half- or reduced- building chamber modes (chapter 5.2.2.1).

Material	LS/HT-LS system	T_b (℃)
PA 2200 virgin	EOSINT P 100	168-169
PA 2200 50/50 virgin/used	EOSINT P 100	168-169
PA 1101	EOSINT P 100	185
PEK HP3	EOSINT P 800	365 (Reduced and Half chamber) 367 (Full chamber)
PEEK 150PF thermally conditioned	EOSINT P 800	338 (Reduced and Half chamber) 340 (Full chamber)
PEEK 450PF thermally conditioned	EOSINT P 800	332 (Reduced and Half chamber) 334 (Full chamber)

Table 27. Part bed temperatures of optimised LS materials and thermally conditioned PEEK grades

By comparing the thermal properties of the powders (Table 25 and Table 26) with their corresponding part bed temperatures (Table 27) it is possible to notice that the part bed temperatures of the PA based grades is lower than the their onset melting temperatures. On the contrary, the part bed temperature of PEK HP3 and thermally conditioned PEEK materials is higher than the onset temperature of melting. This is an interesting result as it proves that the HT-LS materials are processed in the EOSINT P 800 system at a temperature where material melting should have already started according to DSC analysis.

A LS processing window based on the knowledge of the thermal properties of the raw powders is currently available in the LS community. The window has been evaluated and discussed in the following paragraph.

6.1.2 Super-cooling window

The super-cooling window is a LS processing window based on the DSC thermoscan of the powder under test [73] and it is largely used in the LS community [58, 75, 77, 106]. This window has been discussed in chapter 2.2 (Figure 7).

For clarity, the super-cooling window is defined as the temperature gap between the onset of the melting event and the onset of the crystallisation event. This window essentially constitutes a wide range of temperature values that can be used as a processing temperature inside a LS system for successful LS manufacturing. This spectrum enables the powder lying in the powder bed of a generic LS system not to melt before exposure to the laser and not to crystallise during laser exposure.

This operating window has been evaluated experimentally as described in chapter 3.1.9 using DSC analysis on established LS materials such as virgin PA 2200, 50 /50 used/ virgin PA 2200, PA 1101 and PEK HP3, and on PEEK 150PF and 450PF virgin and thermally conditioned grades.

Figure 185 shows the DSC thermoscan of virgin PA 2200 and 50/50 virgin /used PA 2200. Figure 186 is instead the DSC thermoscan of PA 1101.
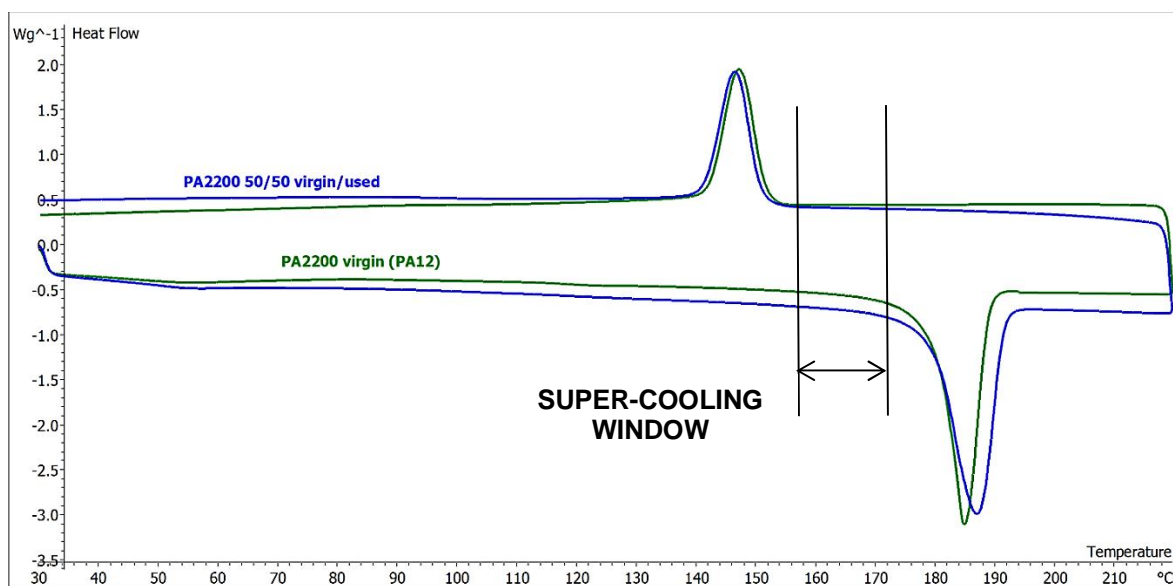
Figure 185. DSC thermoscan showing the super-cooling window applied to PA 2200 powders: virgin and 50/50 virgin/used
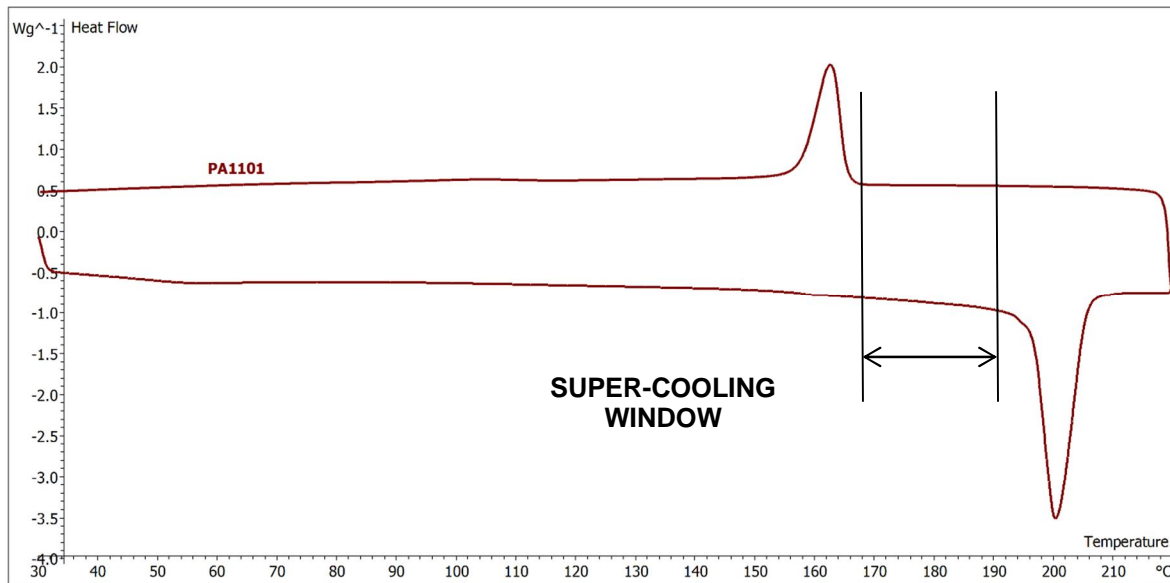
Figure 186. DSC thermoscan showing the super cooling window applied to PA 1101

Both mixtures of PA 2200 (Figure 185) and PA 1101(Figure 186) confirm to exhibit the super-cooling window. A wide temperature spectrum between the onset of the melting phenomenon and the onset of the crystallisation event is clearly visible for these three grades. Both PA 2200 grades and PA 1101 also show sharp and clear peaks corresponding to the melting and crystallisation phenomena. These characteristics are well-known in the LS community and they have been considered to be the reason why PA-based materials are successful in LS processing. The super-cooling window method can be fully validated in these two materials by noticing that the LS part bed temperature of these materials, shown in Table 27, (168-169 °C) are located within the temperature interval defined by the super-cooling window.

Figure 187 shows the DSC thermoscan of PEK HP3, while the DSC thermoscans of PEEK 450PF and 150PF, virgin and thermally conditioned are shown in Figure 188 and Figure 189, respectively.
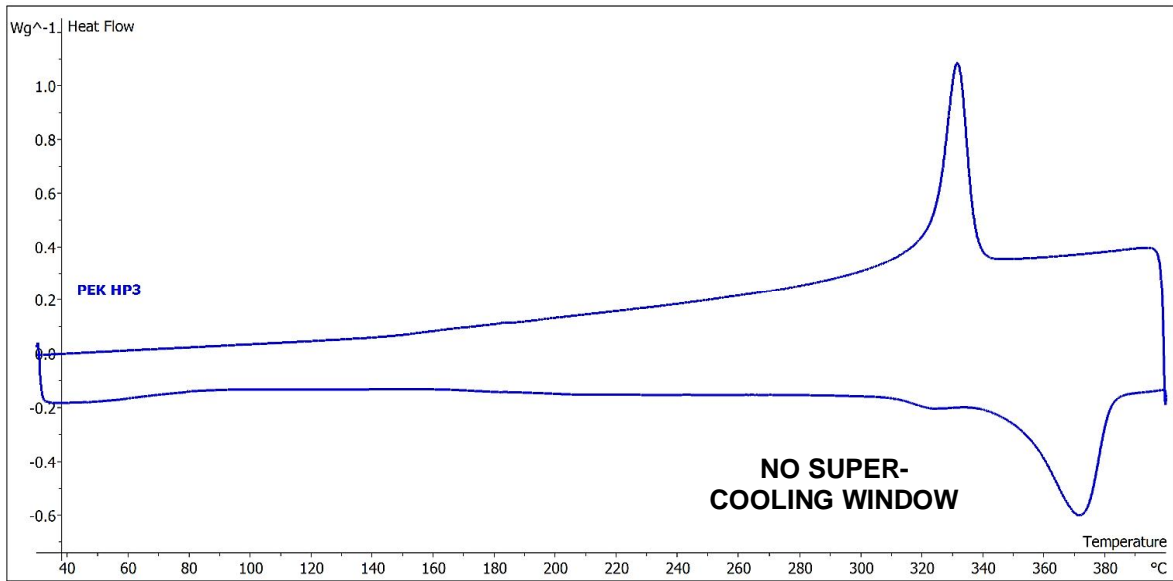
Figure 187. DSC thermoscan showing that the super-cooling window does not apply to PEK HP3
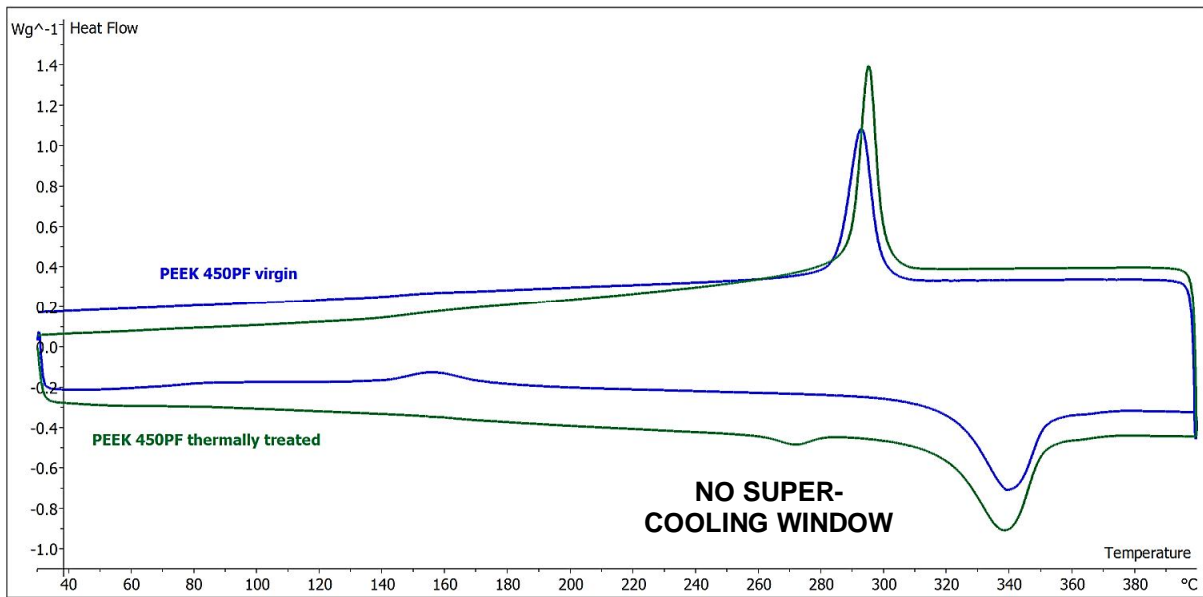
Figure 188. DSC thermoscan showing that the super-cooling window does not apply to virgin and thermally conditioned PEEK 450PF

278
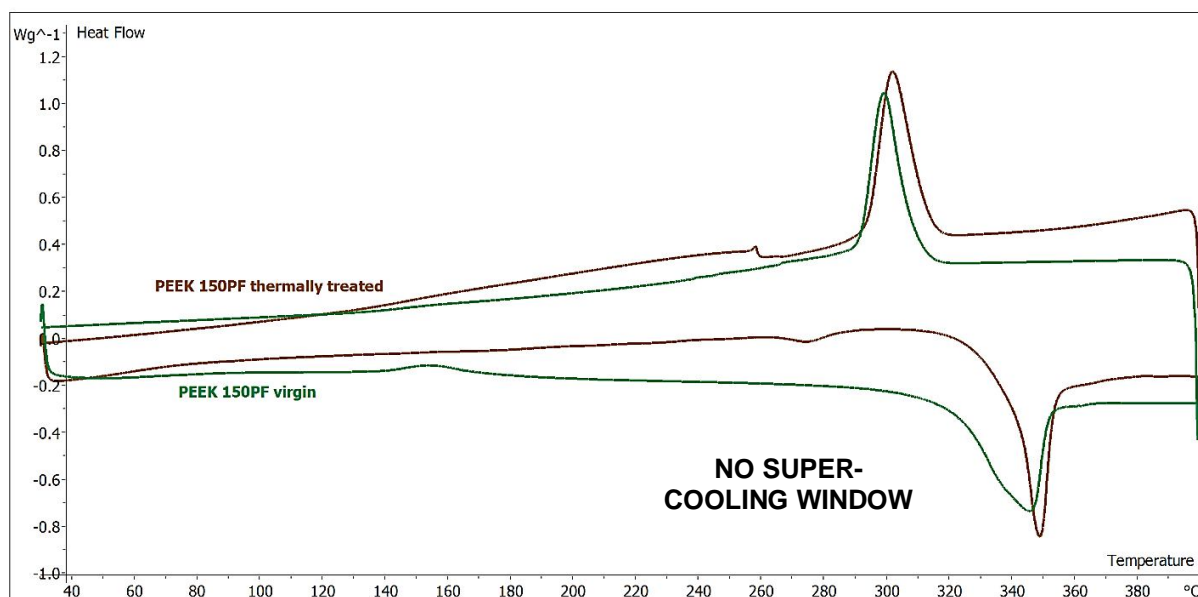
Figure 189. DSC thermoscan showing that the super-cooling window does not apply to virgin and thermally conditioned PEEK 150PF

HP3 PEK exhibits a thermal profile with double melting peak. The melting and crystallisation areas are broad and overlap indicating the lack of temperature gap between the end of the melting region and the onset of the crystallisation phase (Figure 187). The super-cooling window does not seem to occur for this material.

PEEK virgin grades show a cold crystallisation event in proximity to the glass transition temperature, which is believed to be due the rapid cooling phase in the manufacturing process of the powders. After thermal conditioning for the improvement of the flow properties, both PEEK grades show a double melting behaviour (Figure 188 and Figure 189). Several interpretations of the double melting peak behaviour are available in the literature [22] and are discussed in chapter 2.1.2.

As seen in PEK HP3, both virgin and thermally conditioned PEEK powders (150PF and 450PF) do not exhibit the super-cooling window; they showed fairly wide melting and crystallisation regions that overlap.

The reason why the low melting temperature polymers show an evident super-cooling window is believed to be related to the chemical structure of those polymers. It can be noted that the super-cooling processing window is not evident in the HT polymers such as PEK HP3 (Figure 187), thermally conditioned and virgin PEEK

279

450PF (Figure 188) and thermally conditioned and virgin PEEK 150PF (Figure 189). These results are not surprising as it was noted in 6.1 that the part bed processing temperature of these material within the HT-LS system EOSINT P 800 was inside the melting region.

Clearly, the super-cooling window can help to select new LS low temperature polymers on the basis of the material proprieties and offers the possibility to approximately estimate LS processing temperatures of new materials before a series of trials-and-error building process. This method results fully correct for low melting temperature and PA based material such a PA 2200, 50/50 PA 2200 and PA1101. However, it does not seem to allow providing processing temperature predictions for those polymers that do not exhibit a clear temperature interval between melting and crystallisation events such as HT polymers and elastomers.

6.1.3 The new first derivative method

A new very basic approach to estimate the part bed temperature for HT-LS PAEK materials is proposed here. This method consists of evaluating the 1st derivative of the heating segment of a DSC thermoscan of the PAEK material under test and calculating the minimum point, as described in chapter 3.1.9. This technique has been applied to all the material presented in this chapter.

The 1st derivative data of PA 2200 grades (virgin and 50/50 used/virgin) are shown in Figure 190. The processing temperature (part bed temperature) of these materials is lower than the minimum temperature found with the first derivative method. This result is not surprising as the processing temperature of PA 12 and 11 is lower than the onset of the melting region (Figure 185, Figure 186). The first derivative method is therefore not useful for this group of polymers.
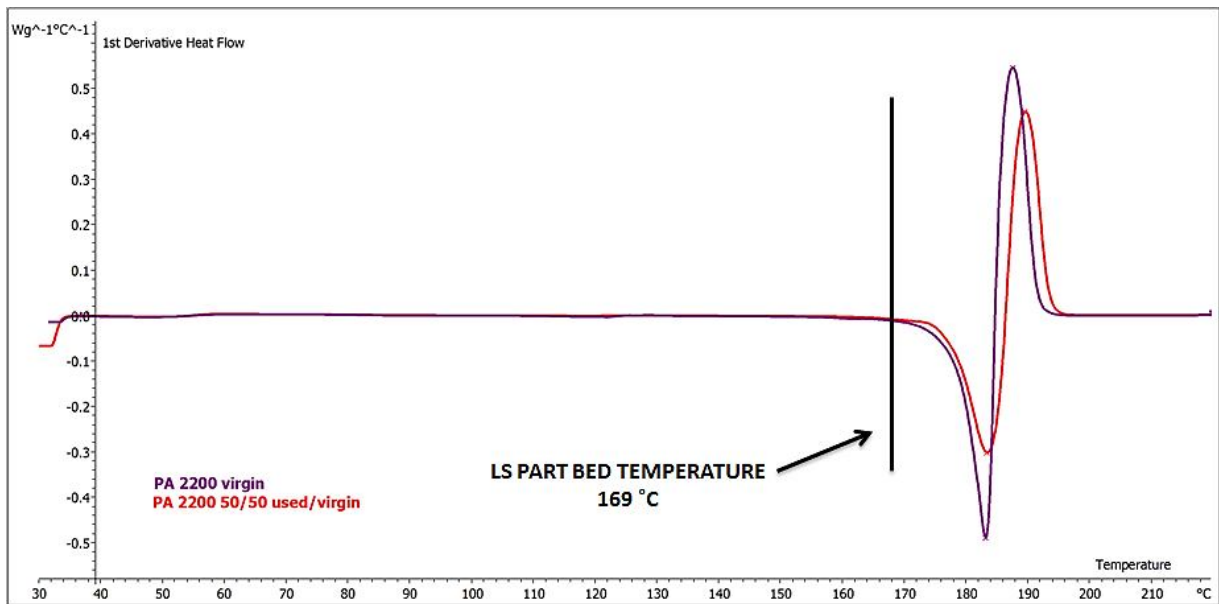
Figure 190. 1st Derivative of the melting segment of the DSC thermoscan of PA 2200 grades
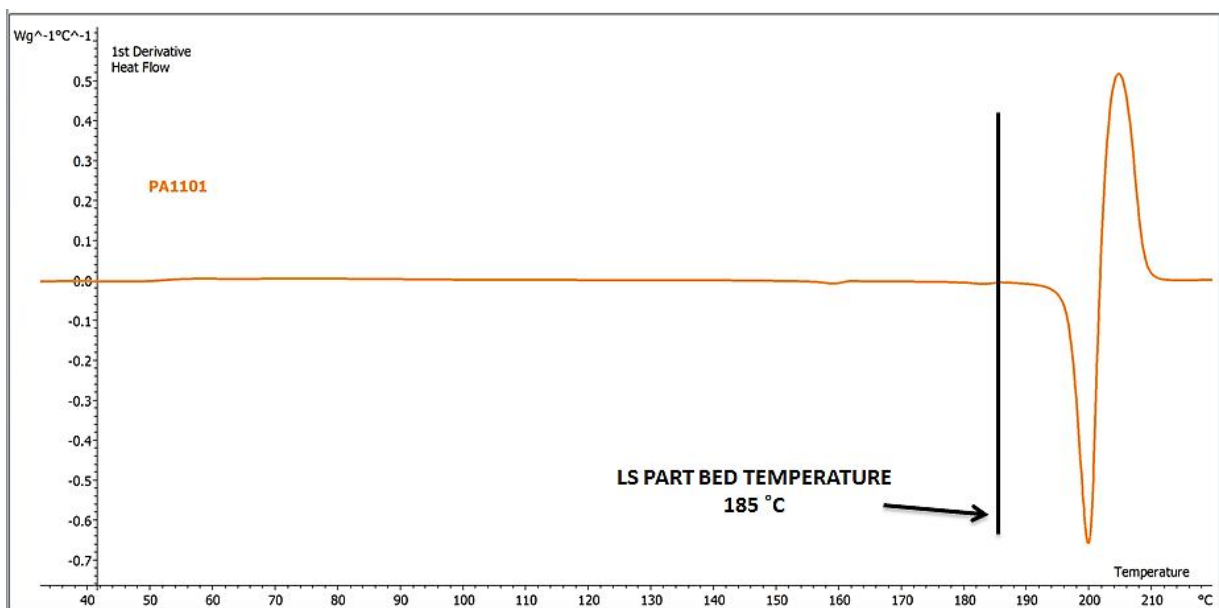
Figure 191. 1st Derivative of the melting segment of the DSC thermoscan of PA 1101 grade

The first derivative of PEK HP3, thermally conditioned PEEK 150PF and thermally conditioned PEEK 450PF are shown from Figure 192 to Figure 194.
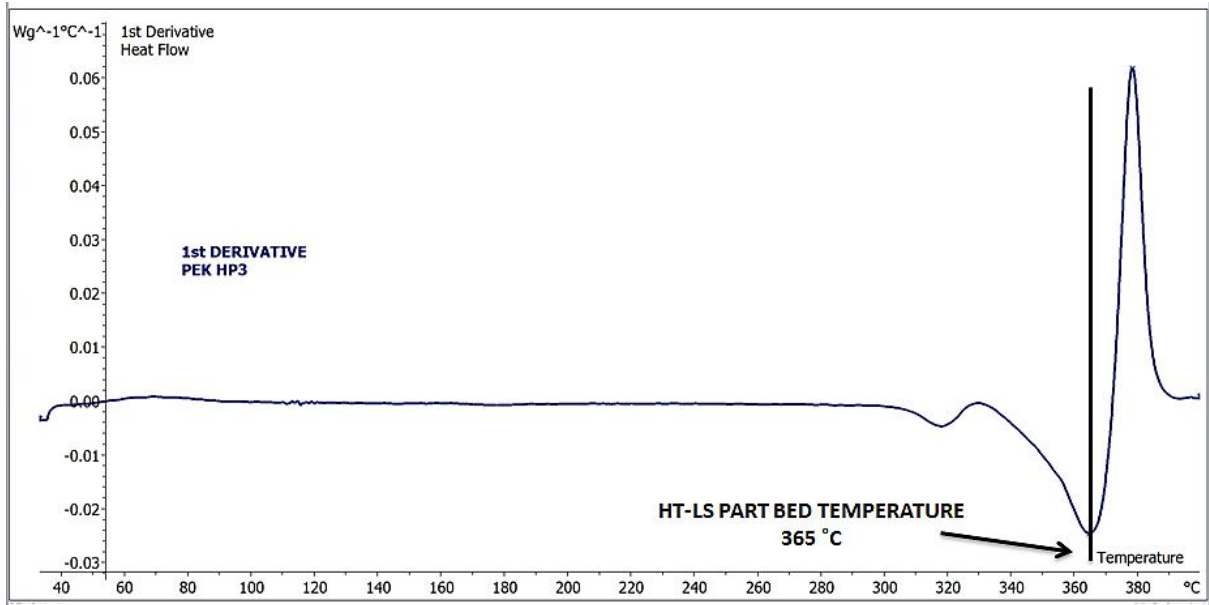
Figure 192. 1st Derivative of the melting segment of the DSC thermoscan of PEK HP3
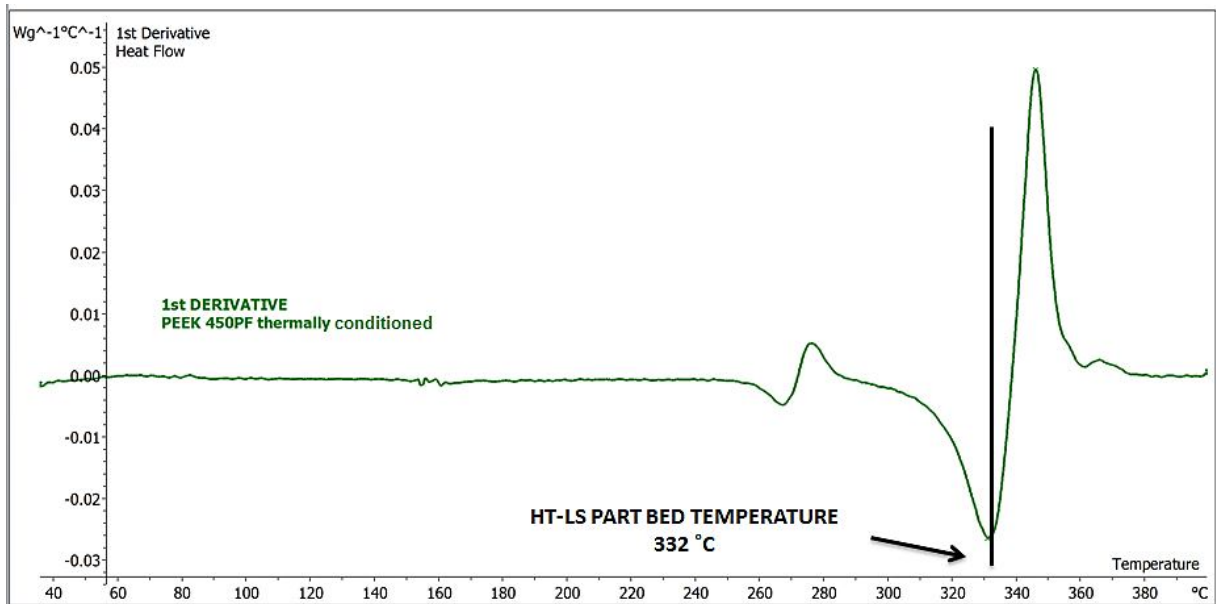
Figure 193. 1st Derivative of the melting segment of the DSC thermoscan of the thermally conditioned PEEK 450PF
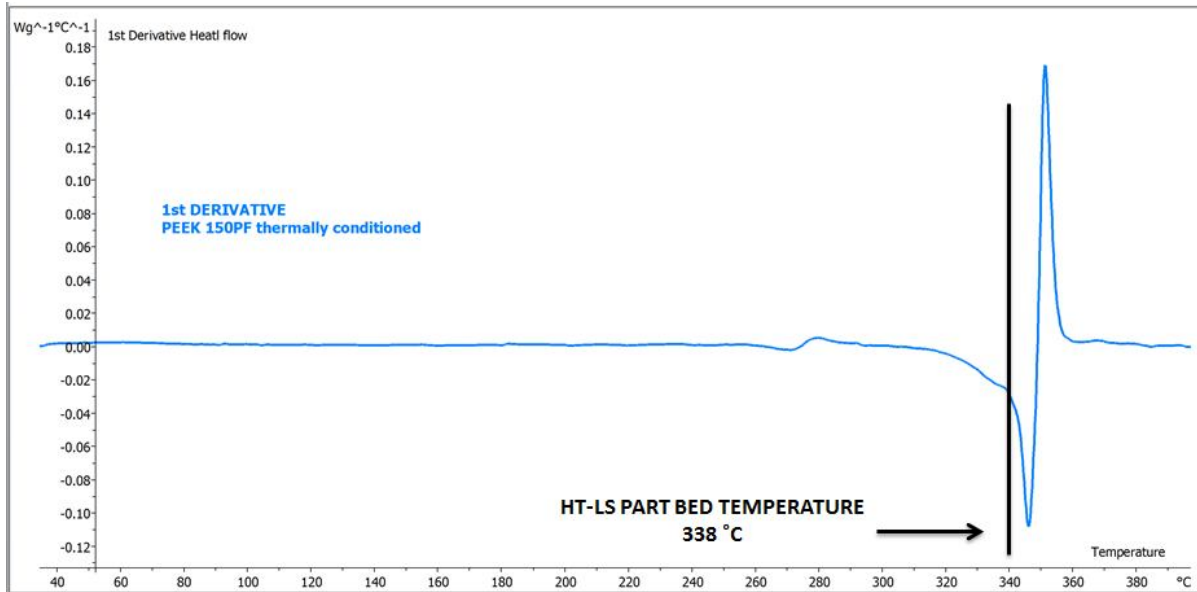
Figure 194. 1st Derivative of the melting segment of the DSC thermoscan of the thermally conditioned PEEK 450PF

The minimum of the first derivative curve of the DSC thermoscans of the HT polymers (Figure 192 to Figure 194) equates the corresponding HT-LS part bed processing temperature. The mean values of the minimum and maximum values obtained by the multiple tests carried out on both materials are listed in Table 28 in parallel with the corresponding part bed temperatures within the HT-LS system EOSINT P 800, EOS recommended PEK HP3 part bed temperature and PEEK temperature found with EOS method (chapter 5.3).

Material	Min (℃)	Max (℃)	Part bed temperature within the EOSINT P 800
PEK HP3	366 ± 2	379 ± 1	365 ℃ (Reduced and Half chamber) 367 ℃ (Full chamber)
PEEK 150PF thermally conditioned	342 ± 3	351 ± 1	338 ℃ (Reduced and Half chamber) 340 ℃ (Full chamber)
PEEK 450PF thermally conditioned	332 ± 1	346 ± 1	332 ℃ (Reduced and Half chamber) 334 ℃ (Full chamber)

Table 28. Thermal properties of the 1ˢᵗ derivative of the melting segment of the DSC thermoscans (average values and standard deviations)

Both PEK HP3 and thermally conditioned PEEK grades show that the part bed temperature required for successful HT-LS within the EOSINT P 800 system seem to equate the minimum of the first derivative.

This method, which appears to be very basic, provided a good estimate of the part bed temperature for PEK HP3 and PEEK 450PF within the HT-LS system P 800. Therefore, this technique could represent a good strategy for estimating the part bed temperature for HT-LS material candidates before trial tests within the HT-LS system. However, a wider range of polymeric powders should be tested and the predicted part bed temperature compared with the actual part bed temperature in order to fully validate this proposed technique.

6.2 Predicting optimal building parameters in HT-LS

6.2.1 Stable sintering region

Stable sintering region is an approach introduced by Vasquez et al. [104] for exploring LS optimised and new potential LS materials in the region above their melting points and below their degradation temperatures. The aim of this method is

not to predict the processing bed temperatures of an unknown material *a priori*. It instead aims to predict the temperatures that lead to thermal degradation of the material in order to avoid them, during a LS building operation, especially during the laser exposure.

The stable sintering region, described in chapter 2.2, is delimited by values found with DSC, hot stage and TGA analyses of polymeric powders. The lower limit is the temperature at which the material is fully molten and is found with the combination of DSC data (melting peak temperature) and hot stage testing (temperature at which the powder particles were fully melted). The upper limit is the temperature at which the 1% weight loss degradation occurs during a TGA experiment that is carried out from room temperature to HT at a heating rate of 10 °C/min. This method clearly does not take into account the crystallisation effect present in semi-crystalline polymers such as PA based powders or PAEK materials and therefore according to Vasquez et al. [104] can be used for more kinds of polymers. The stable sintering region for a LS PA 12 grade is shown again in Figure 8.

PA 12 showed a stable sintering region of 120 °C, with lower limit of 200 °C and upper limit of 320 °C. According to this study, the processing parameters of the LS process and more precisely those of the laser exposure - laser power, scan distance, scan count and scan speed - should cause an increase in the temperature of the powder particles higher than 200 °C in order to achieve complete melting but lower than 320 °C in order to avoid their thermal degradation.

The evaluation of the stable sintering region for thermally conditioned PEEK 450PF is shown in Figure 195. The DSC and TGA data were measured as described in chapter 3.1.9 and 3.1.10, respectively. The black line represents the TGA data "Weight loss", while the blue trace is the heat flow signal resulting from DSC analysis ("Heat flow"). As hot stage testing was not carried out for thermally conditioned PEEK 450PF, the lower limit of its stable sintering region was chosen well above the melting region.
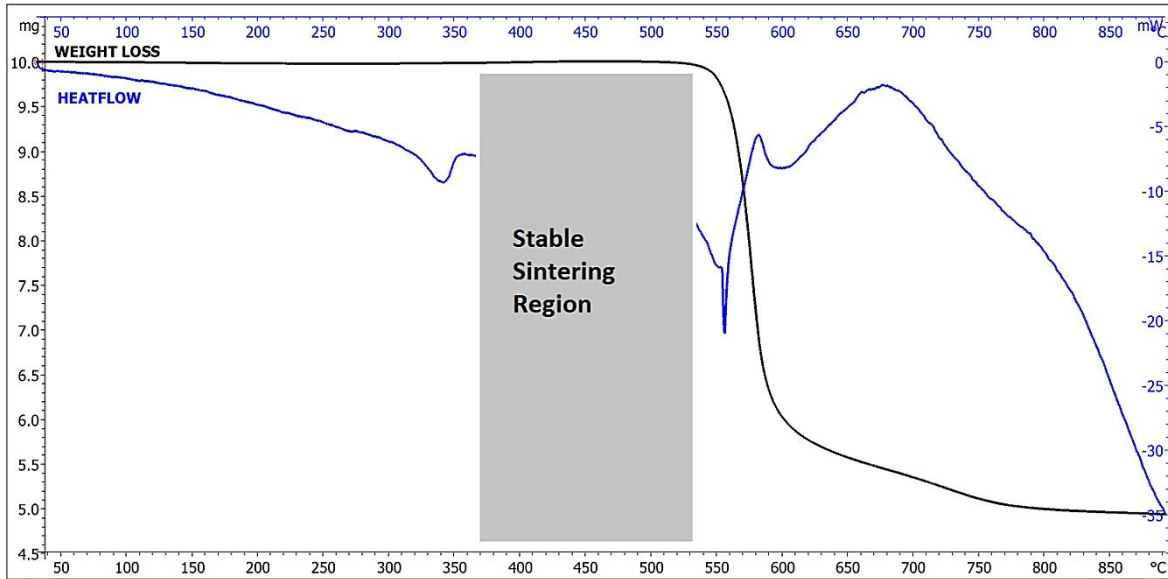
Figure 195. Stable sintering region for thermally conditioned PEEK 450PF found by combining DSC (heat flow) and TGA (weight loss) experimental data.

PEEK 450PF thermally conditioned shows a stable sintering region starting at 380 °C and finishing at 530 °C with a temperature width of 250 °C. This wide range of possible stable sintering temperatures is due to the high onset material degradation temperature, a known characteristic of the PEEK materials. Therefore the optimal processing parameters of the laser exposure strategy - laser power, scan distance, scan count and beam speed - should be chosen to raise the temperature of the PEEK particles higher than 380 °C but lower than 530 °C.

Interestingly, the stable sintering region approach seems to outline that a HT-LS material such as thermally conditioned PEEK 450PF might offer a wider operating window in terms of laser exposure parameters than a well-established previously optimised LS material such as PA 12.

6.2.2 Energy melt ratio

The Energy Melt Ratio (EMR) is a numerical parameter introduced by Starr et al.[181] and later in-depth investigated by Vasquez et al. [104] when studying the relationship between manufacturing parameters and mechanical properties of laser sintered specimens of a discrete number of polymers. This parameter, described in

chapter 2.2.2.2, was used by Vasquez et al. [104] to predict the laser exposure settings leading to material degradation on the basis of the powder material properties. In order to validate the results of this technique, the authors laser sintered specimens of a discrete number of polymers at different ED values and tested their mechanical performance. The EMR value at which the drop of the mechanical property under test occurred was compared to the predicted EMR value responsible for degradation.

6.2.2.1 Activation energy

The evaluation of EMR_D was carried out for the measurement of the activation energy occurring in thermal degradation. The value of this parameter for the thermally conditioned PEEK 450PF material has been calculated using the Kissinger method on the results of several TGA experiments carried out at different heating rates (β) as described in chapter 3.1.10.

The results of the TGA experiments at different heating rates are shown in Figure 196, while the numerical values are listed in Table 29 along with the onset degradation temperatures at which 1% weight loss occurred.
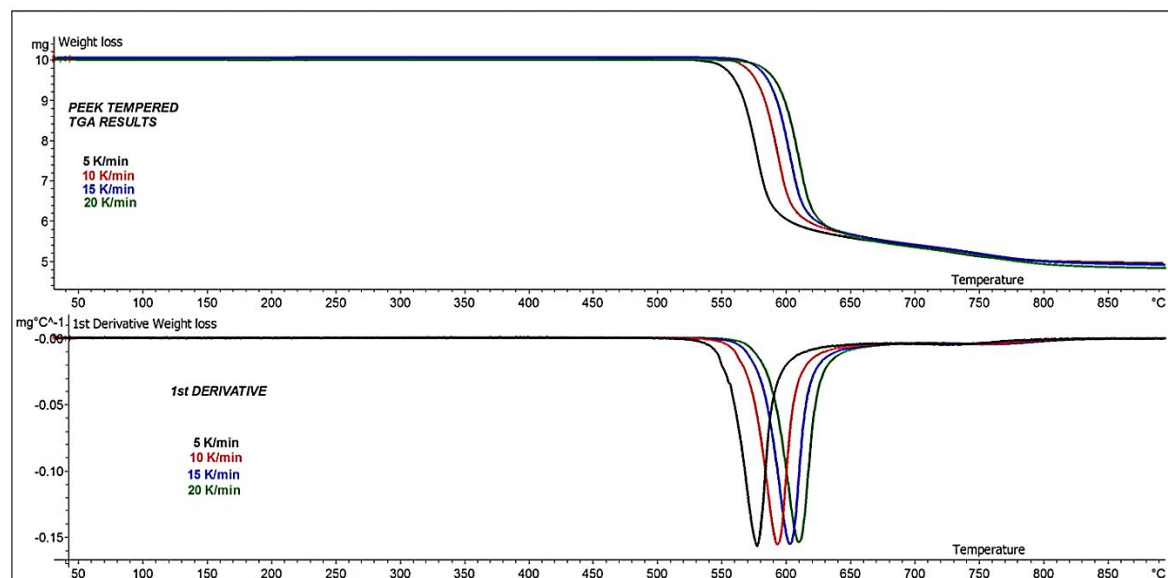
Figure 196. TGA data of thermally conditioned PEEK 450PF used for the evaluation of the activation energy

β (K/min)	T_{max} (K)	T_D (K)
5	850.06	817.53
10	865.89	833.12
15	875.76	841.89
20	882.8	848.82

Table 29. TGA data used for evaluation of the activation energy with the Kissinger method for the thermally conditioned PEEK 450PF material

Thermally conditioned PEEK 450PF showed a higher degradation limit when tested at higher heating rates. Similarly, the maximum temperature of the first derivative of the TGA results (T_{max}) increases with higher heating rates. The heating rate changes the time scale of the degradation process. The lower the heating rate, the longer the material samples is kept at a range of temperature that are critical for triggering degradation and the sooner it will then degrade. This behaviour is not surprising as it was also noticed in other polymeric specimens [197].

Figure 197 represents the Kissinger plot for PEEK 450PF grade obtained as described in chapter 3.1.12.1.
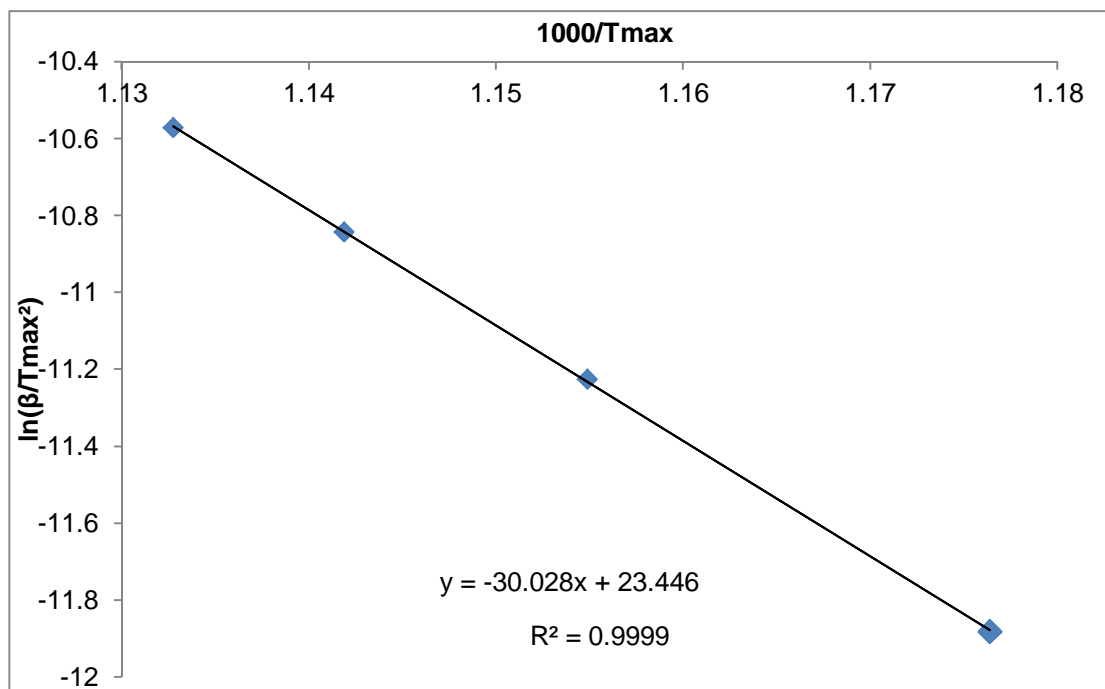
Figure 197. Kissinger plot for PEEK 450PF thermally conditioned

As described in chapter 3.1.12.1, the activation energy of thermally conditioned PEEK 450PF has been evaluated by multiplying the coefficient of the straight line fit found in the Kissinger plot by the gas constant. The value is reported in Table 30.

Material	E_A (kJ/mol)
Thermally conditioned PEEK 450PF	249.7

Table 30. Activation energy for the thermally conditioned PEEK 450PF

This value has then been used in the calculation of the EMR_D value.

6.2.2.2 Bulk density and packing fraction

The values obtained for the bulk density (Q) and packing fraction (Φ) of thermally conditioned PEEK 450PF measured as described in chapter 3.1.11 are listed in Table 31.

Material	$Q\left(\frac{g}{cm^3}\right)$	Φ
PEEK 450PF thermally conditioned	0.385	0.29

Table 31. Powder material density and packing fraction of thermally conditioned PEEK 450PF

6.2.2.3 EMR value leading to thermal degradation

The evaluation of the EMR value leading to thermal degradation (EMR_D) and the corresponding laser power (P_D) have been carried out as described in chapter 3.1.12.1. The values utilised for the degradation limit are shown in Table 32.

Parameter	Value
c_p	$2200 \, kJ \cdot kg^{-1} \cdot °C^{-1}$ [180]
T_D	559.97 ℃
T_m	339 ℃
E_A	$249.7 \, kJ \cdot mol^{-1}$
M_w	$115000 \, g \cdot mol^{-1}$ [4]
Q	0.383 [148]
SC	1
SS	0.2 mm [118]
v	$2550 \, mm \cdot s^{-1}$ [118]
z	0.12 mm

Table 32. Material and HT-LS processing parameters utilised for the evaluation of the EMR value leading to degradation for the thermally conditioned PEEK 450PF powder

The values of the EMR_D and the corresponding laser power (P_D) that should cause degradation of thermally conditioned PEEK 450PF are reported in Table 33.

Material	EMR_D	P_D (W)
Thermally conditioned PEEK 450PF	22.7	11.4

Table 33. EMR value and laser power that lead to thermal degradation during laser exposure strategy in the HT-LS process

The value EMR_D of thermally conditioned PEEK 450PF has been found to equal 22.7 with the corresponding laser power degradation approximately 11 W.

6.2.2.4 EMR analysis for thermally conditioned PEEK 450PF

The EMR values due to the varied processing settings - build 1 to build 6 of chapter 5.5.2 - have been calculated as described in chapter 3.1.12.

The values used for the evaluation of the EMR corresponding to different processing parameters and the tensile strength values of the corresponding HT laser sintered PEEK 450PF (both sets found in chapter 5) samples are reported in Table 34.

Parameter	Value
c_p	$2200\ kJ \cdot kg^{-1} \cdot {}^{\circ}C^{-1}$ [180]
T_B	$332\ {}^{\circ}C$
T_m	$339\ {}^{\circ}C$
h_f	$58.6\ J \cdot g^{-1}$
Q	$0.383\ g \cdot cm^{-3}$
Φ	0.29
SC	1
SS	0.2 mm [118]
v	$2550\ mm \cdot s^{-1}$[118]
z	0.12 mm
P_1	7.5 W
P_2	9.0 W
P_3	12.0 W
P_4	13.5 W
P_5	15.0 W
P_6	16.5 W

Table 34. Values used for EMR related to varied manufacturing parameters

A plot of the tensile strength of thermally conditioned PEEK 450PF HT-LS specimens against the EMR values is shown in Figure 198.
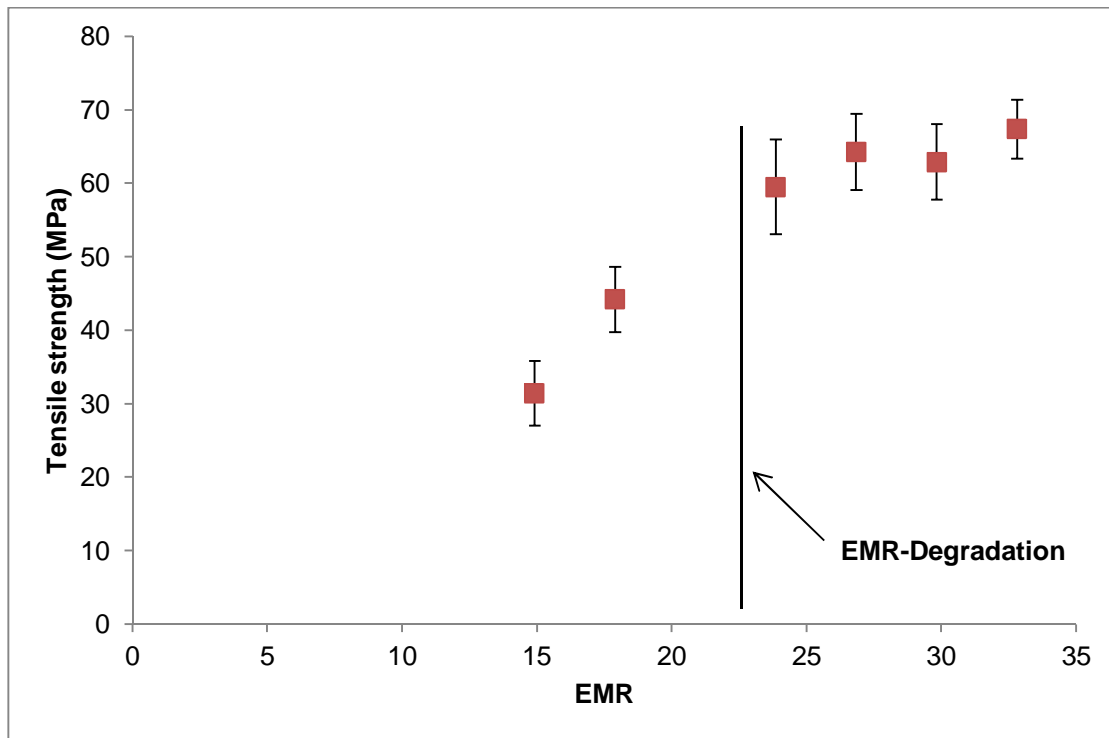
Figure 198. Tensile strength versus EMR for HT-LS specimens of thermally conditioned PEEK 450PF. The EMR value leading to degradation of thermally conditioned PEEK 450PF has been found to equal 22.7 with the corresponding laser power degradation approximately 11 W.

Figure 198 shows that increasing values of the EMR parameter are associated with higher values of tensile strength of the HT laser sintered PEEK components, until the tensile strength values stabilise.

Clearly, the results obtained with the EMR analysis on PEEK (Figure 198) are slightly different from the trend found by Vasquez et al. [104] of the mechanical performance the PA 12 laser sintered components (Figure 8). PA 12 structures showed increasing values of tensile strength ("peak stress" in the graph) with increasing values of EMR up to peak when they start to drop, indicating the occurrence of material degradation. The EMR_D factor was found to be a relatively good prediction of the occurrence of the drop of the mechanical properties of the PA 12 laser sintered components and therefore of the degradation during laser exposure on the basis of the powder material properties

It is important to outline that the EMR analysis has been applied to thermally conditioned PEEK 450PF only, because virgin PEEK 450PF specimens have not been HT laser sintered and tested in terms of tensile strength. The poor spreading performance exhibited by the unconditioned PEEK 450 PF polymer in the EOSINT P 800 shown in chapter 4.7 fully hindered further HT-LS processing such as the manufacture of tensile test samples.

The EMR values of thermally conditioned PEEK 450PF (Figure 198) are much higher than the results found for PA 12 (Figure 8) by Vasquez et al. [104]. This EMR value difference could suggest a poor absorption of the laser energy or could be due to the intrinsic properties of the PEEK material which exhibit higher onset degradation temperature, lower specific heat capacity, lower enthalpy of melt and packing fraction than the PA 12 powder.

To further check upon the robustness of the EMR analysis, a hypothetical EMR value equal to one has been selected. The laser power corresponding to EMR equal to 1 should be 0.5 W. The optimisation results in chapter 5.5.1 have shown that when a sample is manufactured with a laser power of 0.85 W (sample A), the specimen is so fragile that it breaks during removal from the powder cake.

The value EMR_D of thermally conditioned PEEK 450PF has been found to equal 22.7 with corresponding P_D of approximately 11 W. This result was surprising because it implies that the PEEK material should exhibit signs of thermal degradation for processing parameters of build 3 (chapter 5.5.2) that led to fairly low mechanical properties. In other words, PEEK 450PF starts to degrade during the HT-LS process before achieving the maximum mechanical performance.

In order to understand better the EMR_D value and its real effect on HT laser sintered structures, a standard TGA scan (chapter 3.1.10 and 3.2.9) has been performed on: virgin PEEK 450PF powder, thermally conditioned PEEK 450PF powder and a laser sintered sample fabricated according to settings of build 3. This test was carried out on both virgin and thermally conditioned PEEK 450PF powders in order to identify the effect of each single thermal event to which the PEEK 450PF powder was subjected, i.e. thermally conditioning and HT-LS processing. The TGA results of all the samples are shown in Figure 199.
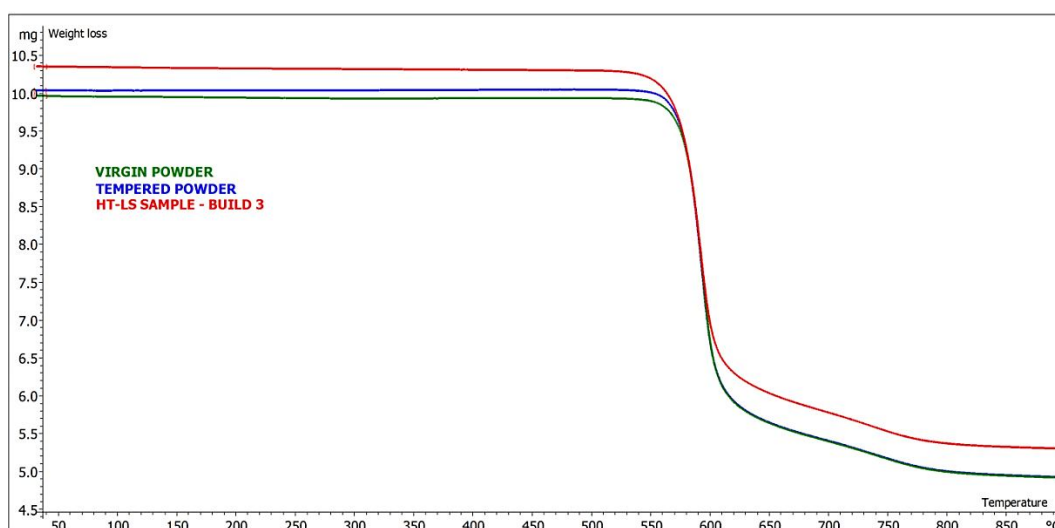
Figure 199. TGA curves of PEEK 450PF virgin and thermally conditioned powder and HT laser sintered specimen manufactured according to build 3

The 1% weight loss degradation has been measured for all the samples, virgin and thermally conditioned powders and laser sintered specimen are listed in Table 35.

Material	T_D (℃)
HT-LS sample – Build 3	545.78
Virgin PEEK 450PF	559.32
Thermally conditioned PEEK 450PF	561.16

Table 35. Degradation temperature causing 1% weight loss evaluated with TGA analysis performed on virgin and thermally conditioned PEEK 450PF powder and on a HT laser sintered sample manufactured with build 3 processing parameters

The 1% weight loss degradation occurred at 559 ˚C for virgin PEEK 450PF powder and at approximately 560 ˚C for the thermally conditioned powder, indicating that no signs of thermal degradation occurred during the thermal conditioning of the powder.

The HT laser sintered specimen instead showed the 1% weight loss degradation at 546 ˚C, nearly 15 ˚C lower than the powder samples. This result indicates that HT-LS process significantly affects the thermal history of the PEEK material leading to

294

earlier degradation than in the powdered samples. It therefore appears that the EMR_D shown in Figure 198 provides a good prediction of the beginning of thermal degradation phenomena in HT-LS, which occur before the material reaches the highest tensile strength performance available through this manufacturing technique.

However, it must be outlined that the 1% degradation limit could be a too strict threshold required on HT laser sintered components and, as shown in Figure 198, too little to cause a significant impact on the mechanical performance. At present a tolerance degradation value acceptable in HT-LS components has not yet been established and therefore it is not clear what degradation level can be allowed in HT-LS applications. The 1% weight loss degradation could in reality be unrequired for the success of a given HT laser sintered PEEK component.

6.3 Conclusions

The general approach in the LS community for testing new polymeric powder candidates is based on performing a series of trial-and-error builds. This strategy is effective at times but very often time-consuming and expensive. A more systematic and less wasteful method would help and speed up the processability investigation of new materials by also providing new insights into the LS phenomenon. In this context, a few studies aware of these issues have developed techniques such as the stable sintering region and the EMR analysis, coupled with the Kissinger method, in order to predict processing parameters and part performance based on the powder material properties.

This chapter applied the stable sintering region and the EMR analyses to PEEK 450PF. The stable sintering region technique showed a wide range of temperature (250 °C) that the PEEK material can undergo during the laser exposure of a HT-LS building process without signs of degradation. The EMR value based on 1% weight loss seems not to accurately fit the results of tensile strength test. Possibly, the 1% weight loss threshold is not significant enough for range of polymers such as HT polymers and PEEK especially, to affect the mechanical performance of the HT laser sintered samples. Clearly, the EMR parameter represents a good starting point for the prediction of optimal parameters, especially those related to the laser exposure

strategy. Yet, a correction of the weight loss limit could lead to better predictions of the optimal HT-LS processing conditions.

Lastly, a new very basic technique for the prediction of the part bed processing temperature within the EOSINT P 800 system is suggested and deemed to be consistent with the limited number of experimental data available.

7 Medical case studies

PEEK is an engineering thermoplastic polymer with high mechanical, thermal and chemical performance which makes it ideal in applications within the automotive and aerospace areas. If produced and processed in clean room conditions (Class 10,000 [4]), PEEK is also a well-established biocompatible material largely used in a broad range of medical applications.

The optimisation of the processing parameters for thermally conditioned PEEK 450PF within the HT-LS system EOSINT P 800 and the characterisation of the physical and mechanical properties of HT laser sintered components have led to the production of two long term medical implants. These implants have been manufactured using the equivalent medical grade of PEEK 450PF, "PEEK OPTIMA® LT1" (chapter 3.1.2.3) and are examined in this chapter.

Cranial implants and several types of spinal inter-body fusion cages were fabricated as described in chapter 3.3.

Only one example of spinal inter-body fusion cages is reported here, while the others are undergoing testing at Invibio biomaterial solutions [3] and protected by intellectual property.

The purpose of this chapter is therefore to provide two case studies of potential HT-LS PEEK medical application on the basis of the previous research work carried out in this project.

7.1 Cranial implants

Cranial implants are medical devices that aim to replace damaged and missing bone of the human skull. Generally custom made, these implants are required to exhibit long term stability, good osseointegration and high geometrical accuracy.

Cranial implants have been manufactured in different building orientations within the HT-LS system and tested in terms of dimensional accuracy. This parameter is the most rigorous requirement on materials and manufacturing processes for cranial implant applications.

No geometrical tolerances of laser sintered cranial implants are available in the literature. However, a company specialised in advanced metal processing technology (Tecomet, USA [198]) for biomedical implants, proposes a tolerance guideline. According to Tecomet, if one considers as a reference a cube with nominal dimensions bigger than 25 mm along each axis (bigger than 25 mm x 25 mm x 25 mm), a good set of nominal tolerances transferable to cranial implant devices [198] is constituted of the following:

- ± 0.125 mm for the first 25 mm and ± 0.08 mm for each additional 25 mm in X (width) and Y (length) axes;
- ± 0.25 mm for the first 25 mm, ± 0.08 mm on every 25 mm thereafter along the Z direction (thickness).

In the LS area, when a component is fabricated for prototyping purposes it is common practice to achieve a 5% resolution on the final parts. However, when LS is used for proper manufacturing higher resolutions are required and a nominal tolerance of ± 100 µm is provided. This resolution can be achieved with: specific laser exposure profiles, enhancing for example sharp edges or skin effects [118, 137]; shrinkage factors, optimised for a given material within a given LS system; lastly, optimal orientation and building position within the building chamber.

In this context, thirteen (13) HT laser sintered cranial implants were manufactured at different orientations with the respect of the building direction (Z axis) within the P 800 system, according to the build 5 processing parameters and in reduced chamber mode. The build assembly of the 13 cranial implants is shown in Figure 200.
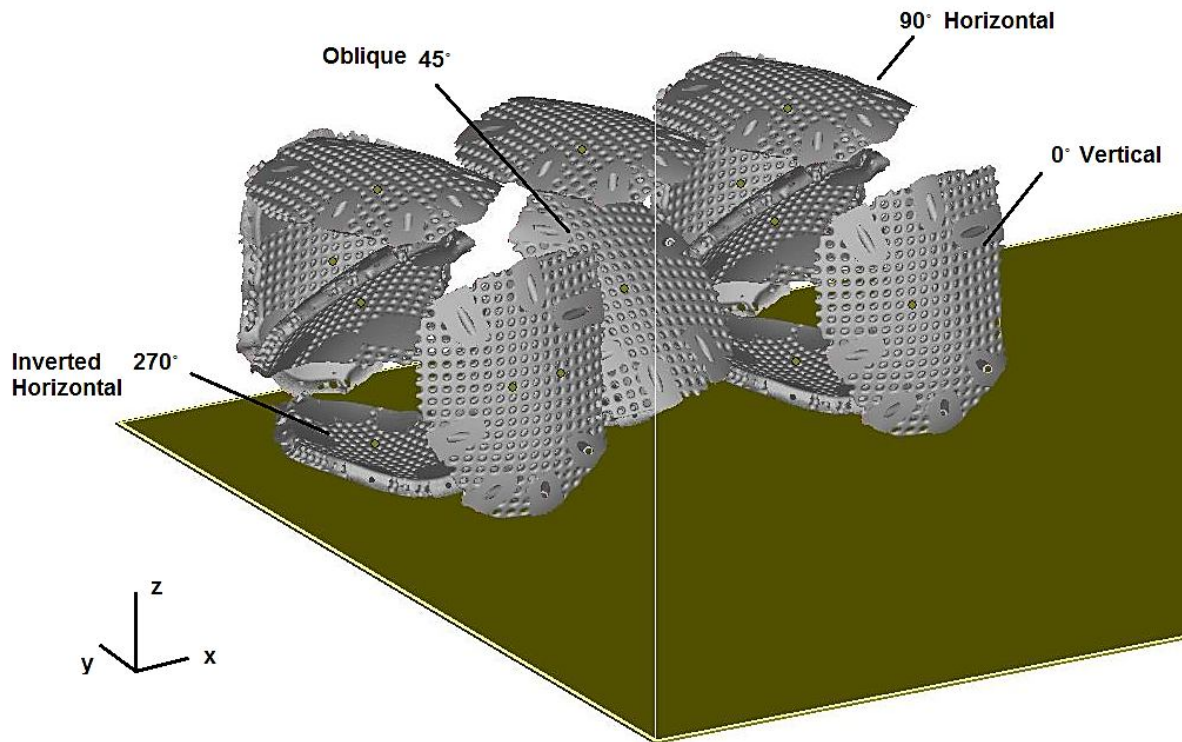
Figure 200. HT-LS build of cranial implants fabricated at several orientations in respect with the building direction (Z axis)

Figure 200 shows the position, orientation and grouping of the parts during the HT-LS process. The legend applied to the implants according to their building orientation in respect with the Z axis is also indicated.

Images of the cranial implant at 0˚ orientation (vertical) in respect with the building direction (Z axis) are reported in Figure 201 and Figure 202.
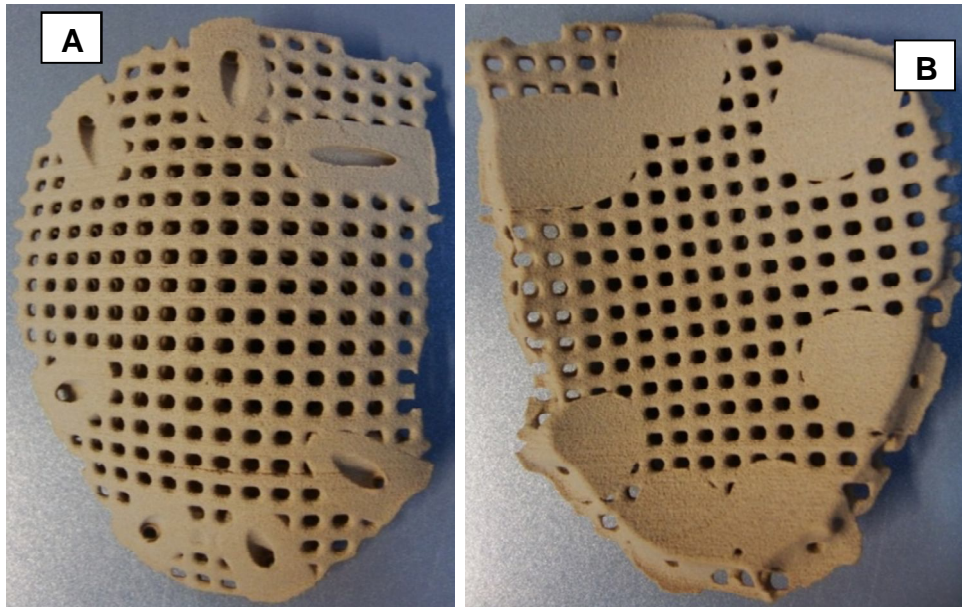
Figure 201. Cranial implant built at 0˚ orientation (vertical) in respect with the building direction (Z axis): (A) exterior and (B) interior surfaces
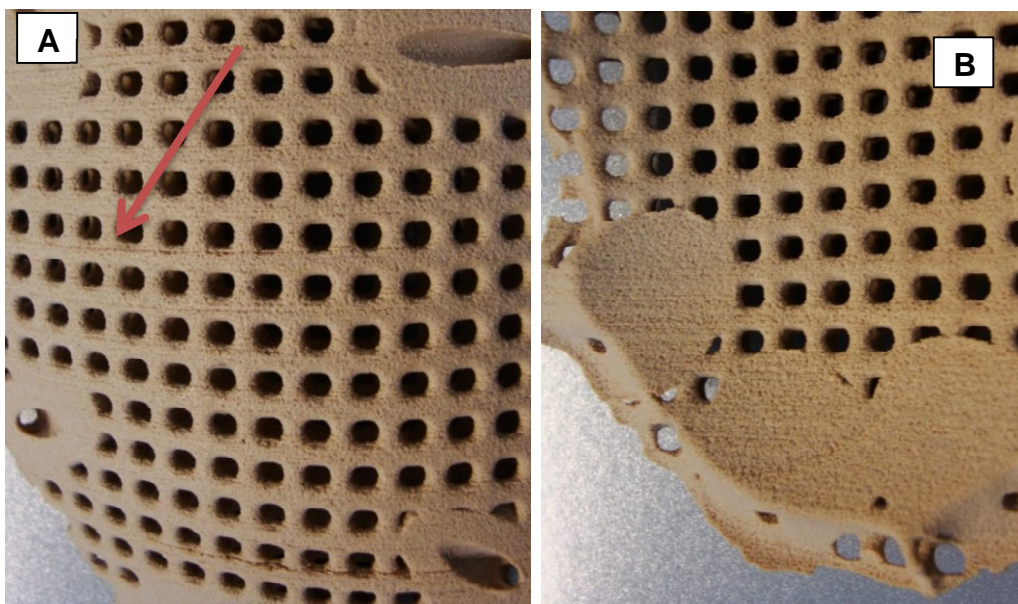
Figure 202. Cranial implant at 0˚ orientation (vertical) in respect with the building direction (Z axis): details of the exterior (A) and interior (B) surfaces

It is possible to notice, especially in Figure 202, horizontal lines all over the surface of the implant. These lines correspond to the powder layers during the HT-LS manufacturing. This characteristic can be called "Layer effect". Figure 203 and Figure 204 show the cranial implant manufactured with a building orientation of 45 ˚ (oblique).
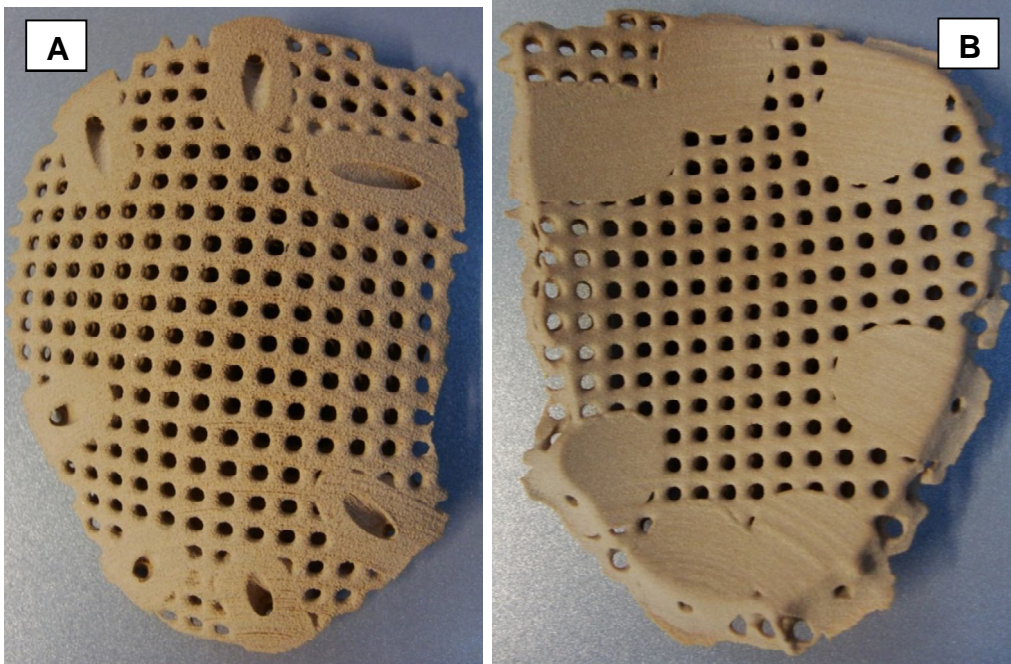
Figure 203. Cranial implant at 45˚ orientation (oblique) in respect with the building direction (Z axis): (A) exterior and (B) interior surfaces
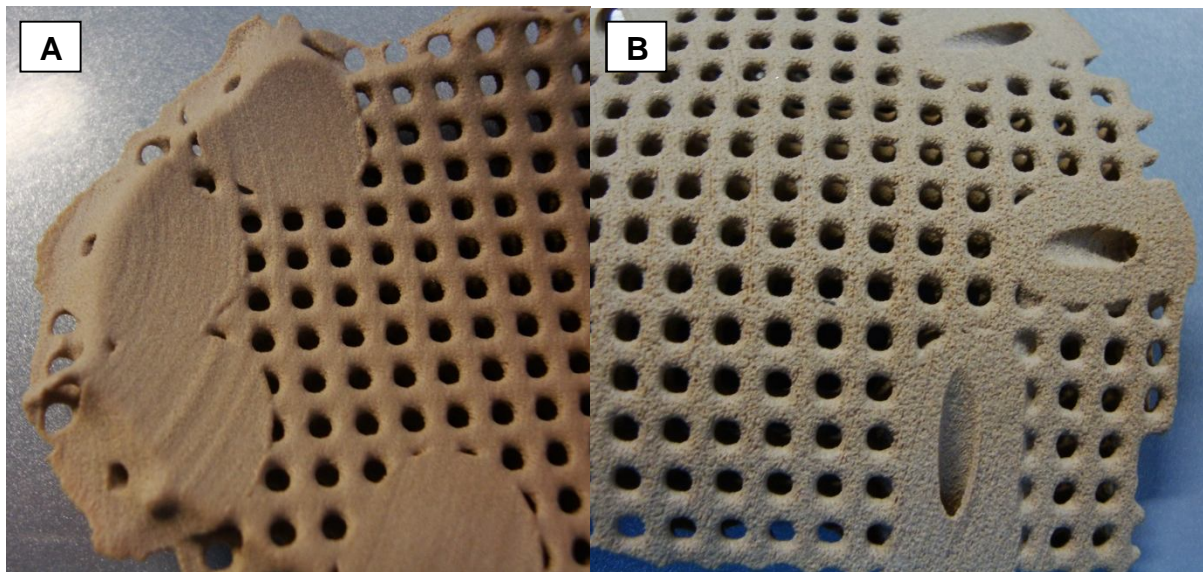
Figure 204. Cranial implant at 45˚ orientation (oblique) in respect with the building direction (Z axis): details of the exterior (A) and interior (B) surfaces

As seen for the vertical implant (Figure 201 and Figure 202) the layer effect is visible also on this implant (Figure 204). Figure 205 and Figure 206 show the cranial implant manufactured with 90˚ building orientation (horizontal). As expected, the layer effect is no longer visible in this part because of the building orientation.
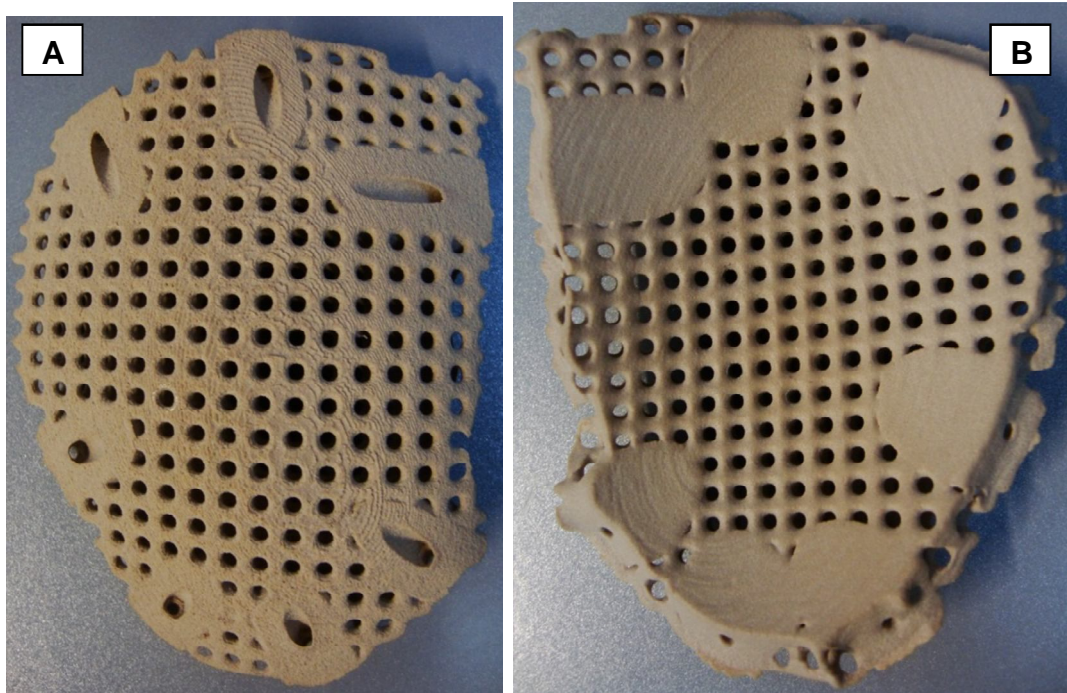
Figure 205. Cranial implant built at 90˚ orientation (horizontal) in respect with the building direction (Z axis): (A) exterior and (B) interior surfaces
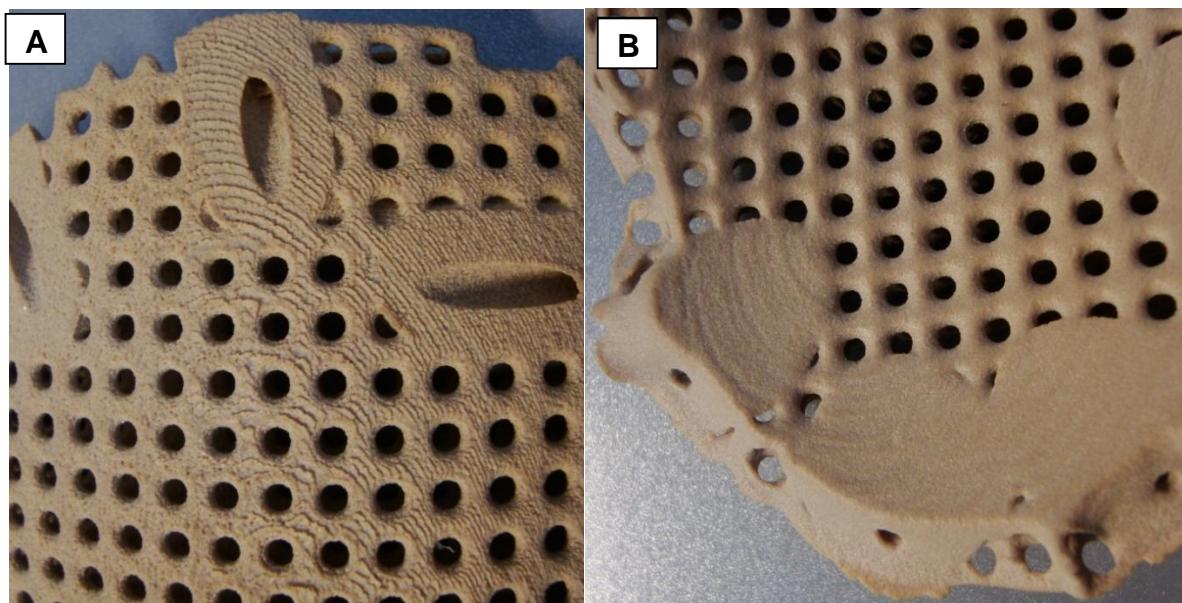
Figure 206. Cranial implant at 90˚ orientation (horizontal) in respect with the building direction (Z axis): details of the exterior (A) and interior (B) surfaces

Lastly, Figure 207 and Figure 208 show the cranial implants manufactured with a building orientation of 270˚ (inverted horizontal). Again, the layer effect is no longer visible because of the building orientation.
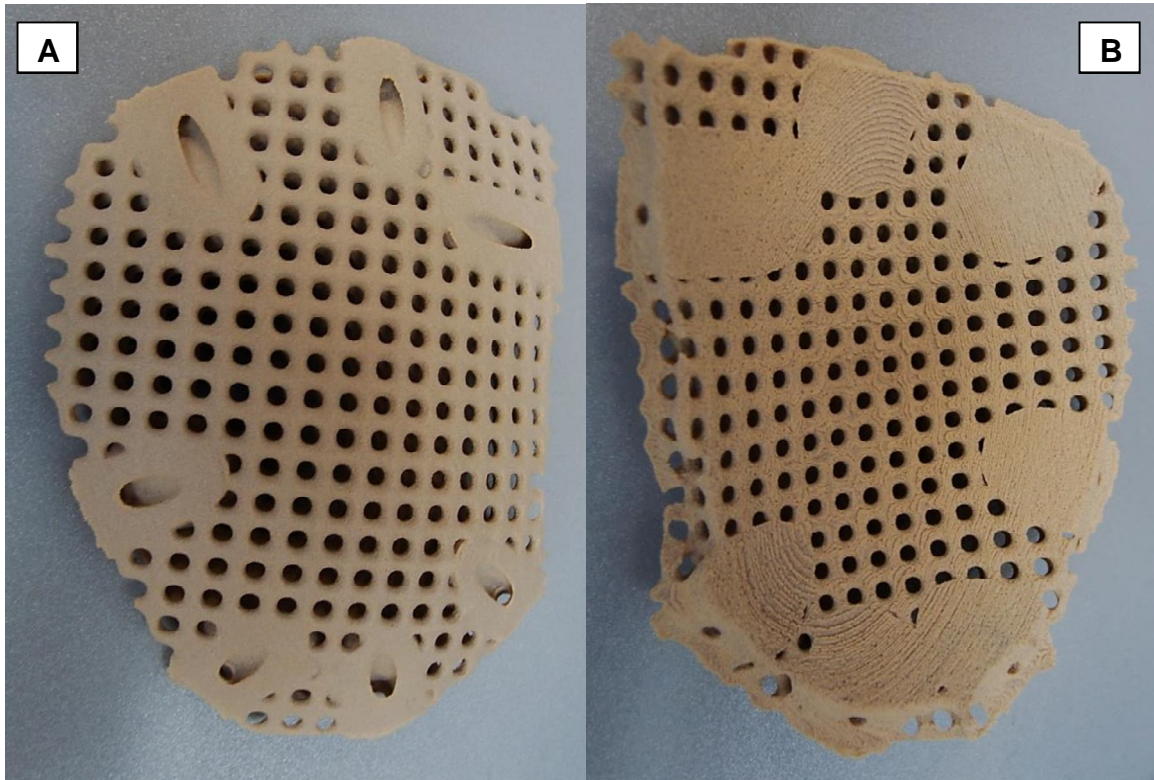
Figure 207. Cranial implant at 270˚ orientation (inverted horizontal) in respect with the building direction (Z axis): (A) exterior and (B) interior surfaces
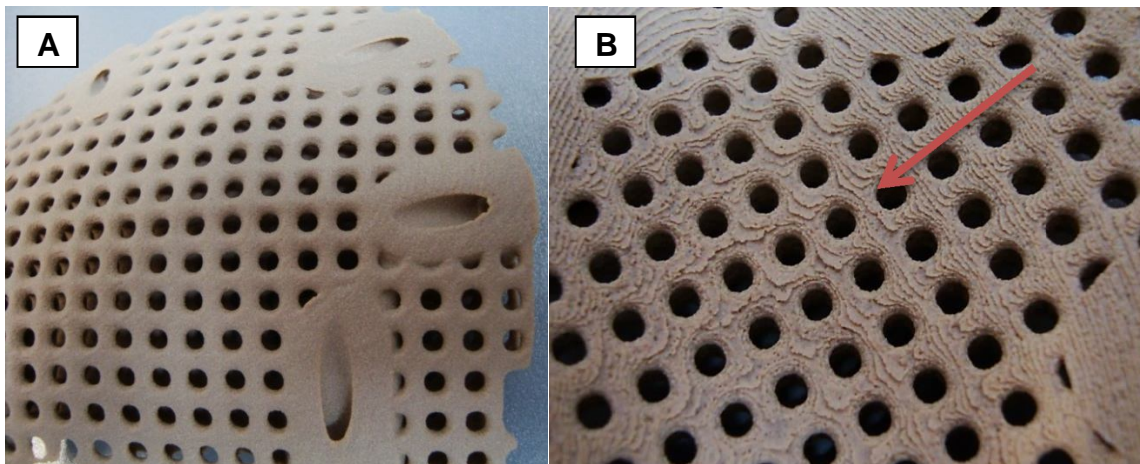
Figure 208. Cranial implant at 270˚ orientation (inverted horizontal) in respect with the building direction (Z axis): details of the exterior (A) and interior (B) surfaces

All implants show closed loop lines similar to flow lines on one surface of the implants. An example is indicated in Figure 208 B. These lines are due to the

combination of the building orientation and complex geometry of the cranial implant components.

7.1.1 Dimensional accuracy measurements

The results of the dimensional accuracy measured as described in chapter 3.3.1.1 are shown from Figure 209 to Figure 212. Figure 209 and Figure 210 are the interior and exterior surface of the implant manufactured with horizontal and vertical orientation, while Figure 211 and Figure 212 represent the interior and exterior surfaces of the implant produced with oblique and inverted horizontal orientation. For clarity, the implants under test are shown in a different colour from the others on the top of the interior surfaces results (Figure 209 and Figure 211).
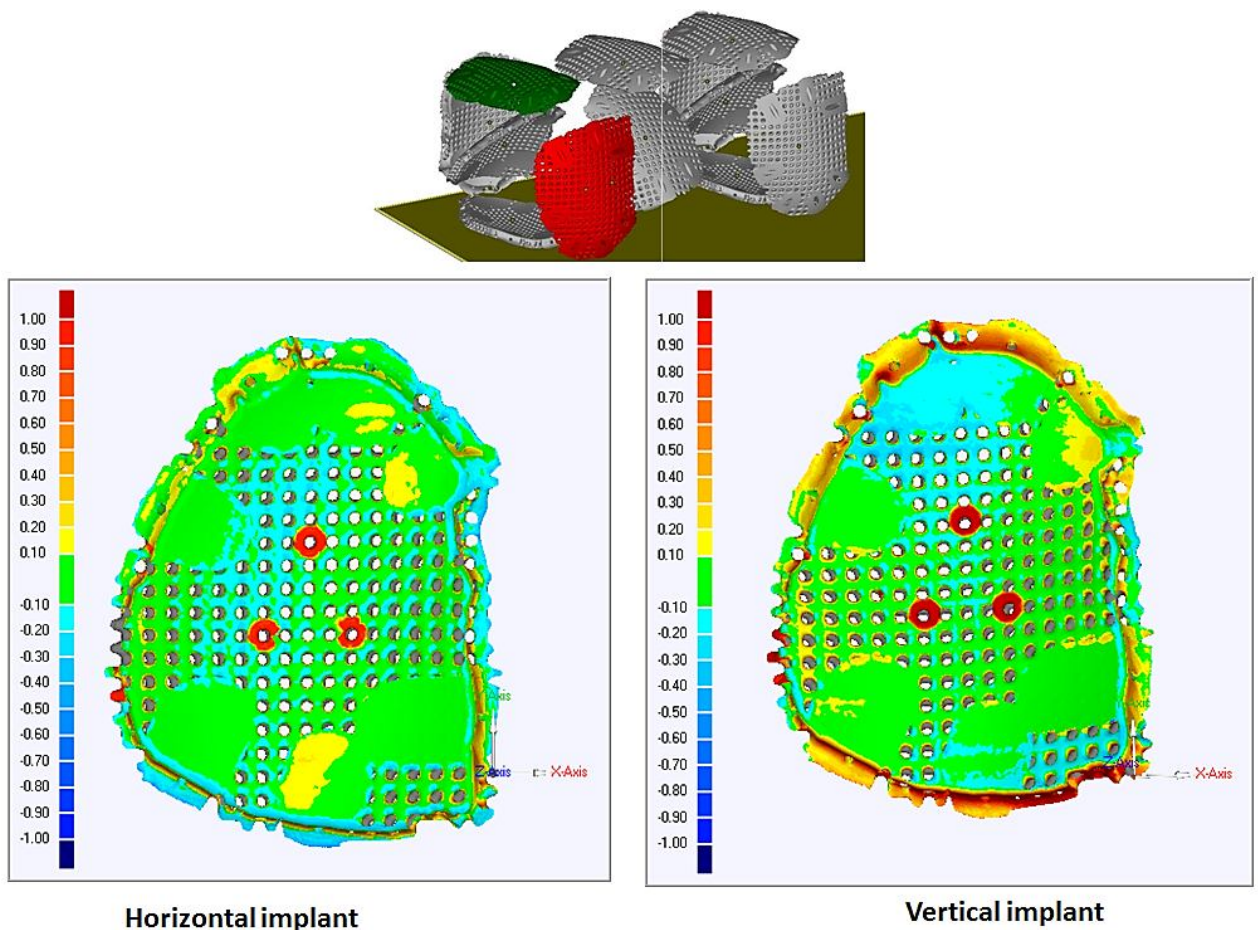
Figure 209. Interior surface of horizontal and vertical cranial implant. Scale bar in mm
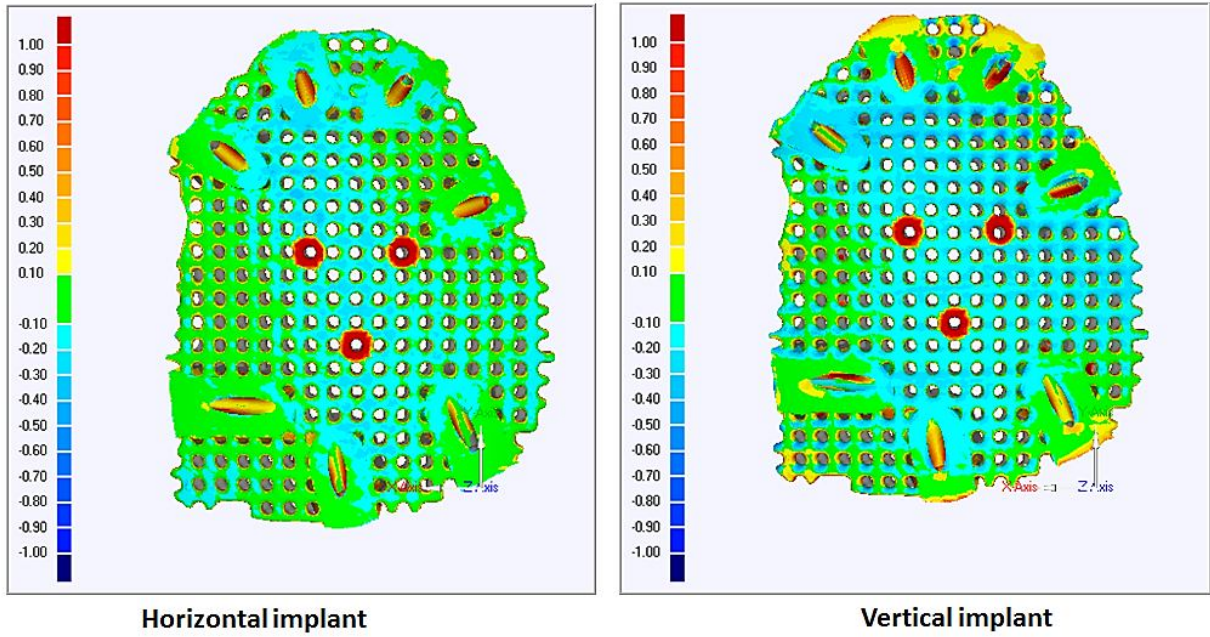
Figure 210. Exterior surface of horizontal and vertical cranial implant. Scale bar in mm
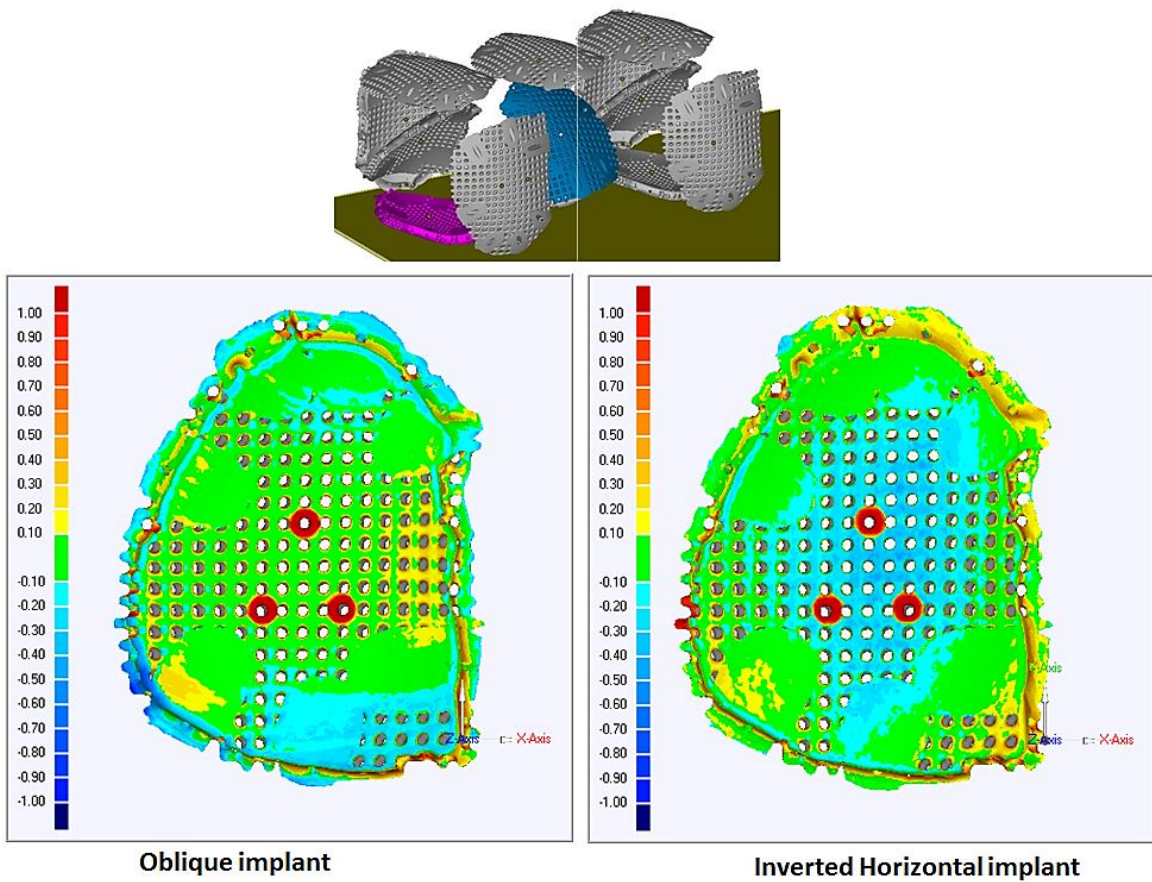
Figure 211. Interior surface of oblique and inverted horizontal cranial implant. Scale bar in mm

305
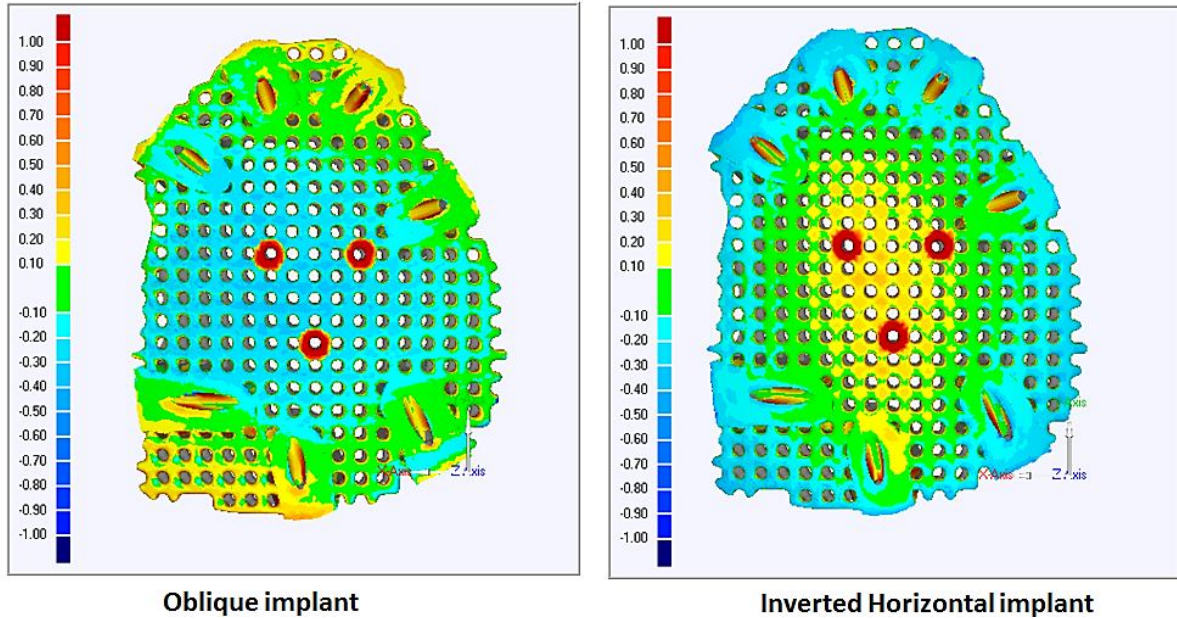
Figure 212. Exterior surface of horizontal and vertical cranial implant. Scale bar in mm

As explained in chapter 3.3.1.1 the nominal tolerances set in this analysis were chosen according to the industry established LS standard of ± 100 μm. The critical values, minimum and maximum, were set equal to ± 1 mm in order to equalise the HT-LS technology resolution limit of 0.5 mm by a factor 2. The implants show different colour maps that correspond to the deviation analysis. The area within the nominal tolerances (green area) is different for every surface of every implant. This expected fact confirms that part orientation affects the dimensional accuracy of a final component.

All the surfaces show a deviation from the original file within ± 0.40 mm at most. This result, although higher than the intended nominal tolerance, might be improved with part positioning and the optimisation of the shrinkage factors applied during HT-LS processing.

The red circular marks exhibited in every scan represent the screws utilised for secure fixation of the implant during the scanning stage.

It is possible to see, especially on the profile of the interior surfaces, that some regions are outside the critical values set in the analysis, i.e. outside the maximum and the minimum values set for the deviation analysis. These characteristics are not

necessarily indication of poor accuracy but they could be artefacts created as consequence of the alignment stage between the STL file generated by the scanning tests and the original CAD STL file.

The area within the nominal tolerances has been measured by using the software Image J as described in chapter 3.3.1.1 for all the implants and all the surfaces. The evaluation of the nominal tolerance ratio as defined in 3.3.1.1 is also provided. The results of the interior and exterior surfaces are listed in Table 36 and Table 37, respectively.

Interior surface Building orientation	Area within nominal tolerances	Overall area	Nominal tolerance ratio (%)
Vertical	46294	88904	52
Oblique	50187	95175	53
Horizontal	57055	97227	59
Inverted horizontal	43815	98470	44

Table 36. Cranial implants: evaluation of the area within the nominal tolerances for the interior surface

Exterior surface Building orientation	Area within nominal tolerances	Overall area	Nominal tolerance ratio (%)
Vertical	27701	89283	31
Oblique	30278	92699	33
Horizontal	43111	93986	46
Inverted horizontal	31044	95042	33

Table 37. Cranial implants: evaluation of the area within the nominal tolerances for the exterior surface

The results of the inner surface (Table 36) highlight the horizontal and the oblique building orientation as the most accurate. The results of the exterior surface (Table 37) show instead that the implants manufactured with horizontal and inverted horizontal building orientations have higher dimensional accuracy. Within the limits of this dimensional accuracy investigation, the horizontal building orientation provided the highest dimensional part accuracy in both surfaces and therefore overall.

When studying the shrinkage characteristics of HT laser sintered PEK structures in the EOSINT P 800 system, Ghita et al. [116] found that PEK HP3 components built along the vertical direction (Z axis) showed more shrinkage than the components built on X and Y axes, i.e. built horizontally. This could be the reason why the vertical and oblique building orientations gave lower accuracy results. The difference found between horizontal and inverted horizontal building orientations instead could be due to the specific geometry of the cranial implant. However, this hypothesis should be validated with further testing.

7.2   Spinal inter-body fusion cages

Spinal inter-body fusion cages are long term implants inserted in the disc space between two vertebral bodies. These implants usually exhibit a high degree of porosity and a hollow structure in order to allow bone graft formation from one vertebral body, through the cage and into the next. The implants were manufactured within the system P 800 at the University of Exeter according the processing parameters defined in profile build 5 (chapter 5.5.2), in reduce chamber building configuration. The design file was released by Invibio biomaterial solutions [3]. The specimens were tested in terms of static uniaxial compression performance and compared with the same components manufactured by traditional machining by Invibio biomaterial solutions.

7.2.1   Static axial compression test

The two types of spinal lumbar cages tested and compared in term of performance are shown in Figure 213. Figure 213 A shows the cages manufactured with traditional from PEEK OPTIMA® Natural stock [3], while the samples manufactured with thermally conditioned PEEK OPTIMA® LT1 by HT-LS are reported in Figure 213-B.
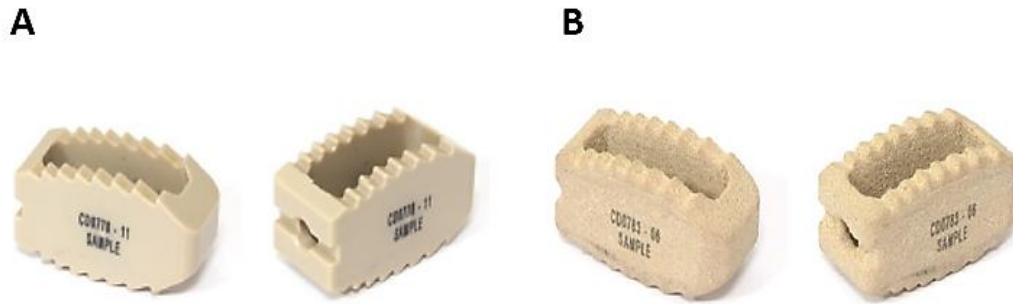
Figure 213. Tested lumbar fusion cages: machined using PEEK OPTIMA® Natural stock (A), HT laser sintered using PEEK OPTIMA® LT1 (B)

The results of machined and HT laser sintered specimens are reported in Figure 214 and Figure 215, respectively.

Figure 214. Results of the machines spinal lumbar cages. (A) Numerical results. (B) Load-Displacement profiles (C) Tested specimens

Specimen	Yield Load	Displacement at Yield Load	Ultimate Load	Displacement at Ultimate Load	Stiffness
	kN	mm	kN	mm	kN/mm
6.1	7.666	1.3	8.294	1.3	8.204
6.2	12.063	1.8	12.324	2.0	8.286
Mean	9.865	1.5	10.309	1.6	8.245
StdDev.	3.109	0.4	2.849	0.5	0.057
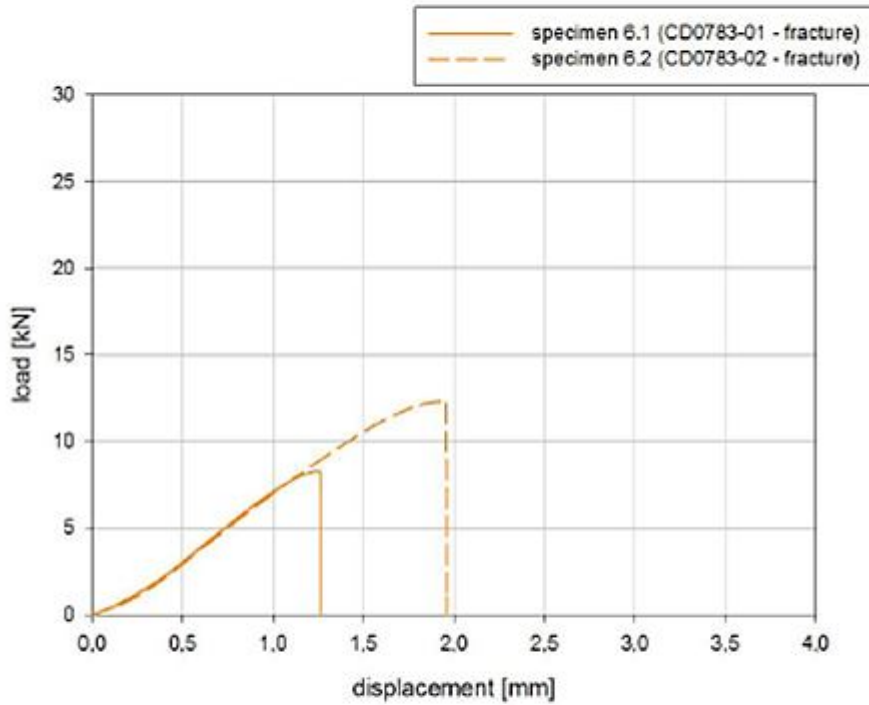
Figure 215. Results of the LS lumbar spinal cages. (A) Numerical results. (B) Load-Displacement profiles. (C) Tested specimens

The machined implants exhibited a mean yield load of 11 kN with a displacement of 1.8 mm. The mean ultimate load was above 11 kN with mean ultimate displacement of approximately 2.2 mm. The stiffness was found to be equal to 8.6 kN/mm and the

samples exhibited clear signs of plastic deformation at the end of the test. The HT laser sintered specimens showed mean yield of 9.8 kN with mean displacement of 1.5 mm and ultimate mean load of 10 kN with ultimate mean displacement of 1.6 mm. Although the stiffness was found fairly similar to value of the machined cages (8.2 kN/mm for the HT laser sintered samples), the HT laser sintered implants fractured when reached the ultimate load.

7.3　Conclusions

Two medical implants, cranial implant and interfusion spinal cages, were HT laser using the medical equivalent grade of PEEK 450PF, namely PEEK OPTIMA® LT1, based on the investigations carried out in the previous stages of this research project. PEEK OPTIMA® LT1 was thermally conditioned before use in the HT-LS technology according to the findings found in the powder characterisation analysis (chapter 4). The HT-LS manufacture was carried out according the set of optimal processing parameters found in the HT-LS manufacturing optimisation stage of this work (chapter 5).

Cranial implants manufactured at different building orientations were analysed in terms of dimensional accuracy. Based on a proposed 100 µm nominal tolerance the horizontal building orientation provided the highest part accuracy.

Inter-body fusion cages for spinal applications were also HT laser sintered using thermally conditioned PEEK OPTIMA® LT1 within the EOSINT P 800. Although several spinal cages with different designs were fabricated at the University of Exeter, the test results of only one design could be reported here, while the remaining are under the intellectual property protection of Invibio biomaterial solutions [3]. The analysis of the static uniaxial compressive behaviour of the HT laser sintered spinal cages was compared against the same design manufactured with traditional machining and equivalent PEEK material. Although the results of the HT laser sintered cages are similar to the benchmark specimens (1 kN difference in ultimate mean load), the HT laser sintered cages show significant lower displacement. This is not a surprising finding as it is well known in the additive

manufacturing community that laser sintered component are generally more brittle than the same models manufactured with traditional manufacturing processes.

Clearly, LS and HT-LS do not aim to fabricate components that are necessarily more performing in terms of mechanical properties than those fabricated with traditional manufacturing methods. However, when the mechanical requirement driven by a specific application are also met by laser sintered parts, then LS and HT-LS offer more design and fabrication freedom than traditional manufacturing techniques and therefore represent a valuable alternative to produce consumer goods and high end value components.

8 Conclusions and future development

8.1 General conclusions

The scope of this thesis, entitled "Poly Ether Ether Ketone (PEEK) polymers for High Temperature Laser Sintering (HT-LS)", has been to assess a new material option in the HT-LS technology where only one polymeric grade, PEK HP3, is commercially available.

A new PEEK polymer has been studied and successfully optimised in the commercial HT-LS system EOSINT P 800 opening the way for HT-LS of PEEK for high demand application areas such as aerospace, medical and automotive fields and new insights into the understanding of the HT-LS process have also been provided.

The first part of this work has focused on the accurate investigation of the physical parameters required on powder materials for their successful use in the LS process.

The second part has involved: the investigation of the mechanical performance of HT laser sintered structures using the optimal of the two PEEK grades analysed, PEEK 450PF; the optimisation of the processing parameters, and the examination of unique characteristics of the HT-LS EOSINT P 800 system such as variable size building chamber and the PS time.

The third part has aimed to explore and understand the relationship between powder properties, material properties and processing parameters within a LS building process. The most recent LS predicting techniques and parameters such as stable sintering region and EMR, have been applied and discussed for the PEEK material and its relative HT laser sintered components. Also a new method for the prediction of the part bed temperatures of those polymers such as HT polymers that lack a temperature gap between melting and crystallisation (super-cooling window) has been suggested.

Lastly, the final part of this project has consisted of providing two case studies of medical applications. Cranial implants and spinal cages were HT laser sintered in the EOSINT P 800 system by using the biocompatible grade PEEK OPTIMA® LT1 and tested in terms of dimensional accuracy and mechanical performance, respectively.

314

This study presents significant innovation aspects and highlights certain areas of polymeric LS that should be further investigated. This is the only work providing a quantitative examination of flow properties of polymeric powders for LS in terms of AOR, attractive forces assessment (Hamaker constant) and particle morphology description (circularity, roundness, solidity and AR). Two effective options for the improvement of powder flow performance have been thoroughly investigated and reported. Prior to this work only general suggestions such as "good flow" and "regular particles" were the main requirements for new potential LS grades.

This research work also offers the first optimisation analysis of PEEK in the commercial HT-LS system. Previous attempts to laser sinter PEEK had been carried out in lab-modified LS systems whose thermal stabilities are questionable and the laser sintered structures were not thoroughly investigated mechanically for high demanding applications, but only developed for tissue engineering applications. Also the novel characteristics of variable size build chamber and PS time are explained and experimentally examined.

The concept of a stable sintering region recently developed in the additive manufacturing community for low temperature polymers, such as elastomers and PA based materials, has been applied for the first time to a HT polymer, such as PEEK. A method for predicting the part bed processing temperature of those polymers such as PAEKs that do not exhibit a temperature gap between melting and crystallisation regions (super-cooling window) is provided. Lastly, the analysis of the EMR parameter for predicting thermal degradation during LS processing on the basis of the material properties was applied and discussed for HT-LS PEEK powder and components.

The methods and the results of this research project have increased the state of the body of knowledge on materials, part performance and efficiency of LS manufacturing at academic level, while the characterisation and optimisation of the HT laser sintered structures are and will be beneficial for users and design product engineers in the industrial sector. The methodologies developed here can be used for a wide range of materials, including not only polymeric grades, hence stimulating and influencing further development and innovation in the additive manufacturing community.

8.2 Specific conclusions

8.2.1 Powder size, morphology and flow performance

The trial and error approach has often been the only way for testing new material candidates in LS. The lack of a more accurate and scientific method has led to vague requirements demanded on powder materials such as "good flow" or "regular particles". This research work helped to outline more quantitative requirements for materials in LS.

1. The PSD results of established LS materials and PEEK grades presented higher volume frequency in the diameter range between 16 and 37.5 µm, while virgin PA 2200 exhibited higher content in the range 37.5 -63 µm. Although this test gives a first screening of the possibility to apply new powders in LS, it is not able to discriminate between good and poor flowing materials when their PSD profiles are very similar. Additionally, this test assumes that the particles under test are spherical, a condition that is not necessarily true for new potential LS materials.

2. The flow behaviour of LS established powders and potential LS candidates have been studied with a highly accessible laboratory test called Angle Of Repose (AOR). Optimised LS grades, i.e. Spheriglass, PA 2200 and PEK HP3 were found to have AOR values of approximately 24, 33-38 according to the blend mixture, and 42, respectively. The improvement of the flow properties of the PEEK powders has been carried out by adding a flow aid additive, which made the AOR drop by 10°, or by applying a thermal conditioning to the powders, which caused a drop of the AOR of 8°. The AOR value of 45° was found to be the upper limit for satisfactory flow conditions in HT-LS and could be considered a threshold value for the selection of new LS materials.

3. The particle shape analysis has provided a detailed and truthful representation of all the powdered material analysed here and has helped to explain the differences found with the AOR technique. When circularity and roundness values are simultaneously higher than 0.65, solidity is higher than 0.86 and AR is lower than 1.81, a given material will likely exhibit successful conditions for the powder spreading in respect of LS processing.

4. An evaluation of the attractive forces acting between particles of the same material and blends can be found with the evaluation of the Hamaker constant. The Hamaker constants calculated here were found to follow the hierarchy of the AOR results.

5. The spreading device available within a LS system affects the flow performance of a material. While a spreading tool applies a certain pressure and imposes compaction on the powder bed, irregularities due to the particle morphology of the material involved are drastically reduced if not fully removed. This is the case of a counter-rotating roller spreading device. However, when a double blade recoater is utilised, the device does not overcome well particle morphology irregularities and the spread layer is extremely rough at best. Materials with higher flowing properties are then required for successful spreading with this spreading device.

8.2.2 HT-LS PEEK processing and optimisation

Although a first selection of new LS material candidates can be carried out effectively by means of accurate powder characterisation methods, the investigation of the mechanical performance of HT laser sintered structures is a necessary requirement for the establishment of a new material. With this intent, several manufacturing conditions have been analysed.

1. The processing of PEEK material has been found possible, reliable and successful within the EOSINT P 800 system.

2. The EOSINT P 800 has been found consistent in terms of mechanical performance for components built using a third, half or full building chamber without significant changes in the tensile properties of the HT laser sintered structures.

3. The PS time which is an additional heating phase added to each sintered layer, does not influence the micro-structure or the mechanical performance of PEEK samples fabricated in the time range 6-15 s. Therefore a shorter PS time might be applied for reducing the whole manufacturing operation without detrimental effects on the performance of the built components.

4. Samples built at different energy densities have been found to be testable only above the ED value of 0.0059 J/mm². ED higher than 0.0327 J/mm² led to a significant amount of smoke during the HT-LS process and black speckles were noticed on the samples, thus indicating potential polymer degradation. The HT-LS manufacture of PEEK components with increasing energy densities led to increasing tensile strength values, until the tensile strength values stabilise.

5. The tensile strength of HT-LS PEEK 450PF components has been found equal to approximately 64 MPa, only 25% lower than PEK HP3. Storage modulus of HT laser sintered PEEK structures has been found to be 2500 MPa, the same value found for HT laser sintered PEK HP3 components.

8.2.3 Predicting processing parameters

Predicting the processing parameters of a LS building process without a series of trial and error builds is a good method that would help to reduce costs, promote the exploration of new material and increasing the understanding of the LS process.

1. The concept of stable sintering region recently introduced in the LS community has been found applicable to HT polymers such as PEEK. PEEK shows a stable sintering region of 250 °C compared to the 125 °C wide stable sintering region previously found by Vasquez et al. [104] for the LS optimised grade PA 12.

2. The EMR factor has been applied to PEEK HT-LS processing parameters and HT laser sintered components. The graph showing the tensile strength of HT laser sintered PEEK specimens plotted against the EMR values has shown how increasing EMR values were associated with increasing values of tensile strength until the tensile values stabilise. The EMR value of degradation was found to occur before the PEEK specimens reached the maximum tensile performance. Possibly, this EMR value is calculated with thermal degradation requirements that might be not significant enough to affect the mechanical performances of the PEEK HT laser sintered components.

3. A new basic technique for the estimate of the part bed temperature within the EOSINT P 800 for HT polymers and based on the thermal properties of the

powder materials under exam is proposed here. This method, based on the analysis of the first derivative of a DSC thermoscan, allowed predicting the part bed temperature used in the EOSINT P 800 for PEK HP3 and PEEK grades.

8.2.4 Case studies of medical applications

The previous investigation carried out on the PEEK powder material and on the HT-LS PEEK manufacturing settings and configurations opened the way to the manufacture of two medical implant components using the medical grade PEEK-OPTIMA® LT1.

1. PEEK-OPTIMA® LT1 HT laser sintered cranial implants have been successfully fabricated within the EOSINT P 800 system. Thirteen parts were produced at different building orientation and tested in terms of dimensional accuracy. The deviation analysis of the implants from the original CAD design highlighted the horizontal building orientation (in reference to the Z axis) as the manufacturing orientation leading to the most accurate implant in the tolerance range of ± 100 µm.

2. Several designs of inter body fusion spinal cages were also manufactured by HT-LS within the EOSINT P 800 system. While most designs are intellectual property of Invibio biomaterial solutions, the test results of one of the models was allowed to be reported here. The specimens were tested under uniaxial static compression and compared against benchmark samples manufactured with traditional machining. The mechanical results of the two types of cages were found to be similar with the exception of a significant lower displacement exhibited by the HT laser sintered parts. This result does not represent a detrimental performance of the HT-LS technology, but only confirms a technology limit which is well known and established in the additive manufacturing community area.

8.3 Limits

When novel findings and testing procedures are carried out, they often become occasions for outlining additional issues and limits of the findings just discovered.

1. The particle shape analysis, which provided truthful results and utilised fully accessible technologies such as SEM, required a significant contribution of manual drawing of the particles. The image J software did not allow accurate recognition of the particles so most of them have been drawn manually for an amount of more than 6000 particles.

2. The evaluation of the Hamaker constant has been carried out by using literature values instead of measured parameters, therefore the possibility to directly detect dielectric constants and refractive indices of LS powders could lead to more accurate results.

3. This research project did not focus into the in-depth investigation of PEEK and PEK particle sintering. Very qualitative experimental tests were performed at the beginning of this project in order to confirm the ability to melt of PEK and PEEK particles within a time scale of the same order of magnitude. However, more investigation into this mechanism could provide new findings in the role of particle morphology and material viscosity during particle sintering, especially in HT-LS processing.

4. The optimisation of the HT laser sintered PEEK components with variable PS time has not been carried out at PS times considerably higher than the EOS standard 12 s PS.

5. While the current prediction methods for LS have been showed and examined, it is still missing any sort of experimental approach for the determination of those temperatures that control the cooling and therefore the crystallisation within the building chamber during a LS process, i.e. exchangeable frame and building platform temperatures.

6. The EMR analysis and the new prediction technique for the part bed temperature have been carried out only for very few materials. More polymers should be tested in order to draw more solid conclusions.

8.4 Suggestions for future work and development

New findings have been provided in this research project. Yet new experimental challenges have become available to be explored.

Additional research on the role of particle morphology and powder material viscosity could be provided by the analysis of particle sintering mechanisms.

The effect of part orientation and part density has not been thoroughly investigated in this project; therefore more experimental building setups could be carried out within this intent. Deeper builds could also provide important results for mechanical and thermo-physical properties of HT laser sintered components.

The characterisation of the HT laser sintered structures mainly focused on the analysis of tensile properties, complex moduli and microstructure. Other tests such as three point bending could be an example for further exploration.

Also different laser exposure strategies could be an occasion for the development of higher performing components. It is well known for example that components built along the Z direction show nearly a 50% drop in the mechanical performance because of sensitivity to the layer manufacturing. However, there is very little research activity carried out in order to improve these characteristics. While the possibility to apply double laser exposure every two or three exposed layers in metal laser sintering has been introduced, such an approach, or a new one, has not been taken into consideration for polymers.

In this research, the thermal degradation associated to 1% weight loss of the original specimen weight was set as a degradation limit acceptable for HT laser sintered components in the EMR analysis. However, this limit could be unrealistic and not required in real scenarios. Therefore, more investigation into the level of tolerable degradation in HT laser sintered parts could lead to better predictions within the EMR analysis and therefore increase the number of applications of the HT-LS technology.

The manufacture of HT laser sintered PEEK components with a much longer PS time could be of great interest for enhancing the tensile strength of the components. As a longer PS time overall can likely lead to over melt across the powder bed and

loss of geometrical accuracy, this investigation should be carried out in parallel with a highly accurate evaluation of geometrical stability of the components.

HT-LS manufacturing of PEEK was based on PEK HP3 optimised shrinkage factors. As PEEK 450PF and PEK HP3 belong to the same chemical family and therefore share similar material performance, applying the same shrinkage factors in the HT-LS process was considered a reasonable assumption. However, the ad-hoc calibration of the PEEK shrinkage factors could provide another opportunity to optimise the process.

Testing more HT-LS polymers could help to further validate the method proposed in chapter 6 for the prediction of the part bed processing temperature inside HT-LS systems.

Lastly, one of the main criticisms often reserved to new LS grades, and especially HT polymers, is the lack of the possibility to recycle these materials. Although this property is not the first priority in in the manufacturing of medical implants, it is of great interest for other industrial sectors. It would therefore be very beneficial to explore properties and performance of PEEK components including overflow or used powders in different amounts.

Novel methodological approaches and conclusive results are included in this three year research project which hence contributes to expand the body of knowledge in an inter-disciplinary field that involves polymer engineering, particle technology, material science and additive manufacturing engineering. A new polymer has been adapted to be ready for use within an area where only one polymeric grade was available hence providing not only new research opportunities for similar materials but a solid accomplishment for the production and development of new industrial applications.

9 Appendix

9.1 Spreading test of PAEK materials at room temperature

Spreading test of HT PAEK polymers within the Sinterstation 2000 and the EOSINT P 800 at room temperature. Layer 3

Spreading test of HT PAEK polymers within the Sinterstation 2000 and the EOSINT P 800 at room temperature. Layer 4

PEK HP3   PEEK 450PF   PEEK 150PF

Spreading test of HT PAEK polymers within the Sinterstation 2000 and the EOSINT P 800 at room temperature. Layer 5

PEK HP3   PEEK 450PF   PEEK 150PF

Spreading test of HT PAEK polymers, PEK HP3, PEEK 150PF and 450PF, within the Sinterstation 2000 (spreading tool: counter-rotating roller) and the EOSINT P 800 (spreading tool: double blade recoater) at room temperature. Layer 7

EOSINT P 800

PEK HP3   PEEK 450PF   PEEK 150PF

SINTERSTATION 2000

Spreading test of HT PAEK polymers within the Sinterstation 2000 and the EOSINT P 800 at room temperature. Layer 8

EOSINT P 800

PEK HP3   PEEK 450PF   PEEK 150PF

SINTERSTATION 2000

Spreading test of HT PAEK polymers within the Sinterstation 2000 and the EOSINT P 800 at room temperature. Layer 9

326

10 Bibliography

1. EOS. *http://www.eos.info/en/home.html*. [cited 2015 April].

2. Victrex. *http://www.victrex.com*. [cited 2015 April].

3. InvibioBiomaterialSolutions. *http://www.invibio.com/*. [cited 2015 April].

4. Kurtz, S.M. and J.N. Devine, *PEEK biomaterials in trauma, orthopedic, and spinal implants.* Biomaterials, 2007. **28**(32): p. 4845-4869.

5. Harsha, A.P., U.S. Tewari, and B. Venkatraman, *Solid particle erosion behaviour of various polyaryletherketone composites.* Wear, 2003. **254**(7–8): p. 693-712.

6. Abraham, R.J. and I.S. Haworth, *Molecular modelling of poly(aryl ether ketones): 2. Chain packing in crystalline PEK and PEEK.* Polymer, 1991. **32**(1): p. 121-126.

7. Dawson, P.C. and D.J. Blundell, *X-ray data for poly(aryl ether ketones).* Polymer, 1980. **21**(5): p. 577-578.

8. Blundell, D.J. and A.B. Newton, *Variations in the crystal lattice of PEEK and related para-substituted aromatic polymers: 2. Effect of sequence and proportion of ether and ketone links.* Polymer, 1991. **32**(2): p. 308-313.

9. Abraham, R.J. and I.S. Haworth, *Molecular modelling of poly(aryl ether ketones). I. Aryl··aryl interactions in crystal structures.* Journal of Computer-Aided Molecular Design, 1990. **4**(3): p. 283-294.

10. Blundell, D.J. and V. Bayon, *The crystal structure of poly(ether ketone) copolymers.* Polymer, 1993. **34**(7): p. 1354-1360.

11. Blundell, D.J. and J. D'Mello, *Variations in the crystal lattice of PEEK and related para-substituted aromatic polymers: 1. Thermal expansion.* Polymer, 1991. **32**(2): p. 304-307.

12. Zimmermann, H.J. and K. Könnecke, *Crystallization of poly(aryl ether ketones): 3. The crystal structure of poly(ether ether ketone ketone) (PEEKK).* Polymer, 1991. **32**(17): p. 3162-3169.

13. Cansado, I.P.P., et al., *PEEK: An excellent precursor for activated carbon production for high temperature application.* Fuel Processing Technology, 2009. **90**(2): p. 232-236.

14. Dr. Stuart Green, J.S., *A Polyaryletherketone Biomaterial for use in Medical Implant Applications.*

15. Harsha, A.P. and U.S. Tewari, *Tribo performance of polyaryletherketone composites.* Polymer Testing, 2002. **21**(6): p. 697-709.

16. Waddon, A.J., et al., *On the crystal texture of linear polyaryls (PEEK, PEK and PPS).* Journal of Materials Science, 1987. **22**(5): p. 1773-1784.

17. Day, M., et al., *Thermal degradation of poly(aryl-ether–ether-ketone) (PEEK): A differential scanning calorimetry study.* Journal of Applied Polymer Science, 1988. **36**(5): p. 1097-1106.

18. Vasconcelos, G.d.C., et al., *Evaluation of crystallization kinetics of polymer of poly (ether-ketone-ketone) and poly (ether-ether-ketone) by DSC.* Journal of Aerospace Technology and Management, 2010. **2**(2): p. 155-162.

19. Hay, J.N. and D.J. Kemmish, *Thermal decomposition of poly(aryl ether ketones).* Polymer, 1987. **28**(12): p. 2047-2051.

20. Day, M., D. Sally, and D.M. Wiles, *Thermal degradation of poly(aryl-ether-ether-ketone): Experimental evaluation of crosslinking reactions.* Journal of Applied Polymer Science, 1990. **40**(9-10): p. 1615-1625.

21. Harper, C.A. and E.M. Petrie, *Plastics Materials and Processes: A Concise Encyclopedia*2003: Wiley.

22. Jin, L., et al., *Crystallization behavior and morphological characterization of poly(ether ether ketone).* Polymer, 2014. **55**(20): p. 5255-5265.

23. Tregub, A., et al., *Deformation and Thermoelastic Behavior of Poly(aryl ether ketones).* Macromolecules, 1995. **28**(11): p. 3890-3893.

24. Bas, C., et al., *Crystallization kinetics of poly(aryl ether ether ketone): Time-temperature-transformation and continuous-cooling-transformation diagrams.* European Polymer Journal, 1995. **31**(10): p. 911-921.

25. Bassett, D.C., R.H. Olley, and I.A.M. Al Raheil, *On crystallization phenomena in PEEK.* Polymer, 1988. **29**(10): p. 1745-1754.

26. Cebe, P. and S.-D. Hong, *Crystallization behaviour of poly(ether-ether-ketone).* Polymer, 1986. **27**(8): p. 1183-1192.

27. Deslandes, Y., F.-N. Sabir, and J. Roovers, *Effect of molecular weight on the spherulitic growth rate of poly(aryl ether ether ketone).* Polymer, 1991. **32**(7): p. 1267-1273.

28. Hsiao, B.S., et al., *Time-resolved X-ray study of poly(aryl ether ether ketone) crystallization and melting behaviour: 1. Crystallization.* Polymer, 1993. **34**(19): p. 3986-3995.

29. Mehmet-Alkan, A.A. and J.N. Hay, *The crystallinity of poly(ether ether ketone).* Polymer, 1992. **33**(16): p. 3527-3530.

30. Mehmet-Alkan, A.A. and J.N. Hay, *The crystallinity of PEEK composites.* Polymer, 1993. **34**(16): p. 3529-3531.

31. Tan, S., et al., *Crystallization kinetics of poly(ether ether ketone) (PEEK) from its metastable melt.* Polymer, 1999. **40**(5): p. 1223-1231.

32. Tierney, J.J. and J.W. Gillespie Jr, *Crystallization kinetics behavior of PEEK based composites exposed to high heating and cooling rates.* Composites Part A: Applied Science and Manufacturing, 2004. **35**(5): p. 547-558.

33. Verma, R.K., et al., *SAXS studies of lamellar level morphological changes during crystallization and melting in PEEK.* Polymer, 1996. **37**(24): p. 5357-5365.

34. Wunderlich, B., *Reversible crystallization and the rigid–amorphous phase in semicrystalline macromolecules.* Progress in Polymer Science, 2003. **28**(3): p. 383-450.

35. Chun, Y.S., et al., *Glass transition temperatures and rigid amorphous fraction of poly(ether ether ketone) and polyarylate blends.* Polymer, 2000. **41**(24): p. 8717-8720.

36. Gupta, H. and R. Salovey, *Thermal behavior of transparent poly(etheretherketone)(PEEK) film.* Polymer Engineering & Science, 1990. **30**(8): p. 453-458.

37. Jonas, A. and R. Legras, *Thermal stability and crystallization of poly(aryl ether ether ketone).* Polymer, 1991. **32**(15): p. 2691-2706.

38. Lattimer, M.P., et al., *On the origin of the multiple endotherms in PEEK.* Polymer, 1992. **33**(18): p. 3971-3973.

39. Lee, Y. and R.S. Porter, *Effects of thermal history on crystallization of poly(ether ether ketone) (PEEK).* Macromolecules, 1988. **21**(9): p. 2770-2776.

40. Lee, Y.C. and R.S. Porter, *Double-Melting Behavior of Poly(Ether Ether Ketone).* Macromolecules, 1987. **20**(6): p. 1336-1341.

41. Mazur, R.L., et al., *Thermal and Rheological Evaluation of PEKK Thermoplastic Matrix for Aeronautical Application.* Polimeros-Ciencia E Tecnologia, 2008. **18**(3): p. 237-243.

42. Medellín-Rodríguez, F.J., P.J. Phillips, and J.S. Lin, *Melting Behavior of High-Temperature Polymers.* Macromolecules, 1996. **29**(23): p. 7491-7501.

43. Nguyen, H.X. and H. Ishida, *Molecular analysis of the melting behaviour of poly(aryl-ether-ether-ketone).* Polymer, 1986. **27**(9): p. 1400-1405.

44. Wei, C.L., M. Chen, and F.E. Yu, *Temperature modulated DSC and DSC studies on the origin of double melting peaks in poly(ether ether ketone).* Polymer, 2003. **44**(26): p. 8185-8193.

45. Bessard E., D.A.O.e.B.G., *Etude et modélisation de la cinétique de cristallisation du PEEK lors de refroidissements isothermes et anisothermes.* Comptes Rendus des JNC 17 - Poitiers 2011, 2011.

46. Cheng, S.Z.D., et al., *Polymorphism and crystal structure identification in poly(aryl ether ketone ketone)s.* Macromolecular Chemistry and Physics, 1996. **197**(1): p. 185-213.

47. Rao, V.L. and P. Sivadasan, *Synthesis and properties of polyether ketones.* European Polymer Journal, 1994. **30**(12): p. 1381-1388.

48. Scholes, S.C. and A. Unsworth, *The wear performance of PEEK-OPTIMA based self-mating couples.* Wear, 2010. **268**(3–4): p. 380-387.

49. Sharma, M., J. Bijwe, and P. Mitschang, *Abrasive wear studies on composites of PEEK and PES with modified surface of carbon fabric.* Tribology International, 2011. **44**(2): p. 81-91.

50. Zhang, G., *Structure–tribological property relationship of nanoparticles and short carbon fibers reinforced PEEK hybrid composites.* Journal of Polymer Science Part B: Polymer Physics, 2010. **48**(7): p. 801-811.

51. Zhang, R., et al., *Study on tribological behaviour of plasma-treated PEEK and its composites.* Wear, 1995. **181–183, Part 2**(0): p. 613-623.

52. Mano, J.F., et al., *Bioinert, biodegradable and injectable polymeric matrix composites for hard tissue replacement: state of the art and recent developments.* Composites Science and Technology, 2004. **64**(6): p. 789-817.

53. Kulkarmi A, H.H., Wong H, *Solis Cage (PEEK) For Anterior Cervical Fusion: Preliminary Radiological Results With Emphasis On Fusion And Subsidence.* The Spine Journal. 2007; 7 (2):205-209, 2007.

54. Nieminen, T., et al., *Amorphous and crystalline polyetheretherketone: Mechanical properties and tissue reactions during a 3-year follow-up.* Journal of biomedical materials research. Part A, 2008. **84**(2): p. 377-83.

55. Han, C.-M., et al., *The electron beam deposition of titanium on polyetheretherketone (PEEK) and the resulting enhanced biological properties.* Biomaterials, 2010. **31**(13): p. 3465-3470.

56. Lethaus, B., et al., *A treatment algorithm for patients with large skull bone defects and first results.* Journal of Cranio-Maxillofacial Surgery, 2011. **39**(6): p. 435-440.

57. Wohlers, T.T. and W. Associates, *Wohlers Report 2012: Additive Manufacturing and Three Dimensional Printing State of the Industry Annual*2012: Wohlers Associates.

58. Goodridge, R.D., C.J. Tuck, and R.J.M. Hague, *Laser sintering of polyamides and other polymers.* Progress in Materials Science, 2012. **57**(2): p. 229-267.

59. Athreya, S.R., K. Kalaitzidou, and S. Das, *Mechanical and microstructural properties of Nylon-12/carbon black composites: Selective laser sintering versus melt compounding and injection molding.* Composites Science and Technology, 2011. **71**(4): p. 506-510.

60.   Chung, H. and S. Das, *Processing and properties of glass bead particulate-filled functionally graded Nylon-11 composites produced by selective laser sintering.* Materials Science and Engineering: A, 2006. **437**(2): p. 226-234.

61.   Chung, H. and S. Das, *Functionally graded Nylon-11/silica nanocomposites produced by selective laser sintering.* Materials Science and Engineering: A, 2008. **487**(1–2): p. 251-257.

62.   Dupin, S., et al., *Microstructural origin of physical and mechanical properties of polyamide 12 processed by laser sintering.* European Polymer Journal.

63.   Gibson, I. and D.P. Shi, *Material properties and fabrication parameters in selective laser sintering process.* Rapid prototyping journal, 1997. **3**(4): p. 129-136.

64.   Goodridge, R.D., R.J.M. Hague, and C.J. Tuck, *Effect of long-term ageing on the tensile properties of a polyamide 12 laser sintering material.* Polymer Testing, 2010. **29**(4): p. 483-493.

65.   Goodridge, R.D., et al., *Processing of a Polyamide-12/carbon nanofibre composite by laser sintering.* Polymer Testing, 2011. **30**(1): p. 94-100.

66.   Kim, J. and T.S. Creasy, *Selective laser sintering characteristics of nylon 6/clay-reinforced nanocomposite.* Polymer Testing, 2004. **23**(6): p. 629-636.

67.   Majewski C.E., H.Z., N.Hopkinson, *Effects of Degree of Particle Melt and crystallinity in SLS Nylon-12 parts.*

68.   Moeskops E., K.N., Van de Vorst B., Knoppers R., *Creep Behaviour Of Polyamide In Selective Laser Sintering.* TNO Industrial Technology, 2004.

69.   Yan, C., et al., *Preparation, characterisation and processing of carbon fibre/polyamide-12 composites for selective laser sintering.* Composites Science and Technology, 2011. **71**(16): p. 1834-1841.

70.   Yan, C., et al., *Preparation and selective laser sintering of nylon-12 coated metal powders and post processing.* Journal of Materials Processing Technology, 2009. **209**(17): p. 5785-5792.

71.   Zarringhalam, H., et al., *Effects of processing on microstructure and properties of SLS Nylon 12.* Materials Science and Engineering: A, 2006. **435–436**: p. 172-180.

72.   Berzins, M., T.H.C. Childs, and G.R. Ryder, *The Selective Laser Sintering of Polycarbonate.* CIRP Annals - Manufacturing Technology, 1996. **45**(1): p. 187-190.

73.   Wendel, B., et al., *Additive Processing of Polymers.* Macromolecular Materials and Engineering, 2008. **293**(10): p. 799-809.

74. Nelson, J.C., et al., *Model of the selective laser sintering of bisphenol-A polycarbonate.* Industrial & Engineering Chemistry Research, 1993. **32**(10): p. 2305-2317.

75. Kruth, J.P., et al., *Lasers and materials in selective laser sintering.* Assembly Automation, 2003. **23**(4): p. 357-371.

76. Zheng, H., et al., *Effect of core–shell composite particles on the sintering behavior and properties of nano-Al2O3/polystyrene composite prepared by SLS.* Materials Letters, 2006. **60**(9–10): p. 1219-1223.

77. Kruth, J.P., et al., *Consolidation phenomena in laser and powder-bed based layered manufacturing.* CIRP Annals - Manufacturing Technology, 2007. **56**(2): p. 730-759.

78. Davidson, C., *Investigating the suitability of laser sintered elastomers for running footwear applications*, 2012, Loughborough University.

79. Vasquez, M., *Analysis and development of new materials for polymer laser sintering*, 2012, Loughborough University.

80. Bartolo, P., et al., *Biomedical production of implants by additive electro-chemical and physical processes.* CIRP Annals - Manufacturing Technology, 2012(0).

81. Fabian Rengier, H.v.T.-K., Christian Zechmann,Hans-Ulrich Kauczor and Frederik L Giesel, *Beyond the Eye – Medical Applications of 3D Rapid Prototyping Objects.* Digital Radiography - EUROPEAN MEDICAL IMAGING REVIEW, 2008.

82. Williams, J.V. and P.J. Revington, *Novel use of an aerospace selective laser sintering machine for rapid prototyping of an orbital blowout fracture.* International Journal of Oral and Maxillofacial Surgery, 2010. **39**(2): p. 182-184.

83. Shapeways. *http://www.shapeways.com/*. [cited 2015 April].

84. Schultz J.P., M.J.P., Kander R.G. and Suchital T.A., *Selective Laser Sintering of Nylon 12-PEEK Blends Formed by Cryogenic Mechanical Alloying*, in *International Solid Freeform Fabrication Symposium* 2000: Austin (TX), USA.

85. Hopkinson, N., R.J.M. Hague, and P.M. Dickens, *Rapid Manufacturing: An Industrial Revolution for the Digital Age* 2006: John Wiley.

86. Seville, J.P., R. Clift, and U. Tüzün, *Processing of Particulate Solids* 2011: Springer London, Limited.

87. Prescott J.K., B.R.A., *On powder flowability.* Pharmaceutical Technology, 2000. **October 2010**

88. Schulze, D., *Powders and Bulk Solids: Behavior, Characterization, Storage and Flow* 2007: Springer Berlin Heidelberg.

89.   Butscher, A., et al., *Structural and material approaches to bone tissue engineering in powder-based three-dimensional printing.* Acta Biomaterialia, 2011. **7**(3): p. 907-920.

90.   Drummer, D., D. Rietzel, and F. Kühnlein, *Development of a characterization approach for the sintering behavior of new thermoplastics for selective laser sintering.* Physics Procedia, 2010. **5, Part B**: p. 533-542.

91.   Tan, K.H., et al., *Scaffold development using selective laser sintering of polyetheretherketone–hydroxyapatite biocomposite blends.* Biomaterials, 2003. **24**(18): p. 3115-3123.

92.   Tan, K.H., et al., *Selective laser sintering of biocompatible polymers for applications in tissue engineering.* Bio-Medical Materials and Engineering, 2005. **15**(1-2): p. 113-124.

93.   Tan, K.H., et al., *Fabrication and characterization of three-dimensional poly (ether-ether-ketone) / hydroxyapatite biocomposite scaffolds using laser sintering.* Proceedings of the Institution of Mechanical Engineers, Part H: Journal of Engineering in Medicine, 2005. **219**(3): p. 183-194.

94.   Evans, R.S., Bourell, D. L., Beaman, J. J. and Campbell, M.I. , *SLS Materials Development Method for Rapid Manufacturing.* Proceedings SFF Symposium, Austin (TX), USA, pp. 184-196., 2005.

95.   McAlea, K., *Selective Laser Sintering Of Polymer Powder Of Controlled Particle Size Distribution*, 1998.

96.   Hao, L., et al., *Characterization of selective laser-sintered hydroxyapatite-based biocomposite structures for bone replacement.* Proceedings of the Royal Society A: Mathematical, Physical and Engineering Science, 2007. **463**(2084): p. 1857-1869.

97.   Liu B., W.R., Tuck C., Ashcroft I., Hague R., *Investigation the Effect of Particle Size Distribution on Processing Parameters Optimisation in Selective Laser Melting Process.* 2011.

98.   Kumar, S., *Selective laser sintering: A qualitative and objective approach.* JOM Journal of the Minerals, Metals and Materials Society, 2003. **55**(10): p. 43-47.

99.   Kolan, K.C.R., et al., *Effect of material, process parameters, and simulated body fluids on mechanical properties of 13-93 bioactive glass porous constructs made by selective laser sintering.* Journal of the Mechanical Behavior of Biomedical Materials, 2012. **13**(0): p. 14-24.

100.   Van der Schueren B., K.J.P., *Powder deposition in selective metal powder sintering.* Rapid Prototyping Journal Volume 1 · Number 3 · 1995 · pp. 23–31, 1995.

101.   Amado A., S.M., Levy G. and Wegener K., *Adavances In SLS Powder Characterization.* 2011.

102. Amado, A.S., M. Wegener, K., *Flowability of SLS powders at elevated temperature* in *Solid Freeform Fabrication Symposium*2014: Austin, Texas.

103. Rietzel D., W.A., Dietmar Drummer, Tim A. Osswald, *Polymer powders for Selective Laser Sintering – Production and Characterization.*

104. Vasquez, M., B. Haworth, and N. Hopkinson, *Methods for quantifying the stable sintering region in laser sintered polyamide-12.* Polymer Engineering & Science, 2013. **53**(6): p. 1230-1240.

105. Rechtenwald T., E.G., Schimdt M. and Pohle D. *Comparison between laser sintering of PEEK and PA using design of experiment methods.* in *Virtual Modelling and Rapid Manufacturing: Advanced Research in Virtual and Rapid Prototyping Proc. 2nd Int. Conf. on Advanced Research in Virtual and Rapid Prototyping, 28 Sep-1 Oct 2005, Leiria, Portugal.* 2005. Taylor & Francis.

106. Kruth, J.-P., et al., *Binding Mechanisms in Selective Laser Sintering and Selective Laser Melting.* Rapid prototyping journal, 2005. **11**(1): p. 26-36.

107. Kruth, P.d.i.J.P., et al., *Benchmarking of different SLS/SLM processes as Rapid Manufacturing techniques*, in *Proceedings of the PMI, paper 525*2005.

108. Shi, Y., et al., *Effect of the properties of the polymer materials on the quality of selective laser sintering parts.* Proceedings of the Institution of Mechanical Engineers, Part L: Journal of Materials Design and Applications, 2004. **218**(3): p. 247-252.

109. Bellehumeur, C.T., M.K. Bisaria, and J. Vlachopoulos, *An experimental study and model assessment of polymer sintering.* Polymer Engineering & Science, 1996. **36**(17): p. 2198-2207.

110. Ch'ng, H.N. and J. Pan, *Sintering of particles of different sizes.* Acta Materialia, 2007. **55**(3): p. 813-824.

111. Frenkel, J., *Viscous flow of crystalline bodies under the action of surface tension.* Journal of Physics 1945. **9**(5): p. 385–91.

112. Vasquez M., H.N., Haworth B., *Laser Sintering Processes: Practical Verification of Particle Coalescence for Polyamides and Thermoplastic Elastomers.* ANTEC, 2010.

113. Tolochko, N., et al., *Selective laser sintering of single- and two-component metal powders.* Rapid prototyping journal, 2003. **9**(2): p. 68-78.

114. Tolochko, N.K., et al., *Absorptance of powder materials suitable for laser sintering.* Rapid prototyping journal, 2000. **6**(3): p. 155-160.

115. Soe, S.P., *Quantitative analysis on SLS part curling using EOS P700 machine.* Journal of Materials Processing Technology, 2012. **212**(11): p. 2433-2442.

116.   Ghita, O., et al., *High Temperature Laser Sintering (HT-LS): An investigation into mechanical properties and shrinkage characteristics of Poly (Ether Ketone) (PEK) structures.* Materials & Design, 2014. **61**(0): p. 124-132.

117.   Senthilkumaran, K., P.M. Pandey, and P.V.M. Rao, *New model for shrinkage compensation in selective laser sintering.* Virtual and Physical Prototyping, 2009. **4**(2): p. 49-62.

118.   EOS, *EOSINT P 800 manual.*

119.   Ho, H.C.H., I. Gibson, and W.L. Cheung, *Effects of energy density on morphology and properties of selective laser sintered polycarbonate.* Journal of Materials Processing Technology, 1999. **89–90**(0): p. 204-210.

120.   Drummer, D., M. Drexler, and F. Kühnlein, *Effects on the Density Distribution of SLS-Parts.* Physics Procedia, 2012. **39**(0): p. 500-508.

121.   Caulfield, B., P.E. McHugh, and S. Lohfeld, *Dependence of mechanical properties of polyamide components on build parameters in the SLS process.* Journal of Materials Processing Technology, 2007. **182**(1–3): p. 477-488.

122.   Franco, A., M. Lanzetta, and L. Romoli, *Experimental analysis of selective laser sintering of polyamide powders: An energy perspective.* Journal of Cleaner Production, 2010. **18**(16-17): p. 1722-1730.

123.   Franco, A. and L. Romoli, *Characterization of laser energy consumption in sintering of polymer based powders.* Journal of Materials Processing Technology, 2012. **212**(4): p. 917-926.

124.   3DSystems. *http://www.3dsystems.com/.* [cited 2015 April].

125.   Pohle, D., et al., *Processing of Three-Dimensional Laser Sintered Polyetheretherketone Composites and Testing of Osteoblast Proliferation in vitro.* Macromolecular Symposia, 2007. **253**(1): p. 65-70.

126.   Evonik. *http://corporate.evonik.com/en/Pages/default.aspx.* [cited 2015 April].

127.   Schmidt, M., D. Pohle, and T. Rechtenwald, *Selective Laser Sintering of PEEK.* CIRP Annals - Manufacturing Technology, 2007. **56**(1): p. 205-208.

128.   von Wilmowsky, C., et al., *Effects of bioactive glass and β-TCP containing three-dimensional laser sintered polyetheretherketone composites on osteoblasts in vitro.* Journal of Biomedical Materials Research Part A, 2008. **87A**(4): p. 896-902.

129.   Von Wilmonsky, C., et al., *In Vivo Evaluation of ß-TCP Containing 3D Laser Sintered Poly(ether ether ketone) Composites in Pigs.* Journal of Bioactive and Compatible Polymers, 2009. **24**(2): p. 169-184.

130.   Wagner, T., et al., *Laser Sintering of High Temperature Resistant Polymers with Carbon Black Additives.* International Polymer Processing, 2004. **19**(4): p. 395-401.

131. Woicke N, Wagner T., Eyerer P., *Carbon Assisted Laser Sintering of Thermoplastic Polymers.* ANTEC conference proceedings, 2005. **7**: p. 36-40.

132. Kroh, M., C. Bonten, and P. Eyerer, *Improvement of mechanical properties by additive assisted laser sintering of PEEK.* AIP Conference Proceedings, 2014. **1593**: p. 724-727.

133. Beard, M., et al. *Material characterisation of Additive Manufacturing components made from a polyetherketone (PEK) high temperature thermoplastic polymer*. in *Advanced Research in Virtual and Rapid Prototyping (VRAP)*. 2011. Leiria, Portugal: CRC Press.

134. Ghita, O.R., et al., *Physico-chemical behaviour of Poly (Ether Ketone) (PEK) in High Temperature Laser Sintering (HT-LS).* Journal of Materials Processing Technology, 2013.

135. El Halabi, F., et al., *Mechanical characterization and numerical simulation of polyether–ether–ketone (PEEK) cranial implants.* Journal of the Mechanical Behavior of Biomedical Materials, 2011. **4**(8): p. 1819-1832.

136. EOS. *PA 2200 material datasheet.*

137. EOS, *EOSINT P 100 manual.*

138. Systems, E.G.-E.O., *EOS PEEK HP3 datasheet.*

139. Margolis, J.M., *Engineering Thermoplastics: Properties and Applications*1985: Dekker.

140. Kurtz, S.M., *Peek Biomaterials Handbook*2011: Elsevier Science Limited.

141. Victrex, *PEEK 150 PF datasheet.*

142. Victrex, *PEEK 450 PF datasheet.*

143. Potters. *http://pottersbeads.com/*. [cited 2013 August].

144. AshGrove. *http://www.ashgrove.com/*. [cited 2015 April].

145. Ashgrove, *Calcium carbonate datasheet.*

146. SigmaAldrich. *http://www.sigmaaldrich.com/sigma-aldrich/home.html*. [cited 2013 August].

147. InvibioBiomaterialSolutions, *Unfilled PEEK OPTIMA Processing Guide.*

148. Leuterer M., M.F., Pfister A., *PAEK powder, in particular for the use in a method for a layer-wise manufacturing of a three-dimensional object, as well as method for producing it*, 2012.

149. Instron. *http://www.instron.com*. [cited 2015 May].

150. Micromeritics. *http://www.micromeritics.com/*. [cited 2015 May].

151. Malvern. *http://www.malvern.com/en/*. [cited 2015 May].

152. ASTM, *ASTM C 1444 – 00 Standard Test Method for Measuring the Angle of Repose of Free-Flowing Mold Powders*.

153. ImageJ, *User manual.*

154. Mora, C.F. and A.K.H. Kwan, *Sphericity, shape factor, and convexity measurement of coarse aggregate for concrete using digital image processing.* Cement and Concrete Research, 2000. **30**(3): p. 351-358.

155. NHS. *ImageJ.* [cited 2013 August]; Available from: *http://rsbweb.nih.gov/ij/*.

156. MATLAB. *http://www.mathworks.co.uk/products/matlab/*. [cited 2015 May].

157. Mahalanobis. *http://www.jennessent.com/arcview/mahalanobis_description.htm*. [cited 2015 April].

158. Ileleji, K.E. and B. Zhou, *The angle of repose of bulk corn stover particles.* Powder Technology, 2008. **187**(2): p. 110-118.

159. Hamaker, H.C., *The London—van der Waals attraction between spherical particles.* Physica, 1937. **4**(10): p. 1058-1072.

160. Lomboy, G., et al., *A test method for determining adhesion forces and Hamaker constants of cementitious materials using atomic force microscopy.* Cement and Concrete Research, 2011. **41**(11): p. 1157-1166.

161. Huang, Q., et al., *Measurement of inter-particle forces by an interfacial force microscope.* Particuology, 2010. **8**(5): p. 400-406.

162. Das S., S.P.A., Raychaudhuri R.K., *A method to quantitatively evaluate the Hamaker constant using the jump-into-contact effect in atomic force microscopy* Nanotechnology, 2007. **18**.

163. Argento C., F.R.H., *Parametric tip model and force–distance relation for Hamaker constant determination from atomic force microscopy.* Journal of Applied Physics, 1996. **80**(11).

164. Israelachvili, J.N., *Intermolecular and Surface Forces: Revised Third Edition*2011: Elsevier Science.

165. Biron, M. and O. Marichal, *Thermoplastics and Thermoplastic Composites*2012: William Andrew.

166. Victrex. *http://www.victrex.com/docs/literature-docs/Victrex_Material%20Properties%20Guide%20%20%203_7_US.pdf*. [cited 2013 August].

167. Goyal R.K., S.J.N., *Fabrication of advanced poly(etheretherketone)/clay nanocomposites and their properties.* Adv. Mat. Lett, 2010. **1**(3): p. 205-209.

168. TWI. *http://www.twi.co.uk/news-events/bulletin/archive/2004/may-june/polymer-performance-in-a-tough-world/*. [cited 2013 August].

169. Polyamide12. *http://www.matweb.com/search/DataSheet.aspx?MatGUID=0e37a459c4eb452faa9d92659f9a0ccc*. [cited 2013 August].

170. Spheriglass. *http://www.matweb.com/search/DataSheet.aspx?MatGUID=d139f411f3c24b8e975f63f625d2142f&ckck=1*. [cited 2013 August].

171. Hydroxyapatite. *http://www.spacekdet.com/tutorials/IOR.html*. [cited 2013 August].

172. Evans, R.W., H.S. Cheung, and D.J. McCarty, *Cultured canine synovial cells solubilize 45Ca-labeled hydroxyapatite crystals.* Arthritis & Rheumatism, 1984. **27**(7): p. 829-832.

173. Hoepfner, T.P. and E.D. Case, *The porosity dependence of the dielectric constant for sintered hydroxyapatite.* Journal of Biomedical Materials Research, 2002. **60**(4): p. 643-650.

174. CalciumCarbonate. *http://www.matweb.com/search/DataSheet.aspx?MatGUID=bea4bfa9c8bd462093d50da5eebe78ac*. [cited 2013 August].

175. Aerosil. *http://www.rafoeg.de/20,Dokumentenarchiv/20,Daten/dielectric_chart.pdf*. [cited 2013 August].

176. RollerSinterstation. [cited 2013 May]; Available from: http://www.mech.kuleuven.be/pp/facilities/dtm.

177. Weidinger, J., F. Muller, and F. Pfefferkorn, *Device and method for a layerwise manufacturing of a three-dimensional object from a building material in powder form*, 2014, Google Patents.

178. Toledo, M. *http://uk.mt.com/gb/en/home.html*. [cited 2015 May].

179. Bailey, M.L., R. Raman, and R.M. German, *Method of making a biocompatible filter*, 1997, Google Patents.

180. Victrex, *PEEK 450 G Datasheet.*

181. Starr, T.L., T.J. Gornet, and J.S. Usher, *The effect of process conditions on mechanical properties of laser-sintered nylon.* Rapid prototyping journal, 2011. **17**(6): p. 418-423.

182. ISO, *527-2-1A Plastics -- Determination of tensile properties.*

183. Gooch, J.W., *Encyclopedic Dictionary of Polymers*2010: Springer.

184. CTPro3D. *http://www.nikonmetrology.com/en_EU/News/US-News/Nikon-Metrology-incorporates-Inspect-X-and-CT-Pro-into-XT-software-Suite-v2.2*. [cited 2015 April].

185. VGStudioMax2.1. *http://vgstudio-max.software.informer.com/2.1/*. [cited 2015 April].

186. SPSS, I. *http://www-01.ibm.com/software/analytics/spss/*. [cited 2015 May].

187. EuropeanCommission. *Stem Cells -European research projects involving stem cells in the 6th Framework Programme.* [cited 2015 April].

188. Renishaw. *http://www.renishaw.com/en/renishaw-enhancing-efficiency-in-manufacturing-and-healthcare--1030*. [cited 2015 May].

189. Geomagic. *http://www.geomagic.com/en/*. [cited 2015 April].

190. Magics. *Materialise http://software.materialise.com/magics*. [cited 2015 April].

191. ImageJ. *http://rsbweb.nih.gov/ij/*. [cited 2015 May].

192. Rimell, J.T. and P.M. Marquis, *Selective laser sintering of ultra high molecular weight polyethylene for clinical applications.* Journal of Biomedical Materials Research, 2000. **53**(4): p. 414-420.

193. Berretta, S., O. Ghita, and K.E. Evans, *Morphology of polymeric powders in Laser Sintering (LS): From Polyamide to new PEEK powders.* European Polymer Journal, 2014. **59**: p. 218-229.

194. Berretta S., G.O., Evans K.E., Anderson A. and Newman C., *Size, shape and flow of powders for use in Selective Laser Sintering (SLS)* in *Advanced research in virtual and rapid prototyping*, P.J.B.e. al., Editor 2013, CRC Press: Leiria, Portugal.

195. RPTools. *http://www.eos.info/systems_solutions*. [cited 2015 May].

196. Mainsah, E., J.A. Greenwood, and D. Chetwynd, *Metrology and Properties of Engineering Surfaces*2001: Springer.

197. Sichina, W.J. *Characterization of Polymers Using TGA*. [cited 2015 May]; Available from: http://depts.washington.edu/mseuser/Equipment/RefNotes/TGA_Notes.pdf.

198. Tecomet. *http://www.tecomet.com/cranial-maxillofacial-implants.html*. [cited 2015 May].